UNIVERSITY OF ALBERTA

CONTRIBUTIONS TO EROSION BY JETS

BY

OLUFEMI ADERIBIGBE ©

A THESIS
SUBMITTED TO THE FACULTY OF GRADUATE STUDIES AND
RESEARCH IN PARTIAL FULFILLMENT OF THE REQUIREMENTS
FOR THE DEGREE OF DOCTOR OF PHILOSOPHY

IN

WATER RESOURCES ENGINEERING

DEPARTMENT OF CIVIL ENGINEERING

EDMONTON, ALBERTA

SPRING, 1996

National Library
of Canada

Acquisitions and
Bibliographic Services Branch

395 Wellington Street
Ottawa, Ontario
K1A 0N4

Bibliothèque nationale
du Canada

Direction des acquisitions et
des services bibliographiques

395, rue Wellington
Ottawa (Ontario)
K1A 0N4

Your file Votre référence

Our file Notre référence

The author has granted an irrevocable non-exclusive licence allowing the National Library of Canada to reproduce, loan, distribute or sell copies of his/her thesis by any means and in any form or format, making this thesis available to interested persons.

L'auteur a accordé une licence irrévocable et non exclusive permettant à la Bibliothèque nationale du Canada de reproduire, prêter, distribuer ou vendre des copies de sa thèse de quelque manière et sous quelque forme que ce soit pour mettre des exemplaires de cette thèse à la disposition des personnes intéressées.

The author retains ownership of the copyright in his/her thesis. Neither the thesis nor substantial extracts from it may be printed or otherwise reproduced without his/her permission.

L'auteur conserve la propriété du droit d'auteur qui protège sa thèse. Ni la thèse ni des extraits substantiels de celle-ci ne doivent être imprimés ou autrement reproduits sans son autorisation.

ISBN 0-612-10563-6

Canada

UNIVERSITY OF ALBERTA

LIBRARY RELEASE FORM

NAME OF AUTHOR: OLUFEMI ADERIBIGBE

TITLE OF THESIS: CONTRIBUTIONS TO EROSION BY JETS

DEGREE: DOCTOR OF PHILOSOPHY

YEAR THIS DEGREE WAS GRANTED: 1996

Permission is hereby granted to the University of Alberta Library to reproduce single copies of this thesis and to lend or sell such copies for private, scholarly or scientific research purposes only.

The author reserves all other publication and other rights in association with the copyright in the thesis, and except as hereinbefore provided, neither the thesis nor any substantial portion thereof may be printed or otherwise reproduced in any material form whatever without the author's prior written permission.

(Signed)..... Olufemi Aderibigbe .....

Permanent Address:

P. O. Box 1848,
Lagos (Marina)
Nigeria, West Africa.

OR

c/o Yemi Adewumi
Apt. 402, 10635 83 Avenue
Edmonton, Alberta.
T6E 2E3

Dated: 18th April 1996

UNIVERSITY OF ALBERTA

FACULTY OF GRADUATE STUDIES AND RESEARCH

The undersigned certify that they have read, and recommend to the Faculty of Graduate Studies and Research for acceptance, a thesis entitled CONTRIBUTIONS TO EROSION BY JETS submitted by OLUFEMI ADERIBIGBE in partial fulfillment of the requirements for the degree of Doctor of Philosophy in Water Resources Engineering.

Supervisor, Dr. N. Rajaratnam

Dr. P.M. Steffler

Dr. F.E. Hicks

Dr. J.D. Scott

Dr. J. Shaw

External Examiner, Dr. A.F. Babb

Date: 19 April 96

Dedication

To God
for His Love

To my parents
for always being there

Abstract

This thesis is written in the paper format and includes five contributions. The following paragraphs are their abstracts.

The first contribution presents the results of an experimental study of erosion of sand/gravel beds by obliquely impinging submerged plane turbulent jets. The main characteristic lengths of the eroded bed profile in the asymptotic state were correlated to the erosion parameter E_p and compared to the correlations for perpendicular impingement.

The results of a laboratory study of the reduction of erosion of sand/gravel beds by screens below submerged impinging circular and plane jets are presented in the second contribution. In this method, a screen is placed on the sand/gravel bed to reduce the impact of the jet on the bed. In the case of impinging circular jets, the dynamic scour depth reduction in these experiments ranged from 47 to 84%. Reduction of the dynamic scour depth was also noticed in the case of impinging plane jets.

The third contribution presents the results of a laboratory study on the erosion of sand beds by submerged circular impinging vertical turbulent jets of water for the erosion parameter E_c less than 5. The variation of the maximum scour depth with impinging distance was studied and this revealed two major flow regimes referred to as the Strongly Deflected and the Weakly

Deflected Jet Regimes. Semi-empirical equations have been developed for the asymptotic characteristic lengths of the eroded bed.

The fourth contribution presents the results of an experimental study on the erosion by deeply submerged plane turbulent wall jets of sand beds made of three sediment mixtures. The characteristic lengths of the eroded bed in the asymptotic state were correlated to the densimetric Froude number based on particle size d_{95} and reductions in these lengths due to armoring were quantified.

The experimental data on erosion by circular horizontal jets from thirteen sources including the present experimental study were compiled and analyzed in the fifth contribution. The compiled data, comprising of over 350 sets of data, cover wide ranges of flow and sediment parameters. Equations relating the asymptotic characteristic lengths of the eroded bed to the F_O have been proposed.

Acknowledgments

I would like to thank my supervisor, Dr. N. Rajaratnam for his patience, guidance, encouragement, understanding and support throughout the research program. I was touched by his constant strong interest in the subject and in my general well being. These contributed very significantly to making this research work possible.

My special thanks to Mr. Sheldon Lovell for setting up all the five different experimental arrangements, his interest in my work, his productive advice and his friendship.

My thanks also go to my colleagues who helped me with the experimental work and for their discussions on the subject and to the professors and other colleagues in the Water Resources group for their friendship.

To my wife, Lara, for her love, encouragement, understanding and support. Also to my parents, brother, sisters and Ms. Adewumi for their love and support.

Finally, I would like to acknowledge the financial assistance I received in the form of a Commonwealth scholarship from the Association of Canadian Colleges and Universities, a scholarship from the Province of Alberta, a research assistantship through an operating grant to my professor from the Natural Science and Engineering Research Council of Canada and a partial financial support from the Central Research Fund of the University of Alberta.

Table of Contents

List of Tables
List of Figures
Notations

Chapter 1: Introduction 1
1.1 Scour by Jets 1
1.2 Organization of this Thesis 2
1.3 References 4

Chapter 2: Erosion of Sand Beds by Oblique Plane Water Jets 5
2.1 Introduction 5
2.2 Experiments and Experimental Results 7
2.3 Analysis of Experimental Results 8
2.3.1 Maximum Scour Depth 8
2.3.2 Other Length Scales 10
2.4 Practical application 11
2.5 Conclusions 12
2.6 References 13

Chapter 3: Reduction of Scour below Submerged Impinging Jets by Screens 26
3.1 Introduction 26
3.2 Impinging Circular Jets 27
3.2.1 Experiments 27
3.2.2 Flow Patterns 28
3.2.3 Dimensional Analysis 29
3.2.4 Regression Analysis 30
3.2.5 Effect of Screen 31
3.3 Impinging Plane Jets 32
3.3.1 Experiments 32
3.3.2 Flow Patterns 33
3.3.3 Dimensional Analysis and Effect of Screen 34
3.4 Conclusions 34
3.5 References 35

Chapter 4: Erosion of Loose Beds by Submerged Circular Impinging Vertical Turbulent Jets 51
4.1 Introduction 51
4.2 Laboratory Experiments 52
4.3 Effects of Impinging Distance 53
4.4 Similarity of Eroded Bed Profiles 54
4.5 Characteristics of Flow Regimes 55
4.5.1 Strongly Deflected Jet Regime 55
4.5.2 Weakly Deflected Jet Regime 56

4.6 Threshold Condition 56
4.7 Governing Equations 57
4.8 Equilibrium Scour Depth 59
4.9 Other Length Scales at Asymptotic State 60
4.10 Effect of Density Difference on Length Scales 62
4.11 Conclusions 62
4.12 References 63

Chapter 5: Effect of Sediment Gradation on Erosion by Plane Turbulent Wall Jets 86
5.1 Introduction 86
5.2 Experiments 87
5.3 Flow Patterns 88
5.4 Effective Diameter 89
5.5 Dimensional Considerations 90
5.6 Characteristic Lengths of the Eroded Bed 91
5.6.1 Maximum Scour Depth 91
5.6.2 Other Length Scales 93
5.7 Conclusions 94
5.8 References 95

Chapter 6: Generalized Study of Erosion by Circular Horizontal Turbulent Jets 116
6.1 Introduction 116
6.2 Literature Review 117
6.3 Experiments and Complied Data 119
6.4 Scour hole Characteristics 120
6.4.1 Description of the Scour Process 120
6.4.2 Evolution of Scour hole with Time 122
6.4.3 Geometric Similarity of Scour hole 123
6.5 Dimensional Considerations 124
6.6 Characteristic Lengths of the Eroded Bed 126
6.6.1 Equilibrium Maximum Scour Depth 126
6.6.1.1 Effect of Jet Submergence 128
6.6.1.2 Effect of Drop Height 129
6.6.2 Other Length Scales 130
6.7 Effect of relative density difference $\Delta\rho/\rho$ 132
6.8 Effects of other non dimensional parameters 133
6.9 Conclusions 134
6.10 References 135

Chapter 7: General Discussion 177
7.1 General Discussion 177
7.2 Application of Results to Prototype Cases 180
7.2 References 182

List of Tables

Table		Page
2-1	Coefficients proposed for equation (2-1)	6
2-2	Experimental Results	14
2-3	Scour depth computations for Cabora Bassa and Kariba Dams	12
	2-3(a) Relevant Parameters	12
	2-3(b) Scour depths	12
3-1	Details of screens	27
3-2	Impinging circular jets - Experimental results	36
3-2	Impinging circular jets - Experimental results (continued)	37
3-3	Impinging plane jets - Experimental Results	38
4-1	Experimental results	65
4-1	Experimental results (Continued)	66
4-2	Experimental results of other researchers	67
	4-2(a) Rajaratnam and Beltaos (1977)	67
	4-2(b) Rajaratnam (1982)	67
	4-2(c) Clarke (1962)	68
	4-2(d) Westrich and Kobus (1973)	68
5-1	Experimental results	97
5-2	Experimental results of Rajaratnam (1981)	98
6-1(a)	Experimental data for evolution of scour with time	138
6-1(b)	Experimental results	139
6-2	Summary of complied data	140
6-3	Experimental results of other researchers	141
	6-3(a) Clarke (1961)	141
	6-3(b) Ofwona (1965)	142
	6-3(c) Opie (1967)	142
	6-3(d) Stevens (1969) - Full flow	143
	6-3(d) Stevens (1969) - Full flow (continued)	144
	6-3(d) Stevens (1969) - Partial flow	145
	6-3(d) Stevens (1969) - Partial flow (continued)	146
	6-3(e) Bohan (1972)	147
	6-3(f) Rajaratnam and Berry (1977)	148
	6-3(g) Mendoza (1980)	149
	6-3(h) Shaihk (1980)	149
	6-3(i) Rajaratnam and Diebel (1981)	150
	6-3(j) Kloberdanz (1982)	150
	6-3(k) Ead (1990)	151
	6-3(l) Lim (1995)	151

List of Figures

Figure		Page
2-1	Definition Sketch	15
2-2	Variation of maximum static scour depth with E_p	16
2-3	Variation of maximum dynamic scour depth with E_p	17
2-4	Variation of ridge height with E_p	18
2-5	Variation of distance of dune with E_p	19
2-6	Variation of scour hole length with E_p	20
2-7	Variation of distance of the max. static scour depth with E_p	21
2-8	Variation of the offset distance with E_p	22
2-9	Similarity of scour profile	23
2-10	Single dominant vortex with suspended sediments	24
2-11	Variation of the height of sediment cloud with E_p	25
3-1(a)	Screen design	39
3-1(b)	Definition sketch	39
3-2	Sediment size distribution curves	40
3-3	Scour profiles with and without screen for circular jets	41
3-4	Scour hole pattern below screen with circular openings	42
3-5	Variation of relative maximum scour depth with E_c	43
3-6	Variation of relative maximum scour depth with other non-dimensional parameters	44
3-7	Variation of relative scour hole radius with other non-dimensional parameters	45
3-8	Variation of η_1 with E_c	46
3-9	Variation of η_2 with E_c	47
3-10	Scour profiles with and without screen for plane jets	48
3-11	Scour and flow patterns due to impinging plane jets using screen PS2	49
3-12	Variation of relative maximum scour depth with E_p	50
4-1	Sediment size distribution curves	69
4-2	Experimental set-up	70
4-3	Definition sketch	71
4-4	Variation of scour depth with impinging distance	72
4-5	Similarity of scour profiles	73
4-6	Variation of $(r_o/\varepsilon_m)_\infty$ with E_c	74
4-7(a)	Strongly deflected jet regime I (SDJR I)	75
4-7(b)	Strongly deflected jet regime II (SDJR II)	75

Figure Page

4-7(c) Weakly deflected jet regime I (WDJR I) 76
4-7(d) Weakly deflected jet regime II (WDJR II) 76
4-8 Variation of relative maximum scour depth with E_C 77
4-9 Dynamic scour depth (predicted against measured) 78
4-10 Variation of scour hole radius with E_C 79
4-11 Variation of (b_∞/h) with E_C 80
4-12 Variation of ridge height with E_C 81
4-13 Variation of relative maximum scour depth with E_C for other fluid-sediment systems 82
4-14 Variation of scour hole radius with E_C for other fluid-sediment systems 83
4-15 Maximum scour depth (measured against predicted) 84
4-16 Scour hole radius (measured against predicted) 85

5-1(a) Experimental set-up 99
5-1(b) Definition sketch 99
5-2 Particle size distributions for the sand mixtures 100
5-3(a-b) Flow patterns due to wall jet 101
5-3(c-d) Flow patterns due to wall jet 102
5-4(a) Sieve analysis of the top layer of bed for Expt. NU 20 103
5-4(b) Sieve analysis of the top layer of bed for Expt. NU 31 104
5-5 Variation of maximum scour depth with F_O 105
5-6 Variation of maximum scour depth with F_O (separated by b_O) 106
5-7 Variation of the reduction in the length scales of the scour hole with F_O 107
5-8 Variation of maximum scour depth with $F_{O(95)}$ 108
5-9 Variation of maximum scour depth difference with F_O 109
5-10 Variation of scour hole length with F_O 111
5-11 Variation of scour hole length with $F_{O(95)}$ 111
5-12 Variation of the distance of the dune with F_O 112
5-13 Variation of the distance of the dune with $F_{O(95)}$ 113
5-14 Variation of the dune height with F_O 114
5-15 Variation of the dune height with $F_{O(95)}$ 115

6-1(a-b) Set-up for the experiments 152
6-2 Definition sketch 153
6-3 Sediment size distribution curves 154
6-4(a) Migrating dunes 155
6-4(b) Eroded sand bed 155
6-4(c) Eroded gravel bed 156
6-4(d) Eroded bed of canola seeds 156
6-5 Variation of longitudinal profile of the eroded bed with time 157

Figure Page

6-6 Variation of the rate of erosion with distance 158
6-7 Variation of the characteristic lengths of the scour hole with time .159
6-8 Variation of x_m/ε_m with F_o 160
6-9 Variation of x_o/ε_m with F_o 161
6-10 Variation of $\bar{b}_m / \varepsilon_m$ with F_o 162
6-11 Variation of V_s / ε_m^3 with F_o 163
6-12 Variation of relative maximum scour depth with F_o 164
6-13 Effect of jet submergence on relative maximum scour depth 165
6-14 Variation of relative maximum scour depth with F_o for unsubmerged flows 166
6-15 Variation of relative maximum scour depth with F_d for overhanging pipes 167
6-16 Variation of relative distance of the maximum scour depth with F_o 168
6-17 Variation of relative scour hole length with F_o 169
6-18 Variation of relative maximum scour hole half width with F_o 170
6-19 Variation of relative distance of dune with F_o 171
6-20 Variation of relative dune height with F_o 172
6-21 Variation of relative volume of scour with F_o 173
6-22 Variation of $\varepsilon_{m\infty}/d$ and $x_{m\infty}/d$ with F_o for other fluid-sediment systems 174
6-23 Variation of $\bar{b}_{m\infty} / d$ and $x_{o\infty}/d$ with F_o for other fluid-sediment systems 175
6-24 Variation of Δ_∞/d and $x_{c\infty}/d$ with F_o for other fluid-sediment systems 176

Notations †

Symbol	Description
A	area of flow at pipe outlet [6]
B	downstream channel width [6]
b	length scale for the profile of eroded bed [3,4]
b_o	half thickness of nozzle of impinging plane jet or thickness of plane wall jet [2,3,5]
$\bar{b}_m$	maximum half-width of scour hole caused by circular wall jet [6]
$C_{1 \text{ to } 5}$	coefficients [4]
C_e	coefficient [5]
C_f	friction coefficient [4]
C_j	diffusion coefficient [4]
C_{jb}	adjusted diffusion coefficient [4]
C_r	correction factor [2]
D (or d_{50})	median size of bed material [2,3,4,5,6]
d	diameter of jet at nozzle [3,4,6]
d_{90} (or d_i)	bed material diameter, 90% (or i%) of which is finer by weight [2,3,5,6]
d_b	depth of partial flow at pipe outlet [6]
d_c	characteristic particle size of bed material [2]
d_e	effective diameter of sediment [5,6]
d_g	geometric mean diameter defined as $\sqrt{(d_{84}d_{16})}$ [5]
d_m	mean bed particle size [2]
d_s	depth of scour measured from tail water level [2]
E_c	erosion parameter for circular jets defined as $F_o/(h/d)$ [3,4]
E_p	the impinging jet erosion parameter defined as $F_o/\sqrt{(h_t/2b_o)}$ [2,3]
f	function (with suffixes) [2,3,4,5,6]
F_d	modified densimetric particle Froude number (see equation (6-18)) [6]
F_o	densimetric particle Froude number defined as $U_o/\sqrt{(gD\Delta\rho/\rho)}$ [3,5,6]
$F_{o(95)}$	modified densimetric particle Froude number defined as $U_o/\sqrt{(d_{95}g\Delta\rho/\rho)}$ [5]
g	acceleration due to gravity [2,3,4,5,6]
GSD	geometric standard deviation (see σ_g)

† The numbers in the square brackets denote the relevant chapter numbers

Symbol	Description
H	difference between the upstream and downstream water levels [2]
h	impinging vertical distance of submerged jet to the original bed level [2,3,4]
h_d	tail water depth [2,5,6]
h_{du}	water depth at pipe outlet [6]
h_p	the difference in culvert (pipe) invert elevation and elevation of tailwater level [6]
h_t	impingement distance of submerged jet measured in the jet direction and it is equal to h for vertical impingement [2]
K	constant [2]
k	exponent [5]
K_c	coefficient [4]
l_c	any characteristic length of the scoured bed [3,5,6]
l_s	diameter of screen opening [3]
M_o	momentum flux from nozzle defined as $\rho\pi d^2U_o^2/4$ for a circular jet and $2\rho b_oU_o^2$ for a unit width for a plane jet. [3]
P	porosity of screen defined as $\pi/(4\lambda^2)$ [3]
Q	discharge at pipe outlet [6]
q	unit discharge [2]
Q_i	discharge intensity defined as $Q/\sqrt{(gd^5)}$ or $Q/\sqrt{(gR_h^5)}$ [6]
r	radial distance [3,4]
r_1	radial distance of the ridge [3,4]
R^2	coefficient of multiple determination [3,5]
R_e	Reynolds number defined as $\rho U_o d/\mu$ [2,3,5,6]
R_h	hydraulic radius [6]
r_o	radius of scour hole at original bed level below circular jets [3,4]
S	height to which the sand particles are lifted above the original bed level [2]
s	relative tail water depth defined as h_d/b_o or h_d/d [5,6]
S_p	pipe slope [6]
S_s	specific gravity [6]
t	time [6]
u_{*c}	critical shear velocity at any slope [4,6]
u_{*cs}	Shields critical shear velocity [4]
U_b	bed velocity very close to jet centerline [4]
U_c	critical velocity [4]
U_m	centerline velocity of a circular jet [4]

Symbol	Description
U_o	velocity of jet at nozzle [2,3,4,5,6]
v	exponent [2]
V_s	volume of scoured material [6]
w	exponent [2]
x	distance along the jet centerline from nozzle or longitudinal distance in the plane of symmetry, from the location of maximum erosion [2,3,4,5,6]
x'	longitudinal distance, measured from the point of erosion, behind the jet [2]
x_1+x_2	length of scour hole [2]
x_b	distance of the location of maximum half width [6]
x_c	distance of the location of maximum dune height [2,5,6]
x_e	total length of the bed profile [5,6]
x_m	distance of the section of maximum erosion from the nozzle [2,5,6]
x_o	scour hole length [3,5,6]
y	exponent [2]
z	exponent [2]
α	non-dimensional screen size [3]
β	exponents [4,5]
$\bar{\beta}$	constant [6]
Δ	height of the ridge (dune) [2,4,5,6]
$\Delta\rho$	difference between the mass densities of the bed material and the fluid[2,3,4,5,6]
Δx	offset distance [2,3]
ε	depth of scour below the original bed level with jet off [2,3,4,5,6]
ε'	depth of scour below the original bed level with jet on [2,3,4,5]
ε'_m	maximum value of ε' [2,3,4,5]
ε'_{md}	the deeper dynamic maximum scour depth [5]
ε'_{ms}	the shallower dynamic maximum scour depth [5]
ε_m	maximum value of ε [2,3,4,5,6]
ϕ	angle of stream wise bed slope [4]
η	percentage reduction in scour depth due to armoring or screen [3,5]
κ	constant [6]
λ	the ratio of the side length of the square grid used for the screen design to the diameter of the screen opening (see Figure 3-1(a)) [3]
μ	dynamic viscosity of water [5,6]
θ	angle of the jet with the horizontal plane of the (uneroded) bed [2]

Symbol	Description
θ_r	submerged angle of repose of the bed material [4]
ρ	mass density of the fluid [2,3,4,5,6]
σ_g	geometric standard deviation of the bed material size defined as $\sqrt{(d_{84}/d_{16})}$ [3,4,5,6]
τ_c	critical shear stress [4]
υ	kinematic viscosity of the fluid [2,3,4]
ψ	relative maximum scour depth difference [5]
∞	suffix to denote asymptotic state [2,3,4,5,6]

CHAPTER 1

Introduction

1.1 Scour by Jets

The nature of flows issuing from hydraulic structures such as vertical gates, flip buckets, roller buckets and hydraulic jump basins is often in the form of turbulent jets. A turbulent jet can be defined as a high velocity fluid discharging into an ambient fluid which may be at rest or in motion. Turbulent water jets downstream of hydraulic structures do occur in different sizes, strengths and shapes and are discharged in different forms. These jets could be classified as; wall (horizontal) or free trajectory (oblique or vertical) jets in terms of their discharge paths, two or three dimensional in terms of their shape and free or submerged in terms of their condition in the ambient fluid.

The interaction of a jet with a sediment bed of sand, gravel, clay or weak rock results in a scour hole. A theoretical analysis of this problem is difficult and complex. It requires an in-depth understanding of jet diffusion in the vicinity of a rapidly changing scour hole geometry, the growth of scour, the movement and behavior of scoured materials at different times of the scour process and the effects of entrained air. Also, the effects of possible substantial variations in the frequencies, duration, magnitudes and turbulence of the spilled discharge on scour hole development need to be thoroughly understood. For these reasons, the general approach to this subject has been mainly empirical.

The scour hole formed could be sizable enough as to endanger the stability of part of or of the whole structure. If this leads to a structural failure, the economical loss could be very substantial, depending on the size of the structure and the extent of the failure. The challenge, therefore, faced by the hydraulic engineer is to devise an effective and economical way based

on the available hydraulic, hydrologic and geological data, to dissipate the energy and ensure a smooth flow transition from the dissipator to the downstream channel without excessive scour. For any design, the choice of energy dissipator will determine the location, growth and ultimate size of the scour that will be formed. In order to evaluate these for control measures, physical model studies are usually carried out for large structures. It is not usually economically justifiable to perform model studies for smaller structures; therefore, some of the standard designs and empirical equations available in the literature are often used.

1.2 Organization of this Thesis

A review of the present knowledge on erosion by turbulent jets reveals that there is still much to be known. This is due mainly to the difficult and complex nature of the problem. A good summary of the present knowledge can be found in Breusers and Raudkivi (1991). This thesis, comprising of five different pieces of work, attempts to contribute to the body of knowledge. This is mainly in the areas of developing equations for the characteristic lengths of scour in the asymptotic state due to different types of jets based on data compiled from many sources, quantifying the effects of screens (alternative method for scour control) on scour by impinging jets and quantifying the effects of sediment gradation on scour size. Each piece of work is written as a chapter and a brief introduction to each chapter is presented below.

In Chapter 2, the results of an experimental study of erosion of sand beds by obliquely impinging submerged plane turbulent jets for angles of impingement equal to 10°, 30°, 45° and 60° are presented. The objective of this study is to propose equations for the size of plunge pool scour. This chapter starts with a review of the earlier proposed formulas, followed by the details of the experiments and the analysis of the experimental results. Finally, the application of the proposed scour depth equation to estimate the scour depths for two prototype cases is presented.

In Chapter 3, the use of protective screens on sand beds to reduce the size of scour caused by impinging circular and plane jets is presented. This idea was prompted by the success of an earlier study (Rajaratnam and Aderibigbe

(1993)) involving using screens to reduce scour caused by deeply submerged plane wall jets. For the present study, the screens, which are nine in number, had circular openings laid out on a square grid (see Figure 3-1(a)). The first part (section 3.3) of this chapter presents the results from the impinging circular jet experiments and the results from the impinging plane jet experiments are presented in the second part (section 3.4). Each part presents the details of the experiments, the flow patterns around the screens, the analysis of the experimental results and finally, the quantification of the reductions (or increments for the scour hole length in some cases) of the length scales of the scour hole.

The asymptotic characteristic lengths of an eroded sand bed profile under submerged circular impinging vertical turbulent jets of water for the erosion parameter E_c less than 5 are analyzed and presented in Chapter 4. These results are based on the data from this study and from other researchers. The results from this study could be used to estimate the scour size below jets issuing from square gates of dams and cantilevered pipe outlets. The details of the experiments are given in section 4.3, followed by the effects of the jet impinging distance on the scour size. In section 4.5, the similarity of the eroded bed profiles is addressed and the characteristics of the different flow regimes are presented in section 4.6. This is followed by sections on the analysis of the experimental results. The effects of the relative density difference on the length scales of the scour hole are addressed in section 4.11 and the conclusions for this study are formulated in section 4.12.

In Chapter 5, the experimental observations and analysis of local scour of non-uniform non-cohesive beds downstream of deeply submerged plane turbulent wall jets are presented. Three sand mixtures of different degrees of non-uniformity are used. The details of the experiments are given in section 5.3. The instability of the jet and the associated flow patterns are discussed in section 5.4. The sections that follow present the analysis, the correlation of the experimental results and the reductions in the scour lengths due to armoring. The concluding remarks are made in section 5.8.

Chapter 6 presents the analysis of over three hundred and fifty sets of scour data at circular pipe outlets, obtained from thirteen sources including

the present experimental study. The present experiments involve water wall jets on sand and gravel beds and air wall jets on a bed of canola seeds. The literature review of past researches is presented in section 6.2, followed by the sections dealing with the experiments conducted. Sections 6.5 to 6.8 deal with the analysis of the compiled database. The length scales are correlated to the erosion parameter F_o and the effects of other parameters are addressed. The conclusions of the study are formulated in section 6.9.

In the last chapter of this thesis, Chapter 7, a general discussion is presented on the five contributions presented in Chapters 2 to 6. For each of these contributions, a brief summary and suggestions for further study are made. The general discussion ends by addressing the practicability of these results to field situations.

1.3 References

Breusers, H.N.C. and Raudkivi, A.J. (1991), Scouring, International Association of Hydraulic Research - Hydraulic Structures Design Manual, A.A. Balkerma, Rotterdam, pp. 143.

Rajaratnam, N. and Aderibigbe, O. (1993), A method for Reducing Scour below Vertical Gates, Proc. Inst. of Civil Engineers, Water, Maritime and Energy, Vol. 101, pp. 73 - 83.

CHAPTER 2

Erosion of Sand Beds by Oblique Plane Water Jets†

2.1 Introduction

Erosion of sand beds by water jets is a problem of considerable importance in hydraulic engineering. Starting with the pioneering investigation of Rouse (1939), a number of studies have been performed on the erosion of sand beds by circular and plane jets, in the impinging as well as in the wall jet modes. Rajaratnam (1981), Whitaker and Schleiss (1984) and Mason and Arumugam (1985) refer to most of the studies on erosion by plane water jets. Erosion of sand beds by oblique plane water jets occurs downstream of drop structures and flip-bucket and high level outlet spillways. Many formulas have been proposed for calculating the maximum scour depth under these jets. A list and a good review of these formulas can be found in Whitaker and Schleiss (1984) and Mason and Arumugam (1985). Most of the formulas generally take the form of equation (2-1).

$$d_s = K \frac{q^v H^y h_d^w}{d_c^z} \qquad (2\text{-}1)$$

where d_s is the scour depth measured from the downstream water level, H is the difference between the upstream and downstream water levels, h_d is the tail water depth, d_c is the characteristic particle size of the bed material which is usually taken as the median size of the bed material D (50% finer by weight than this size). K is a constant and v, y, w and z are exponents. On the average, v and y have been experimentally determined to be about 0.6 and 0.3 respectively. The value for z varies between 0 and 0.5, w is usually taken as zero and K generally ranges between 0.2 and 3.0. The reason for the wide variation in the value of K might be attributed to the differences in the model

† The main content of this chapter has been published in the Proceedings of the Institution of Civil Engineers (London), Water, Maritime and Energy Journal, Vol. 112, 1995, pp. 31 - 38.

set-up or prototype situation. Mason and Arumugam (1985) assessed the accuracy of most of these empirical formulas and also proposed one based on model and prototype data. Table 2-1 has been reproduced mainly from Mason and Arumugam (1985). It shows some of the previously proposed formulas. The mean bed particle size is represented by d_m and d_{90} (or d_i) represents the bed material diameter, 90% (or i %) of which is finer by weight.

Table 2-1: Coefficients proposed for equation (2-1)

	Author	Year	K	v	y	z	w	d_c
1	Schoklitsch	1935	0.521	0.57	0.2	0.32	0	d_{90}
2	Veronese	1937	0.202	0.54	0.225	0.42	0	d_m
3	Veronese	1937	1.9	0.54	0.225	0	0	-
4	Jaeger	1939	0.6	0.5	0.25	0.333	0.333	-
5	Eggenburger	1944	1.44	0.6	0.5	0.4	0	d_{90}
6	Hartung	1959	1.4	0.64	0.36	0.32	0	d_{85}
7	Franke	1960	1.13	0.67	0.5	0.5	0	d_{90}
8	Damle (model data)	1966	0.543	0.5	0.5	0	0	-
9	Damle (prototype data)	1966	0.362	0.5	0.5	0	0	-
10	Damle (both)	1966	0.652	0.5	0.5	0	0	-
11	Chee and Padiyar	1969	2.126	0.67	0.18	0.063	0	d_m
12	Wu	1973	1.18	0.51	0.235	0	0	-
13	Chee and Kung	1974	1.663	0.6	0.2	0.1	0	d_m
14	Martins	1975	1.5	0.6	0.1	0	0	-
15	Taraimovich	1978	0.633	0.67	0.25	0	0	-
16	Machado	1980	1.35	0.5	0.3145	0.0645	0	d_{90}
	Mean of non-zero values		1.08	0.57	0.31	0.28	0.333	

The general approach to this subject has been empirical because a theoretical analysis is difficult and complex. It requires a thorough understanding of jet diffusion in the vicinity of a rapidly changing scour hole geometry, the scouring process, the movement and behavior of scoured materials and the effects of entrained air.

This chapter presents another formula for calculating the characteristics of scour under oblique jets. In an earlier study by Rajaratnam (1981), it was found that for a perpendicularly impinging submerged jet with a thickness of $2b_o$, a velocity of U_o at the nozzle and a vertical impingement distance of h, the maximum depth of erosion in the asymptotic state $\varepsilon_{m\infty}$ occurring under

the jet, in terms of h, was found to be mainly a function of the erosion parameter E_p. This erosion parameter can be interpreted as a measure of the ratio of the force of the plane jet acting on a bed particle directly under the jet and at the original bed level to its resistive force. It is defined as $U_o\sqrt{(2b_o/h)}/\sqrt{(gD\Delta\rho/\rho)}$ where g is the acceleration due to gravity and $\Delta\rho$ being the difference between the mass density of the sand and the density of the fluid ρ. It was also found that the maximum dynamic scour depth $\varepsilon'_{m\infty}$ (with the jet on and measured from the original bed level) in terms of maximum static scour $\varepsilon_{m\infty}$ (with the jet off) is a function of E_p and it is as large as 2 for E_p equal to about 6.

Other non-dimensional characteristic lengths of the eroded bed like Δ_∞/h, $x_{c\infty}/h$, wherein Δ_∞ is the height of the ridge that is formed at the outer edge of the scour hole and $x_{c\infty}$ is the distance of this ridge from the axis of the impinging jet, are functions of mainly the parameter E_p. Further, the profile of the eroded bed, when expressed in a non-dimensional form, was found to be similar with the non-dimensional length scales of the profile being functions of E_p. The present study extends the results of this previous study to obliquely impinging submerged water jets.

2.2 Experiments and Experimental Results

The experimental arrangement used is the same as that described in Rajaratnam (1981). The experiments were performed in a rectangular flume 0.15 m wide, 0.305 m deep and 1.83 m long with plexiglas sides, placed symmetrically in a larger flume, 0.305 m wide, 0.66 m deep and 5.5 m long. The water depth in the larger flume was maintained at about 0.5m. The depth of sand in the test flume was about 0.15m. Two sands of median size D of 1.2 and 2.38 mm were used. The jet was produced from a well designed nozzle of thickness $2b_o$ equal to 2.54 mm, located at the end of a plenum. Water was supplied to the nozzle from a submersible pump placed in the laboratory sump. The velocity U_o of the jet was measured by means of a total head tube of 1.07 mm diameter placed in the potential core of the jet. This nozzle could be positioned at any desired height above the original level of the sand bed and at any desired angle with the horizontal plane (see Figure 2-1).

Some preliminary experiments were performed and it was found that to study asymptotic erosion profiles within the range of experimental conditions expected, each experiment should be run for a period of at least 24 hours. Hence, in the present study every experiment was run for at least 24 hours and some were run for even much longer periods. Scour measurements were taken only in the asymptotic state.

Experiments were performed with the angle of the jet θ, equal to 10, 30, 45 and 60 degrees. In total, 33 experiments were performed and for every experiment, the asymptotic profile of the eroded bed was measured from which the significant characteristic lengths like $\varepsilon_{m\infty}$, the height of the ridge Δ_∞, its distance from the nozzle $x_{c\infty}$, the length of scour hole $(x_1 + x_2)_\infty$ and Δx_∞ the distance between the point of impingement and the location of maximum erosion were measured. In addition, $\varepsilon'_{m\infty}$ the maximum depth of dynamic scour was also measured approximately and these results are given in Table 2-2.

2.3 Analysis of Experimental Results

2.3.1 Maximum Scour Depth

Considering first, the maximum depth of (static) erosion $\varepsilon_{m\infty}$. It can be shown based on dimensional arguments and the analysis presented in Rajaratnam (1981), that equation (2-2) is applicable for large values of jet Reynolds number R_e, equal to $2b_oU_o/\upsilon$ (υ is the kinematic viscosity of the fluid) and large values of h/D.

$$\frac{\varepsilon_{m\infty}}{h_t} = f\left(E_p = \frac{U_o}{\sqrt{g\frac{\Delta\rho}{\rho}D}}\sqrt{\frac{2b_o}{h_t}}, \theta \right) \qquad (2\text{-}2)$$

where h_t, equal to $h/\sin\theta$, is the impingement distance measured in the jet direction. The experimental results for maximum scour depth are presented in Figure 2-2. It appears possible to draw a mean line through all the experimental results for the oblique jets which deviates somewhat from the corresponding curve for $\theta = 90°$ for E_p in the range of 2 to 6. The equation for the mean line is

$$\frac{\varepsilon_{m\infty}}{h_t} = 0.43\left(E_p - 0.5\right) \qquad (2\text{-}3)$$

This equation is different in form from equation (2-1). It expresses the actual scour depth whereas equation (2-1) expresses the depth of scour as a summation of tail water depth and actual scour depth. The use of $\varepsilon_{m\infty}$ instead of d_s surely gives a better appreciation of the magnitude of scour. Equation (2-3) can however be re-written in a form similar to that of equation (2-1) by defining $U_o = C_r\sqrt{(2gH)}$, $\varepsilon_{m\infty} = d_s - h$, $q = 2b_oU_o$, $\Delta\rho/\rho = 1.65$. C_r is a correction factor accounting for head loss due to friction and aeration. The resulting equation after the substitutions is,

$$d_s = 0.4\sqrt{\frac{C_r}{\sin\theta}}\frac{q^{0.5}H^{0.25}h^{0.5}}{g^{0.25}D^{0.5}} - 0.22\frac{h}{\sin\theta} + h \qquad (2\text{-}4a)$$

or

$$\varepsilon_{m\infty} = 0.4\sqrt{\frac{C_r}{\sin\theta}}\frac{q^{0.5}H^{0.25}h^{0.5}}{g^{0.25}D^{0.5}} - 0.22\frac{h}{\sin\theta} \qquad (2\text{-}4b)$$

The value of C_r is less than 1.0 and can be roughly estimated using Figure 15 in Peterka (1964). An estimate for θ can be obtained using equation (5) in Whitaker and Schleiss (1984). Approximate values can be obtained from equations (2-4a) and (2-4b) if constant values for C_r and θ are assumed. If these are assumed to be 1.0 and 45° respectively, equation (2-4a) can be approximated as,

$$d_s = 0.47\frac{q^{0.5}H^{0.25}h^{0.5}}{g^{0.25}D^{0.5}} + 0.7h \qquad (2\text{-}5)$$

Figure 2-3 shows the results for $\varepsilon'_{m\infty}$ the maximum depth of dynamic scour. It is interesting to note that for E_p less than about 3.5, the results for the oblique impingement lie on the line for normal impingement (except for the case with θ equal to 10°) whereas for E_p greater than 3.5, the obliquely impinging jets produce smaller values of $\varepsilon'_{m\infty}/h_t$. The ratio of $\varepsilon'_{m\infty}/\varepsilon_{m\infty}$

was found to depend on E_p and could be as high as 1.25 for E_p equal to about 6.

2.3.2 Other Length Scales

The characteristic lengths for the ridge that forms at the downstream end of the scour hole are shown in Figures 2-4 and 2-5. In Figure 2-4, values of Δ_∞/h_t are plotted against E_p along with the curve for the normal impingement case. A mean line could be drawn as an approximation through the results for the obliquely impinging jets and this line is located above the corresponding line for the normally impinging jet. The mean line for the obliquely impinging jets can be described by equation (2-6).

$$\frac{\Delta_\infty}{h_t} = 0.38\left(E_p - 0.5\right) \tag{2-6}$$

The results for the horizontal distance of the ridge from the jet (x_c) are shown in Figure 2-5. They indicate somewhat larger values than those for the case of normal impingement. For practical purposes, a mean line could be drawn through these data points and this line is described by equation (2-7).

$$\frac{x_{c\infty}}{h_t} = 1.9\left(E_p - 0.5\right) \tag{2-7}$$

Regarding the length of the scour hole, (see Figure 2-1), it was found that for θ equal to 30° to 60°, $x_1 \approx x_2$ whereas for $\theta = 10°$, x_1 was somewhat larger than x_2. The variation of $(x_1 + x_2)_\infty/h_t$ with the parameter E_p is shown in Figure 2-6 wherein it is seen that the lengths for oblique impingement are somewhat larger than those for normal impingement. The present results are described approximately by equation (2-8).

$$\frac{(x_1 + x_2)_\infty}{h_t} = 1.5\left(E_p - 0.5\right) \tag{2-8}$$

If $x_{m\infty}$ is the distance of the section of maximum scour from the nozzle, the variation of $x_{m\infty}/h_t$ with E_p is shown in Figure 2-7 wherein it can be

noticed that the results for $\theta = 10^\circ$ and 45° are located together, but the results for $\theta = 30^\circ$ and 60° are located separately. If Δx_∞ is the distance between the point of impingement and the location of maximum erosion, the variation of $\Delta x_\infty/h_t$ with E_p is shown in Figure 2-8 wherein it is seen that $\Delta x_\infty/h_t$ increases with E_p and the results for each value of θ are different.

During this study, it was observed that the eroded bed profiles for the different experiments appeared to be similar and the profiles were tested for similarity by plotting the results for a few typical experiments in a non-dimensional form in Figure 2-9 in which $(x_1 + x_2)_\infty$ and $\varepsilon_{m\infty}$ have been used as the respective length scales. The scour holes were found to be fairly similar.

Another interesting aspect that was observed during the experimental work was that for some angles of impingement, a single dominant vortex existed on the forward side of the nozzle which kept some bed material in suspension (see Figure 2-10). If S_∞ is the height of this sediment cloud above the original bed level of the sand, as indicated in Figure 2-11, S_∞/h_t appears to be mainly a function of E_p for $\theta = 45^\circ$ and 60° and is described by equation (2-9).

$$\frac{S_\infty}{h_t} = 1.1\left(E_p - 0.5\right) \qquad (2\text{-}9)$$

2.4 Practical application

The proposed formula for calculating the maximum depth of scour (equation (2-4a)), was used to estimate the maximum depths of scour downstream of Cabora Bassa Dam in Mozambique and Kariba Dam in Zimbabwe. These dams are arch dams with outlet spillways.

The relevant parameters for these dams (obtained from a reviewer and Whitaker and Schleiss (1984)) are given in Table 2-3a and a comparison of predicted depths of scour by various formulas to measured depths. A d_c value of 0.3 m was assumed for the prototype bed material. It can be seen from these values that the proposed formula performs reasonably well compared to other formulas. The equation of Mason and Arumugam (1978),

which is probably the most refereed to, also estimates the scour depths quite well. Table 2-3(b) shows that all the formulae predict greater depths of scour at Cabora Bassa Dam because of its higher values of q, H and h_d, whereas, the measured scour depth is lesser. This poor prediction might be due to the use of the same value of d_c for the two dams. It might also be due to the difference in the erodibility of the downstream bed which should be reflected in the value of K. It will be suggested that a method of choosing values for d_c and K to reflect different site conditions should be considered in further work.

Table 2-3: Scour depth computations for Cabora Bassa and Kariba Dams
Table 2-3(a): Relevant parameters

	Cabora Bassa Dam	Kariba Dam
Built	1974	1962
q (m^2/s)	120	96
H (m)	102.64	91.5
h_d (m)	42.1	16
D (m)	0.3	0.3
θ (°)	42	59
C_r	0.84	0.86

Table 2-3(b): Scour depths

Depth of scour d_s (m)	Cabora Bassa Dam 67 (in 1982)	Kariba Dam 89 (in 1978)
Equation (2-4a)	135.9	62
Equation (2-5)	139.2	70
Mason and Arumugam (1985)*	72.6	54.6
Mason and Arumugam (1985)**	110.4	79.8
Chee and Padiyar (1969)	130.5	110.1
Chee and Kung (1974)	83.7	71.6
Veronese (1937)	71.5	61.7
Martins (1973)	42.1	36.4
Taraimovich (1978)	49.8	41.7
Damle (1966)	72.4	61.1

* Equation obtained from model data.
** Equation obtained from model and prototype data.

2.5 Conclusions

On the basis of on an experimental study of erosion of sand beds by obliquely impinging submerged plane turbulent jets for angles of impingement equal to 10°, 30°, 45° and 60°, the following conclusions can be made. In the asymptotic state, scour hole profiles are approximately similar. The main characteristics of the eroded bed profile like the maximum depth of erosion $\varepsilon_{m\infty}$, the height of the downstream ridge Δ_∞, the length of the scour hole $(x_1 + x_2)_\infty$ in terms of h_t the impingement distance are functions of mainly the parameter E_p. But these functional relationships are somewhat different from those for the case of perpendicular impingement. The equation for the maximum depth of scour was rewritten in a form generally used for plunge pools for easier comparison and the predictions for two prototype cases are encouraging.

2.6 References

Rouse, H. (1939), Criteria for similarity in the transportation of sediment, Bull. 20, University of Iowa, Iowa City, USA, pp. 33 - 49.

Rajaratnam, N. (1981), Erosion by plane turbulent jets, Journal of Hydraulic Research, Vol. 19, No. 4, pp. 339 - 358.

Whitaker, J.G., and Schleiss, A. (1984), Scour related to Energy Dissipators for High Head Structures, Mitteilungen der Versuchsanstalt für Wasserbau, Hydrologie and Glaziologie, Zürich, 73 pp.

Mason, P.J. and Arumugam, K. (1985), Free Jet Scour Below Dams and Flip Buckets, Journal of Hydraulic Engineering, Vol. 111, No. 2, pp. 220 - 235.

Peterka, A.J. (1964), Hydraulic Design of Stilling Basin and Energy Dissipation, United States Department of the Interior, Bureau of Reclamation, Washington, 222 pp.

Written comments from a reviewer

Wu, C.M. (1973), Scour at downstream end of dams in Taiwan, IAHR International Symposium on River Mechanics, Bangkok, pp. A13 - 1 - A13 - 6.

Table 2-2: Experimental Results

#	Expt. name	$2b_o$ (mm)	D (mm)	θ (°)	h_t (mm)	U_o (m/s)	E_p	$\varepsilon_{m\infty}$ (mm)	Δ_∞ (mm)	$(x_1+x_2)_\infty$ (mm)	$x_{c\infty}$ (mm)	$x_{m\infty}$ (mm)	Δx_∞ (mm)	$R = 2b_oU_o/\upsilon$ ($X\ 10^{-3}$)	Duration of Expts. (hr.)
1	A4511	2.54	2.38	45	42	2.53	1.00	48	40	170	230	57	27.3	6.43	26
2	A4512	2.54	2.38	45	41	2.46	0.99	44	46	173	224	70	41	6.25	24.9
3	A4513	2.54	2.38	45	41	1.58	0.63	26	26	103	149	48	19	4.01	23.7
4	A4514	2.54	2.38	45	61	2.77	0.91	55	58	187	294	74	30.9	7.04	24
5	A4515	2.54	2.38	45	58	2.04	0.69	42	39	159	228	82	41	5.18	111.9
6	A4516	2.54	2.38	45	58	1.39	0.47	31	34	111	178	66	25	3.53	24
7	A4517	2.54	2.38	45	57	1.84	0.63	34	36	125	196	72	31.7	4.67	24.5
8	A4521	2.54	1.2	45	41	1.86	1.05	42	44	148	228	68	39	4.72	66.5
9	A4522	2.54	1.2	45	41	2.31	1.30	60	52	173	270	66	37	5.87	24
10	A4523	2.54	1.2	45	41	2.52	1.42	69	57	221	310	88	59	6.40	24
11	A4524	2.54	1.2	45	59	1.62	0.76	60	55	208	298	86	44.3	4.11	24
12	A4525	2.54	1.2	45	58	2.53	1.20	69	65	236	344	105	64	6.43	24.8
13	A4526	2.54	1.2	45	58	1.62	0.77	56	55	194	282	84	43	4.11	66.1
14	A4527	2.54	1.2	45	41	1.42	0.80	44	38	140	206	62	33	3.61	24
15	A6021	2.54	1.2	60	19.6	2.09	1.71	38	32	140	163	33	23.2	5.31	24
16	A6022	2.54	1.2	60	18.4	2.08	1.75	41	34	141	171	32	22.2	5.28	24
17	A6023	2.54	1.2	60	17.3	2.26	1.96	43	40	148	175	27	18.3	5.74	24
18	A6024	2.54	1.2	60	17.3	1.76	1.53	31	26	109	132	23	14.3	4.47	66
19	A6025	2.54	1.2	60	32.3	1.89	1.20	38	31	126	157	33	16.8	4.80	24
20	A6026	2.54	1.2	60	33.5	2.45	1.53	56	43	192	223	44	27.2	6.22	24
21	A6027	2.54	1.2	60	34.6	2.05	1.26	41	36	140	180	41	23.7	5.21	24
22	A6028	2.54	1.2	60	34.6	1.12	0.69	23	23	78	116	36	18.7	2.84	24
23	A3021	2.54	1.2	30	74	1.98	0.83	83	93	321	468	171	106.6	5.03	24
24	A3022	2.54	1.2	30	74	1.43	0.60	54	60	215	355	136	71.6	3.63	24
25	A3023	2.54	1.2	30	74	1.23	0.52	44	51	183	302	118	53.6	3.12	41
26	A3024	2.54	1.2	30	98	2.16	0.79	93	96	370	549	208	122.7	5.49	49.7
27	A3025	2.54	1.2	30	98	1.27	0.46	45	48	183	324	142	56.7	3.23	69.5
28	A3026	2.54	1.2	30	98	1.63	0.60	67	76	264	426	170	84.7	4.14	24
29	A3027	2.54	1.2	30	98	1.43	0.52	56	68	221	382	159	73.7	3.63	24
30	A1021	2.54	1.2	10	248	1.27	0.29	28	48	160	303	160	-83	3.23	24
31	A1022	2.54	1.2	10	248	1.53	0.35	35	64	197	359	179	-64	3.89	24
32	A1023	2.54	1.2	10	248	2.24	0.51	92	114	426	590	241	-2	5.69	24
33	A1024	2.54	1.2	10	248	1.74	0.40	48	78	300	422	199	-44	4.42	25

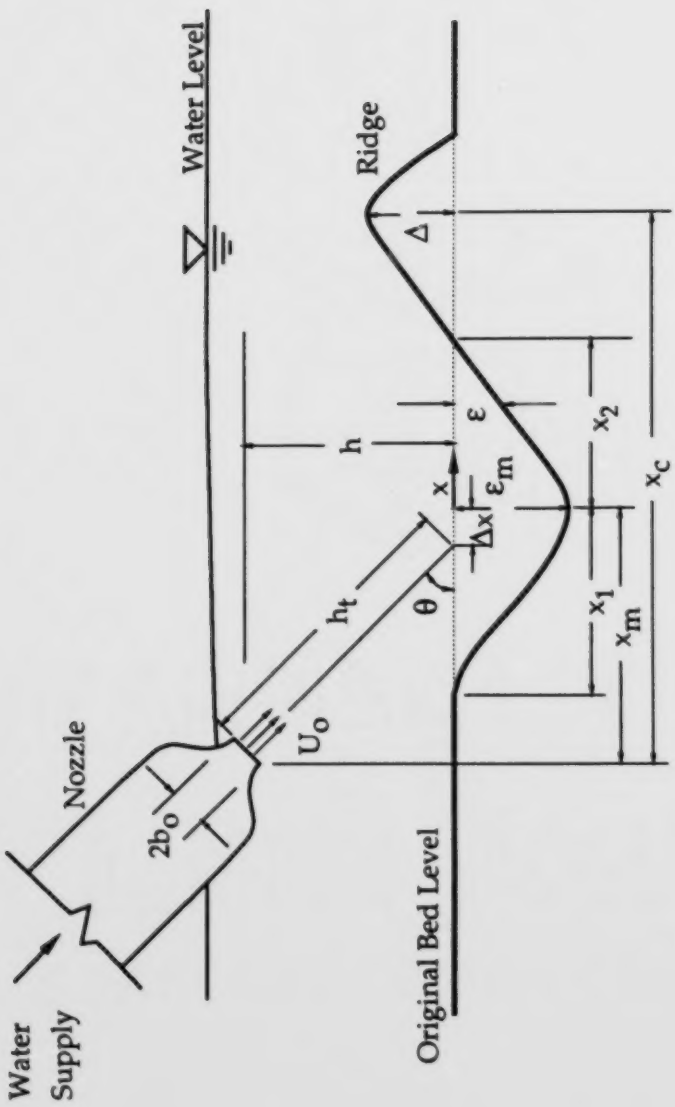

Figure 2-1 Definition Sketch

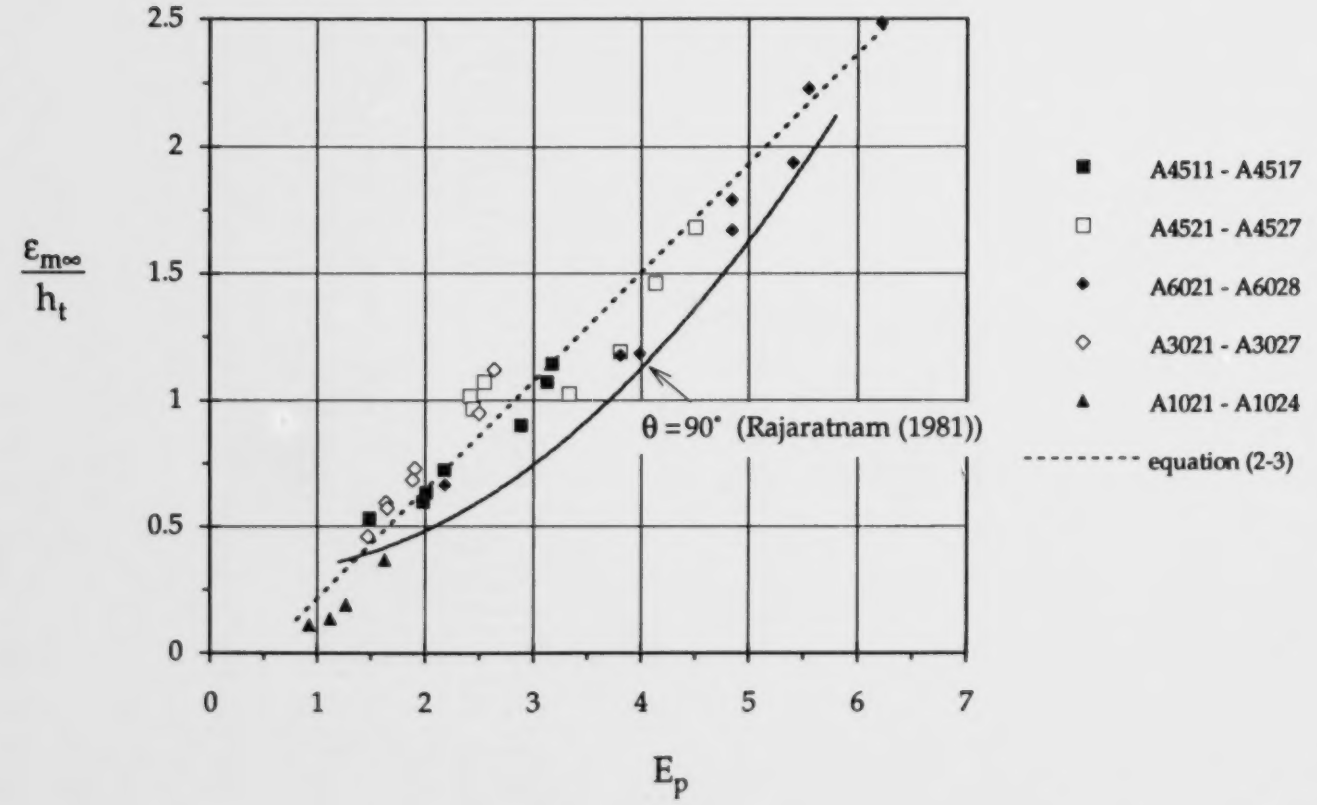

Figure 2 – 2: Variation of maximum static scour depth with E_p

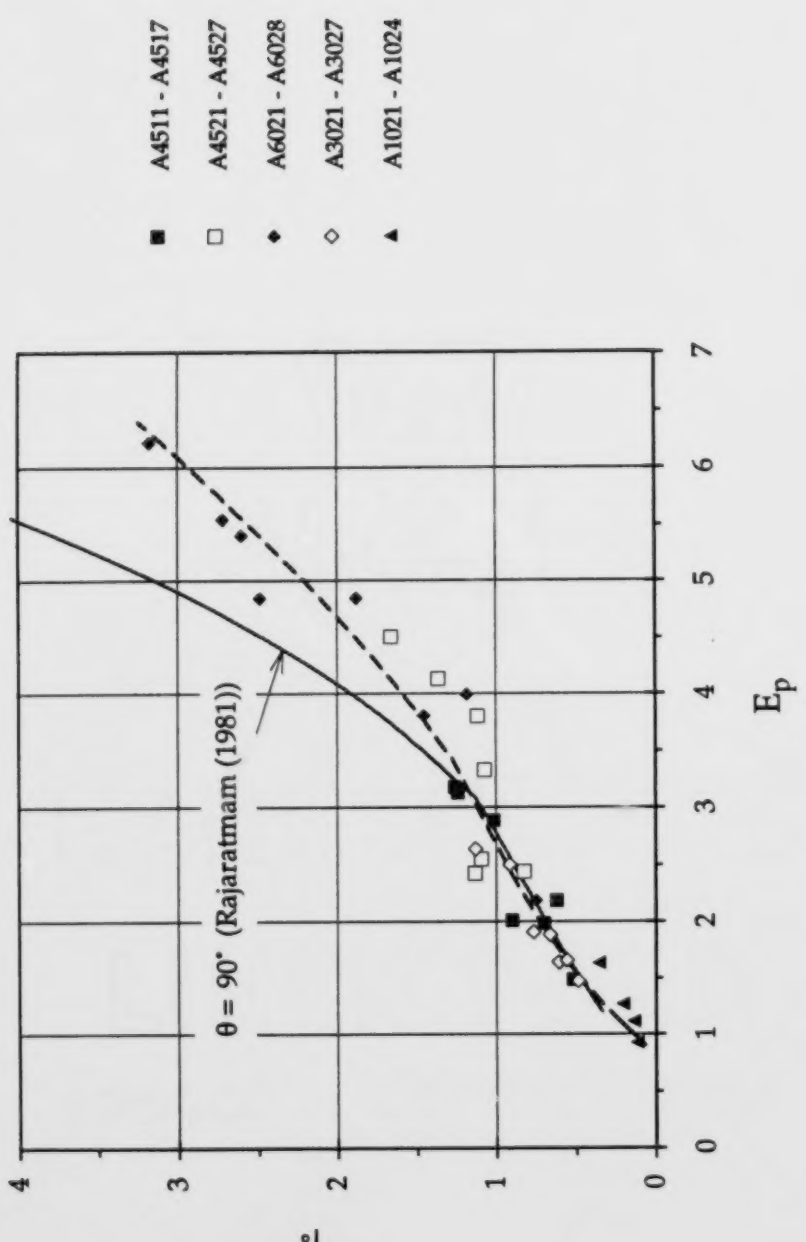

Figure 2 – 3: Variation of maximum dynamic scour depth with E_p

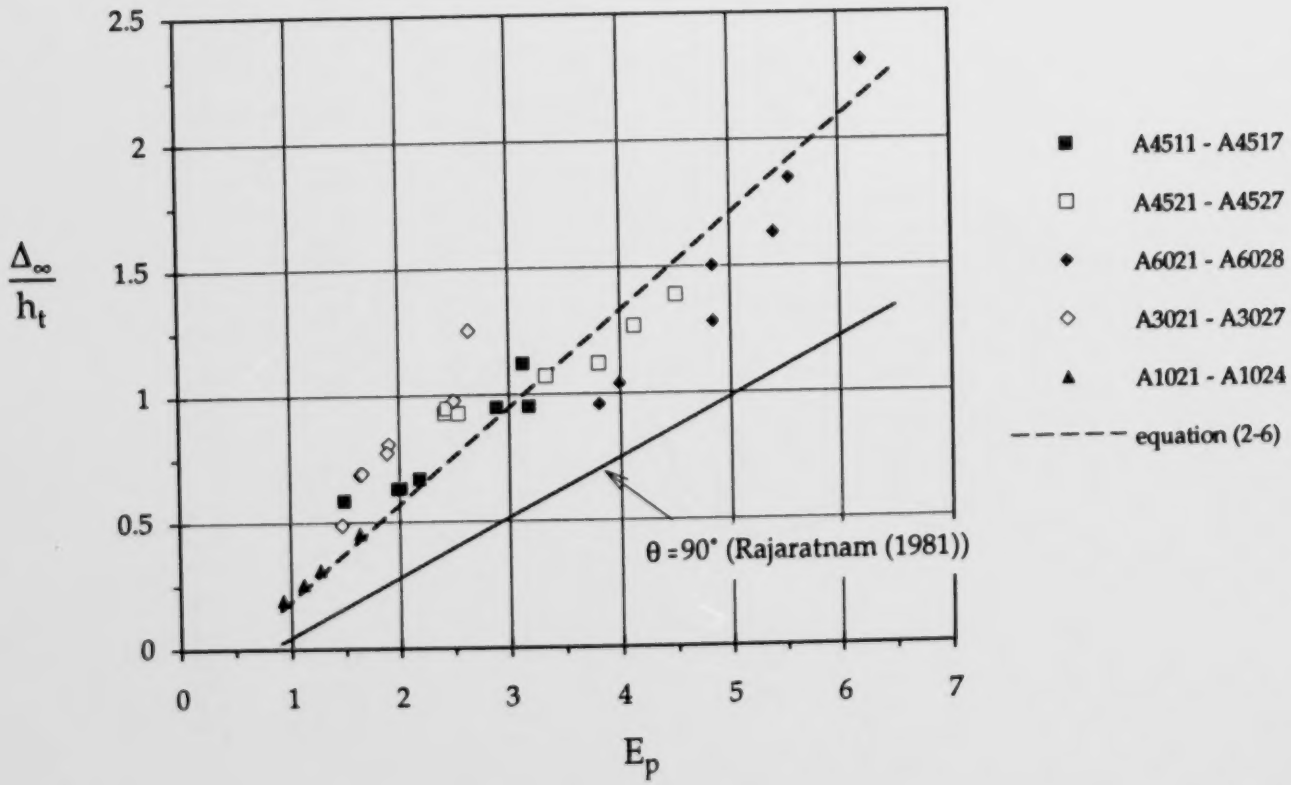

Figure 2 – 4: Variation of ridge (dune) height with E_p

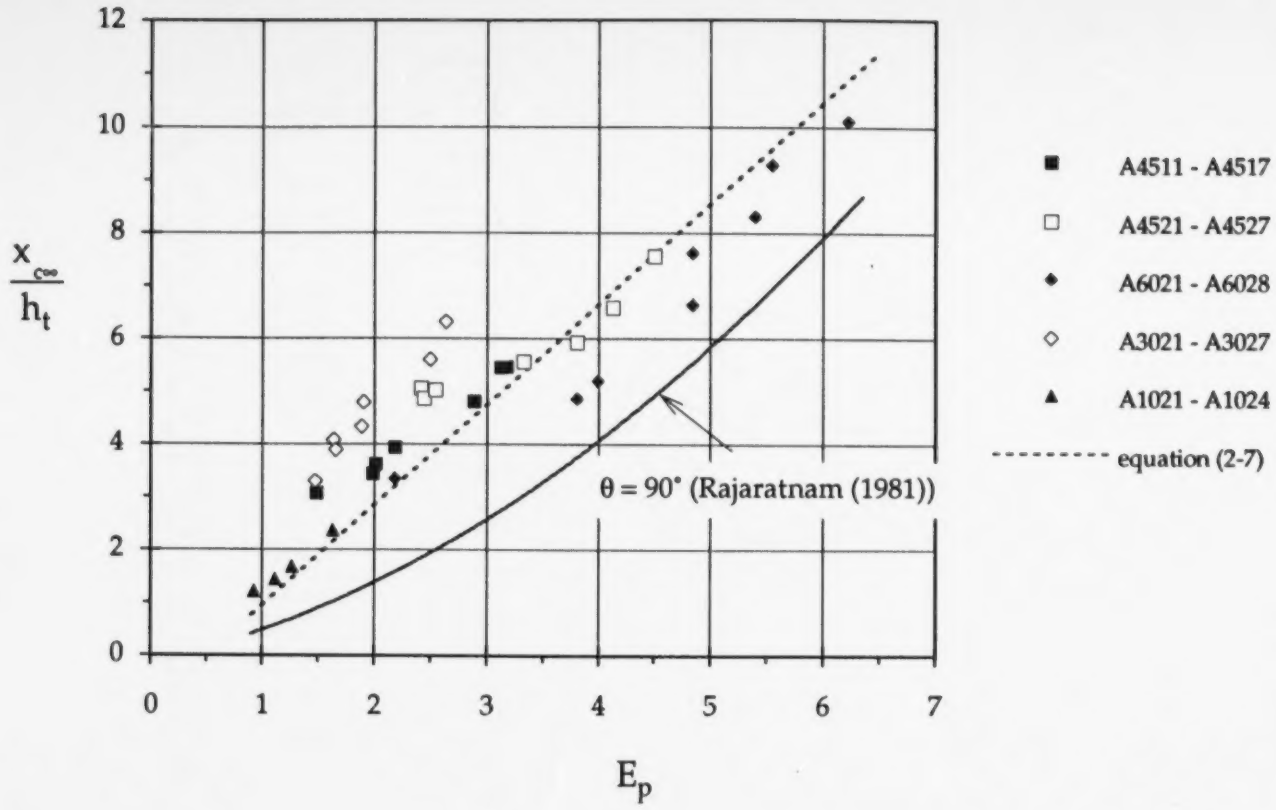

Figure 2 – 5: Variation of distance of ridge (dune) with E_p

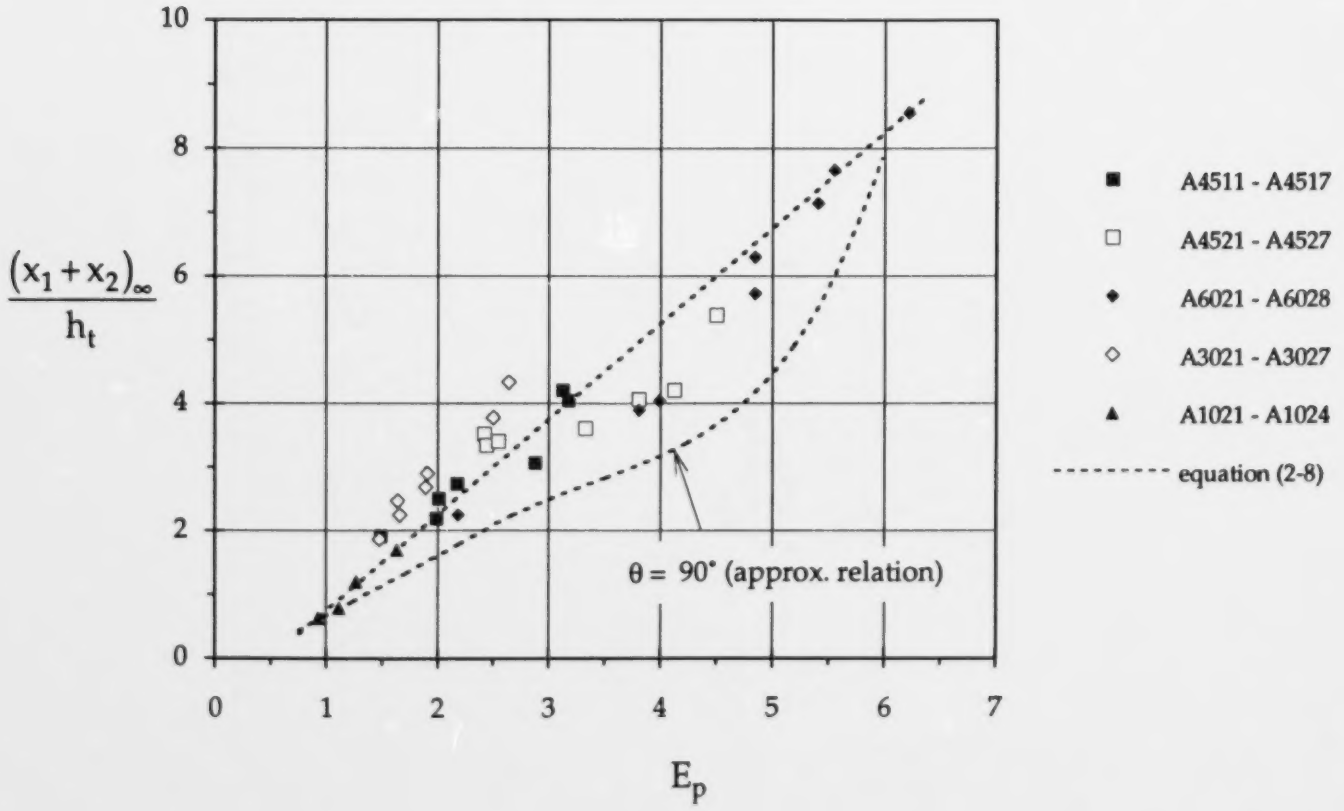

Figure 2 – 6: Variation of scour hole length with E_p

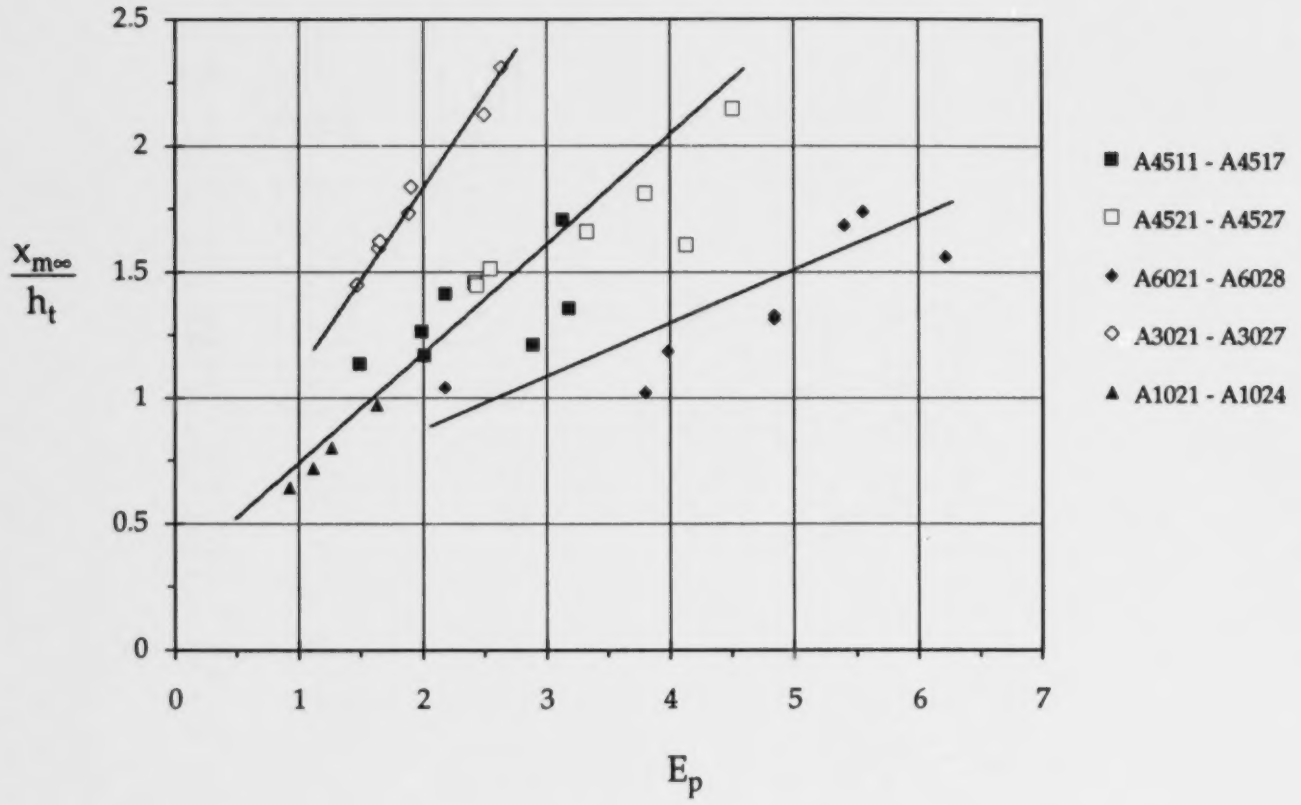

Figure 2-7: Variation of the distance of the maximum static scour depth with E_p

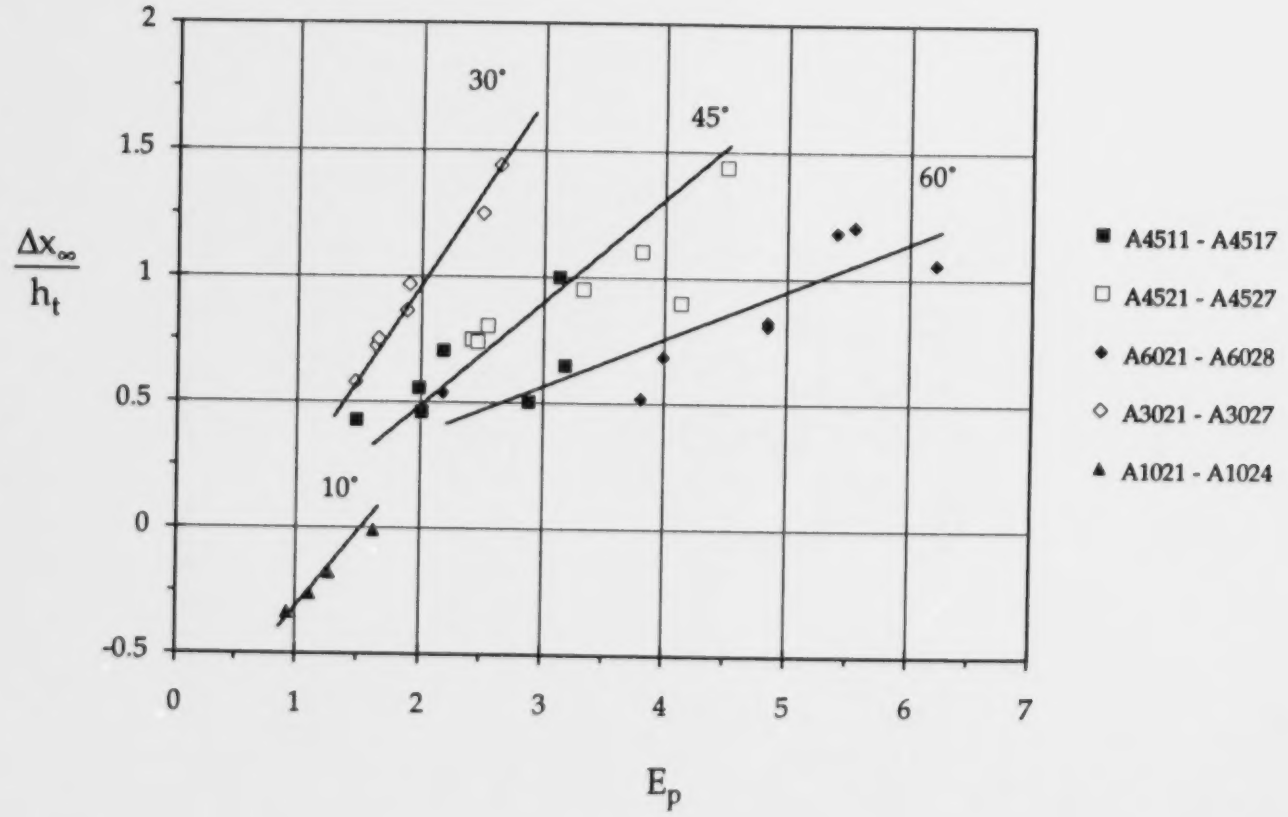

Figure 2 – 8: Variation of the offset distance with E_p

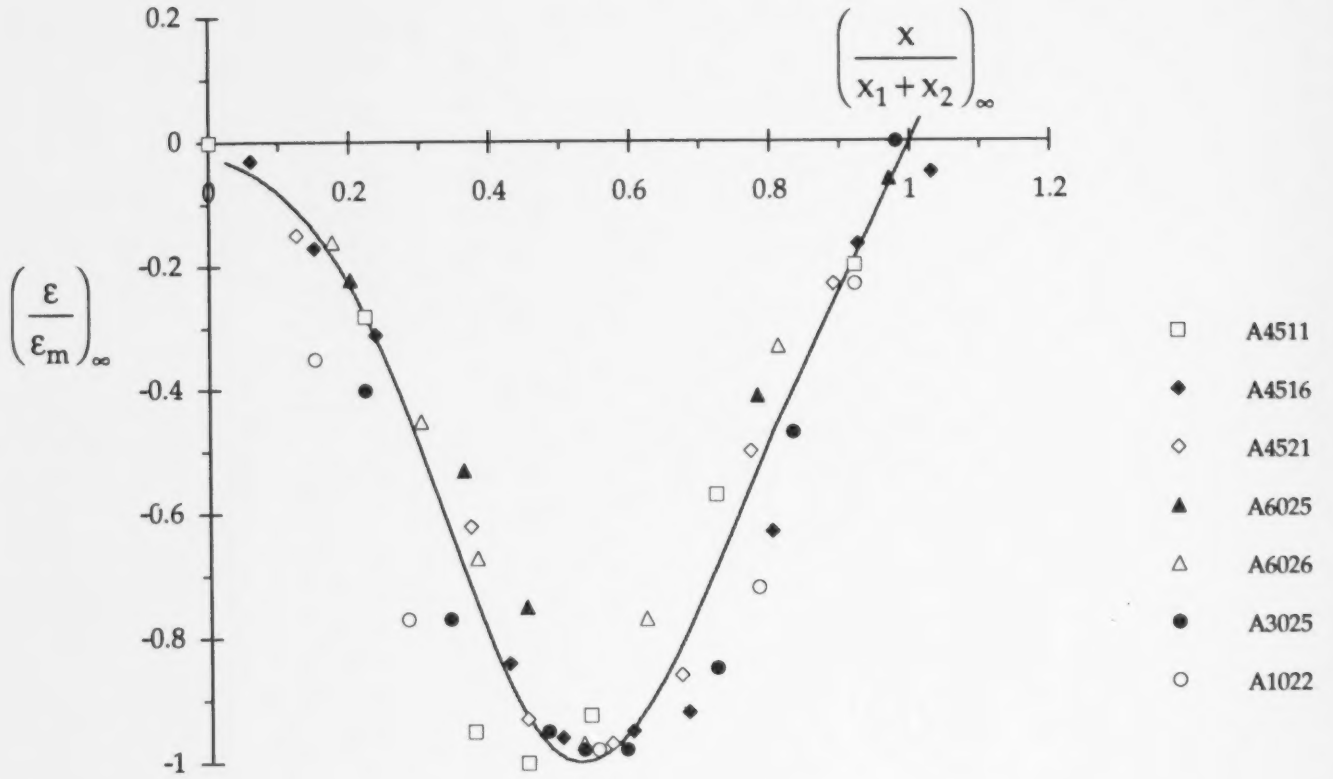

Figure 2 – 9: Similarity of scour hole profile

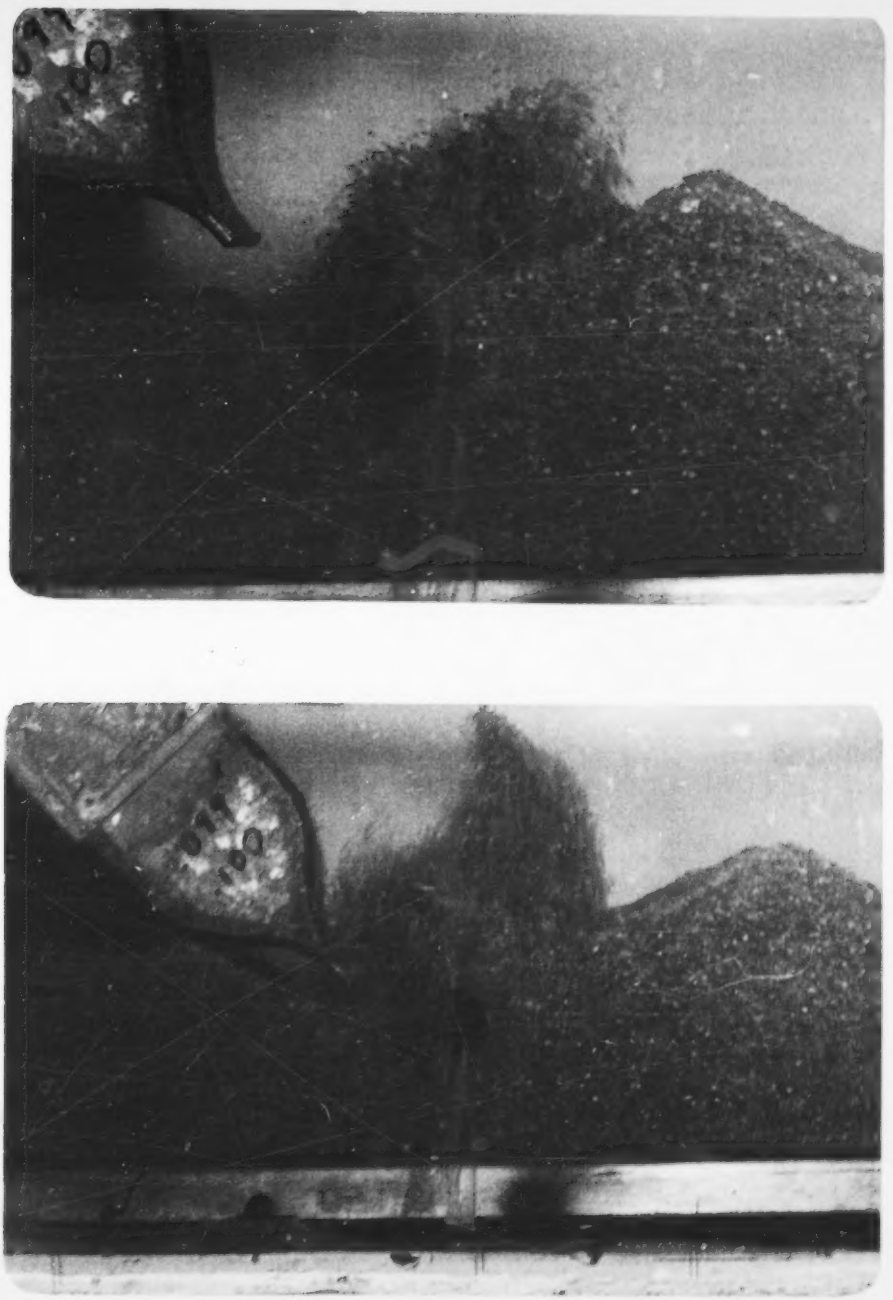

Figure 2 - 10: Single Dominant Vortex with Suspended Sediments

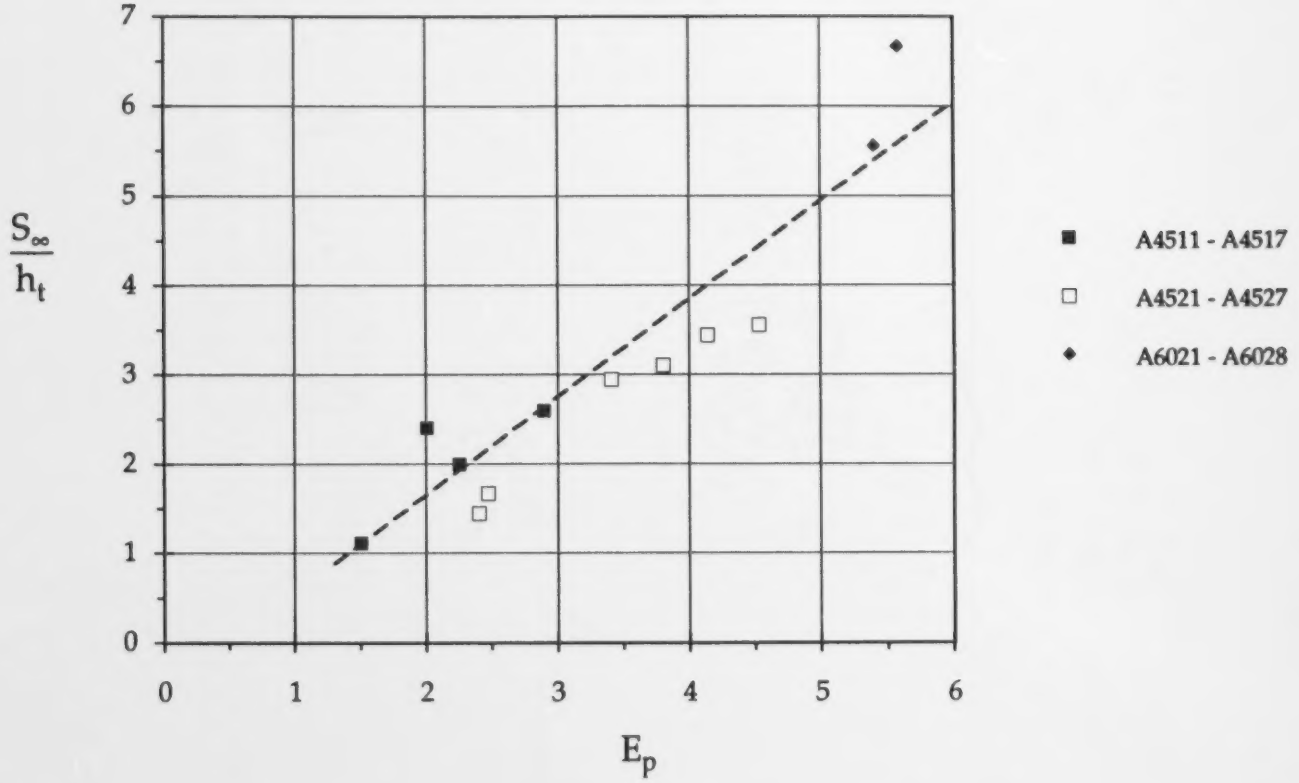

Figure 2–11: Variation of the height of sediment cloud with E_p

CHAPTER 3

Reduction of Scour below Submerged Impinging Jets by Screens †

3.1 Introduction

Erosion of sand and gravel beds by water jets is an area of hydraulic engineering that has received considerable attention in recent years. This is because it is important to predict and control erosion near hydraulic structures. To prevent erosion caused by jets, it is common to build a concrete apron or line the bed with rip rap. These arrangements, when properly designed and constructed, are known to be generally reliable. This study presents an alternative method using screens. In an earlier study involving deeply submerged plane wall jets (Rajaratnam and Aderibigbe (1993)), a reduction in maximum scour depth of about 85% was obtained at a high F_O value of about 14 for a screen having a porosity (screen opening per unit area) of 55% and a 114 mm^2 screen opening area. F_O is the densimetric particle Froude number which can be interpreted as a measure of the ratio of the tractive force of a wall jet on a grain to its resistive force. It is defined as $U_O/\sqrt{(gD\Delta\rho/\rho)}$. This success prompted the idea to investigate such effects in the case of impinging submerged circular and plane jets as might be present in plunge pools below free overfalls and pipe or culvert outlets. In order to simplify the experimental study, the jets were assumed to be vertically impinging and non-aerated. The screen which helps to divert the jet and reduce its impact on the bed was made of a strong plastic plate having circular openings arranged on a grid as shown in Figure 3-1(a). The openings help to prevent any structural damage due to uplift pressures as might be in the case of a concrete apron. Another advantage is the dissipation of some of the energy from the jet by the interaction of the jets issuing from these

---

† The main content of this chapter has been published in the Proceedings of the Institution of Civil Engineers (London), Water, Maritime and Energy Journal, Vol. 112, 1995, pp. 215 - 226.

openings in the eroded space below the screen. In the field, the screen could be made of precast concrete slabs designed to withstand the impact force of the jet and the associated pressure fluctuations. The slabs could be supported on piles in between.

3.2 Impinging Circular Jets

3.2.1 Experiments

The experimental setup for this study is the same as that used by Rajaratnam (1982). An octagonal plastic box having a side length of 0.235 m and a height of 0.6 m was filled with sand/gravel to a depth of about 0.18 m and gently filled with water after placing the screen, in a supported position, on the erodible bed. The impinging jet nozzle was attached to the bottom of a cylinder of 150 mm diameter and variable length, with a suitable constant-head arrangement. It was centrally located in the octagonal plastic box and the vertical distance of the nozzle above the original bed h was varied between 70 and 410 mm. The jet nozzle diameters d were 8, 13 and 19 mm and the exit velocities U_o ranged from 2.65 to 4.67 m/s.

Table 3 -1: Details of Screens

Name of Screen	l_s (mm)	λ	P (Porosity, %)
CS1	5	2	19.6
CS2	10	2	19.6
CS3	15	2	19.6
CS4	10	2.5	12.6
CS5	14.4	1.46	36.9
CS6	7.2	3.06	8.4
PS1	10	2	19.6
PS2	14.4	1.39	40.7
PS3	7	3.06	8.4

Six plastic screens, referred to as CS1, CS2, CS3, CS4, CS5 and CS6 , were used and the details of the screens are given in Table 3-1. At a later stage of the experimental work, thin circular plates with a radius of 50 mm (which is approximately equal to the radial distance where the maximum boundary shear stress occurs for an impinging distance of about 350 mm) were

mounted centrally on the screens CS1 and CS5 and these series of experiments are refereed to as CS1P and CS5P respectively. This was done to further reduce the jet's impact on the sand/gravel beds. Two sizes of sand/gravel having median sizes of 0.88 and 2.42 mm were used. Their particle size geometric standard deviations σ_g were 1.22 and 1.24 respectively (σ_g is equal to $\sqrt{(d_{84}/d_{16})}$). Their size distribution curves are shown in Figure 3-2. Figure 3-1 shows the definition sketch for erosion as well as the pattern of holes for the screens. The jet velocity was measured by means of a pitot tube placed in the potential core of the jet. Each experiment was run until an asymptotic state (when the rate of scour growth is very small) was reached. It was also noticed that within the range of experimental conditions expected for the test runs, the scoured bed would approach this state after about 18 and 10 hours for sand/gravel size 0.88 mm and 2.42 mm respectively. The scoured bed profile was measured using a point gauge after the tank had been carefully drained.

A few preliminary experiments were performed to determine the effectiveness of the screen in reducing the scour depth. In one set of experiments, scour depth reductions in terms of the dynamic scour depth $\varepsilon'm_\infty$ (the scour depth with the jet on) of about 65% and 78% were obtained using CS5 and CS5P respectively, as shown in Figure 3-3. In total, 82 experiments were performed and the details are given in Table 3-2.

3.2.2 Flow Patterns

Some flow observations were made on the behavior of the jet. On reaching the screen, the diffusing jet divides into an impinging jet, heading into the sand/gravel bed and a radial wall jet, traveling away from the center of the screen. The impinging jet erodes the sand/gravel bed and some part of the eroded bed material is carried away by the radial wall jet. Further, the radial wall jet moves the ridge which is generally formed at the periphery of the scour hole, towards the walls of the box. In most cases, the ridge was moved very close to the side walls and as a result, characteristic lengths of the ridges were not taken. The impinging jet forms several small circular jets on passing through the circular openings of the screen. The strength of the small jet decreases with increasing radial distance. It appears that each individual jet digs a small scour hole resulting in a honeycomb pattern in the main scour

hole as shown in Figure 3-4. The flow underneath the screen was cloudy with sand/gravel in suspension and very turbulent and as a result, it was difficult to make detailed observations especially at high velocities. At low velocities, it appears that the stronger small jets which are located closer to the center dig relatively bigger scour holes and transport the eroded sand/gravel from their scour holes into the scour holes of the neighboring weaker jets. A continuation of this process is believed to be responsible for the transport of eroded sand/gravel out of the scour hole, over the screen into the fast flowing radial wall jet on the screen. In the case of impinging plane jets, the flow patterns at high velocities were easier to observe and this is explained in section 3.4.2.

3.2.3 Dimensional Analysis

The characteristic lengths of the scour hole in the asymptotic (or end) state, chosen for analysis, are the static scour depth $\varepsilon_{m\infty}$ and the radius of the scour hole $r_{o\infty}$. Using $l_{c\infty}$ to represent any of the characteristic lengths, it can be shown that:

$$l_{c\infty} = f_1\left(M_o = \rho\frac{\pi}{4}d^2U_o^2, g\Delta\rho, \rho, l_s, \lambda, h, \upsilon, D\right) \qquad (3\text{-}1)$$

where M_o is the momentum flux from the nozzle, l_s is the diameter of the screen opening and λ is a spacing parameter as shown in Figure 3-1(a). Using the method of dimensional analysis, equation (3-1) can be rewritten in terms of six non-dimensional parameters as

$$\frac{l_{c\infty}}{h} = f_2\left(E_c = \frac{U_o}{\sqrt{g\frac{\Delta\rho}{\rho}D}}\frac{d}{h}, \lambda, \frac{l_s}{h}, \frac{l_s}{D}, R_e = \frac{U_o d}{\upsilon}\right) \qquad (3\text{-}2)$$

This equation is valid for the large impingement case ($h/d > 8.3$), as shown by Rajaratnam and Beltaos (1977), and this was the situation for most of the experiments. The erosion parameter E_c can be interpreted as a measure of the ratio of the force of the circular jet acting on a bed particle directly under the jet and at the original bed level to its resistive force. For the value

of the jet Reynolds number R_e, greater than a few thousand, the effect of viscosity on the growth of jets is generally known to be small and thus the Reynolds number can be neglected in equation (3-2). Intuitively, it appears that l_s/D will not be important if it is much greater than 1 which happens to be the case here. This idea was later found to be valid from the multiple regression analysis performed, which consistently showed that the exponent for l_s/D was very small. Equation (3-2) can then be simplified as

$$\frac{l_{c\infty}}{h} = f_3\left(E_c, \lambda, \frac{l_s}{h}\right) \tag{3-3}$$

For this study, the ranges of E_C, λ and l_s /h are 0.4 to 5.7, 1.46 to 3.06 and 0.01 to 0.13 respectively. The variation of the relative scour depth $\varepsilon_{m\infty}/h$ with the erosion parameter E_C has been plotted in Figure 3-5 for all the screens and compared to the no-screen case. The effect of each screen on the relative scour depth reduction in terms of the dynamic scour depth is obvious. Some of the data are surprisingly above the curve for the static scour. This was more noticeable in the experiments involving impinging plane jets and an explanation is given in section 3.4.2.

3.2.4 Regression Analysis

Using multiple regression analysis, equations were developed for the characteristic lengths of the scour hole. Equation (3-4) is the relationship developed for the maximum depth of erosion data with a correlation coefficient R^2 of 0.97 and may be simplified as equation (3-5). Figure 3-6 shows the plot obtained using equation (3-5) for all the screens.

$$\frac{\varepsilon_{m\infty}}{h} = 0.66 E_c^{0.93}\left(\frac{1}{\lambda}\right)^{0.88}\left(\frac{l_s}{h}\right)^{0.33} \tag{3-4}$$

$$\frac{\varepsilon_{m\infty}}{h} \cong 0.69\frac{E_c}{\lambda}\left(\frac{l_s}{h}\right)^{\frac{1}{3}} \tag{3-5}$$

The result of the analysis for the scour hole radius $r_{O\infty}$, is given by equation (3-6) with a correlation coefficient of 0.96. Figure 3-7 shows the results obtained from this equation.

$$\frac{r_{o\infty}}{h} = 1.1E_c^{0.78}\left(\frac{1}{\lambda}\right)^{0.11}\left(\frac{l_s}{h}\right)^{0.27} \qquad (3\text{-}6)$$

3.2.5 Effect of Screen

To quantify the effects of the protective screens on the characteristic lengths of the scour hole, the reductions or increments were expressed as ratios and are defined by equation (3-7).

$$\eta_1 = \left[1 - \frac{\left(\varepsilon'_{m\infty}/h\right)_{(screen)}}{\left(\varepsilon'_{m\infty}/h\right)_{(no\ \ screen)}}\right]100\% \qquad (3\text{-}7)$$

$$\eta_2 = \left[1 - \frac{\left(r_{o\infty}/h\right)_{(screen)}}{\left(r_{o\infty}/h\right)_{(no\ \ screen)}}\right]100\% \qquad (3\text{-}8)$$

Approximate equations for E_C less than 5 were obtained for the denominators in equations (3-7) and (3-8) using data from an on-going study, Rajaratnam (1982) and Westrich and Kobus (1973). To evaluate the numerator for η_1, the static scour depths were used since they were generally found to be approximately equal to the dynamic scour depths. Equations (3-7) and (3-8) can then be respectively expressed by the following equations.

$$\eta_1 = \left[1 - \frac{0.66E_c^{0.93}\left(\frac{1}{\lambda}\right)^{0.88}\left(\frac{l_s}{h}\right)^{0.33}}{0.02 + 0.38E_c}\right]100\% \qquad (3\text{-}9)$$

$$\eta_2 = \left[1 - \frac{1.1E_c^{0.78}\left(\frac{1}{\lambda}\right)^{0.11}\left(\frac{l_s}{h}\right)^{0.27}}{0.15 + 0.21E_c}\right]100\% \qquad (3\text{-}10)$$

From Table 2-2, it can be seen that the ratios from the above equations vary over a wide range. For η_1, the range is from 47 to 84% and η_2 varies from -75 to 16%. For the first ratio, a scour depth reduction of about 98% was obtained from one of the experiments (ICJ 79) using screen CS1P. The range for the second ratio indicates that the scour hole radius $r_{o\infty}$ was both reduced and enlarged depending on the experimental conditions. The variations of η_1 and η_2 with E_c for all the screens for h equal to (an arbitrary value of) 300 mm in equations (3-9) and (3-10) are shown in Figures 3-8 and 3-9 respectively.

In Figure 3-8, it can be seen that the values of η_1 for the screens are approximately independent of E_c. The average values range from about 56% for CS5 to about 82% for CS6. Equation (3-9) can be simplified to express approximate values of η_1 by using E_c equal to 2.5. The resulting equation is

$$\eta_1 \cong \left[1 - \frac{1.64}{\lambda} \left(\frac{l_s}{h}\right)^{\frac{1}{3}}\right] 100\% \qquad (3\text{-}11)$$

The relationships for CS4 and CS1 are about the same. This behavior can be explained by equation (3-5) which requires different screens to have the same value of $l_s^{0.33}/\lambda$ in order to have the same value of $\varepsilon_{m\infty}/h$. This value is same for CS4 and CS1 and it is 0.86. In Figure 3-9, η_2 is weakly dependent on E_c when E_c is greater than about 1.5 and in this range, an approximate equation can be obtained for η_2 by substituting E_c equal to 2.5. The resulting expression is equation (3-12). The increment in scour hole radius can be seen to be as high as about 40%. This can be attributed to the erosive action of the radial wall jet on the screen.

$$\eta_2 \cong \left[1 - 3.34 \left(\frac{l_s}{h\sqrt[3]{\lambda}}\right)^{\frac{1}{3}}\right] 100\% \qquad (3\text{-}12)$$

3.3 Impinging Plane Jets

3.3.1 Experiments

These experiments were performed in a rectangular flume 0.15 m wide, 0.52 m deep and 1.83 m long, placed inside a larger flume 0.32 m wide, 0.6 m

deep and 4.8 m long. The depth of sand/gravel in the test flume was about 0.2 m. Two almost uniform sands/gravels of median sizes 2.42 and 1.52 mm were used and their particle size geometric standard deviations were 1.24 and 1.27. The size distribution curves are shown in Figure 3-2. The jet was produced from two well designed nozzles of thickness $2b_o$ equal to 5 and 13.7 mm. Three screens referred to as PS1, PS2 and PS3 were used and their details are given in Table 3-1. Water was supplied to the nozzle from a submersible pump placed in the reservoir supplying water to the larger flume. The jet velocity U_o was measured by means of a pitot tube placed in the potential core of the jet. The nozzle could be placed at any desirable height not greater than 0.35 m above the original bed level. Eroded bed profiles were photographed only at the asymptotic state. The ridges formed by the eroded sand/gravel were generally poorly formed and as a result were not measured.

In one set of preliminary experiments using screen PS3, a scour depth reduction (in terms of dynamic scour depth) of about 30% was obtained. The maximum static scour depth with screen installed was found to be more compared to the case without screen but less than the dynamic scour depth without screen as shown in Figure 3-9 and also in Figure 3-11. This was earlier experienced as was seen in Figure 3-4. It appears that the flow pattern is responsible for this and an explanation is given in the next paragraph. Each experiment was run for at least 11 and 18 hours for sand/gravel sizes S2 and S3 respectively. In total, 38 test experiments were performed and the details are given in Table 3-3.

3.3.2 Flow Patterns

At low velocities, the flow pattern is similar to that observed in the case of impinging circular jets. At high velocities, it is as shown in Figure 3-11. Part of the impinging jet splits into two wall jets in opposite directions on reaching the screen, assisting in eroding the bed material immediately below the screen and thus widening the scour hole. The remaining part flows through the screen openings. It was found that the flow from the central screen openings is mainly downwards and is diverted outwards on reaching the bed, carrying sand/gravel particles along with it. Part of this diverted flow on reaching a higher elevation below the screen rejoins the central downward flow to form

two vortices. The remainder of the diverted flow forms oblique jets carrying sand/gravel particles out of the scour hole. The eroded sand/gravel particles are then moved downstream by the wall jets on the screen forming the ridges. It appears that in some cases, because of the wider scour width, these oblique jets are able to transport more bed material out of the scour hole resulting in scour depths deeper than static scour depths (without screens). Also, for the case without screen, the ratio of dynamic scour depth to static scour depth could be as high as 2 at E_p equal to 6 (Figure 3-10 and Rajaratnam (1981)). This implies that a lot of bed material is not transported out of the scour hole but deposited in it when the jet is shut off. The strength of the vortices appear to increase with the erosion parameter E_p. Sometimes, one vortex dominated over the other and could be on either side of the impinging jet and could also alternate its position.

3.3.3 Dimensional Analysis and Effect of Screen

Following the earlier approach, equation (3-3) has been modified as

$$\frac{l_{c\infty}}{h} = f_4\left(E_p = \frac{U_o}{\sqrt{g\frac{\Delta\rho}{\rho}D}}\sqrt{\frac{2b_o}{h}}, \lambda, \frac{l_s}{h} \right) \qquad (3\text{-}13)$$

In this case, the ranges for E_p, λ and l_s/h are respectively 1.4 to 5.9, 1.39 to 3.06 and 0.02 to 0.15. A comparison of the variation of the relative scour depth $\varepsilon_{m\infty}/h$ with the erosion parameter E_p for all the screens to that without screen is shown in Figure 3-12. The scour depth reduction in terms of dynamic scour depth is not as large as in the earlier case. The average reduction is about 45%. This experimental study is not as extensive as in the earlier case and as a result, robust regression equations could not be obtained for the scour depth $\varepsilon_{m\infty}$ and the scour hole length $x_{o\infty}$. It is however clear that the screen does help to reduce the dynamic scour depth.

3.4 Conclusions

It has been found that the presence of protective screens on sand and gravel beds being subjected to impinging circular and plane jets reduces the depths of scour depending on the screen design. In some cases, the scour

hole radii were found to be enlarged. In the case of impinging circular jets, expressions involving the erosion parameter E_C, the diameter of screen opening l_s, and the ratio of the side length of the square grid used for the screen design to the diameter of the screen opening λ have been developed for the non-dimensional characteristic lengths of the scour hole in the asymptotic state and also for the reduction or increment ratios for these lengths. The dynamic scour depth reduction in these experiments ranged from 47 to 84% and the reduction or increment in scour hole radius ranged between a reduction of 16% and an increment of 75%. Simple approximate equations were also developed for quantifying the reductions in the dynamic scour depth and reductions or increments in scour hole radius. In the case of impinging plane jets, the study was not as extensive. It was however noticed that the screens were also effective in reducing the dynamic scour depth. The average scour depth reduction was about 45%.

3.5 References

Rajaratnam, N. (1981), Erosion by Plane Turbulent Jets, Journal of Hydraulic Research, Vol. 19, No. 4, pp. 339 - 358.

Rajaratnam, N. (1982), Erosion by Submerged Circular Jets, Journal of Hydraulic Engineering, ASCE, Vol. 108, pp. 262-267.

Rajaratnam, N. and Aderibigbe, O. (1993), A method for Reducing Scour below Vertical Gates, Proc. Inst. of Civil Engineers, London. Vol. 101, pp. 73-83.

Rajaratnam, N. and Beltaos, S. (1977), Erosion by Impinging Circular Turbulent Jets, Journal of Hydraulic Division, Vol. 103, No. HY10, pp. 1191 - 1205.

Westrich, B. and Kobus, H. (1973), Erosion of a Uniform Sand Bed by Continuous and Pulsating Jets, Proceedings, IAHR, Istanbul, Turkey, Vol. 1, pp. A13 -1-8.

Table 3-2: Impinging Circular Jets - Experimental Results

Expt. #	Code	Time (hrs)	Screen l_s (mm)	λ	d (mm)	D (mm)	$\varepsilon_{m\infty}$ (mm)	$r_{o\infty}$ (mm)	U_o (m/s)	h (mm)	$\varepsilon_{m\infty}/h$	$r_{o\infty}/h$	h/d	l_s/h	E_c	η_1 (%)	η_2 (%)
1	ICJ7	12	5	2	19	2.42	43.75	102.5	3.06	188	0.23	0.55	9.89	0.027	1.56	72.5	-13.8
2	ICJ8	11	5	2	19	2.42	41.5	140	3.53	337	0.12	0.42	17.74	0.015	1.01	76.9	8.8
3	ICJ9	13	5	2	8	2.42	14	78.75	4.12	255	0.05	0.31	31.88	0.020	0.65	74.7	11.7
4	ICJ10	12	5	2	8	2.42	20	80	3.73	101	0.20	0.79	12.63	0.050	1.49	66.4	-33.9
5	ICJ17	13	5	2	12.7	2.42	30.5	105	4.47	409	0.07	0.26	32.20	0.012	0.70	78.3	20.7
6	ICJ18	15	5	2	12.7	2.42	36	100	4.01	201	0.18	0.50	15.83	0.025	1.28	72.9	-9.2
7	ICJ19	18	5	2	8	0.88	27	87.5	3.99	205	0.13	0.43	25.63	0.024	1.31	73.1	-8.9
8	ICJ20	26	5	2	8	0.88	23.5	112.5	4.47	407	0.06	0.28	50.88	0.012	0.74	78.2	19.5
9	ICJ25	19	5	2	19	0.88	59.75	185	3.59	364	0.16	0.51	19.16	0.014	1.57	77.7	4.8
10	ICJ26*	42	5	2	19	0.88	69.25	170	2.66	75	0.92	2.27	3.95	0.067	5.65	65.4	-42.3
11	ICJ31	26	5	2	12.7	0.88	39	117.5	3.52	338	0.12	0.35	26.61	0.015	1.11	77.0	7.2
12	ICJ32*	22	5	2	12.7	0.88	44.5	137.5	2.65	70	0.64	1.96	5.51	0.071	4.02	63.9	-49.4
13	ICJ1	11	10	2	12.7	2.42	26.5	105	3.64	360	0.07	0.29	28.35	0.028	0.65	71.8	3.3
14	ICJ2	12	10	2	12.7	2.42	26	110	3.11	196	0.13	0.56	15.43	0.051	1.02	65.7	-27.6
15	ICJ3	12	10	2	19	2.42	34	130	3.11	196	0.17	0.66	10.32	0.051	1.52	66.1	-35.3
16	ICJ4	12	10	2	19	2.42	34	150	3.52	333	0.10	0.45	17.53	0.030	1.01	71.1	-10.5
17	ICJ11	14	10	2	8	2.42	23	85	3.73	101	0.23	0.84	12.63	0.099	1.49	58.1	-61.5
18	ICJ12	16	10	2	8	2.42	18.5	80	4.46	405	0.05	0.20	50.63	0.025	0.45	73.1	17.9
19	ICJ21	28	10	2	8	0.88	26.25	110	4.47	407	0.06	0.27	50.88	0.025	0.74	72.8	2.9
20	ICJ22	18	10	2	8	0.88	30.25	90	4.05	230	0.13	0.39	28.75	0.043	1.18	67.6	-25.4
21	ICJ27*	27	10	2	19	0.88	74	205	2.66	75	0.99	2.73	3.95	0.133	5.65	56.8	-71.6
22	ICJ28	21	10	2	19	0.88	53.75	200	3.65	388	0.14	0.52	20.42	0.026	1.50	72.7	-12.3
23	ICJ33*	18	10	2	12.7	0.88	41.1	140	2.70	80	0.51	1.75	6.30	0.125	3.59	56.6	-75.0
24	ICJ34	22	10	2	12.7	0.88	34	140	3.65	384	0.09	0.36	30.24	0.026	1.01	72.4	-6.3
25	ICJ13	14	15	2	8	2.42	27.25	95	4.46	405	0.07	0.23	50.63	0.037	0.45	69.4	8.4
26	ICJ14	16	15	2	8	2.42	33.5	100	3.99	201	0.17	0.50	25.13	0.075	0.80	61.2	-34.1
27	ICJ15	15	15	2	12.7	2.42	48.25	142.5	3.99	201	0.24	0.71	15.83	0.075	1.27	61.5	-46.8
28	ICJ16	16	15	2	12.7	2.42	41.8	132.5	4.47	409	0.10	0.32	32.20	0.037	0.70	69.1	-6.7
29	ICJ5	11	15	2	19	2.42	49	152.5	3.52	333	0.15	0.46	17.53	0.045	1.01	67.1	-23.3
30	ICJ6	13	15	2	19	2.42	64	157.5	3.06	188	0.34	0.84	9.89	0.080	1.56	60.9	-53.1
31	ICJ23	19	15	2	8	0.88	47	147.5	4.05	230	0.20	0.64	28.75	0.065	1.18	63.1	-39.9
32	ICJ24	20	15	2	8	0.88	34.5	132.5	4.46	405	0.09	0.33	50.63	0.037	0.74	69.0	-8.6
33	ICJ29	22	15	2	19	0.88	67.5	200	3.51	335	0.20	0.60	17.63	0.045	1.67	67.6	-31.7
34	ICJ30	23	15	2	19	0.88	68.75	197.5	3.05	185	0.37	1.07	9.74	0.081	2.62	61.6	-57.2
35	ICJ35	20	15	2	12.7	0.88	51.75	152.5	3.28	257	0.20	0.59	20.24	0.058	1.36	64.5	-38.5
36	ICJ36	39	15	2	12.7	0.88	62.5	165	3.06	186	0.34	0.89	14.65	0.081	1.75	60.9	-54.9
37	ICJ 37	15	10	2.5	12.7	0.88	32	135	3.37	280	0.11	0.48	22.05	0.036	1.28	75.3	-17.4
38	ICJ 38	13	10	2.5	12.7	0.88	30.5	132.5	3.72	405	0.08	0.33	31.89	0.025	0.98	77.9	-1.5
39	ICJ 39	17	10	2.5	12.7	0.88	38.5	150	4.35	355	0.11	0.42	27.95	0.028	1.30	77.1	-10.4
40	ICJ 40	17	10	2.5	12.7	0.88	49.5	145	4.05	223	0.22	0.65	17.56	0.045	1.93	73.8	-29.8
41	ICJ 41	18	10	2.5	8	0.88	27	95	4.29	324	0.08	0.29	40.50	0.031	0.89	76.3	-5.6
42	ICJ 42	15	10	2.5	8	0.88	33	125	3.97	193	0.17	0.65	24.13	0.052	1.38	72.2	-31.1

Table 3-2: Impinging Circular Jets - Experimental Results (Continued)

Expt. #	Code	Time (hrs)	Screen l_s (mm)	λ	d (mm)	D (mm)	$\varepsilon_{m\infty}$ (mm)	$r_{o\infty}$ (mm)	U_o (m/s)	h (mm)	$\varepsilon_{m\infty}/h$	$r_{o\infty}/h$	h/d	l_s/h	E_c	η_1 (%)	η_2 (%)
43	ICJ 43	19	10	2.5	8	0.88	22.5	95	3.57	361	0.06	0.26	45.13	0.028	0.66	77.1	5.0
44	ICJ 44	20	10	2.5	8	0.88	25	90	3.20	235	0.11	0.38	29.38	0.043	0.91	73.7	-15.9
45	ICJ 45	21	10	2.5	8	0.88	21.5	102.5	3.71	407	0.05	0.25	50.88	0.025	0.61	78.0	10.3
46	ICJ 46	22	10	2.5	8	2.42	14.5	72	3.71	407	0.04	0.18	50.88	0.025	0.37	78.4	26.1
47	ICJ 47	25	10	2.5	8	2.42	15	60	3.27	261	0.06	0.23	32.63	0.038	0.51	74.7	5.2
48	ICJ 48	22	10	2.5	12.7	2.42	28	85	3.91	178	0.16	0.48	14.02	0.056	1.41	71.5	-34.4
49	ICJ 49	23	10	2.5	12.7	2.42	27.5	100	3.85	188	0.15	0.53	14.80	0.053	1.32	72.0	-31.3
50	ICJ 50	23	10	2.5	19	2.42	34	125	3.65	387	0.09	0.32	20.37	0.026	0.91	77.6	-1.1
51	ICJ 51	16	10	2.5	19	2.42	28	85	3.13	212	0.13	0.40	11.16	0.047	1.42	73.1	-28.2
52	ICJ 52	22	14.4	1.46	19	2.42	63.5	155	3.64	388	0.16	0.40	20.42	0.037	0.90	58.5	-18.2
53	ICJ 53	24	14.4	1.46	19	2.42	52.5	110	3.04	183	0.29	0.60	9.63	0.079	1.60	47.9	-58.2
54	ICJ 54	22	14.4	1.46	12.7	2.42	48	135	3.72	407	0.12	0.33	32.05	0.035	0.59	59.2	-3.6
55	ICJ 55	20	14.4	1.46	12.7	2.42	41.5	103.7	3.06	185	0.22	0.56	14.57	0.078	1.06	47.5	-49.2
56	ICJ 56	28	14.4	1.46	8	2.42	34.5	102.5	4.35	353	0.10	0.29	44.13	0.041	0.50	57.5	-1.7
57	ICJ 57	16	14.4	1.46	8	2.42	31	80	3.98	197	0.16	0.41	24.63	0.073	0.82	48.4	-38.6
58	ICJ 70	29	14.4	1.46	19	0.88	64	137.5	3.05	180	0.36	0.76	9.47	0.080	2.70	48.8	-62.1
59	ICJ 71	23	14.4	1.46	19	0.88	74.5	180	3.71	405	0.18	0.44	21.32	0.036	1.46	59.5	-26.5
60	ICJ 72	17	14.4	1.46	12.7	0.88	57	140	3.52	335	0.17	0.42	26.38	0.043	1.12	56.6	-28.3
61	ICJ 73	24	14.4	1.46	12.7	0.88	50.5	130	3.22	233	0.22	0.56	18.35	0.062	1.47	51.6	-47.0
62	ICJ 74	18	14.4	1.46	8	0.88	46	130	4.47	405	0.11	0.32	50.63	0.036	0.74	59.0	-11.2
63	ICJ 75	21	14.4	1.46	8	0.88	41	105	4.05	227	0.18	0.46	28.38	0.063	1.20	50.9	-44.1
64	ICJ 76	24	14.4	1.46	12.7	0.88	63.5	180	4.31	335	0.19	0.54	26.38	0.043	1.37	56.8	-32.2
65	ICJ 58	22	7.2	3.06	19	2.42	28.5	120	4.34	350	0.08	0.34	18.42	0.021	1.19	82.8	2.1
66	ICJ 59	21	7.2	3.06	19	2.42	21	115	3.72	407	0.05	0.28	21.42	0.018	0.88	83.5	11.4
67	ICJ 60	16	7.2	3.06	12.7	2.42	18	82.5	4.11	251	0.07	0.33	19.76	0.029	1.05	80.8	-4.9
68	ICJ 61	16	7.2	3.06	12.7	2.42	18.5	100	3.79	125	0.15	0.80	9.84	0.058	1.95	76.5	-35.9
69	ICJ 62*	23	7.2	3.06	19	2.42	28.5	117.5	3.79	125	0.23	0.94	6.58	0.058	2.91	76.9	-36.6
70	ICJ 63	24	7.2	3.06	19	2.42	25	110	4.05	230	0.11	0.48	12.11	0.031	1.69	80.5	-14.2
71	ICJ 64	36	7.2	3.06	19	0.88	42.5	180	4.36	360	0.12	0.50	18.95	0.020	1.93	83.2	-2.1
72	ICJ 65	24	7.2	3.06	19	0.88	52.5	205	4.11	253	0.21	0.81	13.32	0.028	2.59	81.5	-13.1
73	ICJ 66	22	7.2	3.06	12.7	0.88	37	150	4.23	203	0.18	0.74	15.98	0.035	2.22	80.0	-19.8
74	ICJ 67	18	7.2	3.06	12.7	0.88	27	160	4.46	401	0.07	0.40	31.57	0.018	1.18	83.5	5.7
75	ICJ 68	22	7.2	3.06	19	0.88	38.5	165	3.52	334	0.12	0.49	17.58	0.022	1.68	82.7	-3.2
76	ICJ 69	26	7.2	3.06	19	0.88	47	180	3.05	180	0.26	1.00	9.47	0.040	2.69	79.4	-23.9
77	ICJ 77†	26	5	2	12.7	0.88	11	140	4.47	405	0.03	0.35	31.89	0.012	1.17	94.2	12.6
78	ICJ 78†	24	5	2	12.7	0.88	7.5	135	4.31	335	0.02	0.40	26.38	0.015	1.37	95.9	7.6
79	ICJ 79†	22	5	2	12.7	0.88	3	130	4.05	222	0.01	0.59	17.48	0.023	1.94	98.2	-5.4
80	ICJ 80†	20	14.4	1.46	12.7	0.88	39.5	225	4.31	335	0.12	0.67	26.38	0.043	1.37	78.3	-53.9
81	ICJ 81†	23	14.4	1.46	12.7	0.88	34	200	4.05	222	0.15	0.90	17.48	0.065	1.94	79.8	-62.2
82	ICJ 82†	25	14.4	1.46	12.7	0.88	38	210	4.47	405	0.09	0.52	31.89	0.036	1.17	80.0	-31.1

* $h/d < 8.3$

† Screen has mounted center plate

Table 3-3: Impinging Plane Jets - Experimental Results

Expt. #	Code Name	Time (hrs.)	l_s (mm)	λ	$2b_o$ (mm)	D (mm)	$\varepsilon_{m\infty}$ (mm)	$x_{o\infty}$ (mm)	U_o (m/s)	$h/2b_o$	E_p	$\varepsilon_{m\infty}/h$	$x_{o\infty}/h$
1	IPJ 1	12	10	2	5	2.42	130	255	3.84	25.40	3.85	1.02	2.01
2	IPJ 2	11	10	2	5	2.42	113	240	3.65	47.40	2.68	0.48	1.01
3	IPJ 3	15	10	2	5	2.42	90	235	3.38	62.40	2.16	0.29	0.75
4	IPJ 4	20	10	2	5	2.42	57	180	2.15	53.40	1.48	0.21	0.67
5	IPJ 5	22	10	2	13.7	2.42	125	350	2.24	13.87	3.03	0.66	1.84
6	IPJ 6	22	10	2	13.7	2.42	120	315	2.29	21.17	2.52	0.41	1.09
7	IPJ 7	23	10	2	13.7	2.42	115	275	2.41	7.08	4.57	1.19	2.84
8	IPJ 26	21	10	2	5	1.52	160	350	3.95	28.40	4.72	1.13	2.46
9	IPJ 27	22	10	2	5	1.52	70	170	1.95	40.40	1.96	0.35	0.84
10	IPJ 28	26	10	2	5	1.52	70	150	2.08	57.00	1.75	0.25	0.53
11	IPJ 29	29	10	2	13.7	1.52	125	340	2.03	13.87	3.47	0.66	1.79
12	IPJ 30	23	10	2	13.7	1.52	55	150	1.06	19.34	1.54	0.21	0.57
13	IPJ 31	22	10	2	13.7	1.52	110	330	2.12	21.39	2.93	0.38	1.13
14	IPJ 8	22	14.4	1.39	13.7	2.42	105	175	1.84	18.83	2.14	0.41	0.68
15	IPJ 9	24	14.4	1.39	13.7	2.42	70	145	1.68	10.80	2.59	0.47	0.98
16	IPJ 10	21	14.4	1.39	13.7	2.42	115	200	1.38	7.30	2.57	1.15	2.00
17	IPJ 17	24	14.4	1.39	5	2.42	135	240	4.16	46.00	3.10	0.59	1.04
18	IPJ 18	18	14.4	1.39	5	2.42	60	130	2.10	46.00	1.56	0.26	0.57
19	IPJ 19	29	14.4	1.39	5	2.42	130	240	4.03	25.60	4.02	1.02	1.88
20	IPJ 20	24	14.4	1.39	5	1.52	170	250	3.66	33.40	4.04	1.02	1.50
21	IPJ 21	36	14.4	1.39	5	1.52	140	265	3.71	48.80	3.39	0.57	1.09
22	IPJ 22	24	14.4	1.39	5	1.52	140	265	3.83	53.00	3.35	0.53	1.00
23	IPJ 32	24	14.4	1.39	13.7	1.52	80	180	1.35	21.39	1.86	0.27	0.61
24	IPJ 33	25	14.4	1.39	13.7	1.52	105	305	1.87	13.50	3.24	0.57	1.65
25	IPJ 34	24	14.4	1.39	13.7	1.52	135	340	2.09	7.15	4.99	1.38	3.47
26	IPJ 11	22	7	3.06	13.7	2.42	103	280	2.25	17.08	2.75	0.44	1.20
27	IPJ 12	20	7	3.06	13.7	2.42	110	290	2.30	21.17	2.52	0.38	1.00
28	IPJ 13	28	7	3.06	13.7	2.42	105	300	2.13	8.98	3.59	0.85	2.44
29	IPJ 14	21	7	3.06	5	2.42	125	350	5.71	58.40	3.77	0.43	1.20
30	IPJ 15	22	7	3.06	5	2.42	175	425	5.34	39.00	4.32	0.90	2.18
31	IPJ 16	24	7	3.06	5	2.42	137	260	3.94	22.60	4.19	1.21	2.30
32	IPJ 23	22	7	3.06	5	1.52	138	365	4.69	53.00	4.11	0.52	1.38
33	IPJ 24	18	7	3.06	5	1.52	83	225	2.81	58.00	2.35	0.29	0.78
34	IPJ 25	18	7	3.06	5	1.52	160	410	4.01	18.60	5.93	1.72	4.41
35	IPJ 35	25	7	3.06	13.7	1.52	120	360	2.10	18.98	3.08	0.46	1.38
36	IPJ 36	24	7	3.06	13.7	1.52	80	230	1.59	20.95	2.21	0.28	0.80
37	IPJ 37	26	7	3.06	13.7	1.52	138	430	2.11	10.00	4.25	1.01	3.14
38	IPJ 38	23	7	3.06	13.7	1.52	130	370	2.16	14.96	3.55	0.63	1.80

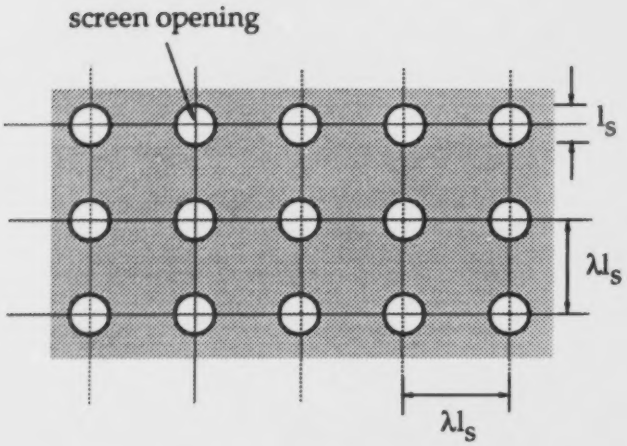

Figure 3-1(a) Screen Design

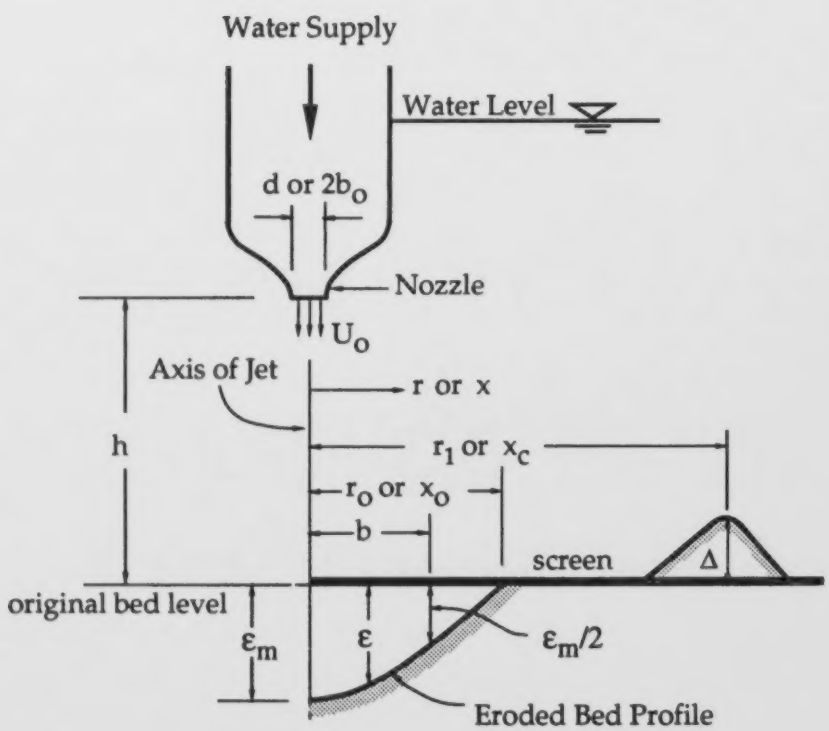

Figure 3-1(b) Definition Sketch

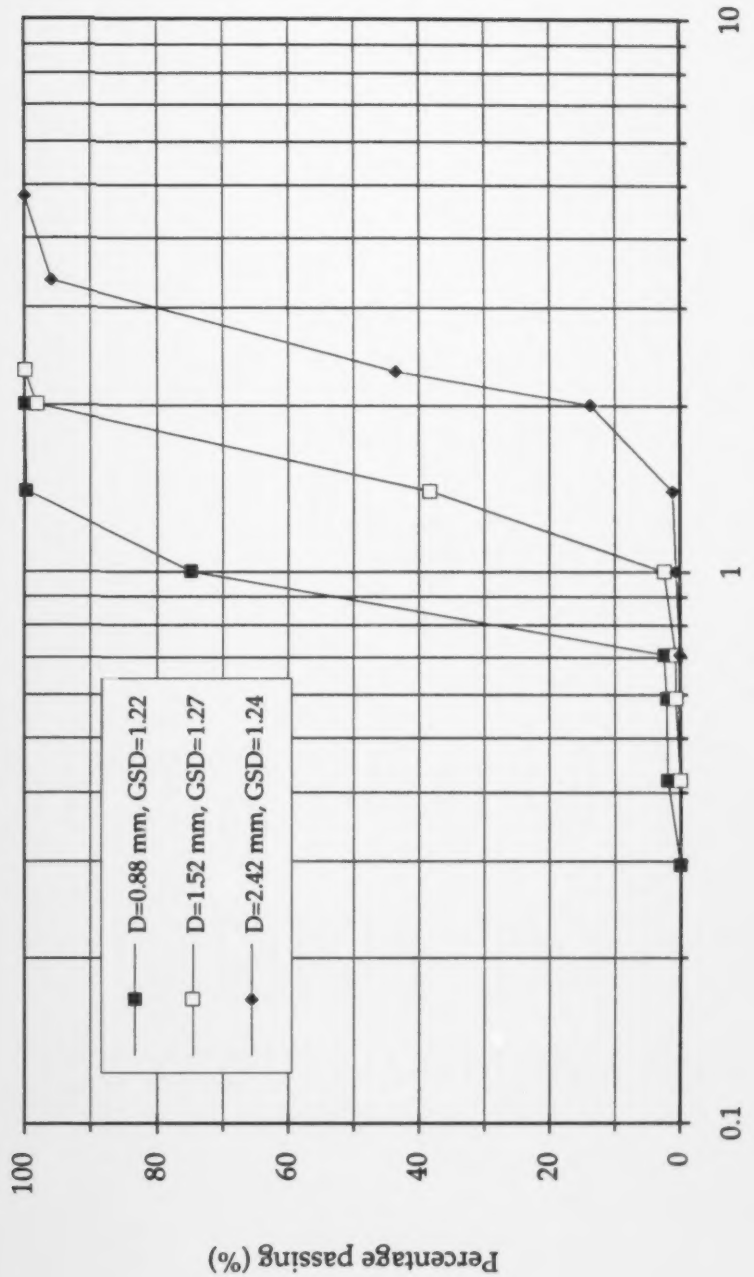

Figure 3-2: Sediment size distribution curves

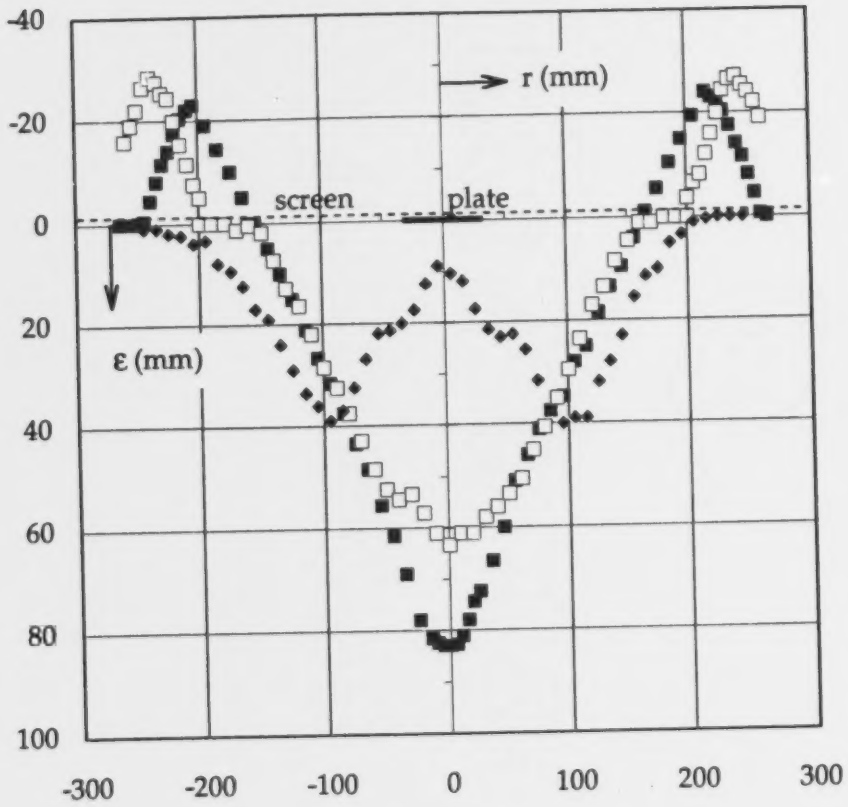

$h = 0.335\,m$
$d = 12.7\,mm$
$D = 0.88\,mm$
$U_o = 4.31\,m/s$
$E_c = 1.37$

■ No screen (static scour), approx. dynamic scour depth = 180mm

□ Screen CS5

◆ CS5 with center plate (diameter = 100 mm), CS5P

Figure 3-3: Scour profiles with and without screen for circular jets

Figure 3-4: Scour hole Pattern below Screen with Circular Openings

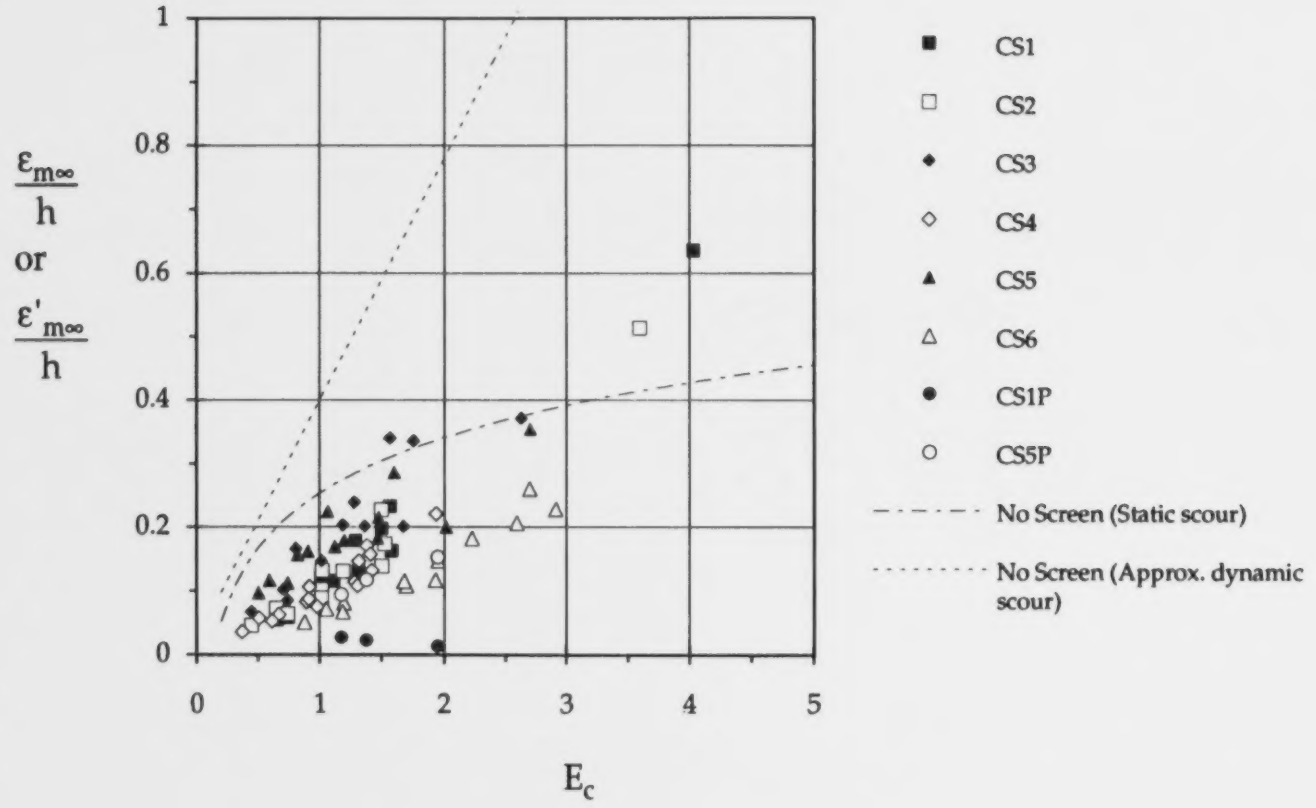

Figure 3–5: Variation of relative maximum scour depth with E_c

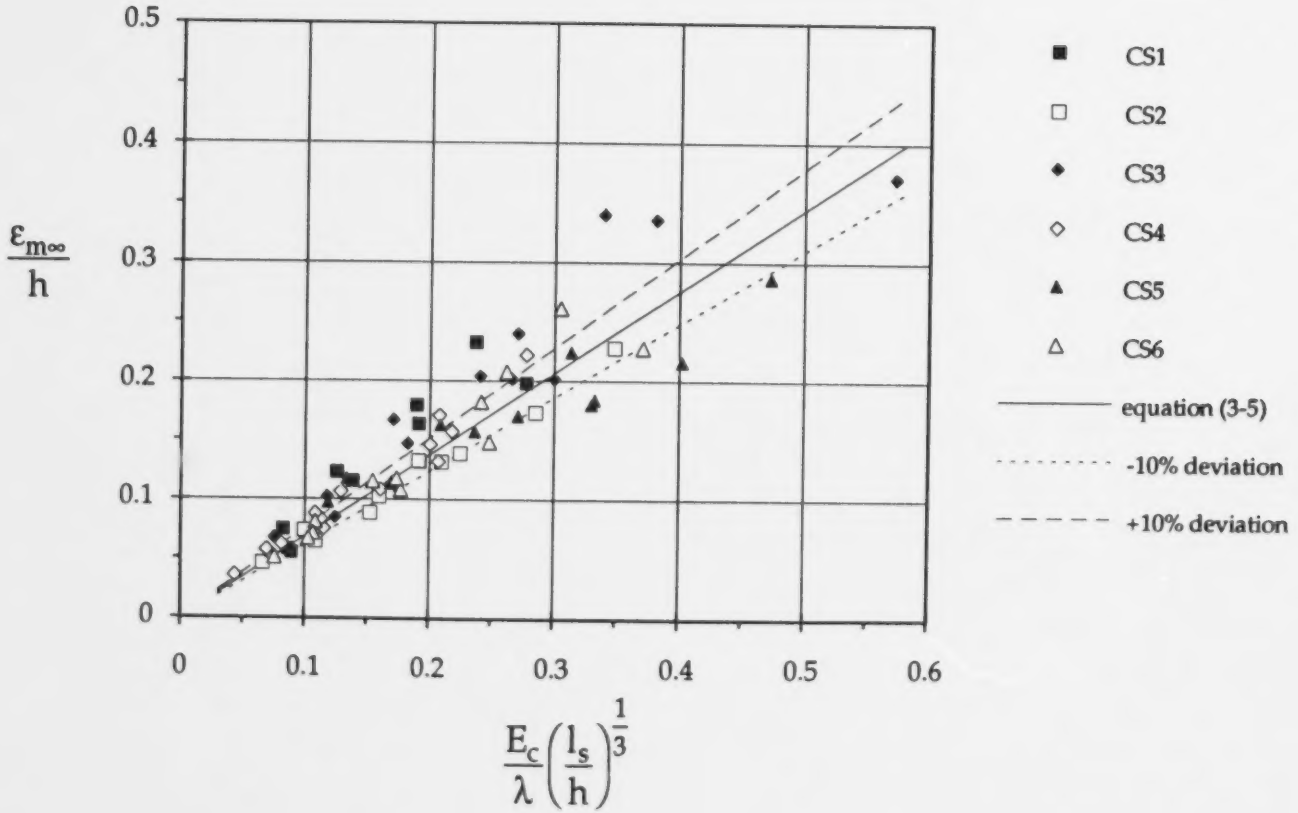

Figure 3 – 6: Variation of relative maximum scour depth with other non – dimensional parameters

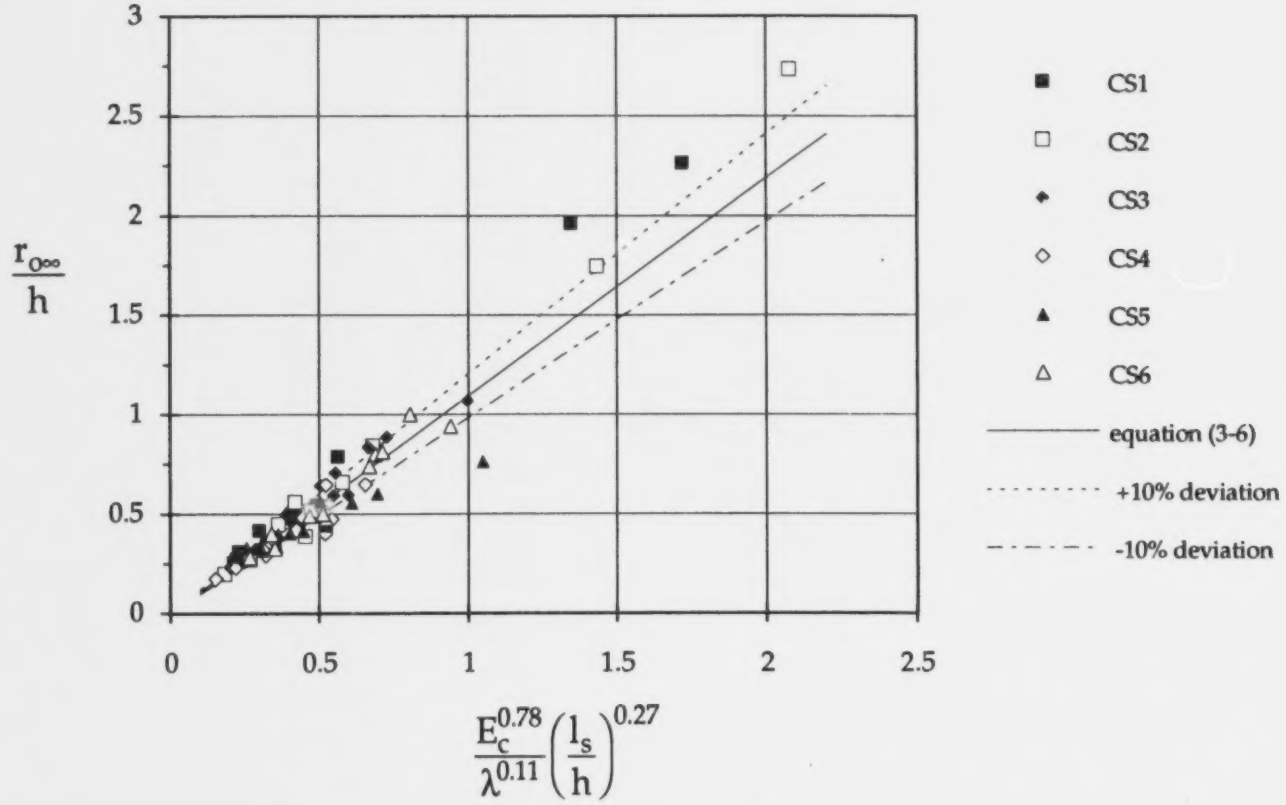

Figure 3-7: Variation of relative scour radius with other non-dimensional parameters

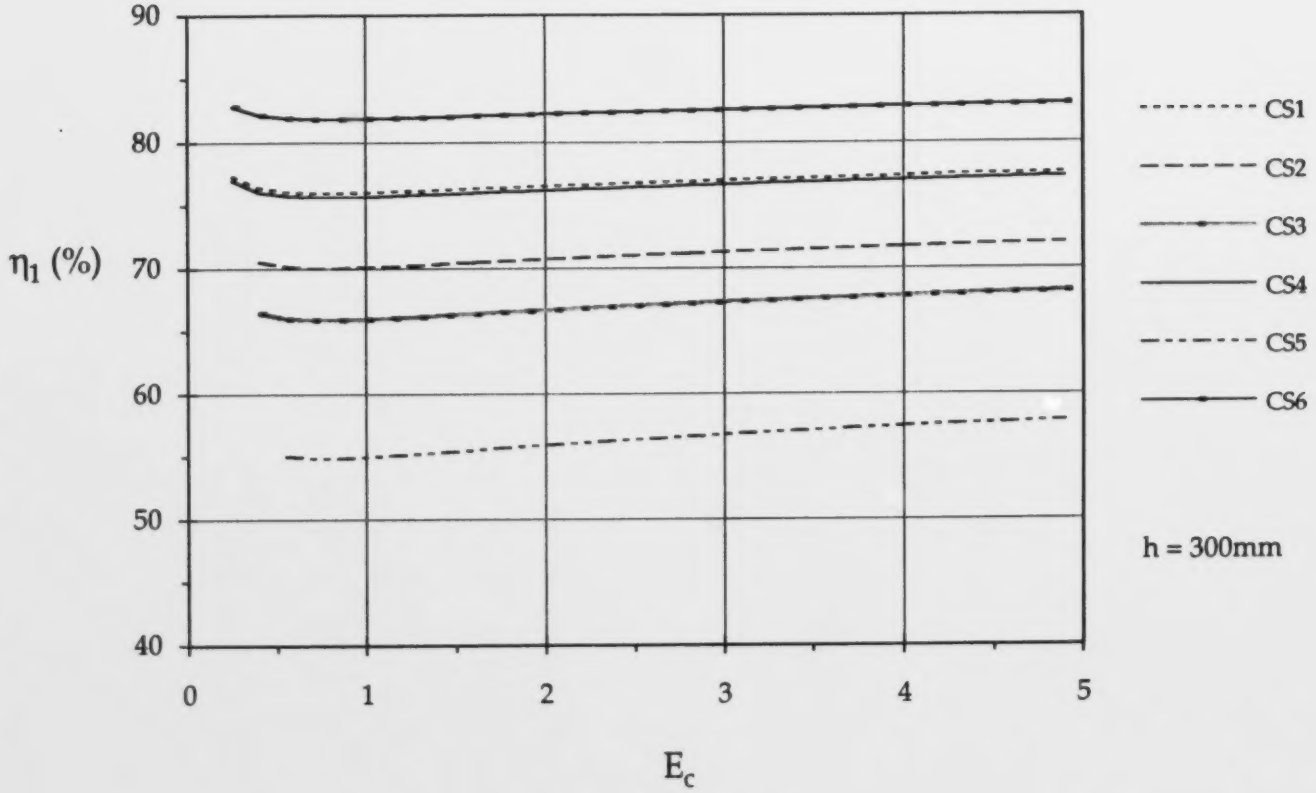

Figure 3 – 8: Variation of η_1 with E_c

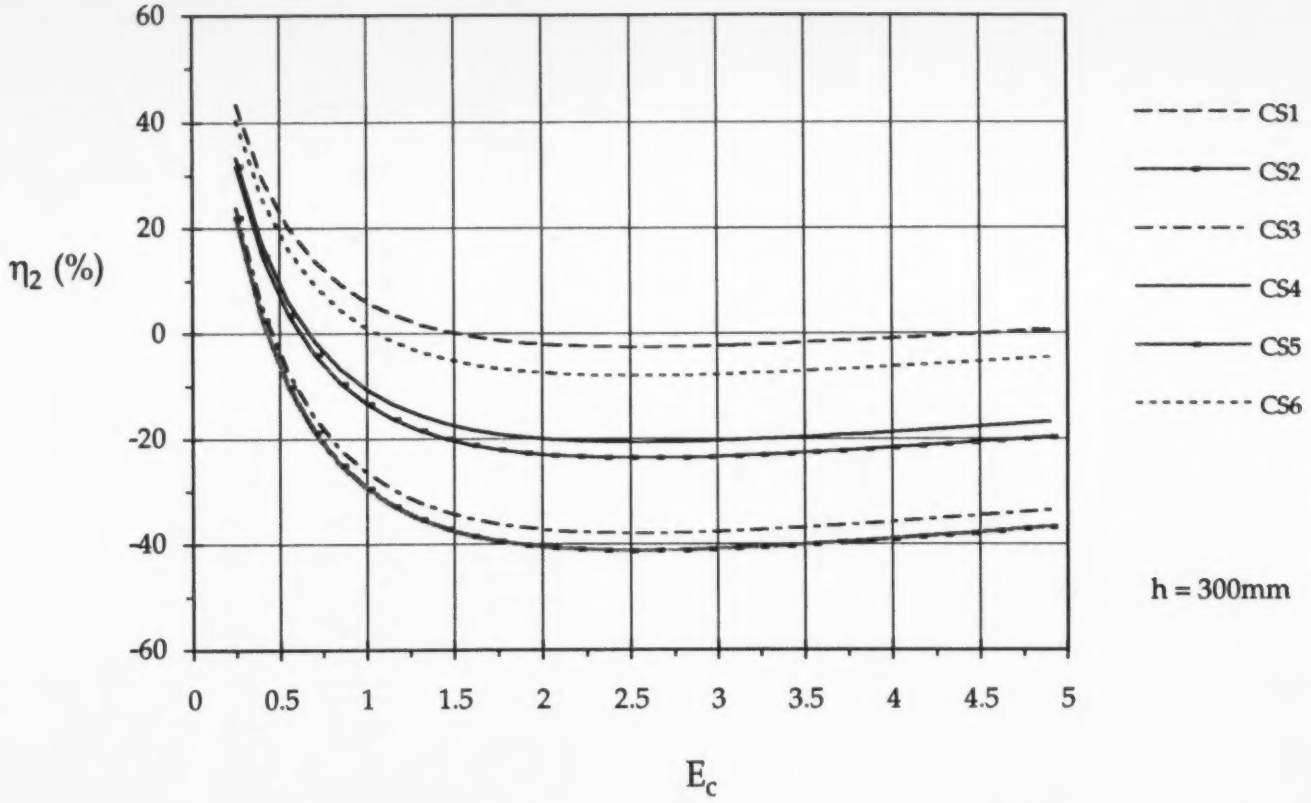

Figure 3-9: Variation of η_2 with E_c

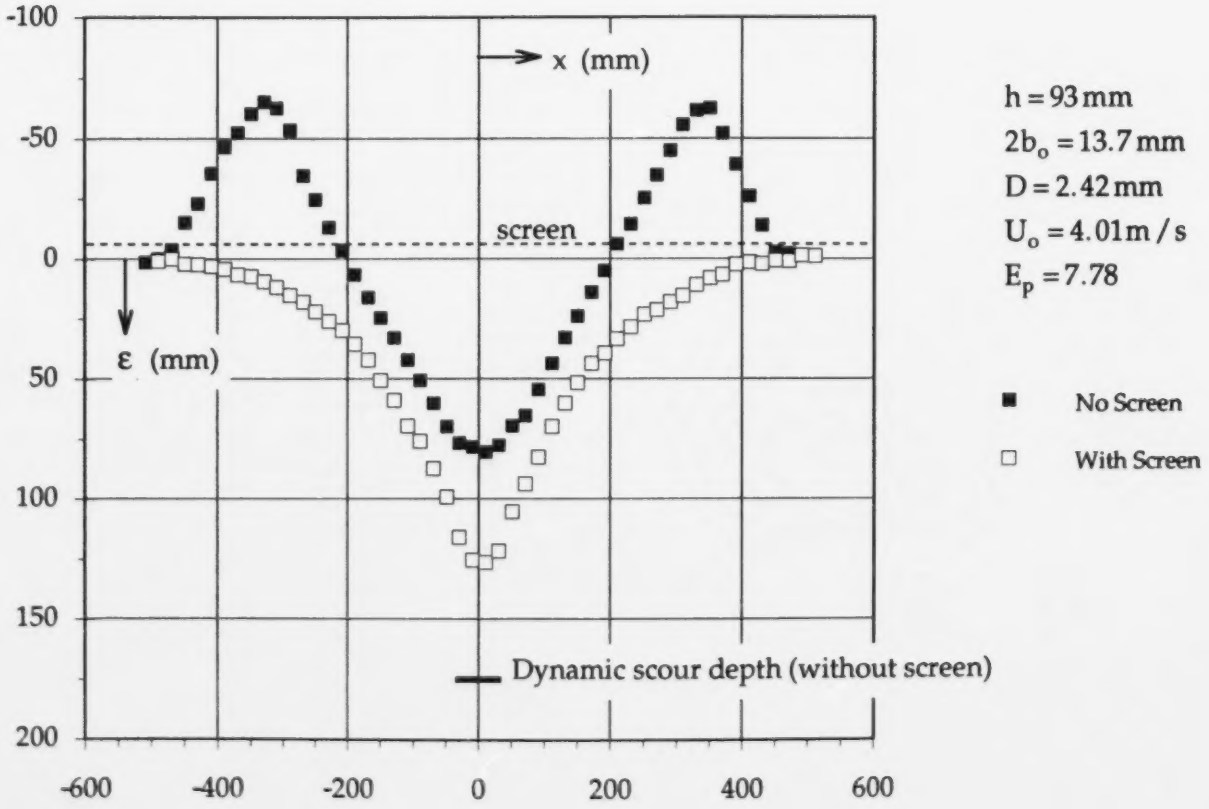

Figure 3-10: Scour profiles with and without screen for plane jets

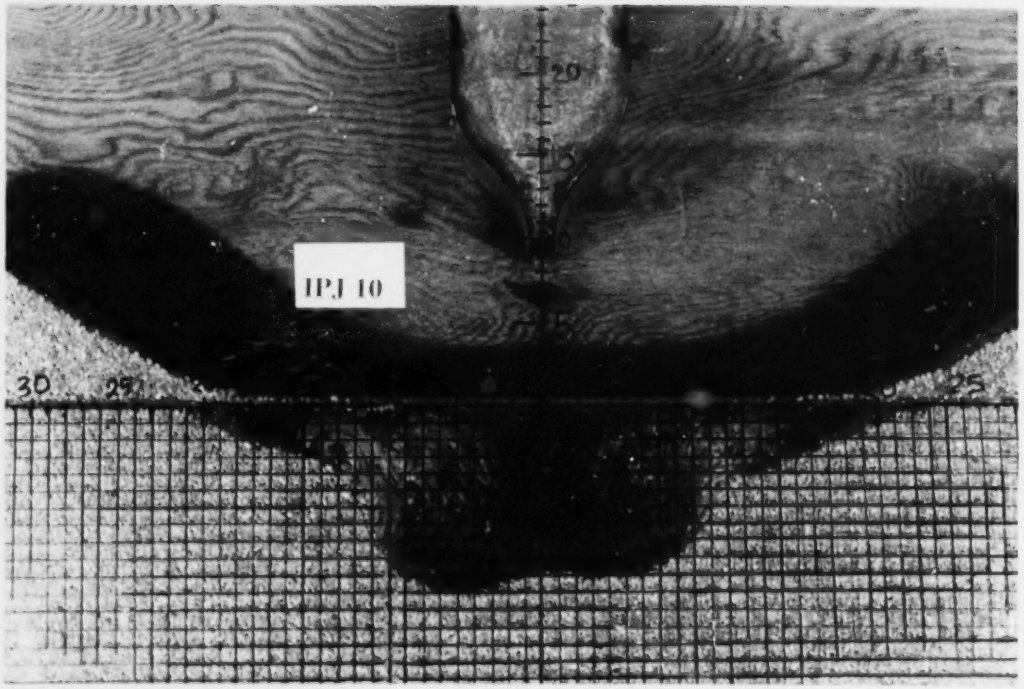

$h = 100\,mm$

$2b_o = 13.7\,mm$

$D = 2.42\,mm$

$U_o = 1.37\,m/s$

$E_p = 2.57$

Figure 3-11: Scour and flow patterns due to impinging plane jet using screen PS2

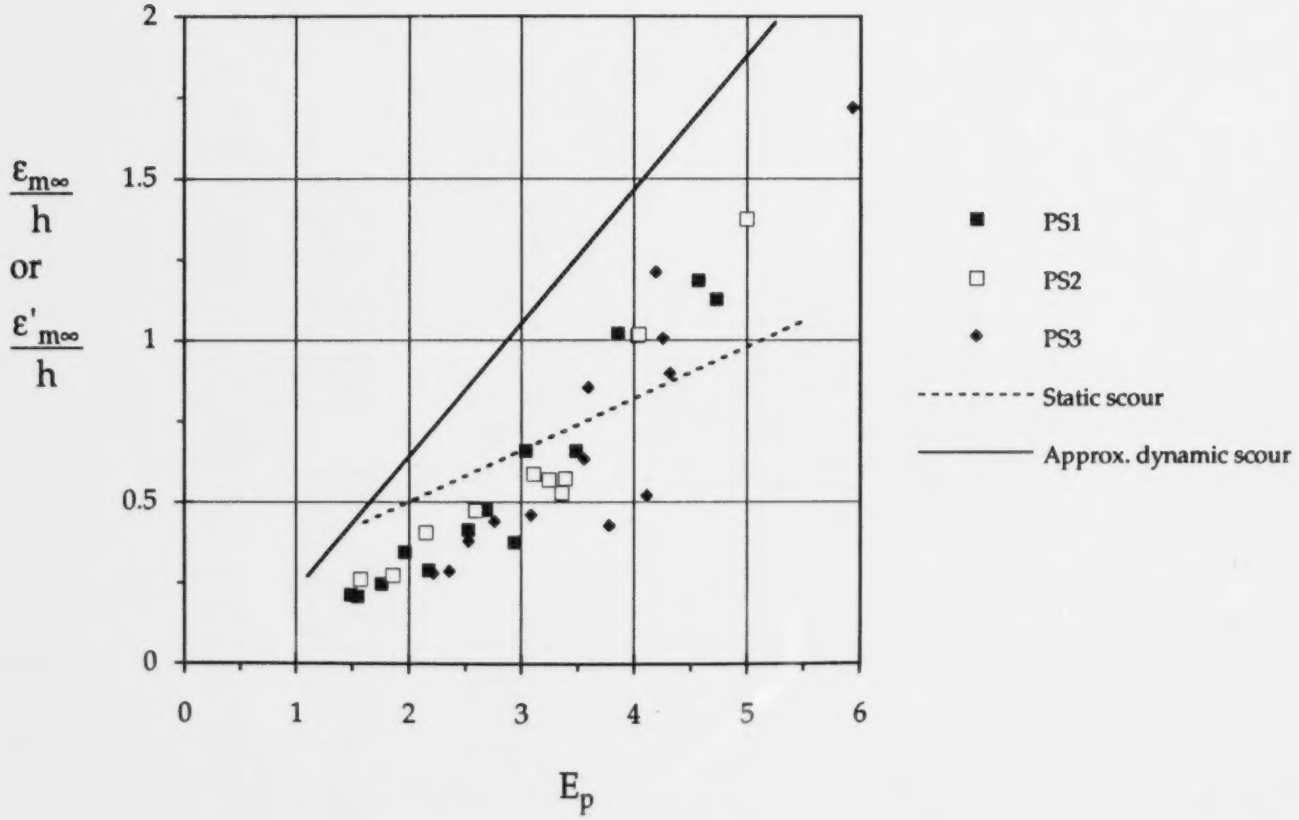

Figure 3-12: Variation of relative maximum scour depth with E_p

CHAPTER 4

Erosion of Loose Beds by Submerged Circular Impinging Vertical Turbulent Jets †

4.1 Introduction

In the field of hydraulic engineering, erosion of beds of sand, gravel, clay and weak rock is of considerable importance because it is necessary to predict and control erosion near hydraulic structures. The cause of erosion could be local flow acceleration as in a constricted reach, secondary flows as in a curved channel, flow concentration as in a high velocity jet and vortices as in flow around a bridge pier. Research on erosion by jets has been mainly empirical because of the complex nature of the flow and its interaction with the sediment bed. Rouse, in 1939, pioneered research work in this area and since then, a number of investigations have been carried out. Some of the important contributions on submerged circular impinging turbulent jets are by Doddiah et al. (1953), Poreh and Hefez (1967), Johnson (1967), Westrich and Kobus (1973), Rajaratnam and Beltaos (1977), Kobus et al. (1979), Rajaratnam (1982) and Blaisdell and Anderson (1988).

This study could be regarded as a simplified study of erosion below cantilevered pipe/culvert outlets. This could also apply to erosion below jets issuing from square gates of dams. Another practical application of this study could be in the use of jets to clean gravel beds for salmon spawners as shown by Mih and Kabir (1983). Although, the practical application of this study is not as common compared to that of erosion due to impinging plane jets, this study could assist in understanding and appreciating erosion due to impinging plane jets.

---

† The main content of this chapter has been published in the Journal of Hydraulic Research (IAHR), Vol. 34, No. 1, pp. 19 - 33, 1996.

This study examines the effect of the impinging distance of submerged circular vertical turbulent jets of water on the characteristic lengths of an eroded sand/gravel bed profile in the asymptotic or end state. The similarity of the eroded bed profiles in the asymptotic state has been examined and the characteristics of the different flow regimes have also been determined. The experimental results were analyzed using a semi-empirical approach. Using data from the literature, regression equations that are usable for different values of the relative density difference $\Delta\rho/\rho$ have been developed for the asymptotic values of the maximum scour depth $\varepsilon_{m\infty}$ and the scour hole radius $r_{o\infty}$. $\Delta\rho$ is the difference between the mass densities of the bed material and the fluid and ρ is the mass density of the fluid.

4.2 Laboratory Experiments

An octagonal plastic box having a side length of 0.235m and a height of 0.6m was used. The impinging jet nozzle was attached to the bottom of a cylinder of 150mm diameter and variable length, with a suitable constant-head arrangement. In order to simplify the experimental study, the jets were arranged to be vertically impinging and non-aerated. The nozzle was centrally located in the octagonal plastic box and always submerged just below the tail water. Six series of experiments were performed. In each series, the jet velocity at the nozzle U_o, the jet diameter at nozzle d and the median size D of the sand/gravel bed particles were kept constant. The impinging distance h was the only parameter varied. This was done by keeping the nozzle position fixed and altering the thickness of the sand/gravel bed. The value of h ranged from 4 to 523 mm. The jet nozzle diameters were 4, 8, 12 and 19 mm and the exit velocities ranged from 2.65 to 4.45 m/s. The median bed particle sizes D of the nearly uniform sand and gravel beds used were 0.88 and 2.42 mm and their respective particle size geometric standard deviations σ_g (equal to $\sqrt{(d_{84}/d_{16})}$) were 1.22 and 1.24. Their size distribution curves are shown in Figure 4-1.

The procedure for each run consisted of establishing a leveled compacted saturated sand or gravel bed at the bottom of the octagonal box which was slowly filled with water. The set-up for the jet was then centrally mounted keeping the jet nozzle blocked and slightly submerged in the pool. The set-up was then fed with water and the nozzle was opened after a constant head was

established. The scour depth grew with time and when the asymptotic state (when the rate of increase of scour depth with time is very small) was reached, the maximum dynamic scour depth $\varepsilon'_{m\infty}$, which is the maximum scour depth when the jet is on, was measured approximately by gradually inserting a thin rod into the scour hole until it touched the bottom. This procedure was repeated until four close values were obtained and the average was used as its value. For this study, the time to reach the asymptotic state varied from 6 to 50 hours. The next step was to stop the experiment and carefully drain the octagonal box to allow an easy measurement of the static scoured bed profile $\varepsilon(r)$, which is the state of scour when the jet is off. In total, 67 experiments were performed and their details are given in Table 4-1. The experimental data obtained from other researchers used in this study are given in Table 4-2. Figure 4-2 and 4-3 respectively show the set-up and a definition sketch.

4.3 Effects of Impinging Distance

Previous research into the effects of impinging distance on maximum scour depth has produced some interesting results. Doddiah et al. (1953) found using hollow and solid circular jets that there exists a critical impinging distance at which an increase or decrease in impinging distance causes a decrease in maximum static scour depth, when the other variables are kept constant. Johnson (1967) also obtained similar results in his studies using semi-circular jets. Westrich and Kobus (1973) showed that the variation of the asymptotic scour volume with impinging distance has two peaks. The present study attempts to study this phenomenon in detail and develop expressions to define the different regimes.

Figures 4-4(a-b) show the variations of the dynamic and static scour depths with impinging distance for two sets of experiments. It can be seen from these two figures that there exists a critical impinging distance at which static scour depth is maximum. The reason for this is explained below under the 'Strongly Deflected Jet Regime' section. For values of h smaller than the critical value, the dynamic scour depth is greater than the corresponding static value. In Figure 4-4(a), the critical impinging distance is about 250 mm and the erosion parameter E_c is equal to 0.37. The erosion parameter E_c can be interpreted as a measure of the ratio of the force of the circular jet acting on

a bed particle directly under the jet and at the original bed level to its resistive force. It is defined as $U_o d/h/\sqrt{(gD\Delta\rho/\rho)}$. In Figure 4-4(b), the critical impinging distance is about 260 mm and E_c is equal to 0.42. For values of h larger than the critical value, the static and dynamic scour depths are approximately equal and by extrapolating the scour curves, the points of no scour (incipient motion) could be roughly estimated to occur at h equal to 505 mm (E_c=0.18) and 790 mm (E_c=0.14) in Figures 4-4(a) and 4-4(b) respectively.

4.4 Similarity of Eroded Bed Profiles

The asymptotic erosion profiles were tested for similarity by plotting $(\varepsilon/\varepsilon_m)_\infty$ against $(r/\varepsilon_m)_\infty$ and the results for a few experiments are shown in Figure 4-5(a). The value of E_c ranged from 0.14 to 3.52. It is seen that all the data points except those for four cases appear to fall on a single curve. It is also interesting that these four cases have the lowest values of E_c. Another plot of interest is the variation of $(r_o/\varepsilon_m)_\infty$ with E_c shown in Figure 4-6. It can be seen that the ratio $(r_o/\varepsilon_m)_\infty$ is approximately 1.7 for E_c greater than about 0.35 and for E_c smaller than this value, it rapidly increases with decreasing E_c. The four odd cases in Figure 4-5(a) fall in this range of E_c. It may be concluded from these two figures that the side slope of the scour hole is very sensitive to E_c when the latter is less than about 0.35.

In order to find a single non-dimensional curve that will describe asymptotic scour hole profiles for a wide range of E_c, another length scale b_∞ was introduced which is equal to the radial distance at which the scour depth is half the maximum scour depth. A plot of $(\varepsilon/\varepsilon_m)_\infty$ against $(r/b)_\infty$ was drawn following the method used by Rajaratnam (1982). Figure 4-5(b) shows that the exponential equation written as equation (4-1) describes this non-dimensional profile reasonably well for $(r/b)_\infty$ up to about 1.6.

$$\frac{\varepsilon_\infty}{\varepsilon_{m\infty}} = \exp\left(-0.693\left(\frac{r}{b_\infty}\right)^2\right) \qquad (4\text{-}1)$$

In order to use this equation, the equations for the variation of $\varepsilon_{m\infty}$ and b_∞ with the erosion parameter E_c have to be determined. These are given later as equations (4-15) and (4-18) respectively.

4.5 Characteristics of Flow Regimes

There have been previous attempts to classify the flow regimes by impinging jets on non-cohesive beds. Rouse (1939) studied the flow patterns by a submerged plane vertical jet on loose sand beds during the scouring process. It was noticed that the flow pattern could start as what was termed 'maximum jet deflection', that is, when the jet is deflected through nearly 180° and later changes after the scour depth has exceeded a certain value to 'minimum jet deflection', that is, when the jet follows the boundary of the scour hole as far as the crest of the dune. Westrich and Kobus (1973) and Kobus et al. (1979) classified asymptotic scour holes as either 'scour form I' or 'scour form II' depending on the interaction of the flow with the bed. The former was attributed to scour holes formed when a defined non-dimensional momentum flux parameter similar to E_C slightly exceeds that for incipient motion and the latter to scour holes formed at high values of E_C. In the present study, the flow patterns over the asymptotic scour holes are classified as either the Strongly Deflected Jet Regime (SDJR) or the Weakly Deflected Jet Regime (WDJR). It appears that the two regimes are linked by a narrow transition regime. WDJR and SDJR were found to be respectively somewhat similar to the earlier defined scour form I and scour form II. Figure 4-7(a-d) show sketches of flow patterns and bed profiles for these regimes.

4.5.1 Strongly Deflected Jet Regime

This regime has been divided into SDJR I and SDJR II according to the value of E_C. An observer can see the bottom of the scour hole in the latter unlike in the former (see Figure 4-7(a-b)). In this regime, the jet always penetrates the bed and thus gets deflected strongly, transporting eroded material out of the scour hole by suspension. Due to reduced transport capacity of the deflected jet at larger radial distances, there is deposition on the inner sides of the scour hole causing the deposited material to slide towards the center of erosion and thereby causing renewed erosion. This is why in the SDJR, the time required for the scouring process to reach an asymptotic state is much less than that in the WDJR. The distinctive flow pattern in this regime is the re-circulatory flow and its interaction with the suspended material. When the jet is shut off, all the suspended particles are deposited to fill the cavity formed by the penetrating jet thereby resulting in a

smaller scour depth (static) compared to the dynamic scour depth. In this case, the scour hole side slope is equal to the submerged angle of repose of the material. The plots showing the variation of scour depth with impinging distance for the six series of experiments (two of which are shown in Figure 4-4(a-b)) showed that the SDJR regime occurs at values of E_c greater than about 0.35 which is fairly close to 0.27 suggested by Westrich and Kobus (1973) for the beginning of 'scour form II'. It was observed that the jet was deflected through an angle that varied approximately between 90° plus θ_r and 180° depending on E_c, where θ_r is the submerged angle of repose of the bed material. As shown in Figure 4-6, in this regime, $(r_o/\varepsilon_m)_\infty$ is approximately a constant.

4.5.2 Weakly Deflected Jet Regime

In this regime, the jet has a weak penetration into the bed and as a result, there is reduced interaction with the bed. This regime has also been divided into WDJR I and WDJR II according to the value of E_c (see Figures 4-7(c-d)). The former occurs close to the transition region and the latter close to the state of incipient motion. This regime occurs at values of E_c less than about 0.35. The static and dynamic profiles are the same. The jet is weakly deflected, traveling along the boundary of the scour hole as far as the crest of the dune. This flow transports the eroded material out of the scour hole, mainly along the bed. From Figure 4-6, it is observed that $(r_o/\varepsilon_m)_\infty$ is very sensitive to E_c which suggests that the scour hole side slope varies significantly. The jet deflection angle varies approximately between 90° and 90° plus θ_r.

4.6 Threshold Condition

The flow over an erodible bed can be assumed to have reached a critical or threshold condition when the hydrodynamic force is balanced by the resisting force of the bed particle. Scouring starts beyond this stage and will continue until this condition is restored. In the case of local scour, the scour hole is continuously enlarged and the eroded bed profile will eventually approach an asymptotic state. At this state, the force of the jet is either insufficient to move the bed particle, or the secondary currents generated in the scour hole are incapable of transporting the suspended particles out of the scour hole. It then appears reasonable to assume that the threshold condition has been attained.

The threshold condition for flow over non-cohesive sediments in nearly horizontal flumes, based on data obtained from several researchers can be described by the Shields curve. A recent study by Chiew and Parker (1994) discussed the effect of stream wise bed slope on the threshold condition. This result in conjunction with the Shields curve, which will be henceforth referred to as the modified Shields criterion, might not be applicable to the asymptotic state in the SDJR. The reason is that scour will continue and another asymptotic state would be attained if the suspended sediments are removed from the scour hole as found by Johnson (1967), Blaisdell and Anderson (1988a and 1988b) and others. However, it may be assumed that the modified Shields criterion is applicable at least at the asymptotic state in the WDJR II, where the side slope of the scour hole is small.

4.7 Governing Equations

In order to develop an equation for the maximum scour depth, the following equations can be combined:

i) the equation for the modified Shields criterion

ii) the equation for the critical shear stress and

iii) the equation for the decay of centerline velocity of the jet.

The Shields curve can be described by equations (4-2) and (4-3). Equation (4-4) as given by Chiew and Parker (1994) accounts for the effect of stream wise bed slope on the Shields critical shear velocity u_{*cs}. It was found from their experiments that K_C varies between 0.5 and 1.5 using an average value of $\theta_r = 36^\circ$ and ϕ, the angle of stream wise bed slope, varying between -4.5° and 30.6°.

$$\frac{u_{*cs}^2}{g\frac{\Delta\rho}{\rho}D} = 0.0166\frac{\left(\frac{u_{*cs}D}{\upsilon}+1\right)^{2.65}}{\left(\frac{u_{*cs}D}{\upsilon}\right)^{2.44}} \qquad \text{for} \quad \frac{u_{*cs}D}{\upsilon} \le 600 \qquad (4\text{-}2)$$

$$\frac{u_{*cs}^2}{g\frac{\Delta\rho}{\rho}D} \cong 0.06 \qquad \text{for} \quad \frac{u_{*cs}D}{\upsilon} > 600 \qquad (4\text{-}3)$$

$$\frac{u_{*c}}{u_{*cs}} \equiv \sqrt{\cos\phi\left(1-\frac{\tan\phi}{\tan\theta_r}\right)} = K_c \qquad (4\text{-}4)$$

The term u_{*c} is the critical shear velocity at any slope and υ is the kinematic viscosity of water. The critical shear stress τ_c is given by equation (4-5) wherein C_f is the friction coefficient and U_c is the critical velocity for incipient motion.

$$\tau_c = \rho u_{*c}^2 = C_f \rho \frac{U_c^2}{2} \qquad (4\text{-}5)$$

Equation (4-2) can be simplified to equation (4-6) and by assuming that $\upsilon = 10^{-6}\ m^2/s$ and $\Delta\rho/\rho = 1.65$, an approximate solution could be expressed as either equation (4-8) or equation (4-9). The former is a better solution. Equation (4-3) can be re-written as equation (4-10). A simplified general solution to equations (4-2) and (4-3) describing Shields curve might then be expressed as equation (4-11) following the format of equation (4-10), where C_3 is an adjustable coefficient.

$$u_{*cs}^{-1.675} + C_1 D u_{*cs}^{-0.675} - C_2 D^{0.543} = 0 \qquad (4\text{-}6)$$

$$\text{where} \quad C_1 = \frac{1}{\upsilon} \quad \text{and} \quad C_2 = \frac{4.7}{\left(g\frac{\Delta\rho}{\rho}\right)^{0.377}\upsilon^{0.92}} \qquad (4\text{-}7)$$

$$u_{*cs} = 0.01 + 14.56D - 579.33D^2 \qquad (4\text{-}8)$$

$$u_{*cs} = 0.91\ D^{0.51} \qquad (4\text{-}9)$$

$$u_{*cs} = 0.245\ \sqrt{g\frac{\Delta\rho}{\rho}D} \qquad (4\text{-}10)$$

$$u_{*cs} = C_3\ \sqrt{g\frac{\Delta\rho}{\rho}D} \qquad (4\text{-}11)$$

Equation (4-12a) expresses the decay of the centerline velocity U_m of a submerged circular free jet with x, which is the distance along the jet centerline, greater than the length of the potential core. C_j is the diffusion coefficient. In the case of jet impingement, this equation is valid for up to 86% of the impinging distance (Beltaos and Rajaratnam (1974)). It appears that this equation can still be used to compute the bed velocity U_b, very close to the jet centerline, by replacing C_j with an experimentally determined coefficient C_{jb} (equation (4-12b)). This approach has been used successfully by Chee and Yuen (1985).

$$\frac{U_m}{U_o} = \frac{C_j}{x/d} \tag{4-12a}$$

$$\frac{U_b}{U_o} = \frac{C_{jb}}{x/d} \tag{4-12b}$$

An expression for the maximum scour depth can now be obtained when U_b is equal to U_c, x is equal to ($\varepsilon_{m\infty}$ + h) and equations (4-4), (4-5), (4-11) and (4-12b) are combined. The final expression is given as equation (4-13). The coefficients might be combined to form another adjustable coefficient C_4 as shown in equation (4-14).

$$\frac{\varepsilon_{m\infty}}{h} = \frac{C_{jb}}{C_3 K_c}\sqrt{\frac{C_f}{2}}\ \frac{U_o}{\sqrt{g\frac{\Delta\rho}{\rho}D}}\frac{d}{h} - 1 \tag{4-13}$$

$$\frac{\varepsilon_{m\infty}}{h} = C_4\ E_c - 1 \tag{4-14}$$

4.8 Equilibrium Scour Depth

The maximum static scour depth data used to find the C_4-coefficient were obtained from Clarke (1962), Westrich and Kobus (1973), Rajaratnam (1982) and this study and they are plotted in Figure 4-8. Clarke's data appear to deviate from the rest of the data beyond E_c equal to 0.8 and these were not used for curve fitting. An examination of his scour depth against time data showed that his experiments were not run long enough (1.5 to 4.67 hours) to

reach an asymptotic state and this might explain why his values are generally lower.

It could be proposed that the adjustable coefficient C_4 is dependent on E_c and by doing so, equation (4-14) could be re-written after some regression analysis as equation (4-15). It is only valid for h/d greater than C_j or preferably for h/d greater than 8.3 as suggested by Rajaratnam and Beltaos (1977).

$$\frac{\varepsilon_{m\infty}}{h} = \left(1.255E_c^{-0.893}\right)E_c - 1 = 1.26E_c^{0.11} - 1 \qquad (4\text{-}15)$$

The erosion parameter corresponding to the critical impinging distance can be found from this equation by partially differentiating $\varepsilon_{m\infty}$ with respect to h and equating the differential to zero. This yields a value of 0.35 for E_c, which is close to the values obtained from Figure 2(a-b). Also from this equation, the value of E_c at incipient motion is 0.12. Westrich and Kobus (1973) suggested 0.17. Rajaratnam and Beltaos (1977) obtained 0.18 from their air jet experiments on loose beds of sand and spherical-polystyrene and Shafai-Bajestan and Albertson (1993) obtained 0.367 from their experiments involving inclined submerged circular impinging jets on a uniform gravel bed.

4.9 Other Length Scales at Asymptotic State

Some of the other characteristic lengths of the eroded bed profile that will be analyzed are $\varepsilon'_{m\infty}$, b_∞, $r_{0\infty}$ and the height of the ridge Δ_∞. In order to obtain an expression for the dynamic scour depth similar to that for the maximum static scour depth (equation (4-15)), a correction term had to be added to E_c. This is to account for the faster decay rate of the velocity of the descending jet due to the ascending flow. This makes the velocity decay equation (equation (4-12b)) inapplicable especially at high values of E_c. Rajaratnam et al. (1993) noticed a similar flow pattern in their study of jet diffusion in storm water drop shafts. The decay of the maximum velocity in the descending jet was found to be greater in relatively smaller drop shafts. Equation (4-16) predicts the dynamic scour depth fairly well despite the crude measuring technique used, as can be seen in Figure 4-9. Figure 4-10 shows

that $r_{o\infty}/h$ appears to increase rapidly with increasing E_C in the WDJR and then increases linearly with E_C in the SDJR. These relationships are described by equation (4-17).

$$\frac{\dot{\varepsilon}_{m\infty}}{h} = 7.32E_c\left(\frac{d}{h}\right)^{\beta} - 1 \quad \text{where} \quad \beta = 1.53E_c^{0.22} - 1 \tag{4-16}$$

$$\frac{r_{o\infty}}{h} = 1.46E_c^{0.15} - 1 \qquad \text{for} \quad E_c \le 0.5 \tag{4-17a}$$

$$\frac{r_{o\infty}}{h} = 0.22 + 0.2E_c \qquad \text{for} \quad 0.5 < E_c < 5 \tag{4-17b}$$

The variation of the length scale b_∞/h with E_C is shown in Figure 4-11. It can be described approximately by equation (4-18). Figure 4-12 shows the variation of the relative height of the ridge (dune) Δ_∞/h with E_C. The data are separated mainly into two groups. In this study, the tail water depth and the impinging distance were approximately equal. This indicates that for lower values of h, that is, higher values of E_C, there were stronger radial currents in the pool which flattened the ridge resulting in lower values of Δ_∞/h. The other data were obtained from experiments where the tail water depths were much greater that the impinging distances resulting in weaker radial currents and therefore, higher values of Δ_∞/h. Equation (4-19) describes the limits for Δ_∞/h in terms of E_C based on the available data. C_5 is equal to 0.077 and -0.02 for the upper and the lower limit respectively and these could be used to obtain rough estimates for practical application.

$$\frac{b_\infty}{h} = 1.2E_c^{0.06} - 1 \qquad \text{for} \quad E_c \le 0.5 \tag{4-18a}$$

$$\frac{b_\infty}{h} = 0.11 + 0.08E_c \qquad \text{for} \quad 0.5 < E_c < 5 \tag{4-18b}$$

$$\frac{\Delta_\infty}{h} = C_5 + 0.044E_c \tag{4-19}$$

4.10 Effect of Density Difference on Length Scales

Scour data on other fluid-sediment systems were collected from Rajaratnam and Beltaos (1977). It contains data on air jets impinging on loose beds of sand and polystyrene. For the air jet-polystyrene system, $\Delta\rho/\rho = 852$, $E_c < 1.2$ and there were eight sets of data. For the air jet-sand system, $\Delta\rho/\rho = 2171$, $E_c < 1.4$ and there were twelve sets of data. Figures 4-13 and 4-14 respectively show the effects of density difference on the maximum static scour depth and the scour hole radius. The trends are different from that of water jets on sand/gravel beds. At higher values of E_c, the scour length scales appear to have the highest values for the air jet-sand system. An attempt was made to develop equations for the maximum scour depth and the scour hole radius that can be used for different values of $\Delta\rho/\rho$. In order to achieve this, these data and those from the water jet-sand system were correlated with erosion parameter E_c and $\Delta\rho/\rho$. Although, $\Delta\rho/\rho$ is contained in E_c to give it a physical meaning, its separate inclusion in the correlation is to account for the effect of the mode of transport in the different fluid-sediment systems on the characteristic lengths of scour. Equations (4-20) and (4-21) were obtained respectively for the maximum scour depth and the scour hole radius. A plot of the measured scour depths against their predicted values is shown in Figure 4-15. A similar plot for the scour hole radius is shown in Figure 4-16.

$$\frac{\varepsilon_{m\infty}}{h} = 0.05\ \left(E_c - 0.14\right)^{0.6} \frac{\left(\frac{\Delta\rho}{\rho}+1\right)^{3.1}}{\left(\frac{\Delta\rho}{\rho}\right)^{2.8}} \tag{4-20}$$

$$\frac{r_{0\infty}}{h} = 11\ E_c^{0.65} \frac{\left(\frac{\Delta\rho}{\rho}\right)^{6.2}}{\left(\frac{\Delta\rho}{\rho}+1\right)^{6.6}} \tag{4-21}$$

4.11 Conclusions

The asymptotic characteristic lengths of an eroded sand/gravel bed profile under submerged circular impinging vertical turbulent jets of water

have been analyzed for the erosion parameter E_C less than 5. Using data from this study and from other researchers, these lengths were found to be mainly functions of the erosion parameter. Using the maximum scour depth as the length scale, the non-dimensional asymptotic eroded bed profiles were found to be very similar except at very low values of the erosion parameter. Another length scale was introduced to achieve similarity for all values of the erosion parameter.

The variation of both the dynamic and the static scour depth with impinging distance was studied. Two different flow regimes were observed and the conditions in which they exist were determined. These regimes are the Strongly Deflected Jet Regime (SDJR) and the Weakly Deflected Jet Regime (WDJR) and they were found to exist in the region $E_C > 0.35$ and $E_C < 0.35$ respectively. It was also found that the maximum static scour depth occurs approximately when the regime changes ($E_C \cong 0.35$). At incipient motion E_C was estimated to be 0.12. Equations were developed for the maximum scour depth and the scour hole radius that can be used for different values of the relative density difference $\Delta\rho/\rho$ using data from the literature on water and air jets impinging on loose beds of sand and polystyrene and this study.

4.12 References

Beltaos, S. and Rajaratnam, N. (1974), Impinging Circular Turbulent Jets, Journal of Hydraulic Engrg., ASCE, Vol. 100, No 10, 1313 - 1328.

Blaisdell, F.W. and Anderson, C.L. (1988a), A Comprehensive Generalized Study of Scour at Cantilevered Pipe Outlets I. Background, Journal of Hydraulic Research, Vol. 26, No. 4, pp. 357 - 376.

Blaisdell, F.W. and Anderson, C.L. (1988b), A Comprehensive Generalized Study of Scour at Cantilevered Pipe Outlets II. Results, Journal of Hydraulic Research, Vol. 26, No. 5, pp. 509 - 524.

Chee, S.P. and Yuen, E.M. (1985), Erosion of Unconsolidated Gravel Beds, Canadian Journal of Civil Engineering, 12. pp. 559 - 566.

Chiew Y. and Parker, G. (1994), Incipient Sediment Motion on Non-horizontal Slopes, Journal of Hydraulic Research, Vol. 32, No. 5, pp. 649 - 660.

Clarke, F.R.W. (1962), The Action of Submerged Jets on Movable Material, M. Sc. Thesis, University of London, U. K., 202 p.

Doddiah, D., Albertson, M., and Thomas, R. (1953), Scour from Jets, Proceedings Minnesota International Hydraulics Convention, Minneapolis, USA, pp. 161-169.

Johnson, G. (1967), The Effect of Entrained Air on the Scouring Capacity of Water Jets, Proceedings 12th IAHR Congress, Fort Collins, USA, pp. 218 - 226.

Kobus, H., Leister, P. and Westrich, B. (1979), Flow Field and Scouring Effects of Steady and Pulsating Jets Impinging on a movable Bed, Journal of Hydraulic Research, Vol. 17, No. 3, pp. 175 - 192.

Mih, W.C. and Kabir, J. (1983), Impingement of Water jets on Non uniform Streambed, Journal of Hydraulic Engineering, ASCE, 109(4), pp. 536 - 548.

Poreh, M. and Hefez, E. (1967), Initial Scour and Sediment Motion due to an Impinging Jet, Proceedings, Twelfth Congress, IAHR, Vol. 3, Fort Collins, USA, pp. 9 - 16.

Rajaratnam, N. (1982), Erosion by Submerged Circular Jets, Journal of Hydraulics Division, ASCE, Vol. 108, No. HY2, pp. 262 - 267.

Rajaratnam, N. and Beltaos, S. (1977), Erosion by Impinging Circular Turbulent Jets, Journal of Hydraulics Division, ASCE, Vol. 103, No. HY10, pp. 1191 - 1205.

Rajaratnam, N., Johnston, G. A. and Barber, M. A. (1993), Energy Dissipation by Jet Diffusion in Storm water Drop Shafts, Canadian Journal of Civil Engineering, Vol. 20, No. 3, pp. 374 - 379.

Rouse H. (1939), Criteria for Similarity in the Transportation of Sediment. Bulletin 20, University of Iowa, Iowa, USA, pp. 33 - 49.

Shafai-Bajestan, M. and Albertson, M. L. (1993), Riprap Criteria Below Pipe Outlet, Journal of Hydraulic Engineering, ASCE, Vol. 119, No. 2, pp. 181 - 200.

Vanoni, V.A. (1975), Sedimentation Engineering, ASCE - Manuals and Reports on Engineering Practice - N0. 54, 745p.

Westrich, B. and Kobus, H. (1973), Erosion of a Uniform Sand Bed by Continuous and Pulsating Jets, Proceedings IAHR, Vol. 1, Istanbul, Turkey, pp. A13 1-8.

Table 4-1: Experimental Results

#	Time (hr.)	D (mm)	d (mm)	U_o (m/s)	h (mm)	$\varepsilon_{m\infty}$ (mm)	$\varepsilon'_{m\infty}$ (mm)	$r_{o\infty}$ (mm)	b_∞ (mm)	Δ_∞ (mm)	$r_{1\infty}$ (mm)	h/d	$\varepsilon_{m\infty}/d$	$\varepsilon'_{m\infty}/d$	E_c
1	21	0.88	4	2.74	18	10.9	-	26.5	12	1.55	50	4.5	2.73	-	
2	20	0.88	4	2.74	22	11	-	19	10	3.3	45	5.5	2.75	-	
3	21	0.88	4	2.74	42	16.8	56.0	28.5	13	4.65	44	10.5	4.20	14.01	2.18
4	25	0.88	4	2.74	63	16.8	44.0	28	13	2.75	42.5	15.8	4.20	10.99	1.46
5	22	0.88	4	2.74	103	17.5	35.3	32.5	16	5.9	45	25.8	4.38	8.83	0.89
6	20	0.88	4	2.74	128	23.4	37.1	39	18.5	7.1	57.5	32.0	5.85	9.27	0.72
7	48	0.88	4	2.74	148	29.6	39.3	50	23.5	8.5	72.5	37.0	7.40	9.83	0.62
8	42	0.88	4	2.74	193	30.2	39.7	54.5	27.5	10.8	77.5	48.3	7.55	9.93	0.48
9	44	0.88	4	2.74	238	31.4	-	58.5	30	10	87	59.5	7.85	-	0.39
10	44	0.88	4	2.74	283	31.5	-	58	33	11.95	90	70.8	7.88	-	0.32
11	50	0.88	4	2.74	328	29.2	29.2	61	35.5	10.8	91.25	82.0	7.30	7.30	0.28
12	46	0.88	4	2.74	373	24.3	24.3	60.5	40.5	10.85	92.5	93.3	6.08	6.08	0.25
13	45	0.88	4	2.74	423	14.4	14.4	57.5	38.5	6.8	91	105.8	3.60	3.60	0.22
14	47	0.88	4	2.74	483	4.8	4.8	44	27	4.35	80	120.8	1.20	1.20	0.19
15	24	2.42	4	2.74	83	21	35.5	28.20	14.10	1.10	37.50	20.8	5.25	8.88	0.67
16	23	2.42	4	2.74	118	21.5	35.2	29.75	18.00	4.25	42.50	29.5	5.38	8.80	0.47
17	23	2.42	4	2.74	148	27.5	30.7	38.60	22.20	4.49	53.50	37.0	6.88	7.67	0.37
18	19	2.42	4	2.74	193	24.2	24.2	42.00	23.75	6.90	55.00	48.3	6.05	6.05	0.29
19	20	2.42	4	2.74	243	18.8	18.8	46.50	34.10	7.40	62.50	60.8	4.70	4.70	0.23
20	24	2.42	4	2.74	283	18.2	18.2	47.00	31.50	6.05	65.00	70.8	4.55	4.55	0.20
21	29	2.42	4	2.74	323	14.5	14.5	48.00	30.00	3.60	65.00	80.8	3.63	3.63	0.17
22	20	2.42	4	2.74	353	5.8	5.8	45.00	24.00	1.70	65.00	88.3	1.45	1.45	0.16
23	23	2.42	4	2.74	403	1.5	1.5	-	-	-	-	100.8	0.38	0.38	0.14
24	6	2.42	8	2.74	65	23.7	63.0	37.50	22.80	3.75	48.75	8.1	2.96	7.87	1.70
25	17	2.42	8	2.74	108	25.8	60.8	37.80	23.00	4.75	47.50	13.5	3.23	7.60	1.02
26	23	2.42	8	2.74	144	33.5	55.2	45.00	24.80	5.55	60.00	18.0	4.19	6.90	0.77
27	22	2.42	8	2.74	179	40	47.7	60.00	28.50	8.75	81.25	22.4	5.00	5.96	0.62
28	22	2.42	8	2.74	218	44	49.7	65.00	33.40	11.15	95.00	27.3	5.50	6.21	0.51
29	22	2.42	8	2.74	257	45	50.3	71.50	40.00	12.00	107.50	32.1	5.63	6.29	0.43
30	20	2.42	8	2.74	303	43.7	46.1	73.50	43.20	13.30	107.50	37.9	5.46	5.76	0.37
31	20	2.42	8	2.74	353	41	41.0	79.00	51.70	17.15	115.00	44.1	5.13	5.13	0.31
32	27	2.42	8	2.74	433	33.5	33.5	85.00	56.40	13.25	117.50	54.1	4.19	4.19	0.26
33	28	2.42	8	2.74	503	28	28.0	87.00	59.50	11.50	120.00	62.9	3.50	3.50	0.22

Table 4-1: Experimental Results (Continued)

#	Time (hr.)	D (mm)	d (mm)	U_o (m/s)	h (mm)	$\varepsilon_{m\infty}$ (mm)	$\varepsilon'_{m\infty}$ (mm)	$r_{o\infty}$ (mm)	b_∞ (mm)	Δ_∞ (mm)	$r_{1\infty}$ (mm)	h/d	$\varepsilon_{m\infty}/d$	$\varepsilon'_{m\infty}/d$	E_c
34	21	2.42	4	3.68	65	21.5	46.0	31.50	16.50	0.80	57.50	16.3	5.38	11.49	1.14
35	27	2.42	4	3.68	103	24.3	35.5	34.00	18.00	2.85	52.50	25.8	6.08	8.87	0.72
36	19	2.42	4	3.68	158	28.3	40.4	44.00	24.40	6.75	62.50	39.5	7.08	10.11	0.47
37	19	2.42	4	3.68	191	31.5	39.8	51.00	28.50	5.70	70.00	47.8	7.88	9.95	0.39
38	23	2.42	4	3.68	266	29	29.0	55.00	35.20	11.15	80.00	66.5	7.25	7.25	0.28
39	20	2.42	4	3.68	300	28.5	28.5	60.20	29.70	10.00	78.75	75.0	7.13	7.13	0.25
40	21	2.42	4	3.68	339	23	23.0	61.50	44.00	9.25	82.50	84.8	5.75	5.75	0.22
41	19	2.42	4	3.68	393	19.5	19.5	63.00	39.50	6.50	85.00	98.3	4.88	4.88	0.19
42	15	2.42	4	3.68	432	12	12.0	56.00	37.00	4.40	80.00	108.0	3.00	3.00	0.17
43	15	2.42	4	3.68	479	4.5	4.5	42.50	28.50	1.75	66.25	119.8	1.13	1.13	0.16
44	16	2.42	4	3.68	523	2.1	2.1	47.50	32.50	1.25	77.50	130.8	0.53	0.53	0.14
45	22	0.88	4	3.78	293	38.5	-	72.5	35	14	105	73.3	9.63	-	0.43
46	22	0.88	4	3.78	324	37.5	-	72.5	40	14.6	105	81.0	9.38	-	0.39
47	20	0.88	4	3.78	365	38	-	73.5	40.4	11.85	110	91.3	9.50	-	0.35
48	20	0.88	4	3.78	457	36	-	87.5	55	13.25	125	114.3	9.00	-	0.28
49	22	0.88	8	3.78	4	24	-	80	35	-	-	0.5	3.00	-	
50	15	0.88	8	3.78	11	18	-	55	29	5.85	75	1.4	2.25	-	
51	22	0.88	8	3.78	32	20.7	-	56.25	30.6	5.95	90	4.0	2.59	-	
52	18	0.88	8	3.78	49	24	-	60	32.4	10.75	97.5	6.1	3.00	-	5.18
53	11	0.88	8	3.78	72	23.8	-	55.5	29.3	10.55	85	9.0	2.98	-	3.52
54	14	0.88	8	3.78	107	33	-	68	29.15	9	95	13.4	4.13	-	2.37
55	14	0.88	8	3.78	137	35	-	64	28.2	10.35	97.5	17.1	4.38	-	1.85
56	16	0.88	8	3.78	179	47	-	81	34.5	9.85	115	22.4	5.88	-	1.42
57	20	0.88	8	3.78	227	54.5	-	95	42.4	16.1	139.5	28.4	6.81	-	1.12
58	21	0.88	8	3.78	412	70	-	131.5	67.4	25.35	192.5	51.5	8.75	-	0.62
60	45	0.88	8	4.45	69	38.3	122.8	73	31	13.8	115	8.6	4.79	15.35	4.32
61	52	0.88	8	4.45	83	35	115.2	68.5	27	13.3	115	10.4	4.38	14.40	3.60
62	46	0.88	8	4.45	98	38.8	114.2	72.5	28.5	11.6	110	12.3	4.85	14.28	3.04
63	68	0.88	8	4.45	110	40.5	120.0	80	32.5	15.25	122.5	13.8	5.06	15.00	2.71
64	44	0.88	8	4.45	133	43.8	115.1	80	32	11.5	115	16.6	5.48	14.39	2.24
65	45	0.88	19	4.45	205	83.7	198.3	173.4	70	27.2	234.5	10.8	4.41	10.44	3.46
66	42	0.88	12	4.45	206	74	135.0	144	63	18.75	192.5	17.2	6.17	11.25	2.17
67	43	0.88	12	4.45	168	61.5	155.1	120	53	15.3	168.5	14.0	5.13	12.92	2.66
68	43	0.88	12	4.45	138	55	155.2	121	53.5	17.65	168.5	11.5	4.58	12.93	3.24

Table 4-2: Experimental Results of other researchers

Table 4-2a: Rajaratnam and Beltaos (1977)

#	Series	Expt. #	U_o (m/s)	d (mm)	D (mm)	h (mm)	$\varepsilon_{m\infty}$ (mm)	$r_{o\infty}$ (mm)	$r_{1\infty}$ (mm)	h/d	$\varepsilon_{m\infty}/h$	$r_{o\infty}/h$	$r_{1\infty}/h$	E_c
1	Air Jets	111	65.99	6.43	0.26	237.7	61.0	106.7	115.8	37.00	0.26	0.45	0.49	0.75
2	on Sand	121	43.28	6.43	0.26	240.8	30.5	54.9	54.9	37.47	0.13	0.23	0.23	0.49
3		122	52.73	6.43	0.26	240.8	43.0	79.2	79.2	37.47	0.18	0.33	0.33	0.60
4		123	66.39	6.43	0.26	240.8	73.5	128.0	134.1	37.47	0.31	0.53	0.56	0.75
5		124	77.57	6.43	0.26	240.8	81.1	146.3	152.4	37.47	0.34	0.61	0.63	0.88
6		131	20.30	6.43	0.26	106.7	22.3	33.5	45.7	16.60	0.21	0.31	0.43	0.52
7		132	32.06	6.43	0.26	106.7	46.3	79.2	88.4	16.60	0.43	0.74	0.83	0.82
8		133	43.28	6.43	0.26	106.7	68.6	121.9	131.1	16.60	0.64	1.14	1.23	1.10
9		134	52.73	6.43	0.26	106.7	77.1	137.2	158.5	16.60	0.72	1.29	1.49	1.34
10		141	52.73	6.43	0.26	323.1	26.8	85.3	91.4	50.28	0.08	0.26	0.28	0.44
11		142	77.57	6.43	0.26	323.1	59.7	121.9	128.0	50.28	0.18	0.38	0.40	0.65
12		143	99.06	6.43	0.26	323.1	102.1	189.0	-	50.28	0.32	0.58		0.83
13	Air Jets on	211	25.30	6.43	1.4	106.7	17.4	64.0	-	16.60	0.16	0.60	-	0.44
14	Polystyrene	212	46.33	6.43	1.4	106.7	25.3	100.6	-	16.60	0.24	0.94	-	0.81
15		213	65.99	6.43	1.4	106.7	32.0	125.0	-	16.60	0.30	1.17	-	1.16
16		221	25.30	6.43	1.4	152.4	11.0	73.2	-	23.72	0.07	0.48	-	0.31
17		231	46.33	6.43	1.4	237.7	20.4	79.2	-	37.00	0.09	0.33	-	0.36
18		232	65.99	6.43	1.4	237.7	43.3	97.5	-	37.00	0.18	0.41	-	0.52
19		241	15.18	23.50	1.4	222.5	38.4	106.7	125.0	9.47	0.17	0.48	0.56	0.47
20		242	20.51	23.50	1.4	222.5	51.8	143.3	167.6	9.47	0.23	0.64	0.75	0.63
21		243	34.26	23.50	1.4	222.5	-	204.2	274.3	9.47	-	0.92	1.23	1.05

Table 4-2b: Rajaratnam (1982)

#	Series	Expt. No.	U_o (m/s)	d (mm)	D (mm)	h (mm)	$\varepsilon_{m\infty}$ (mm)	$\varepsilon'_{m\infty}$ (mm)	$r_{o\infty}$ (mm)	$r_{1\infty}$ (mm)	Δ_∞ (mm)	b_∞ (mm)	h/d	E_c	$\varepsilon_{m\infty}/h$	$\varepsilon'_{m\infty}/h$
1	Water jets	11	3.11	9.8	2.38	171.5	41.8	57.9	109.8	-	11.3	31.2	17.50	0.91	0.24	0.34
2	on Sand	12	3.48	9.8	2.38	279.4	78.3	78.3	112.8	-	24.1	51.7	28.51	0.62	0.28	0.28
3		13	3.23	9.8	2.38	247.7	63.4	69.5	91.4	137.2	22.6	41	25.28	0.65	0.26	0.28
4		14	2.99	9.8	2.38	174.8	49.1	58.8	65.5	91.4	11.6	34	17.84	0.85	0.28	0.34
5		15	4.54	9.8	2.38	225.6	61.6	88.1	88.3	128	16.2	49	23.02	1.00	0.27	0.39
6		16	4.38	9.8	2.38	149.2	50.3	-	70.1	94.5	10.4	36	15.22	1.47	0.34	-
7		17	4.60	9.8	1.2	250.8	79.3	108.8	129.8	175.3	24.7	55	25.59	1.29	0.32	0.43
8		18	3.36	9.8	1.2	276.2	71.6	86	121.9	164.6	24.4	57	28.18	0.86	0.26	0.31
9		19	3.00	9.8	1.2	200.0	56.7	72.5	88.4	128	18	45	20.41	1.05	0.28	0.36

Table 4-2c: Clarke (1962)

#	Expt.#.	Time (hr.)	U_o (m/s)	d (mm)	h (mm)	D (mm)	ε_m (mm)	r_o (mm)	r_1 (mm)	Δ (mm)	ε_m/h	r_o/h	h/d	E_c
1	13.0	8.7	3.03	4.78	127	0.82	-	62.9	87.6	14.0	-	0.50	26.57	0.99
2	12.0	125.0	1.71	4.78	127	0.82	-	54.5	78.4	13.2	-	0.43	26.57	0.56
3	15.0	2.3	3.28	4.78	127	0.82	-	61.7	86.6	14.5	-	0.49	26.57	1.07
4	16.0	1.0	1.20	4.78	127	0.82	-	40.6	57.3	10.9	-	0.32	26.57	0.39
5	9.0	3.3	2.86	4.78	127	0.82	-	56.6	79.9	12.2	-	0.45	26.57	0.93
6	24.0	3.0	7.43	4.78	127	0.82	27.9	102.1	145.5	22.4	0.22	0.80	26.57	2.43
7	22.0	2.0	5.08	4.78	127	0.82	22.1	77.5	108.0	18.3	0.17	0.61	26.57	1.66
8	23.0	3.5	6.08	4.78	127	0.82	25.7	90.2	125.9	20.1	0.20	0.71	26.57	1.99
9	21.0	4.0	4.12	4.78	127	0.82	19.8	68.3	96.9	17.0	0.16	0.54	26.57	1.34
10	28.0	3.5	2.99	2.38	127	0.82	26.7	52.1	75.6	14.2	0.21	0.41	53.36	0.49
11	26.0	3.0	0.83	4.78	127	0.82	20.3	29.8	46.6	9.4	0.16	0.24	26.57	0.27
12	27.0	3.0	1.63	2.38	127	0.82	19.6	29.8	46.4	9.7	0.15	0.24	53.36	0.27
13	25.0	4.7	8.16	4.78	127	0.82	34.5	114.0	161.3	25.7	0.27	0.90	26.57	2.67
14	32.0	3.0	11.69	2.38	127	0.82	25.4	88.1	121.9	19.8	0.20	0.69	53.36	1.90
15	30.0	3.0	5.03	2.38	127	0.82	19.1	59.1	82.7	14.5	0.15	0.47	53.36	0.82
16	31.0	4.3	8.13	2.38	127	0.82	22.1	70.6	100.3	16.8	0.17	0.56	53.36	1.32
17	29.0	3.0	4.07	2.38	127	0.82	20.3	55.9	80.1	14.2	0.16	0.44	53.36	0.66
18	35.0	1.5	2.17	3.05	127	0.82	-	43.8	66.3	13.0	-	0.35	41.64	0.45
19	33.0	4.5	12.12	3.05	127	0.82	-	108.8	151.8	23.6	-	0.86	41.64	2.53
20	34.0	2.0	8.47	3.05	127	0.82	-	81.9	115.4	18.0	-	0.65	41.64	1.76
21	41.0	1.7	2.41	2.38	127	2.02	20.8	28.6	36.8	-	0.16	0.23	53.36	0.25
22	37.0	5.8	8.13	2.38	127	2.02	-	52.7	69.9	11.2	-	0.42	53.36	0.84
23	39.0	4.3	3.18	2.38	127	2.02	-	36.2	49.5	9.1	-	0.29	53.36	0.33
24	38.0	7.5	4.58	2.38	127	2.02	-	41.3	59.1	11.9	-	0.33	53.36	0.47
25	40.0	4.0	1.97	2.38	127	2.02	15.0	26.7	33.7	5.8	0.12	0.21	53.36	0.20
26	36.0	7.5	11.69	2.38	127	2.02	-	61.5	90.2	16.3	-	0.48	53.36	1.21

Table 4-2d: Wetrich and Kobus (1973)†

D = 1.5 mm

$\varepsilon_{m\infty}/h$	0.06	0.08	0.08	0.10	0.10	0.10	0.10	0.11	0.13	0.15	0.15	0.16	0.20	0.23
E_c	0.18	0.20	0.21	0.23	0.27	0.27	0.29	0.31	0.35	0.38	0.39	0.39	0.46	0.52

† Data were extracted from one of the graphs in their publication

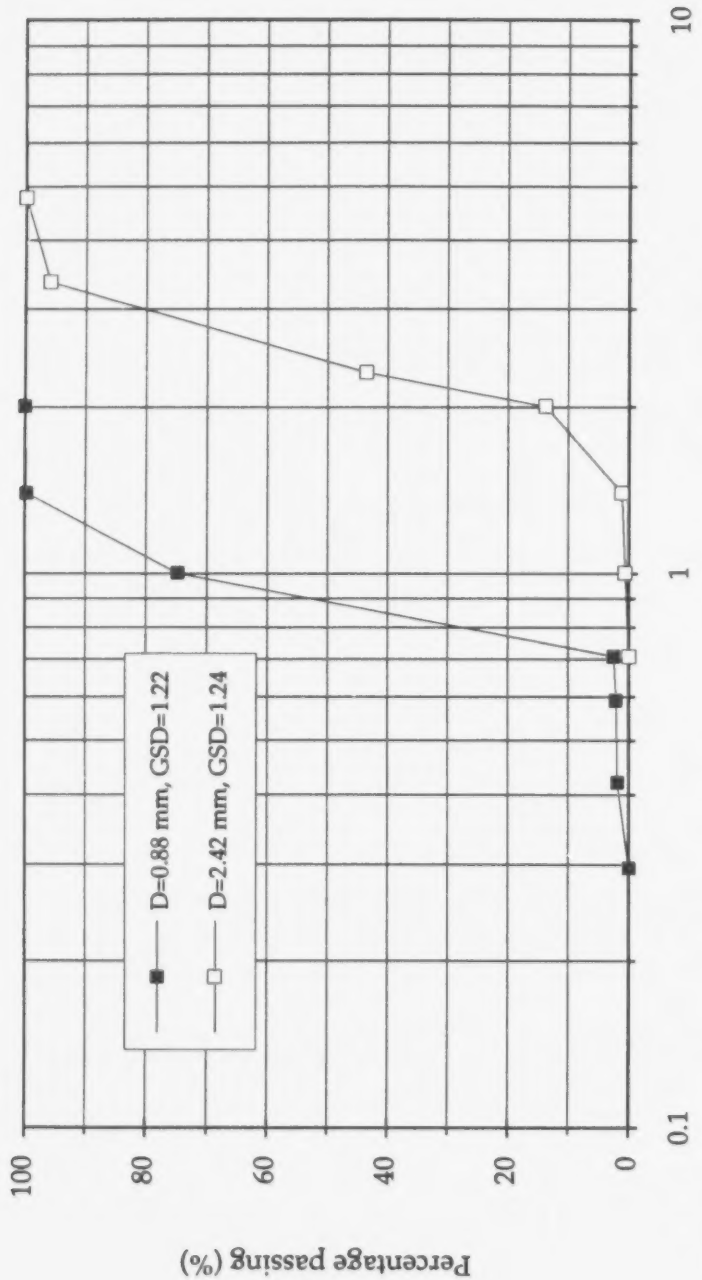

Figure 4-1: Sediment size distribution curves

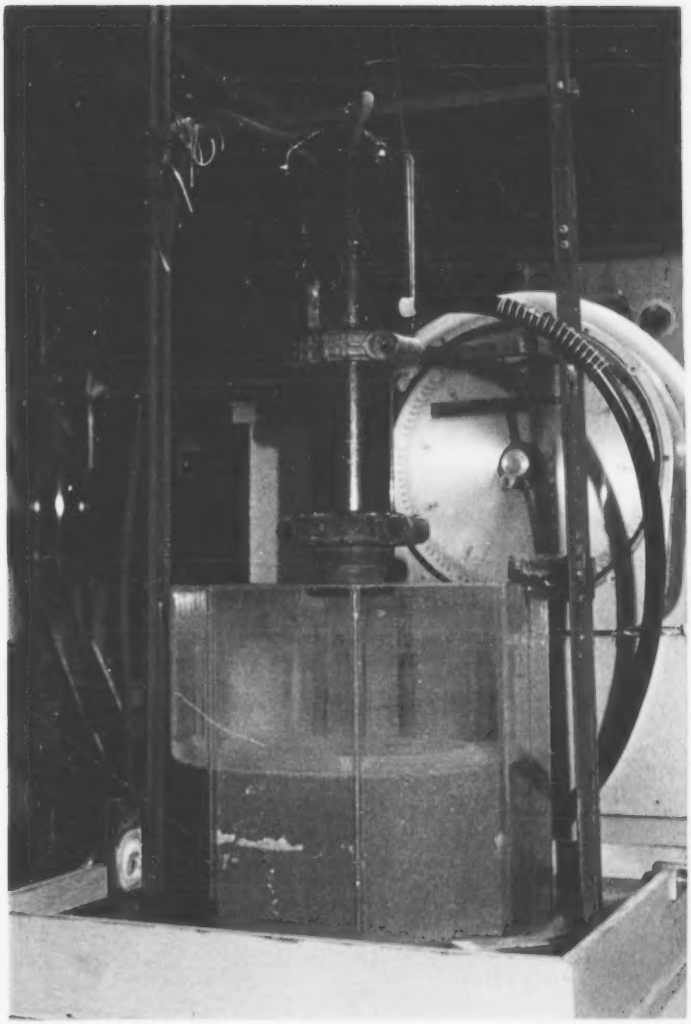

Figure 4-2: Experimental Set-up

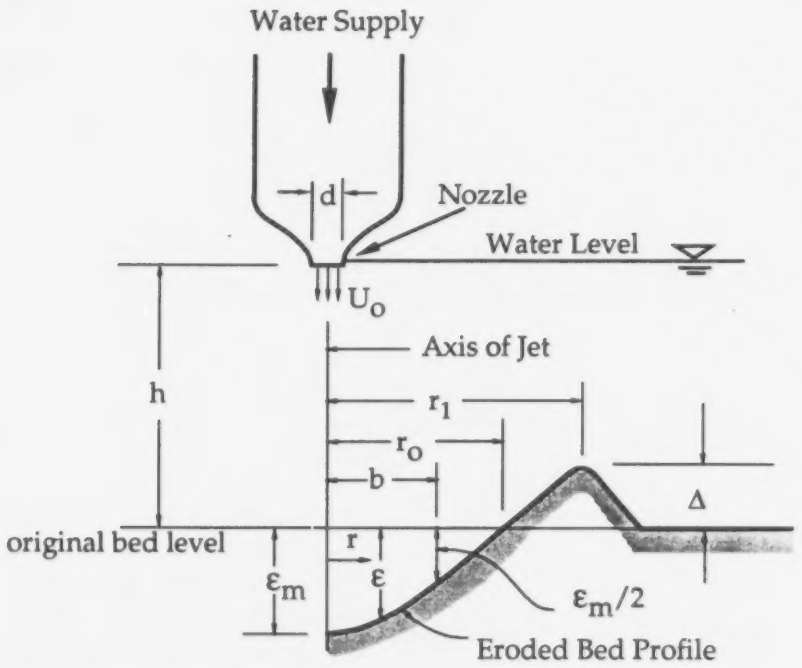

Figure 4-3 Definition Sketch

Figure 4-4a

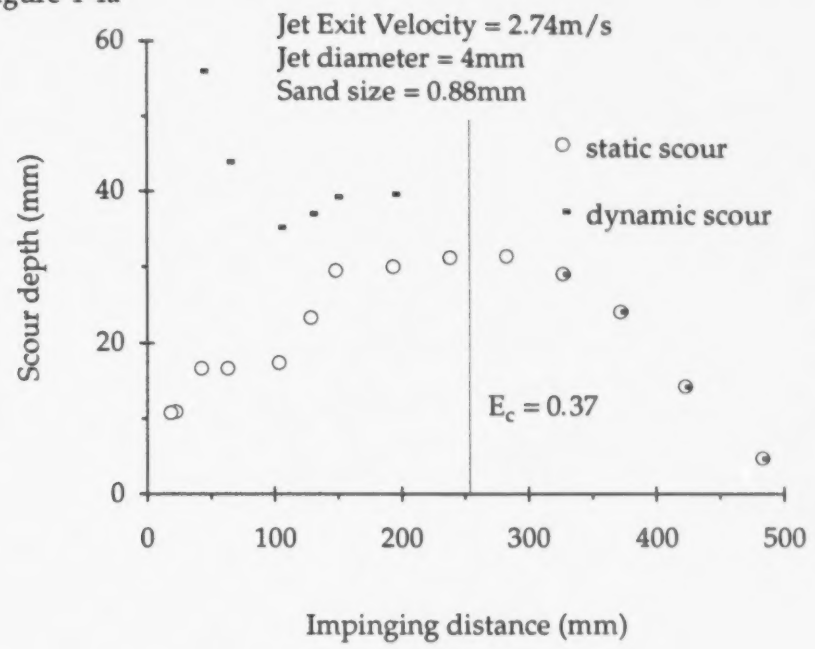

Figure 4-4b

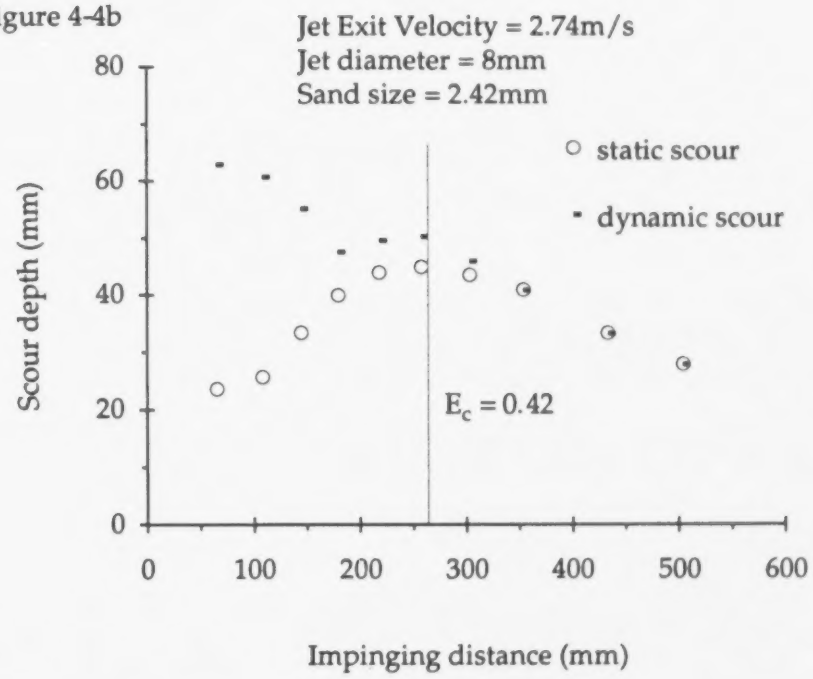

Figure 4-4(a-b): Variation of scour depth with impinging distance

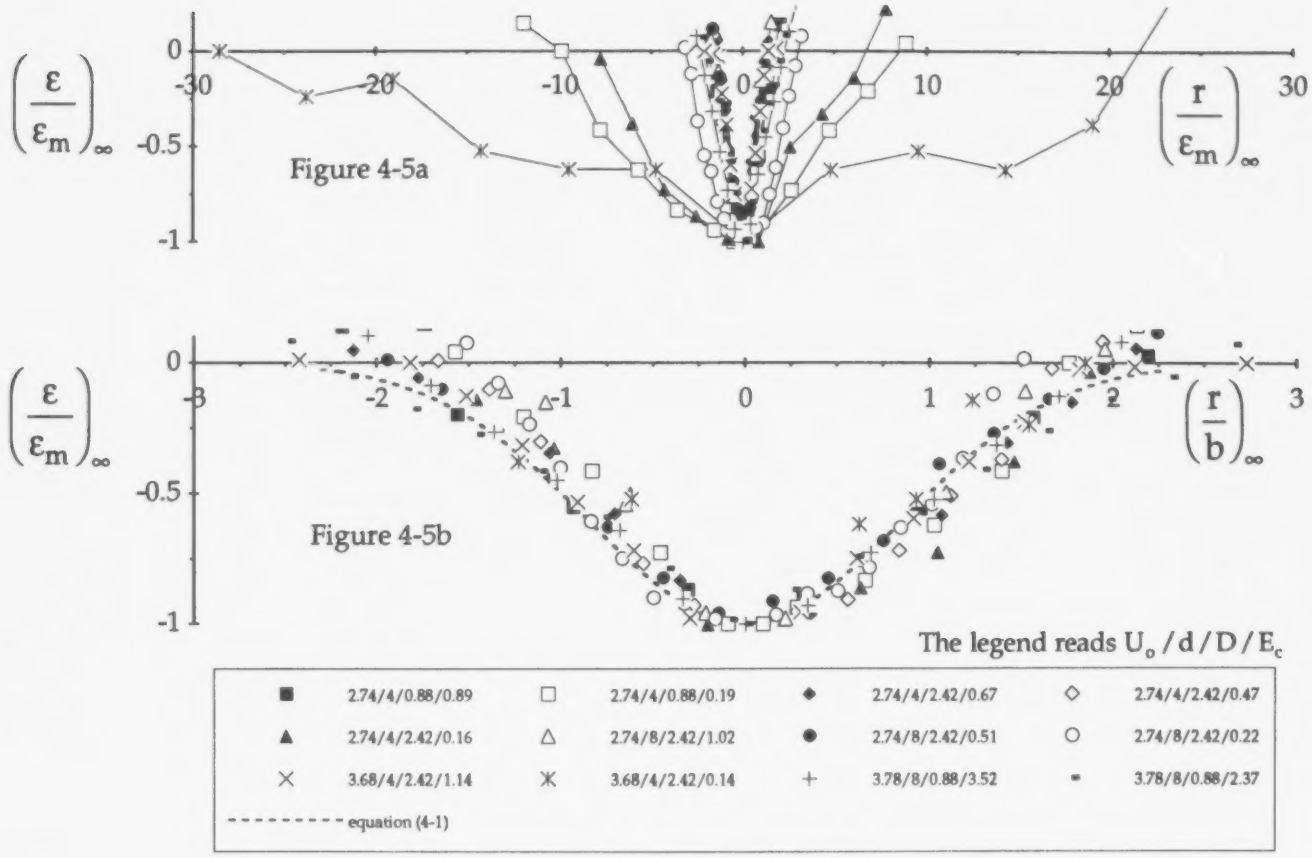

Figure 4-5: Similarity of scour profiles

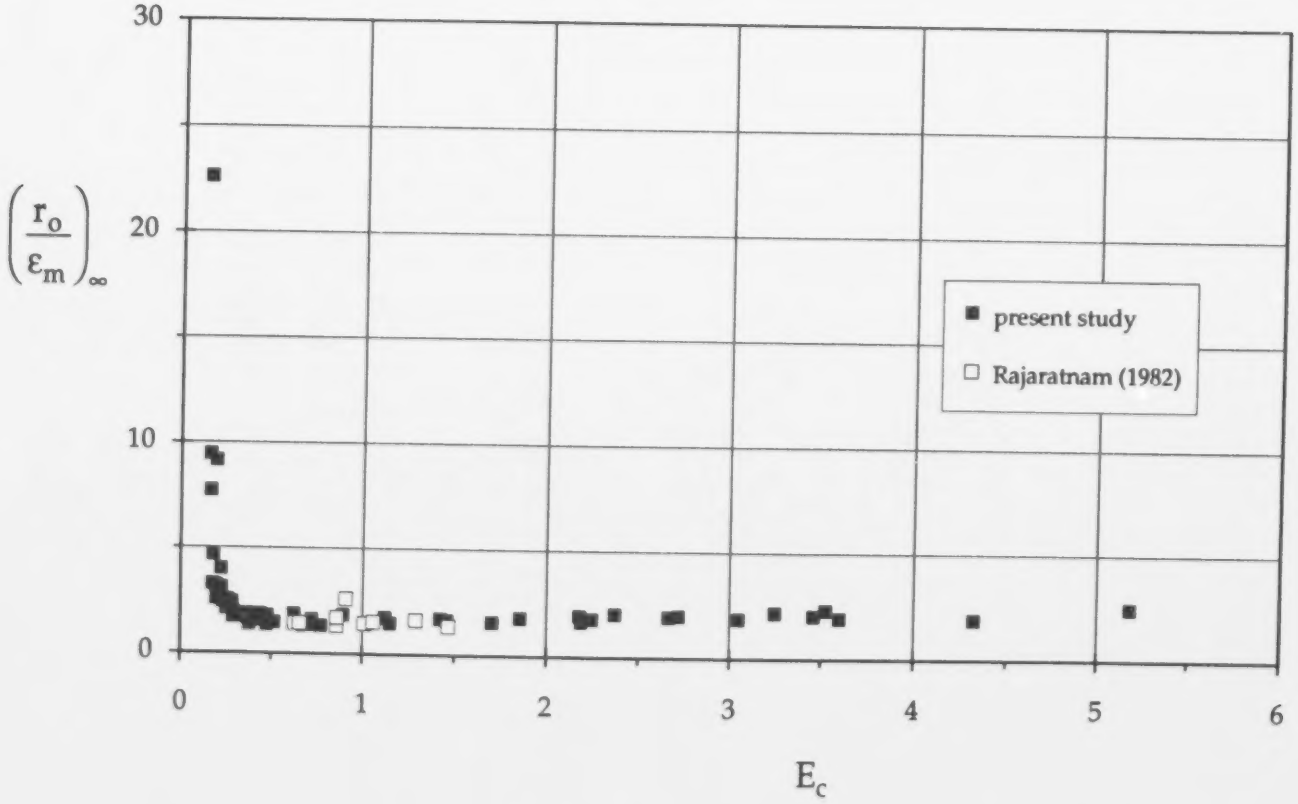

Figure 4 – 6: Variation of $\left(\frac{r_o}{\varepsilon_m}\right)_\infty$ with E_c

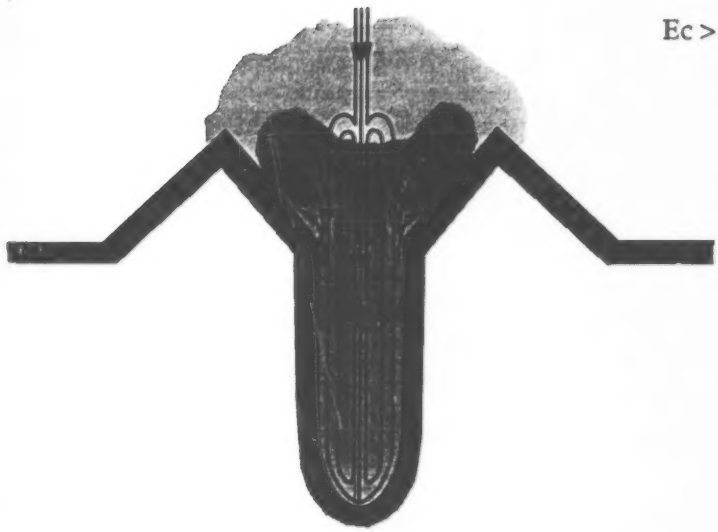

Figure 4-7(a): Strongly Deflected Jet Regime I (SDJR I)

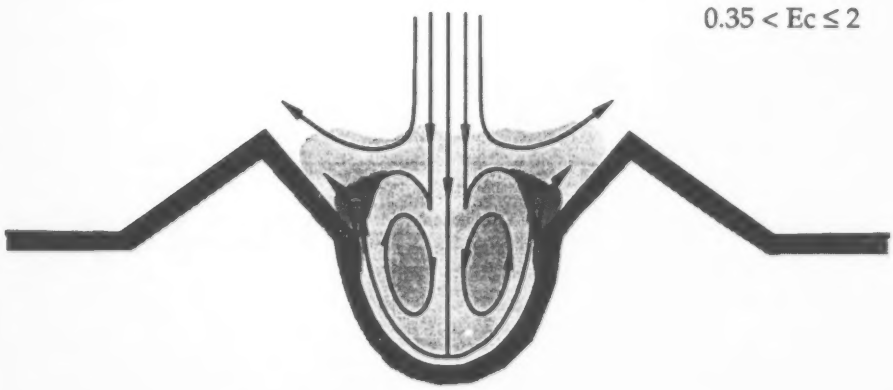

Figure 4-7(b): Strongly Deflected Jet Regime II (SDJR II)

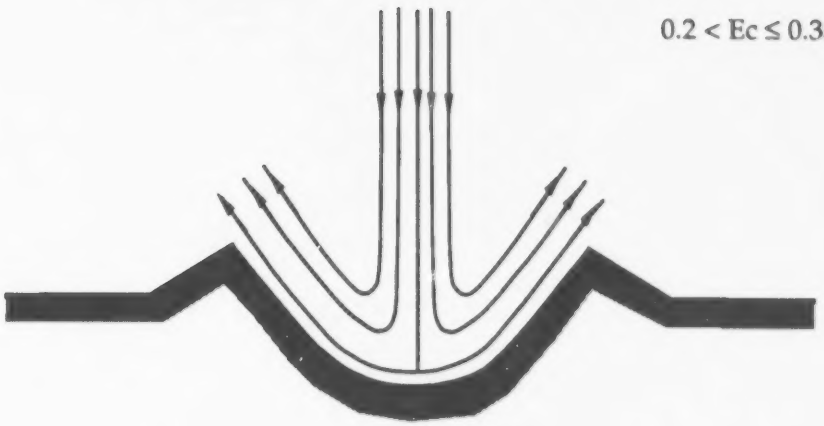

Figure 4-7(c): Weakly Deflected Jet Regime I (WDJR I)

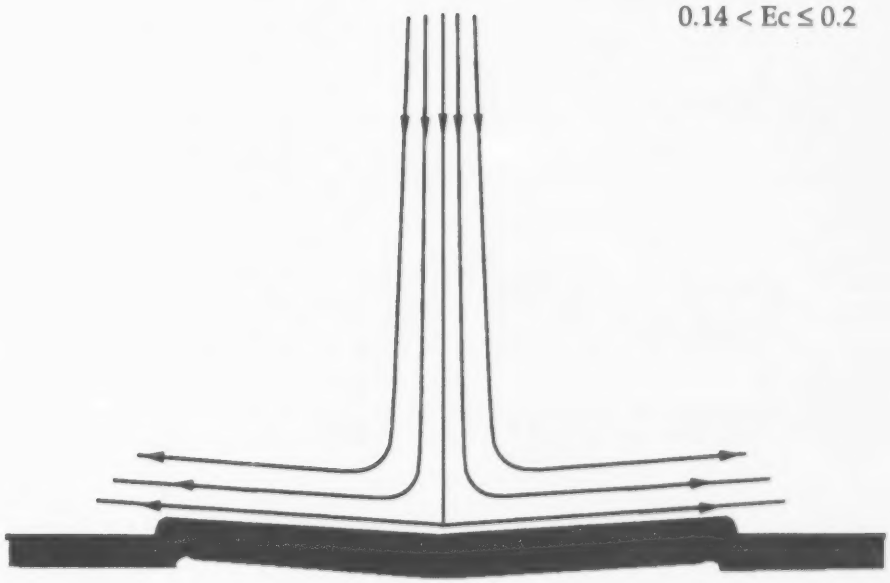

Figure 4-7(d): Weakly Deflected Jet Regime II (WDJR II)

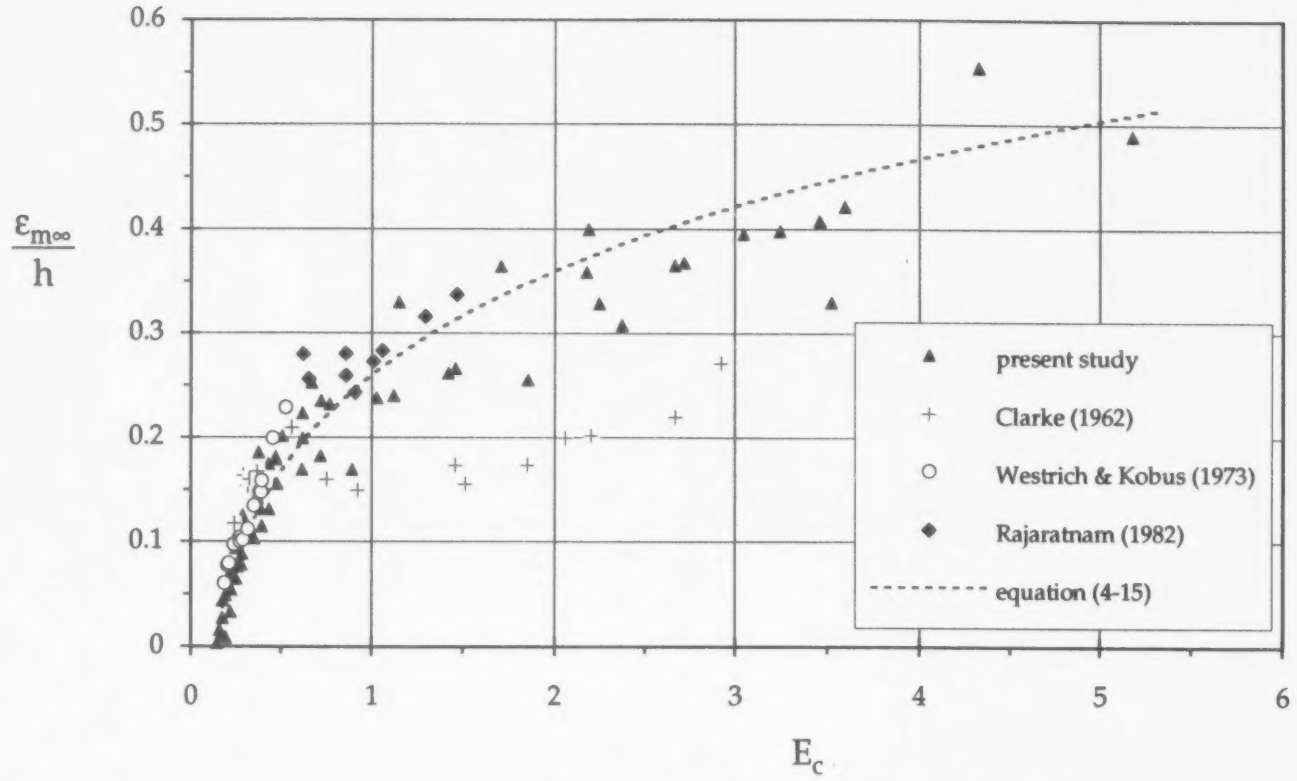

Figure 4 – 8: Variation of relative maximum static scour depth with E_c

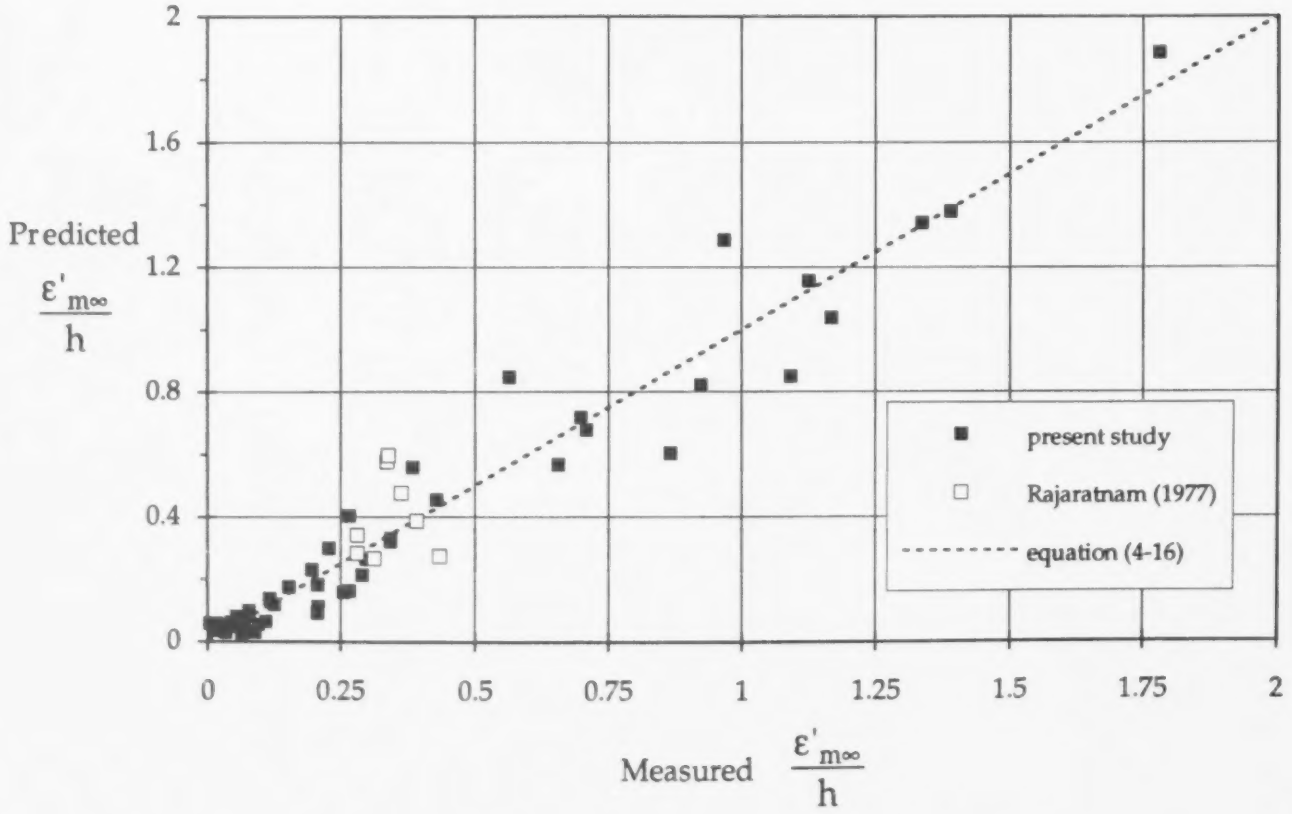

Figure 4-9: Dynamic scour depth

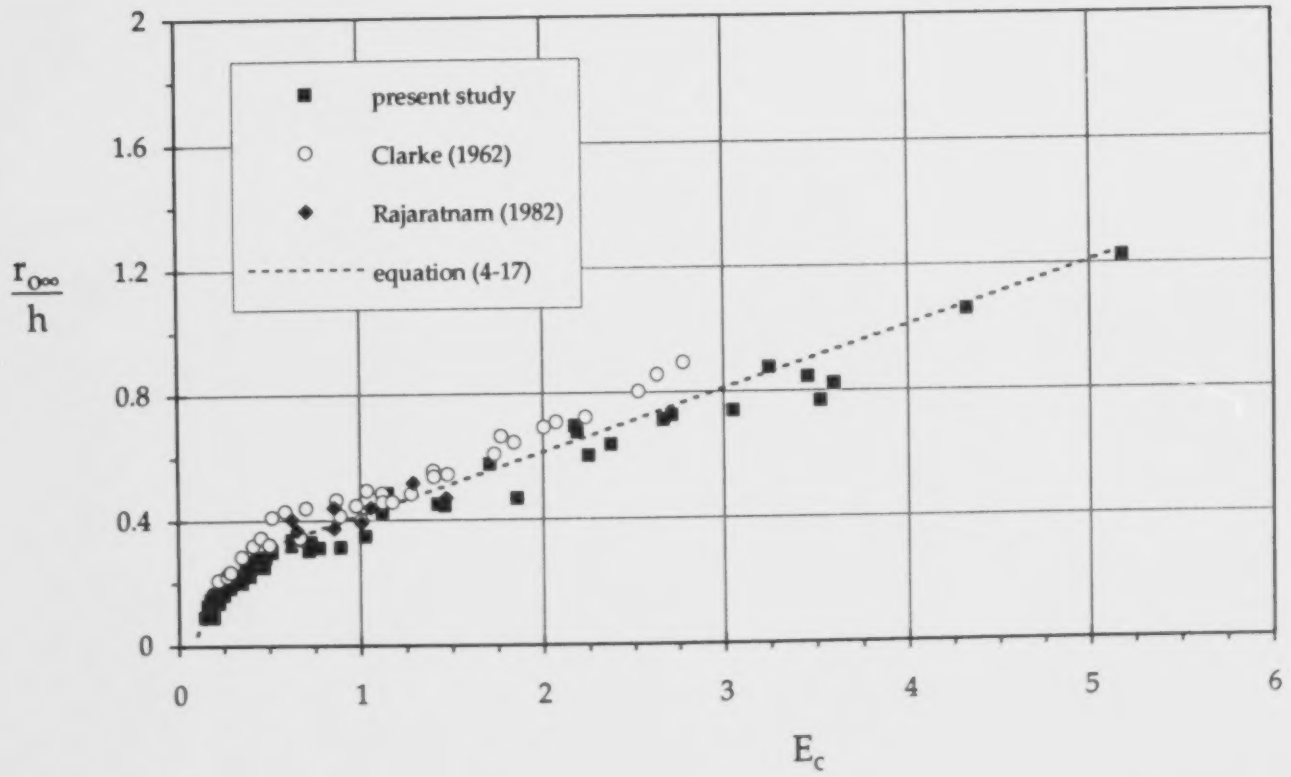

Figure 4 – 10: Variation of scour hole radius with E_c

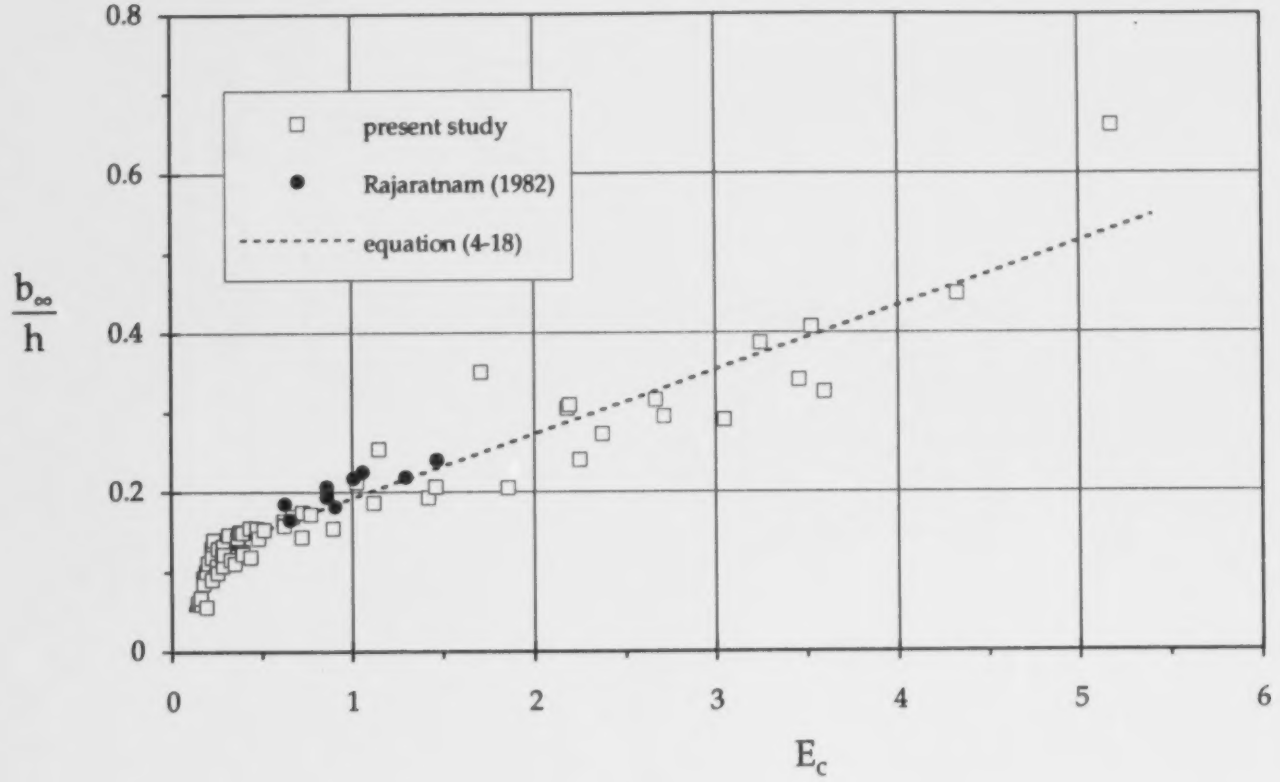

Figure 4–11: Variation of $\frac{b_\infty}{h}$ with E_c

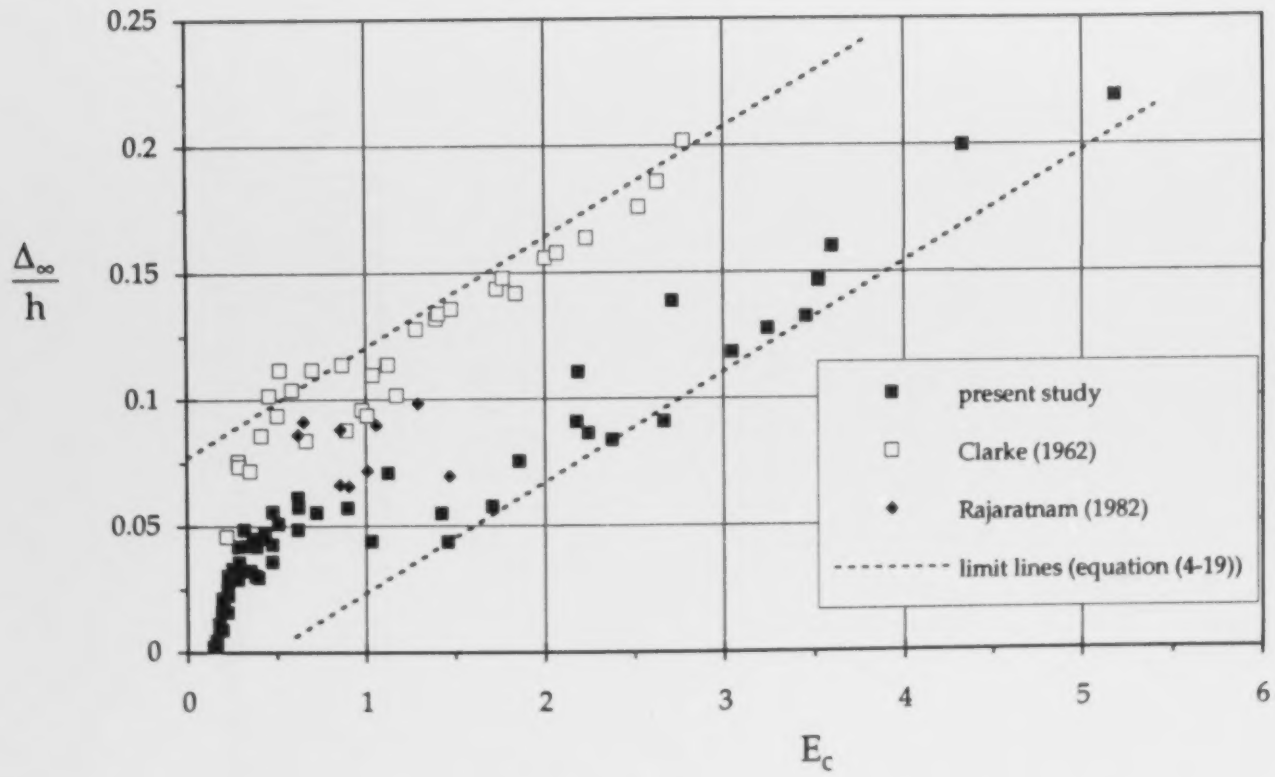

Figure 4 – 12: Variation of ridge (dune) height with E_c

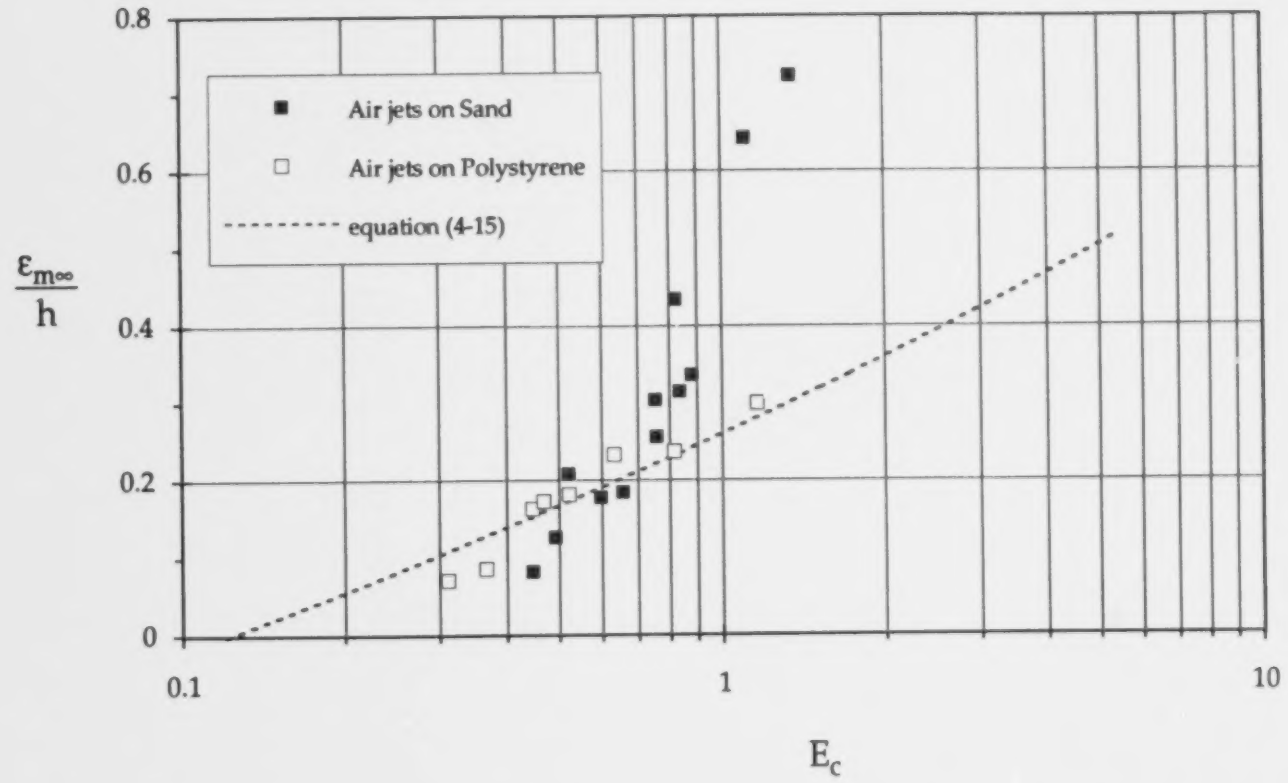

Figure 4 – 13: Variation of maximum static scour depth with E_c for other fluid – sediment systems

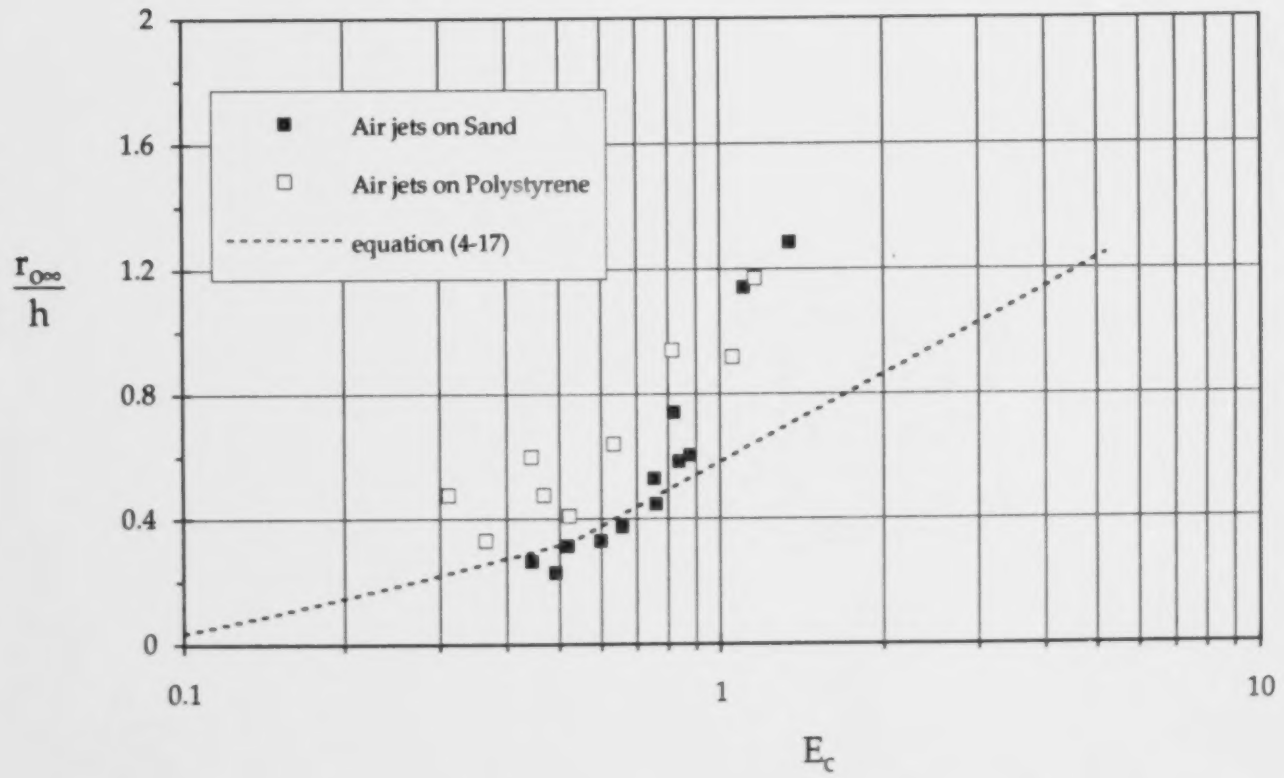

Figure 4 – 14: Variation of scour hole radius with E_c for other fluid – sediment systems

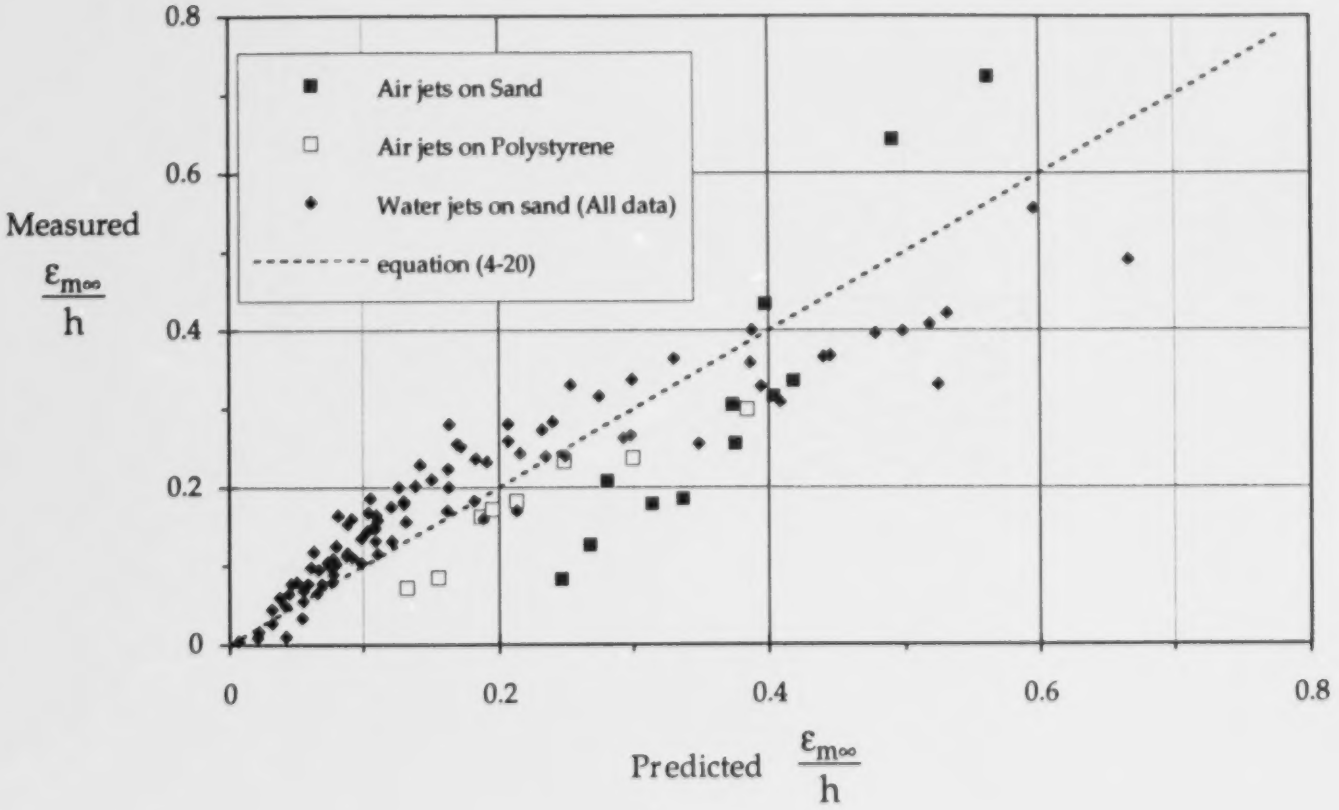

Figure 4-15: Maximum scour depth

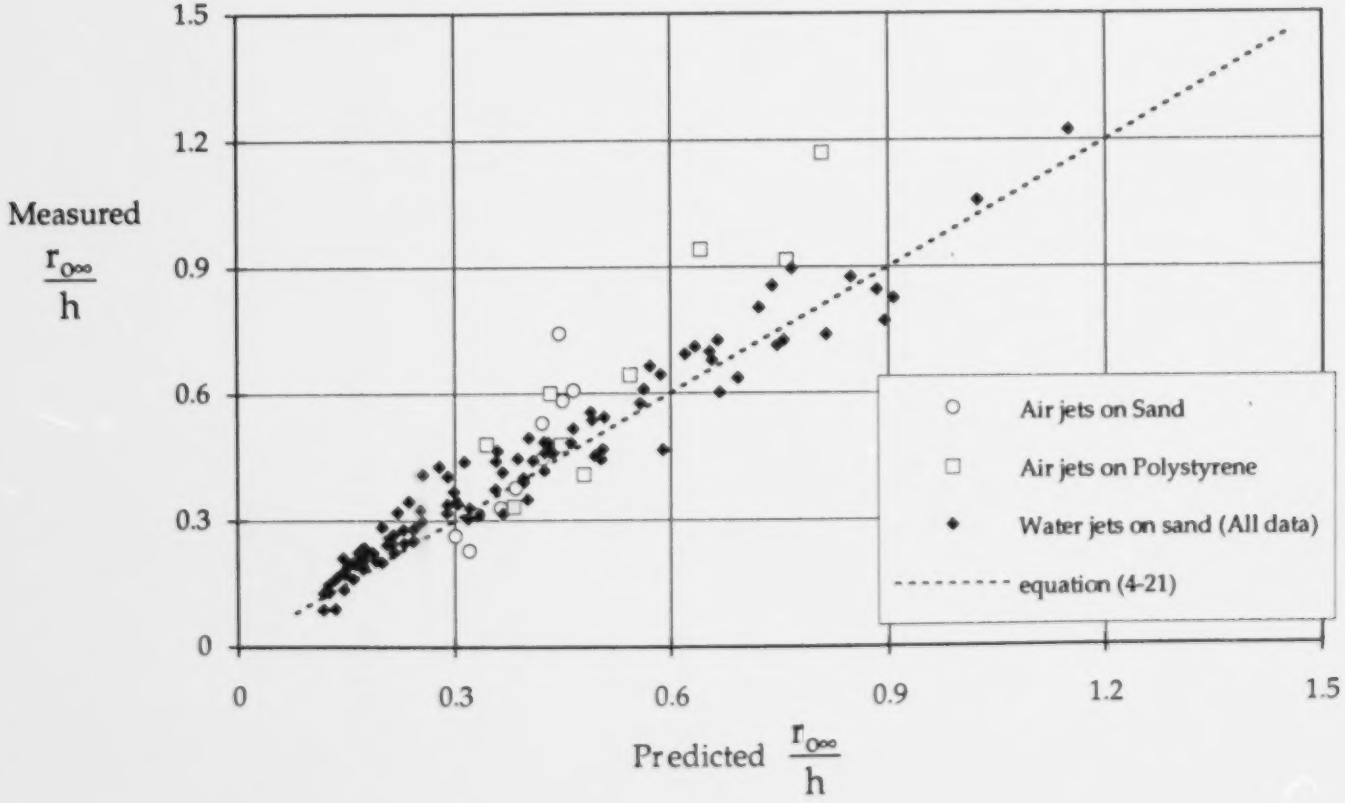

Figure 4-16: Scour hole radius

CHAPTER 5

Effect of Sediment Gradation on Erosion by Plane Turbulent Wall Jets†

5.1 Introduction

Erosion due to plane turbulent submerged wall jets can be found downstream of vertical gates and hydraulic jump stilling basins. The safety of these structures depends on the prediction and control of the localized scour around them. The general approach to estimating the size of the scour hole has been mainly empirical because of the complex nature of the flow and its interaction with the sediment bed. Some of the approaches to this problem can be found in the studies of Valentin (1967), Rajaratnam (1981), Ali and Lim (1986), Uyumaz (1988) and Chatterjee et al. (1994) among others. In most of these studies, nearly uniform sand or gravel was used to model the prototype sediment bed which is generally well-graded (non-uniform).

It is known that when a well-graded sediment bed is subjected to low velocities, the smaller grains are more easily moved while the coarser grains remain in place. If this hydraulic segregation is allowed to continue for some time, the rate of sediment transport will decrease and eventually approach zero. The top layer of the bed will eventually be transformed into a layer of mainly coarser grains with few sheltered smaller grains. This layer, which is referred to as the armor coat, gives the bed a greater resistance to scour.

It is therefore expected that the results based on the study of nearly uniform sand or gravel, having the same median size as the non-uniform sand, would give conservative estimates of the scour hole size because of the process of armoring. This study attempts to quantify the reduction in scour hole size in terms of the densimetric particle Froude number F_o due to the

---

† Submitted to the Journal of Hydraulic Engineering, American Society of Civil Engineers (ASCE)

sediment gradation in the bed and determine an effective grain size for the bed. F_o is defined as $U_o/\sqrt{(gD\Delta\rho/\rho)}$ and can be interpreted as a measure of the ratio of the tractive force of a wall jet on a grain to its resistive force. U_o is the jet velocity at the nozzle outlet, D is the median size of the sediment mixture, g is the acceleration due to gravity and $\Delta\rho$ is the difference between the mass density of the sand or gravel and the density of the fluid ρ.

5.2 Experiments

The experimental arrangement and definition sketch are shown in Figure 5-1(a-b). It was set up in a flume, 0.32 m wide, 0.65 m deep and 5 m long. This flume was partitioned along its length so that only a width of 0.155 m was used. The water jets, which were deeply submerged, were produced from well designed nozzles with nozzle opening b_o of 5, 14 and 25 mm. The jet velocities were measured using a Prandtl tube of external diameter of 3 mm. Water was supplied from a pump to the nozzle from a reservoir attached to the flume and was re-circulated. Three sediment mixtures referred to as S1, S2 and S3 were used. Their median sizes D and geometric standard deviations σ_g (equal to $\sqrt{(d_{84}/d_{16})}$) were 7.2 mm and 1.33, 1.15 mm and 2.09 and 1.62 mm and 3.13 respectively. The sieve analysis curves are shown in Figure 5-2.

The sediment mixtures were prepared in small portions and carefully poured into the 0.2m deep sediment compartment to prevent mechanical segregation. The sediment bed was then saturated and leveled to the elevation of the invert of the nozzle outlet. The next step was to fill the flume with water and run the experiment at a constant discharge. It was observed in most of the experiments, especially at higher F_o values, that the diffusing jet was unstable. It was oscillating between the horizontal direction and along the eroded bed. A shallower maximum scour depth ε'_{ms}, and a deeper dynamic maximum scour depth ε'_{md}, were produced in these states respectively. Section 5.4 explains this phenomenon in more detail. The experiments were run for a duration of about 22 hours on the average. They were stopped when the sediment transport over the dune was insignificant. This state is referred to as the asymptotic state. It was noticed that the profile of the scour hole section, unlike the profile of the dune section, was dependent on the direction of the jet at the time the experiment was stopped.

After the flume had been carefully drained, the (static) profile of the eroded bed $\varepsilon(x)$ was measured (see Figure 5-1(b)). The depth of erosion below the original bed level is denoted as ε and x is the longitudinal distance from the nozzle. On the whole, 31 experiments were performed, with F_o varying from 2.7 to 29.5. The jet submergence s, defined as the ratio of the tail water depth h_d to nozzle size, varied from 12 to 60. The experimental results are shown in Table 5-1.

5.3 Flow Patterns

It was noticed that during the scouring process, the jet from the nozzle became unstable. It was continuously oscillating between a position along the bed to a horizontal direction. Figures 5-3(a-d) show these positions and the jet interaction of the jet with the bed. The period of oscillation was generally between 5 and 10 seconds and it appears that it might be weakly dependent on F_o. When the jet is attached to the bed, it transports a lot of material, some of which (mostly finer particles) are transported over the dune. The coarser particles are continuously deposited and piled at the far end of the scour hole (at the beginning of the dune) resulting in the steepening of the bed slope which is supported by the jet (see Figure 5-3(a)). When the steepness exceeds a certain value as shown in Figure 5-3(b), the jet can no longer support the bed and attacks the mid section of the scour hole like an inclined jet, strongly erodes the bed and generates a big sediment cloud immediately downstream of it. Most of the hydraulic segregation occurs here. A sediment-laden vortex is formed upstream of the impingement area between the bed and the jet. The maximum depth occurs at this point and it is referred to as the deeper dynamic maximum scour depth ε'_{md}. The jet then starts to rise (see Figure 5-3(c)), towards the horizontal direction, causing the impingement area to move downstream into the piled deposits which at the same time are falling back into mid section of the scour hole. By the time the impingement area has reached the end of the scour hole (i.e. the jet path is horizontal), all the piled deposits are back in the scour hole and the maximum depth at this point is referred to as the shallower dynamic maximum scour depth ε'_{ms} (see Figure 5-3(d)). This process is continuously repeated resulting in a scour hole with mainly coarser particles and a dune covered with mainly finer particles. The armor layer in this study was never stable.

The particle size distributions of sections of the top layer of the hydraulic segregated bed were studied. Figures 5-4(a) and 5-4(b) show these distributions for experiments NU 20 and NU 31 respectively. It can be seen from these figures that the section of coarsest particles is located approximately between $0.37x_o$ and $0.75x_o$. The median size d_{50} of the particles in these coarsest sections correspond approximately to the d_{95} of the original sediment mixtures. The finest particles on the eroded bed were found on the downstream slope of the dune and from these plots, correspond approximately to the d_{50} of the original sediment mixtures. The finest particles of the original sediment mixtures were deposited further downstream of the dune.

5.4 Effective Diameter

A sediment mixture is considered to be non-uniform if d_{95}/d_5 is greater than 4 or 5 or if the geometric standard deviation σ_g, defined as $\sqrt{(d_{84}/d_{16})}$, is greater than 1.35 according to Breusers and Raudkivi (1991). Little and Mayer (1976) suggested a slightly lower value of 1.3 and Gessler (1971) suggested a d_{84}/d_{50} (also equal to σ_g) ratio exceeding 2.

In the calculation of a scour hole size in a non-uniform sediment bed, it is necessary to determine the sediment size within the range of sizes contained in the sediment mixture, that will adequately represent it in the scouring process. It appears reasonable therefore to define this sediment size, that is, the effective diameter d_e, as the size of a uniform sediment mixture that is scoured to the same final state as the non-uniform sediment mixture under the same conditions. One of the approaches to choosing an effective size is to use a size of such as d_{65}, d_{75}, d_{90} or d_{95}. Another approach is to use some kind of an average of all the sizes in the sediment mixture, as given by equation (5-1), wherein β is an exponent:

$$d_e = \left\{ \frac{1}{10} \sum_{i=1}^{10} \left[\frac{d_{10(i-1)} + d_{10i}}{2} \right]^{\beta} \right\}^{\frac{1}{\beta}} \qquad (5\text{-}1)$$

The effective diameter is equal to:

i) the arithmetic mean of all the particle sizes when β is equal to 1. The geometric mean size d_g is defined as $\sqrt{(d_{84}d_{16})}$.

ii) the particle size for which the surface area is equal to the average surface area of all the particles when β is equal to 2

iii) the particle size with a volume is equal to the average volume of all the particles when β is equal to 3

iv) the particle size with a surface area/volume ratio equal to the average surface area/volume ratio of all particles when β is equal to -1.

Stevens (1969) used the third condition for his definition. Smith (1955) found the fourth condition to be the most satisfactory compared to conditions (ii) and (iii) for his analysis of slurry flow in pipes. Using an analytical approach, Christensen (1969) obtained an equation similar to equation (5-1) with β equal to -1. Another approach worth mentioning is the combination of two statistical parameters of the sediment distribution, an example of which is given by equation (5-2), wherein, C_e and k are respectively a constant and an exponent.

$$d_e = C_e d^* \sigma_g^k \qquad \text{where} \quad d^* = d_{50}, d_g, \ldots\ldots \tag{5-2}$$

This approach has been used by Abt et al. (1984) and Kothyari et al. (1992) among others. In this study, an attempt will be made to determine which of these approaches gives the best correlation.

5.5 Dimensional Considerations

The asymptotic characteristic lengths of the eroded bed such as the shallower dynamic scour depth $\varepsilon'_{ms\infty}$, the deeper dynamic scour depth $\varepsilon'_{md\infty}$, the scour hole length $x_{O\infty}$, the distance of the location of maximum dune height $x_{C\infty}$ and dune height Δ_∞, as shown in Figure 5-1(b), can be made non-dimensional and related to other non-dimensional parameters using dimensional arguments. Following the approach of Rajaratnam (1981), equation (5-3) can be formulated with $l_{C\infty}$ representing any characteristic length of the asymptotic scour profile. Equation (5-3) is applicable for uniform sediments and could be made applicable for non-uniform sediments by replacing D with d_e.

$$\frac{l_{c\infty}}{b_o} = f_1\left(F_o = \frac{U_o}{\sqrt{g\frac{\Delta\rho}{\rho}D}}, R_e = \frac{\rho U_o b_o}{\mu}, \frac{b_o}{D} \right) \qquad (5\text{-}3)$$

The jet Reynolds number R_e can be neglected if it is greater than a few thousand, as in the present study (Rajaratnam 1976). The effect of b_o/D has been assumed to be quite secondary to that of F_o. Equation (5-3) therefore reduces to equation (5-4).

$$\frac{l_{c\infty}}{b_o} = f_2\left(\frac{U_o}{\sqrt{g\frac{\Delta\rho}{\rho}d_e}} \right) \qquad (5\text{-}4)$$

5.6 Characteristic Lengths of the Eroded Bed

5.6.1 Maximum Scour Depth

Figure 5-5 shows a plot of the relative deeper dynamic asymptotic maximum scour depth $\varepsilon'_{md\infty}/b_o$ against F_o. The observations of Rajaratnam (1981) on erosion of two nearly uniform sands (D=1.2 and 2.38 mm) are also shown in Figure 5-5. Table 5-2 shows the details of his experimental results. It can be seen in Figure 5-5 that the data are divided into two groups, one with σ_g (GSD) less than about 1.35 and the other with σ_g between 2 and 3.2. For any given value of F_o, the latter group gives a lower value of $\varepsilon'_{md\infty}/b_o$. This further confirms the effect of armoring on scour depth. This figure also suggests that $\varepsilon'_{md\infty}$ is proportional to b_o for a given value of F_o. The data were re-plotted according to b_o as shown in Figure 5-6, which shows clearly that b_o is the scale for the maximum depth of scour.

The effect of armoring in terms of F_o can be quantified by determining the ratio between the curves in Figure 5-5. If the percentage scour size reduction η is defined by equation (5-5), the variation of η for the $\varepsilon'_{md\infty}$ with F_o is shown in Figure 5-7.

$$\eta = \left[1 - \frac{\left(\frac{l_{c\infty}}{b_o}\right)_{2<\sigma_g<3.2}}{\left(\frac{l_{c\infty}}{b_o}\right)_{\sigma_g<1.35}} \right] 100\% \qquad (5\text{-}5)$$

The percentage reduction for $\varepsilon'_{md\infty}$ has an average value of 60% for F_o between 2 and 14. This is quite close to 50% obtained by Lim and Chin (1992) from their experiments on scour of non-uniform sediments by circular wall jets.

The effective size d_e of the sediment mixture was determined by finding the particle size that gives the best correlation between $\varepsilon'_{md\infty}/b_o$ and a modified F_o (using another particle size instead of $D=d_{50}$). Many particle sizes such as sizes between d_{50} and d_{95}, d_g and sizes from equation (5-1) with β equal to -1, 1, 2 and 3 were tried. The best correlation was obtained using d_{95} and the poorest using d_{50}. This is in agreement with the results of the sieve analysis of the coarsest section of the scour hole. The use of d_{90} was almost as good as using d_{95}.

Figure 5-8 shows the variation of $\varepsilon'_{md\infty}/b_o$ with $F_{o(95)}$ and the best fit line is expressed as equation (5-6). This relationship describes reasonably well the observations of Rajaratnam (1981). The d_{95} sizes of his two nearly uniform sands (each sorted from two sieve sizes) were estimated to be 1.94 and 3.49 mm from the log-normal plots of the size distributions. The subscripts for the coefficients in equation (5-6) are the standard deviation values. $F_{o(95)}$ is defined as $U_o/\sqrt{(d_{95}g\Delta\rho/\rho)}$. An attempt was made to express the effective diameter in the form of equation (5-2). This was deduced from equation (5-7a) with has a coefficient of multiple determination R^2 of 0.81 which is less than that of equation (5-6). The effective diameter is thus given as equation (5-7b).

$$\frac{\varepsilon_{md\infty}}{b_o} = -6.35_{\pm 2.2} + 3.43_{\pm 0.04} F_{o(95)} \qquad R^2 = 0.9 \qquad (5\text{-}6)$$

$$\frac{\varepsilon'_{md\infty}}{b_o} = 0.44 F_o^{1.77} \sigma_g^{-1.16} \qquad R^2 = 0.81 \qquad (5\text{-}7a)$$

$$d_e = d_{50} \sigma_g^{1.31} \qquad (5\text{-}7b)$$

Going back to the two values of the maximum depths of erosion $\varepsilon'_{md\infty}$ and $\varepsilon'_{ms\infty}$ produced by the oscillating jet, Figure 5-9 shows the variation of the relative maximum difference in scour depth ψ, defined by equation (5-8), with F_o. From Figure 5-9, it can be seen that ψ is zero at very low values of F_o and has an average value of 0.281 ± 0.064 (0.064 is the standard deviation) for F_o greater than 5 for σ_g less than 1.35 and for F_o greater than 8 for σ_g between 2 and 3.2.

$$\psi = \frac{\frac{\varepsilon'_{md\infty}}{b_o} - \frac{\varepsilon'_{ms\infty}}{b_o}}{\frac{\varepsilon'_{md\infty}}{b_o}} \qquad (5\text{-}8)$$

As can be seen from Table 5-1, the values of $\varepsilon_{m\infty}$ are always between the corresponding values of $\varepsilon'_{md\infty}$ and $\varepsilon'_{ms\infty}$.

5.6.2 Other Length Scales

Figure 5-10 shows the variation of the relative scour hole length $x_{o\infty}/b_o$ (defined by equation (5-5)) with F_o and it can be seen that the scour hole is significantly shorter for the graded material. Figure 5-11 shows the variation of $x_{o\infty}/b_o$ with $F_{o(95)}$ and the best fit line is described by equation (5-9).

$$\frac{x_{o\infty}}{b_o} = -7.87 + 9.06 F_{o(95)} \qquad (5\text{-}9)$$

A plot of the percentage reduction in scour hole length due to armoring can be seen in Figure 5-7 with an average reduction of about 53 %.

Variation of the normalized distance to the crest of the dune from the jet outlet $x_{c\infty}/b_o$ with F_o is shown in Figure 5-12 where the reduction in $x_{c\infty}/b_o$ can be seen for the graded material. Equation (5-10) expresses the relation in

Figure 5-13. The percentage reduction in the distance of the dune due to armoring was found to have an average value of about 52%. Figure 5-13 shows that the variation of $x_{c\infty}/b_o$ with $F_{o(95)}$ can be described by the equation (5-10).

$$\frac{x_{c\infty}}{b_o} = -17.13 + 15.56 F_{o(95)} \tag{5-10}$$

A similar analysis was done for the maximum dune height as shown in Figures 5-14 and 5-15. In Figure 5-15, the best line fit is described by equation (5-11).

$$\frac{\Delta_\infty}{b_o} = -4.32 + 2.7 F_{o(95)} \tag{5-11}$$

In this case, the average percentage reduction in maximum dune height due to armoring was found to be 62% (see Figure 5-7).

5.7 Conclusions

The experimental observations and analysis presented in this study on local scour of non-uniform non-cohesive beds downstream of deeply submerged plane turbulent wall jets has established that the sediment non-uniformity has a significant effect on the size of the scour hole produced by the jet. The particle size distributions of sections of the top layer of the hydraulic segregated eroded bed show that the coarsest section lies approximately between 0.37 and 0.75 of the scour hole length. The median size of the particles in this section was found to correspond approximately to the d_{95} of the original sediment mixture. The effective size of the sediment mixture for obtaining a good correlation for the depth of scour was determined to be d_{95} rather than d_{50} for defining the densimetric particle Froude number F_o. The average reduction due to armoring in the maximum scour depth and dune height was found to be about 60% and 50% for the scour hole length and the distance of the dune.

5.8 References

Abt, S. R., Kloberdanz, R. L. and Mendoza, C. (1984), Unified Culvert Scour Determination, Journal of Hydraulic Engineering, Vol. 110, No. 10, pp. 1475 - 1479.

Ali, K.H.M. and Lim, Y. (1986), Local Scour caused by Submerged Wall Jets, Journal of Institution of Civil Engineers, Part 2, Vol. 81, pp. 607 - 645.

Breusers, H.N.C. and Raudkivi, A.J. (1991), Scouring, International Association of Hydraulic Research - Hydraulic Structures Design Manual, A.A. Balkerma, Rotterdam, 143 pp.

Chatterjee, S.S. Ghosh, S.N. and Chatterjee, M. (1994), Local Scour due to Submerged Horizontal Jet, Journal of Hydraulic Engineering, ASCE, Vol. 120, No. 8, pp. 973 - 992.

Lim, S.Y. and Chin, C.O.(Wang S.S.Y. (Ed.)) (1992) , Scour by Circular Wall Jets with Non-uniform Sediments, Advances in Hydro-science and Engineering, Vol. 1, pp. 1989 - 1994.

Christensen, B.A. (1969), Effective Grain Size in Sediment Transport, Proceedings 13th Congress IAHR, Kyoto, 3, PP. 223 - 231.

Gessler, J. (1971), Critical Shear Stress for Sediment Mixtures, Proceedings 14th Congress of IAHR, Vol. 3, C1-1 - C1-8.

Kothyari, U.C., Garde, R.J. and Ranga Raju, K.G. (1992), Temporal Variation of Scour Around Circular Bridge Piers, Journal of Hydraulic Engineering, Vol. 118, No. 8, pp. 1091 - 1106.

Little, W.C. and Mayer, P.G. (1976), Stability of Channel Beds by Armoring, ASCE, Journal of Hydraulic Engineering, Vol. 102, No. HY11, pp. 1647 - 1661.

Rajaratnam, N. (1976), Turbulent Jets, Elsevier Scientific Publication Company, Amsterdam, The Netherlands, 304 pp.

Rajaratnam, N. (1981), Erosion by Plane Turbulent Jets, Journal of Hydraulic Research, Vol. 19, No. 4, pp. 339 - 358.

Smith, R.A. (1955), Experiments on the Flow of Sand-Water Slurries in Horizontal Pipes, Transactions of the Institution of Chemical Engineers, Vol. 33., pp. 85 - 92.

Stevens, M. A. (1969), Scour in Rip rap at Culvert Outlets, Ph.D. Dissertation, Colorado State University, Fort Collins, Colorado.

Uyumaz Ali (1988), Scour Downstream of Vertical Gate, Journal of Hydraulic Engineering, Vol. 114, No. 7, pp. 811 - 816.

Valentin, F. (1967), Considerations Concerning Scour in the case of Flow Under Gates, Proceedings, Twelfth Congress, IAHR, Fort Collins, Colorado, Vol. 3, pp. 92 - 96.

Table 5-1: Experimental Results

Expt. #.	Time (hr.)	U_o (m/s)	b_o (mm)	D (mm)	σ_g	$\varepsilon_{m\infty}$ (mm)	$\varepsilon'_{ms\infty}$ (mm)	$\varepsilon'_{md\infty}$ (mm)	$x_{m\infty}$ (mm)	$x_{o\infty}$ (mm)	$x_{c\infty}$ (mm)	$x_{e\infty}$ (mm)	Δ_∞ (mm)	F_o	$\varepsilon'_{md\infty}/b_o$
NU 1	5	0.922	14	7.2	1.33	63	63	63	140	327	475	660	69.8	2.70	4.50
NU 2	10	1.974	14	7.2	1.33	86	83.9	105	190	420	660	820	119.5	5.78	7.50
NU 3	40	2.187	14	7.2	1.33	110	97.5	141.7	230	500	780	1000	144	6.41	10.12
NU 4	12	1.586	5	7.2	1.33	41.5	41.5	41.5	80	165	230	295	38	4.65	8.30
NU 5	11	2.363	5	7.2	1.33	76	58.3	78.1	140	268	395	505	73	6.92	15.62
NU 6	15	2.98	5	7.2	1.33	99.5	76.5	103.5	140	340	500	655	88	8.73	20.70
NU 7	50	3.861	5	7.2	1.33	108.5	99.4	146.7	240	440	680	855	125	11.31	29.34
NU 21	5	1.071	25	7.2	1.33	33	33	33	180	270	400	600	60	3.14	1.32
NU 8	15	0.582	14	1.15	2.09	35.8	35.8	35.8	110	200	270	530	32.5	4.27	2.56
NU 9	21	0.74	14	1.15	2.09	44.2	44.2	44.2	140	233	350	550	44.8	5.42	3.16
NU 10	24	1.093	14	1.15	2.09	70.3	59.7	70.4	190	337	560	715	67.5	8.01	5.03
NU 11	20.5	1.339	14	1.15	2.09	100	83	101.3	220	420	700	900	90	9.82	7.24
NU 12	22	1.57	14	1.15	2.09	109.5	102.8	133.9	230	527	870	1080	111.5	11.51	9.56
NU 13	12	1.082	5	1.15	2.09	36	36	36	80	150	240	285	30.8	7.93	7.20
NU 14	17	1.412	5	1.15	2.09	53.7	47.4	66.7	125	220	370	470	47	10.35	13.34
NU 15	16	1.757	5	1.15	2.09	78.3	56.8	84.2	120	265	450	600	68.3	12.88	16.84
NU 16	40	2.45	5	1.15	2.09	107.3	91	130.2	220	410	720	915	108	17.96	26.04
NU 17	14	0.602	25	1.15	2.09	38.7	38.7	38.7	150	260	390	480	50.3	4.41	1.55
NU 18	23	0.707	25	1.15	2.09	49.5	49.5	49.5	170	295	465	595	63	5.18	1.98
NU 19	29	0.804	25	1.15	2.09	58.5	58.5	58.5	180	335	520	650	56.7	5.89	2.34
NU 20	26	0.929	25	1.15	2.09	75.3	75.3	75.3	200	365	630	810	74.7	6.81	3.01
NU 22	13.5	0.863	25	1.62	3.13	54	54	54	180	320	520	660	57	5.33	2.16
NU 23	20	0.84	14	1.62	3.13	37.5	37.5	37.5	110	210	280	430	34.2	5.19	2.68
NU 24	17	1.566	14	1.62	3.13	95	79.4	119.4	200	415	710	930	82.5	9.67	8.53
NU 24b	20	1.844	14	1.62	3.13		104	147.2						11.39	10.51
NU 25	16	1.076	14	1.62	3.13	54	54	54	160	265	420	515	48.5	6.65	3.86
NU 26	18	1.343	14	1.62	3.13	72.5	64.5	87.5	190	355	560	740	71	8.30	6.25
NU 27	52	1.675	14	1.62	3.13	119	96.3	128.5	190	475	805	1050	84.5	10.35	9.18
NU 28	15.5	1.62	5	1.62	3.13	46	41.5	59.25	120	202	340	450	49	10.01	11.85
NU 29	22	2.509	5	1.62	3.13	73.5	64.5	107	150	293	550	690	81.5	15.50	21.40
NU 30	18	2.867	5	1.62	3.13	83.3	72.9	121	130	325				17.71	24.20
NU 31	45	4.77	5	1.62	3.13	122	118.9	163.7	190	467	810	1053	138	29.46	32.74

Table 5-2: Experimental Results of Rajaratnam (1981)

Expt. No.	D (mm)	b_o (mm)	U_o (m/s)	$\varepsilon_{m\infty}$ (mm)	$x_{m\infty}$ (mm)	$x_{o\infty}$ (mm)	$x_{c\infty}$ (mm)	Δ_∞ (mm)	F_o	$\varepsilon_{m\infty}/b_o$
31	2.38	24.89	1.31	199.64	405.38	740	1240.54	20.12	6.66	8.02
32	2.38	3.56	1.80	81.38	134.11	260	411.48	68.28	9.16	22.89
33	2.38	3.56	1.95	94.79	152.40	300	463.30	70.10	9.92	26.66
34	2.38	3.56	2.22	105.77	152.40	326	518.16	85.65	11.29	29.74
35	2.38	6.60	1.34	76.81	158.50	268	435.86	77.11	6.83	11.63
36	2.38	3.56	1.73	76.20	152.40	237	381.00	66.45	8.84	21.43
37	1.2	3.56	1.79	103.33	128.02	347	530.35	88.70	12.86	29.06
38	1.2	3.56	0.92	35.97	57.91	130	192.02	32.00	6.60	10.11
39	1.2	3.56	1.95	111.25	128.02	367	573.02	97.23	13.97	31.29
310	1.2	3.56	1.80	104.24	176.78	348	527.30	86.87	12.88	29.31
311	1.2	3.56	1.22	69.19	106.68	245	344.42	44.81	8.77	19.46
312	2.38	24.89	0.87	83.21	237.74	374	579.12	84.43	4.41	3.34
313	2.38	6.60	1.11	60.96	143.26	230	350.52	56.69	5.65	9.23
314	2.38	6.60	1.34	72.54	152.40	262	414.53	68.28	6.85	10.98

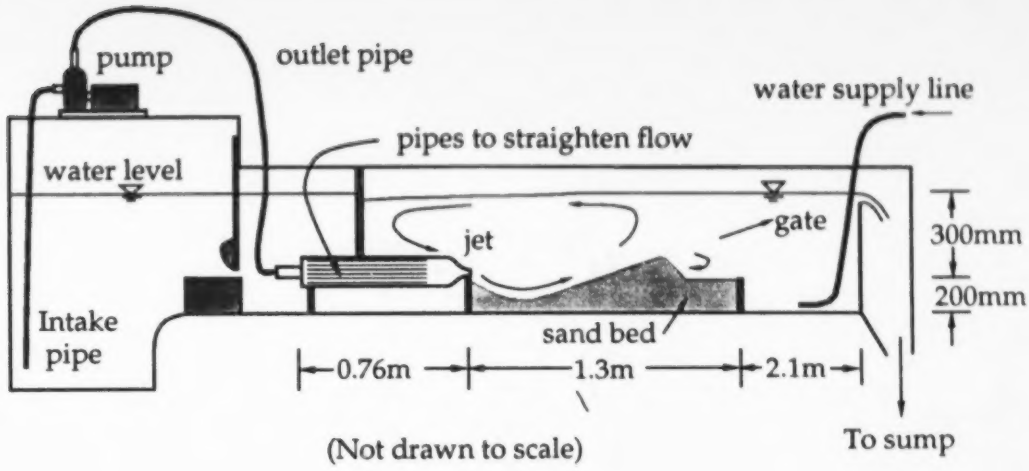

Figure 5-1(a) Experimental Set-up

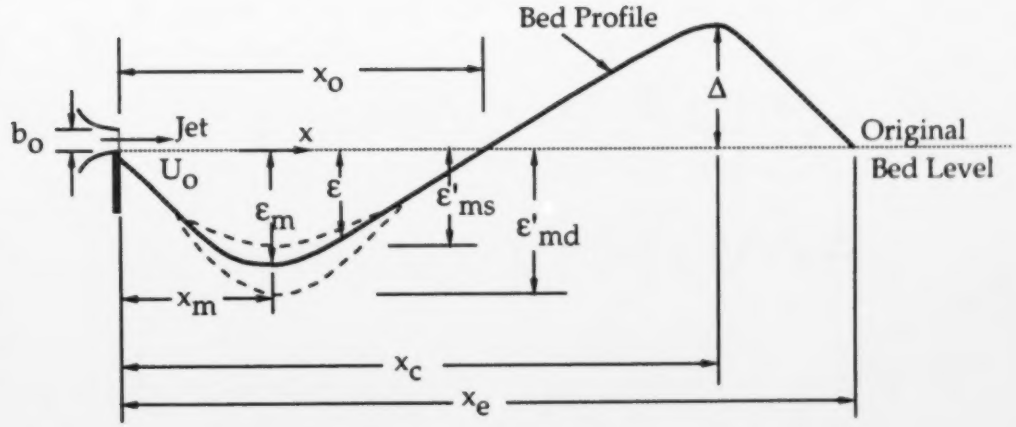

Figure 5-1(b) Definition Sketch

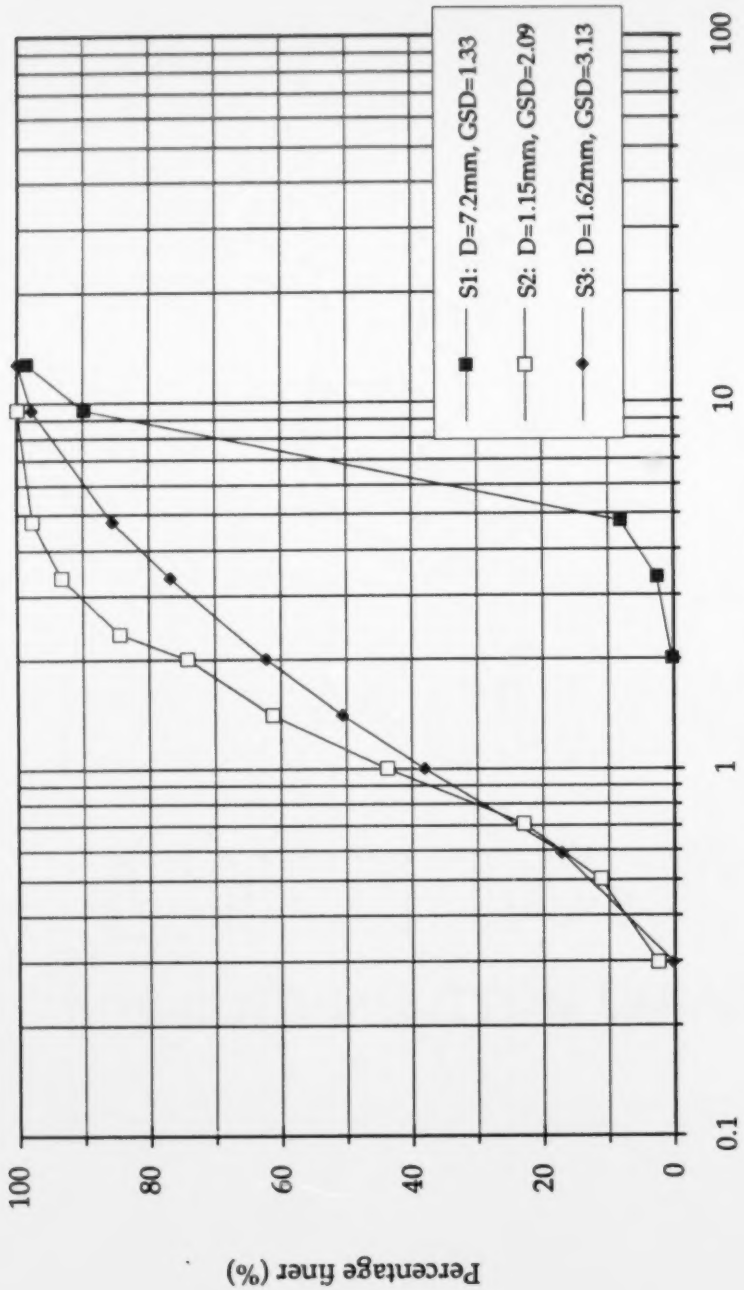

Figure 5-2: Particle size distributions for the sand mixtures

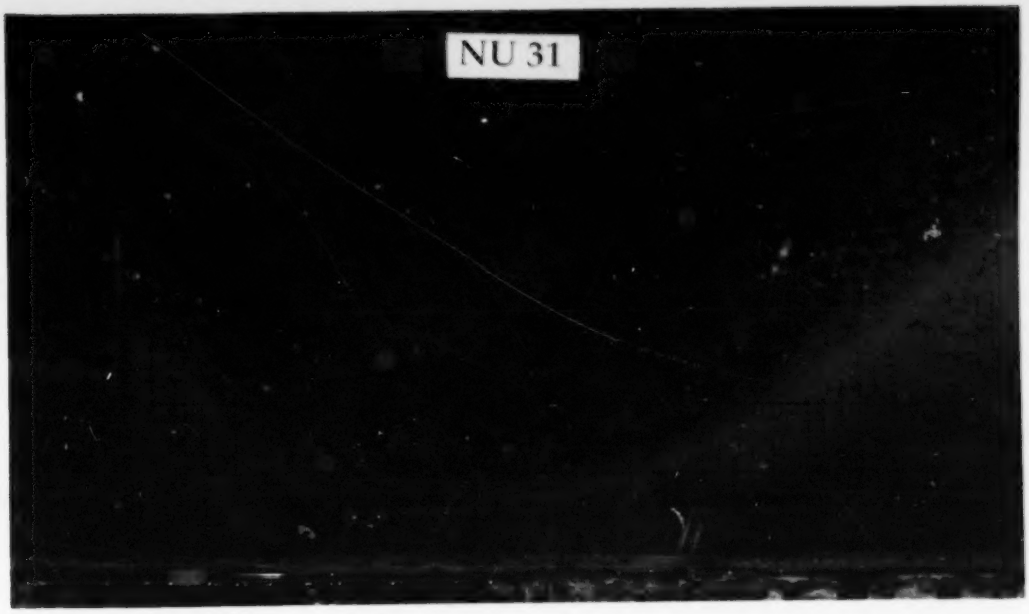

Figure 5-3(a)

Figure 5-3(b)

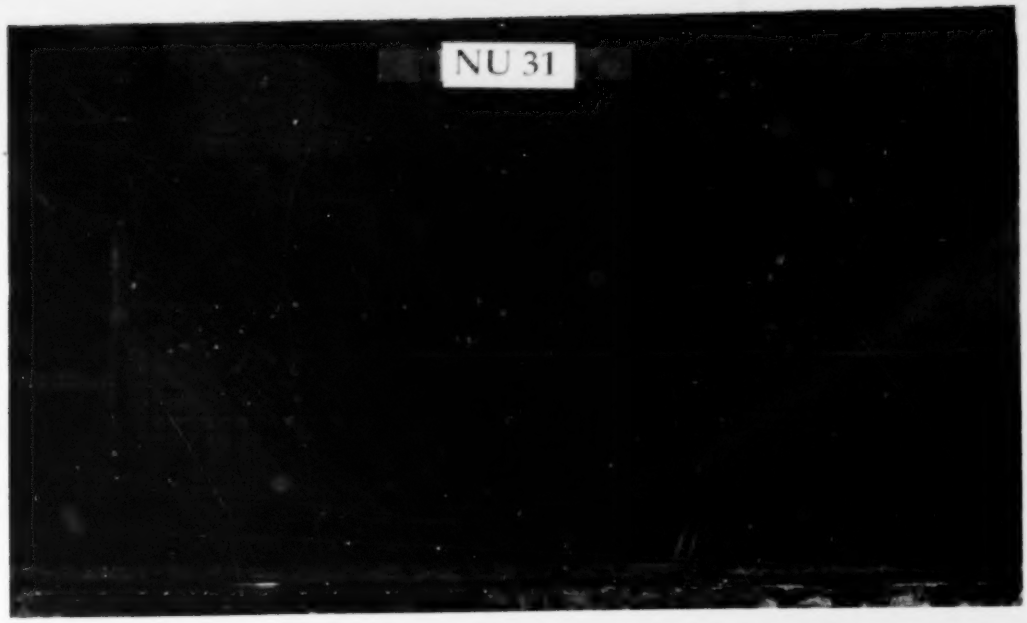

Figure 5-3(c)

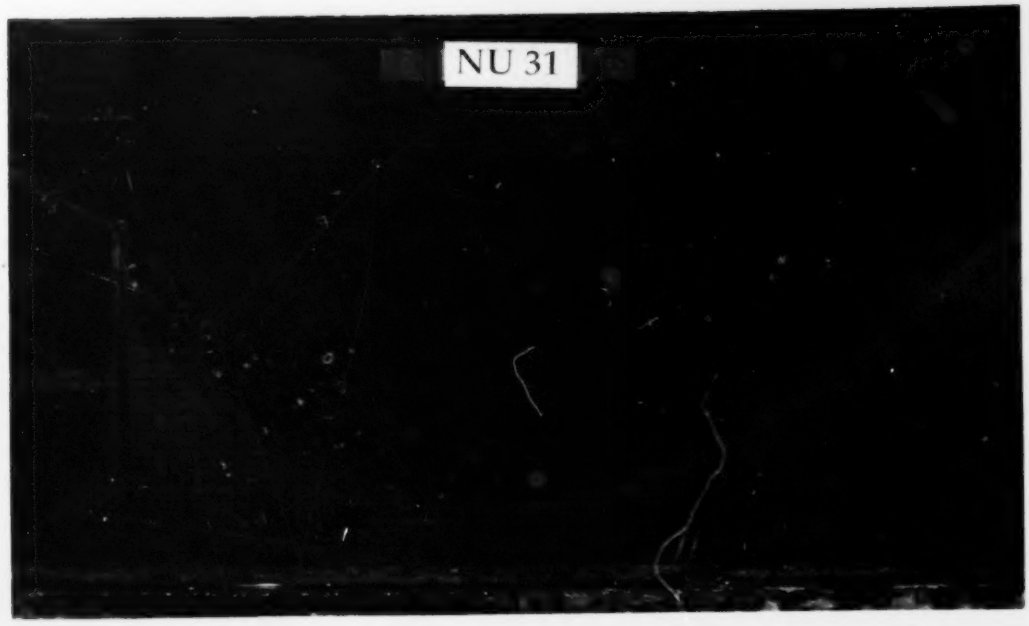

Figure 5-3(d)

Figure 5-3(a-d): Flow Patterns due to Wall jet

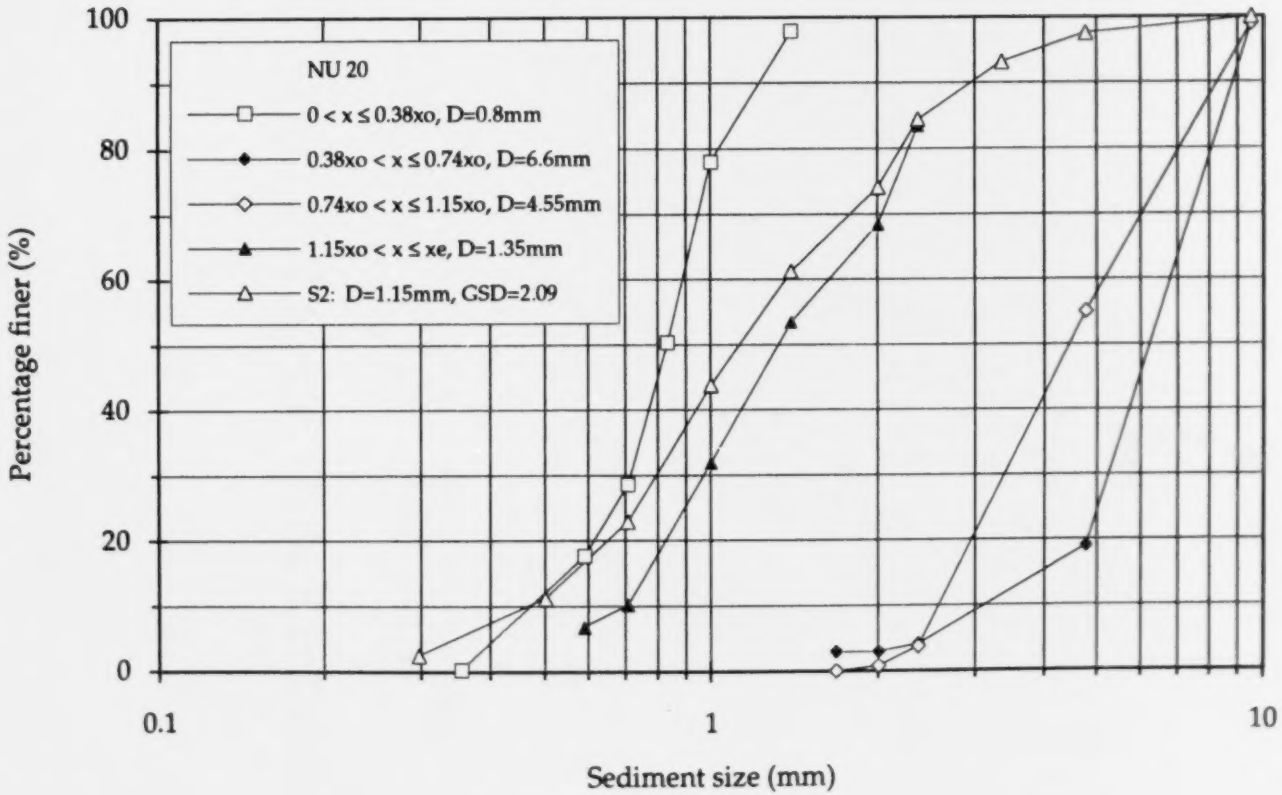

Figure 5-4(a): Sieve analysis of the top layer of bed for Expt. NU 20

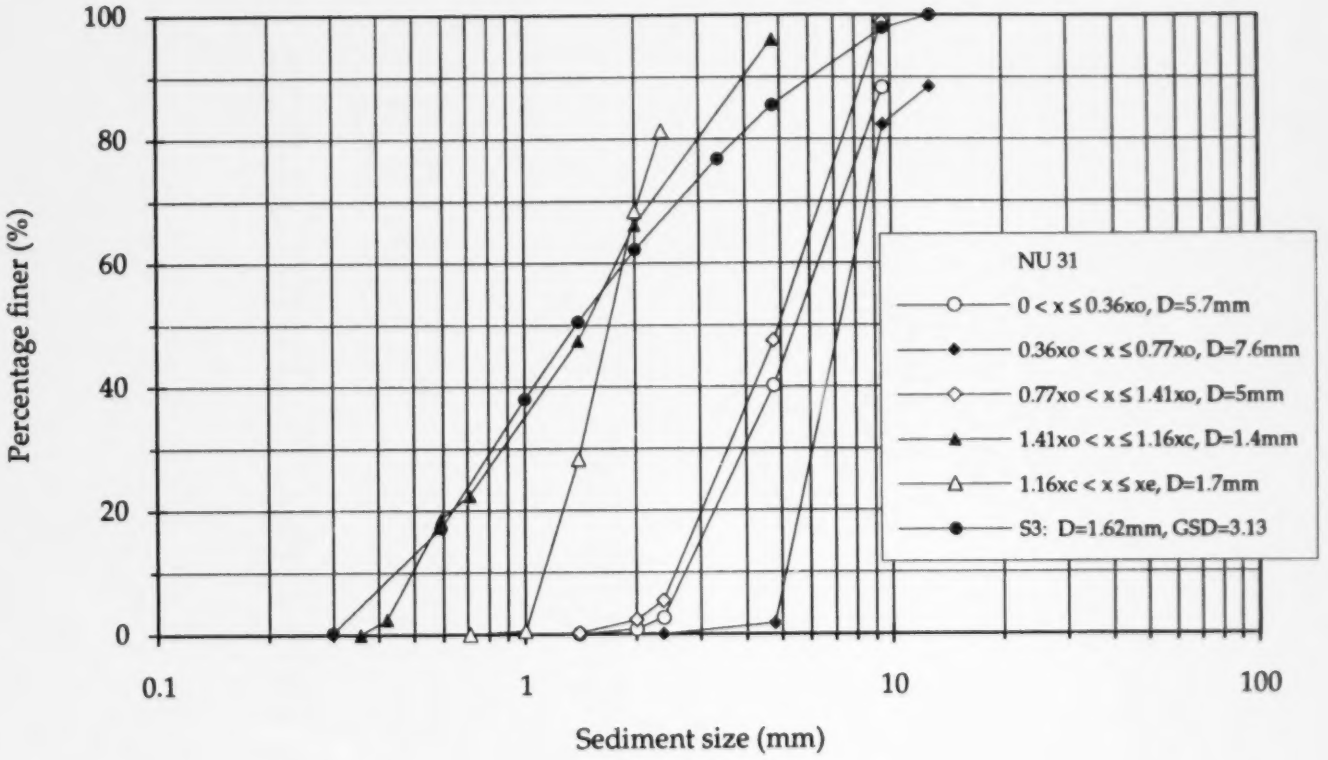

Figure 5-4(b): Sieve analysis of the top layer of bed for Expt. NU 31

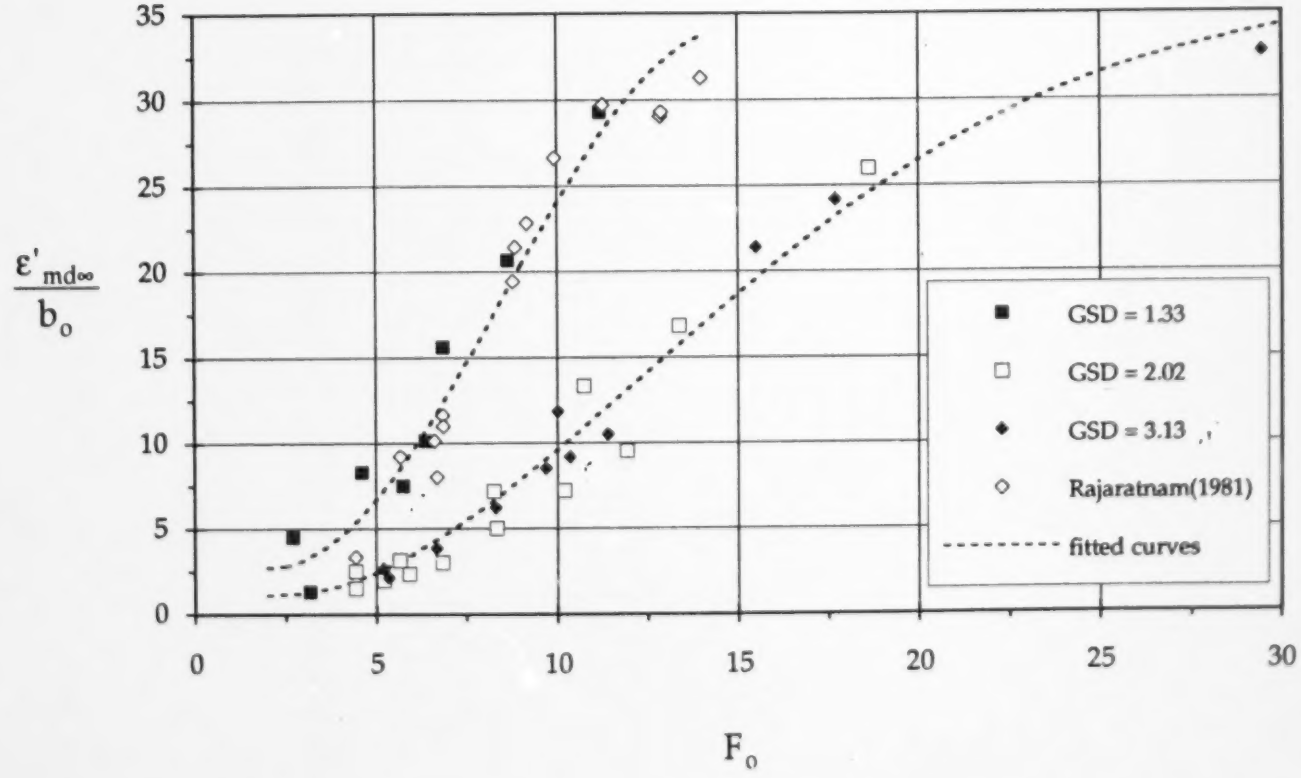

Figure 5-5: Variation of maximum scour depth with F_o

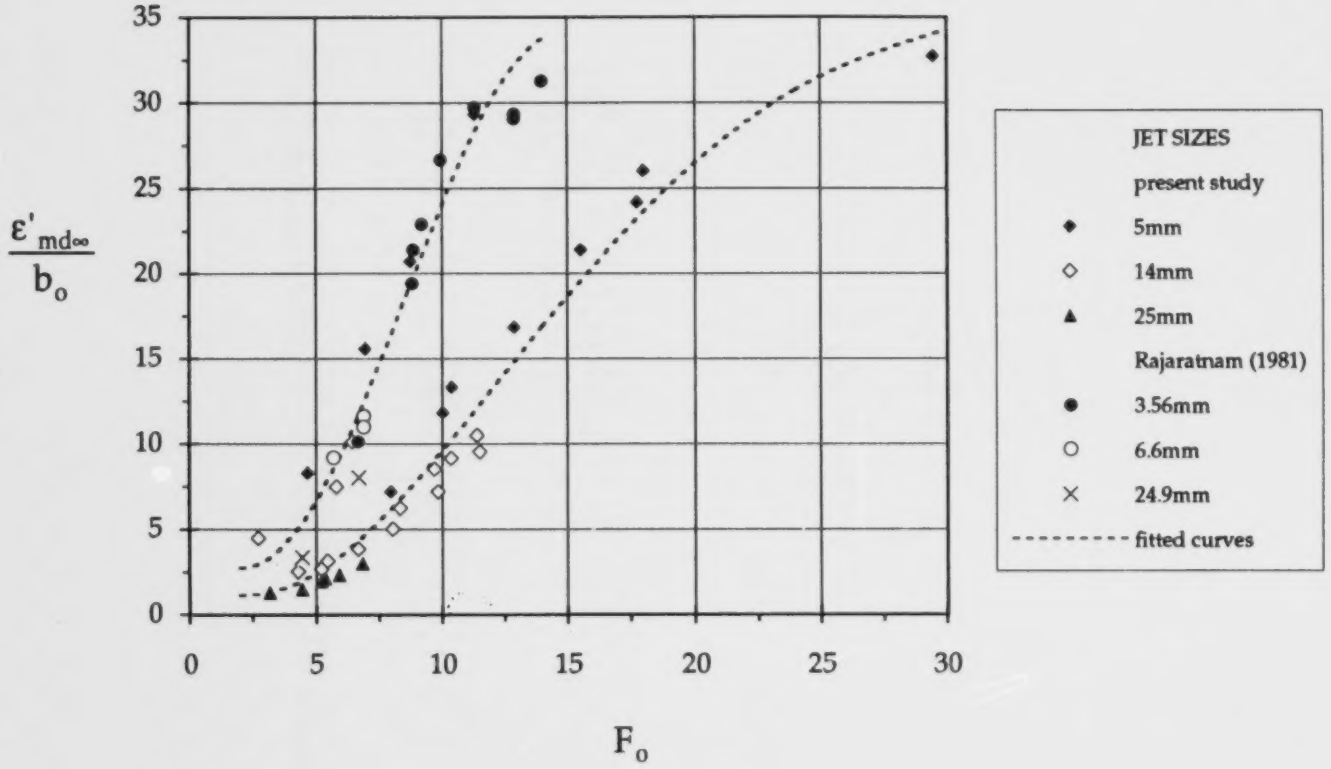

Figure 5-6: Variation of maximum scour depth with F_o (seperated by b_o)

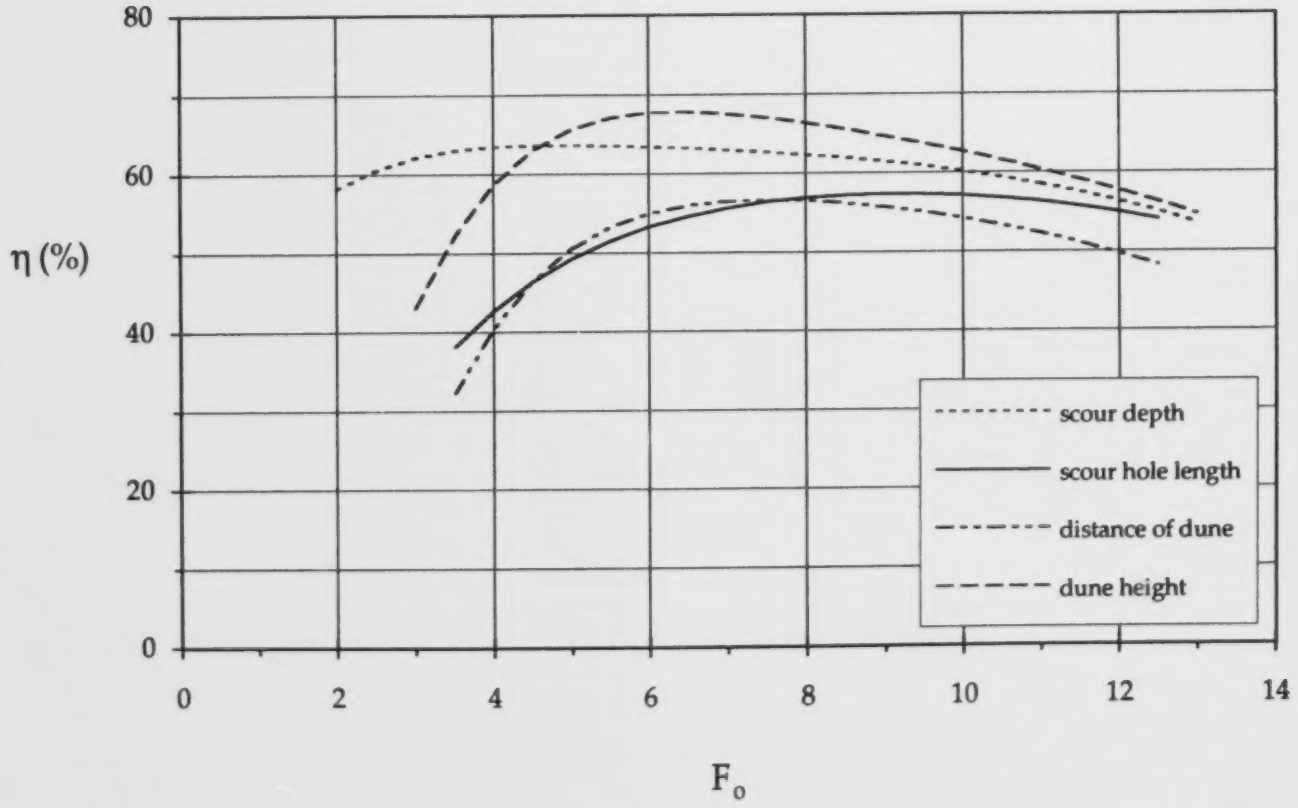

Figure 5–7: Variation of the reduction in the length scales of the scour hole with F_o

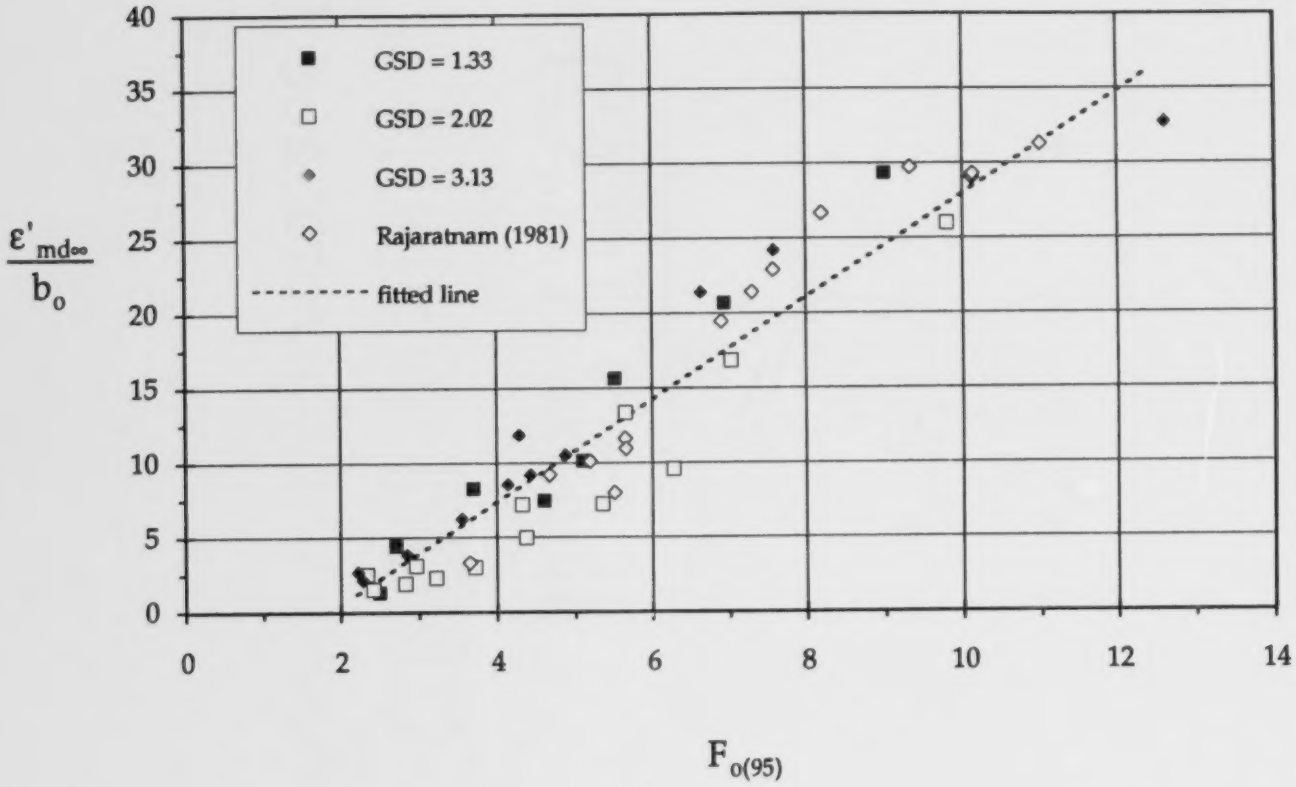

Figure 5 – 8: Variation of maximum scour depth with $F_{o(95)}$

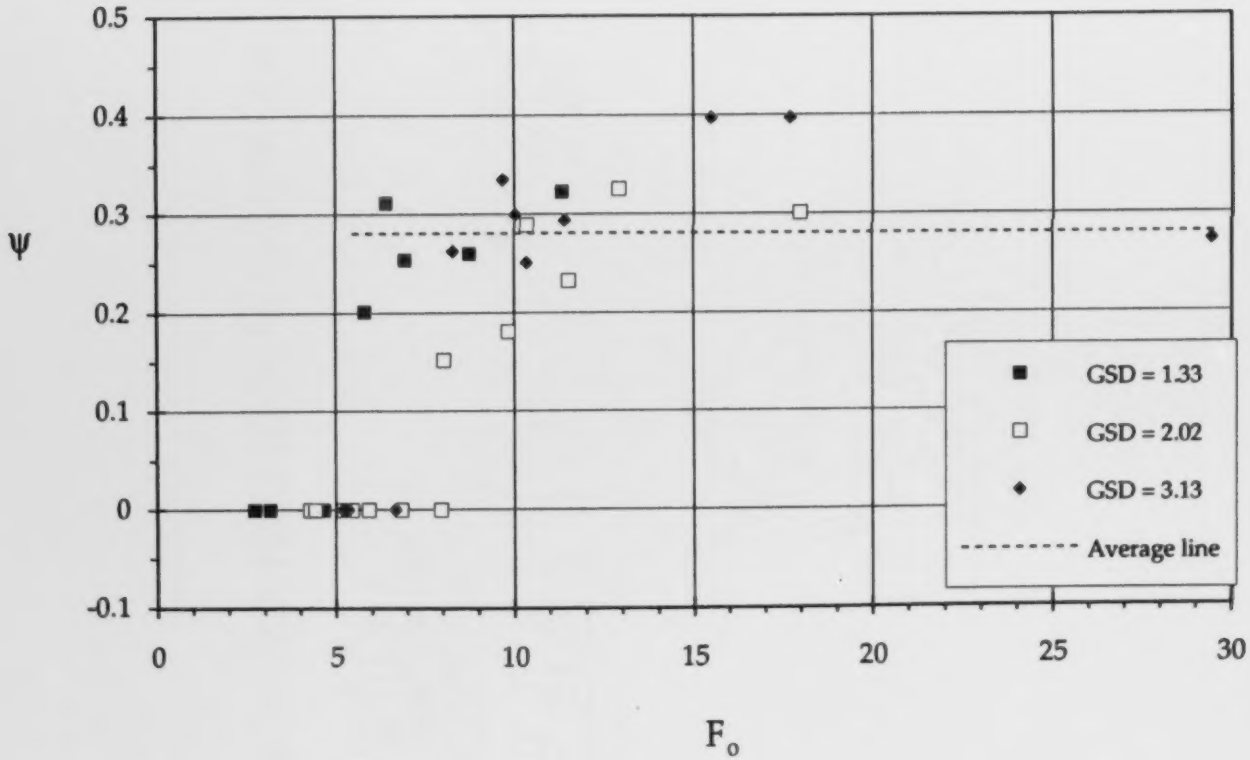

Figure 5-9: Variation of maximum scour depth difference with F_o

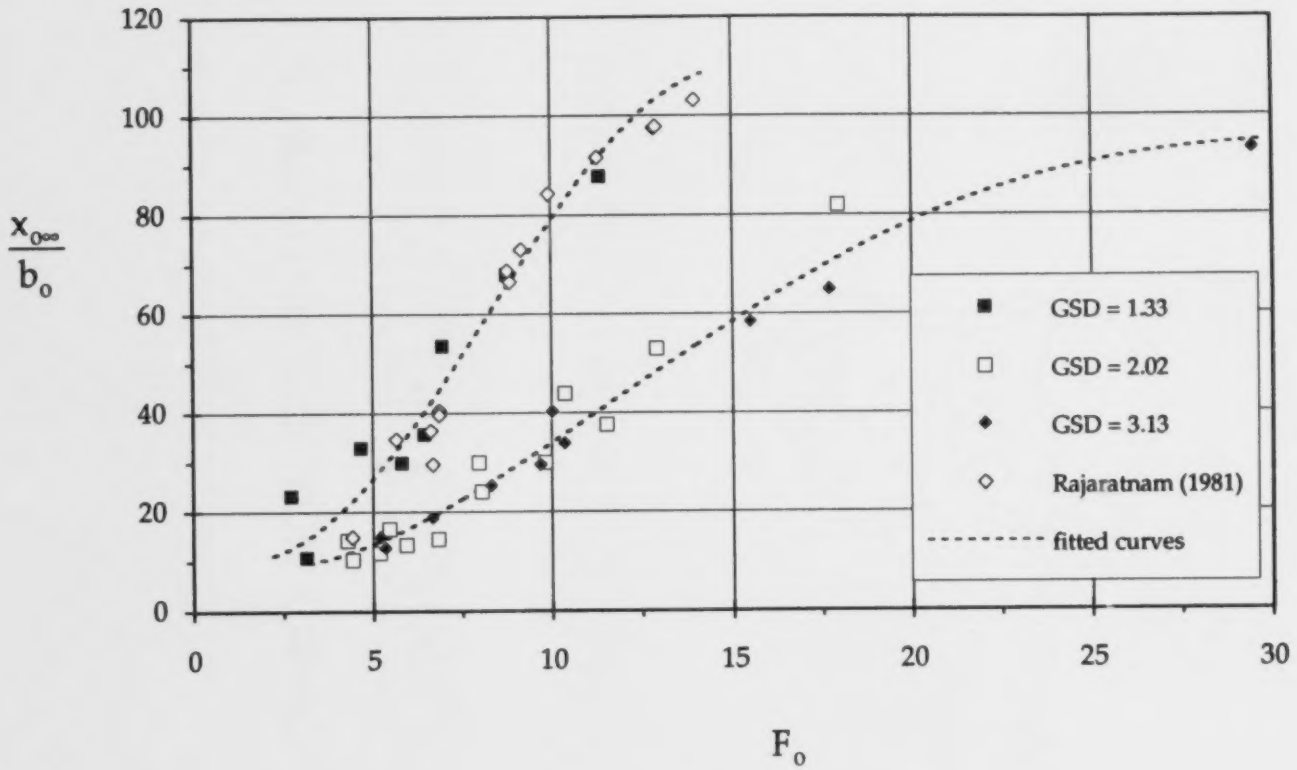

Figure 5–10: Variation of scour hole length with F_o

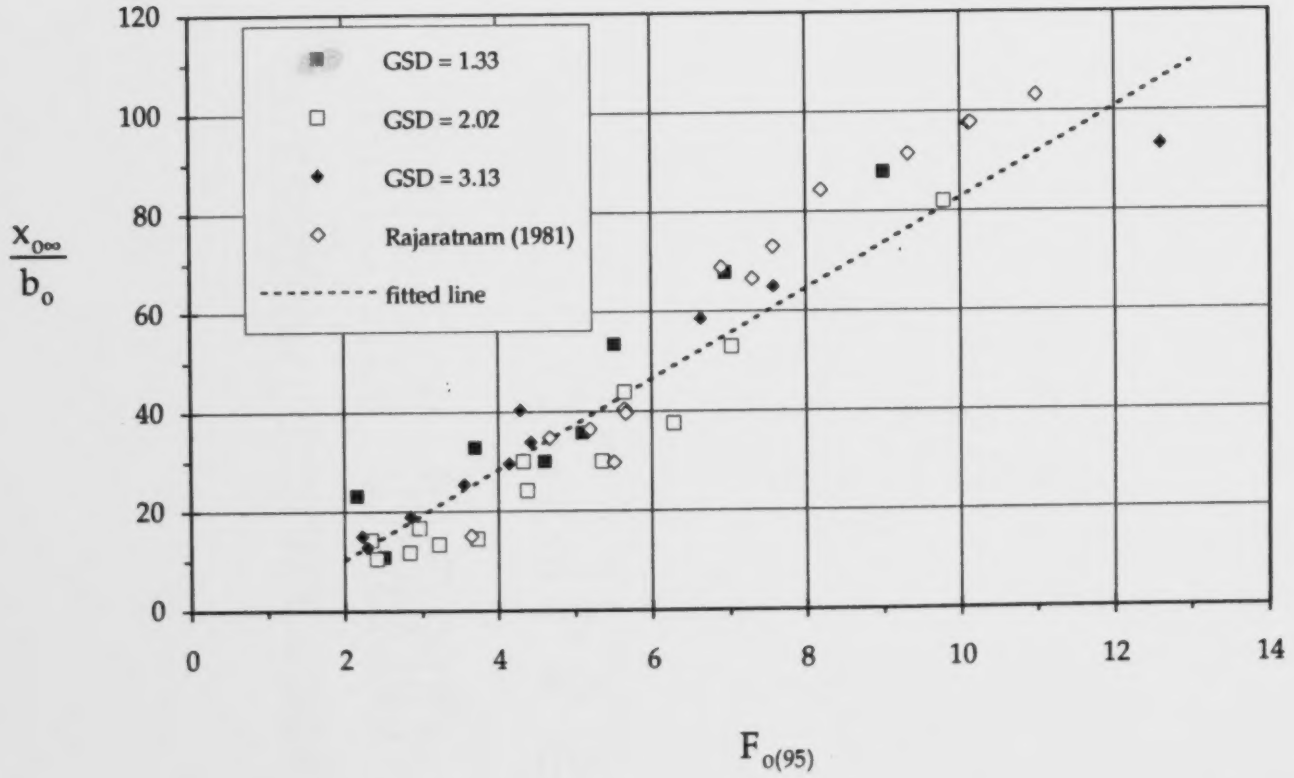

Figure 5–11: Variation of scour hole length with $F_{o(95)}$

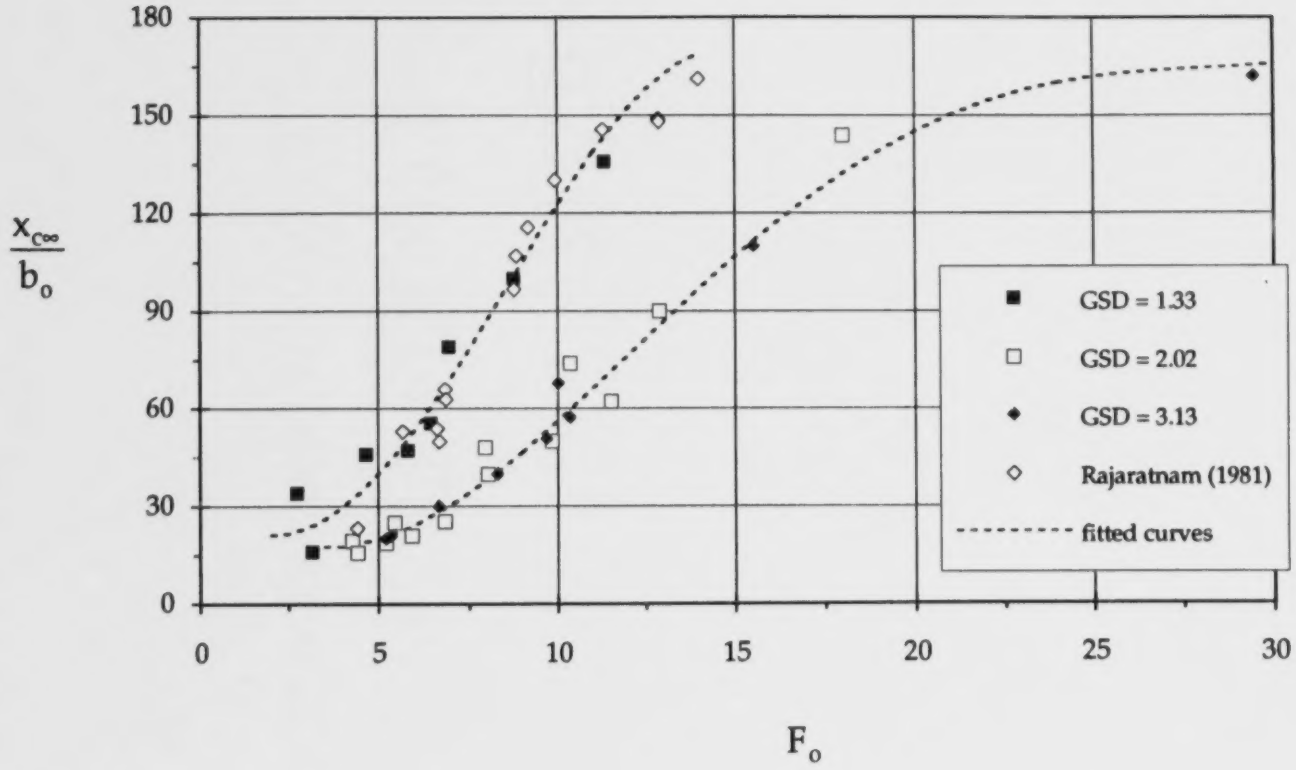

Figure 5–12: Variation of the distance of dune with F_o

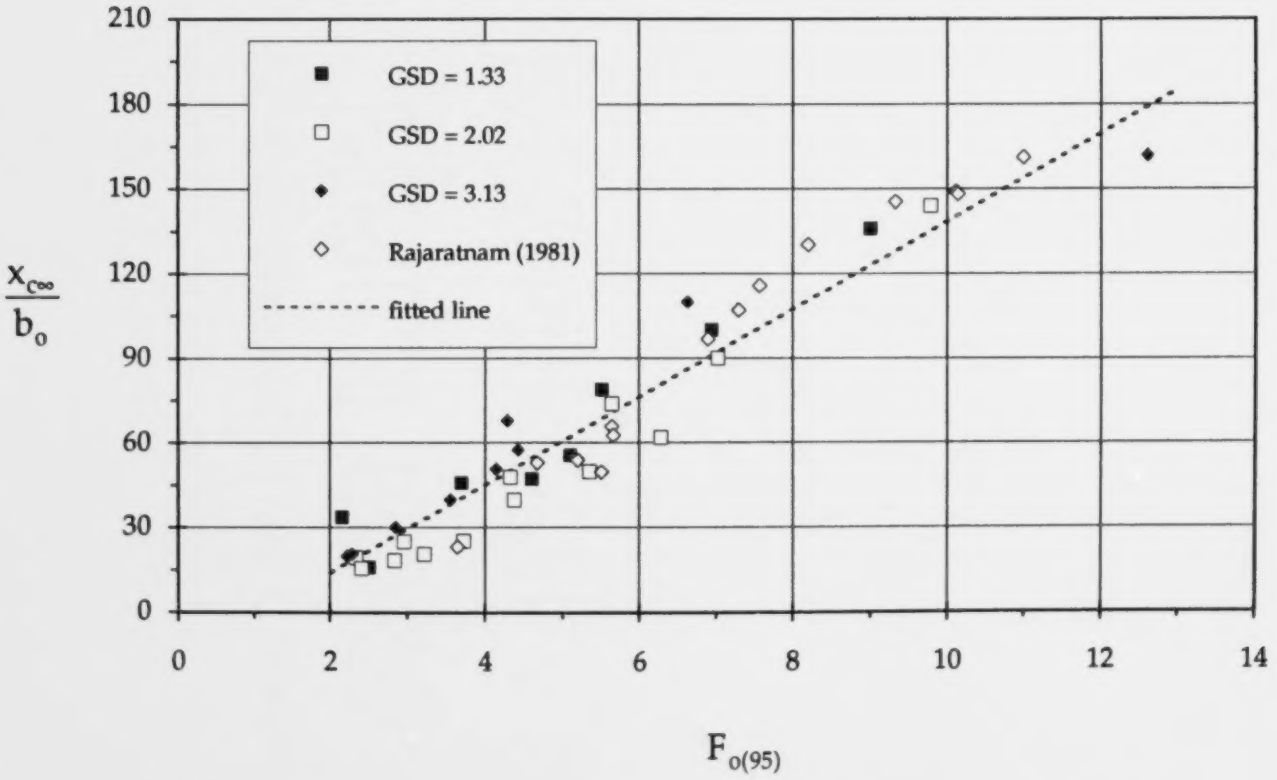

Figure 5 – 13: Variation of the distance of dune with $F_{o(95)}$

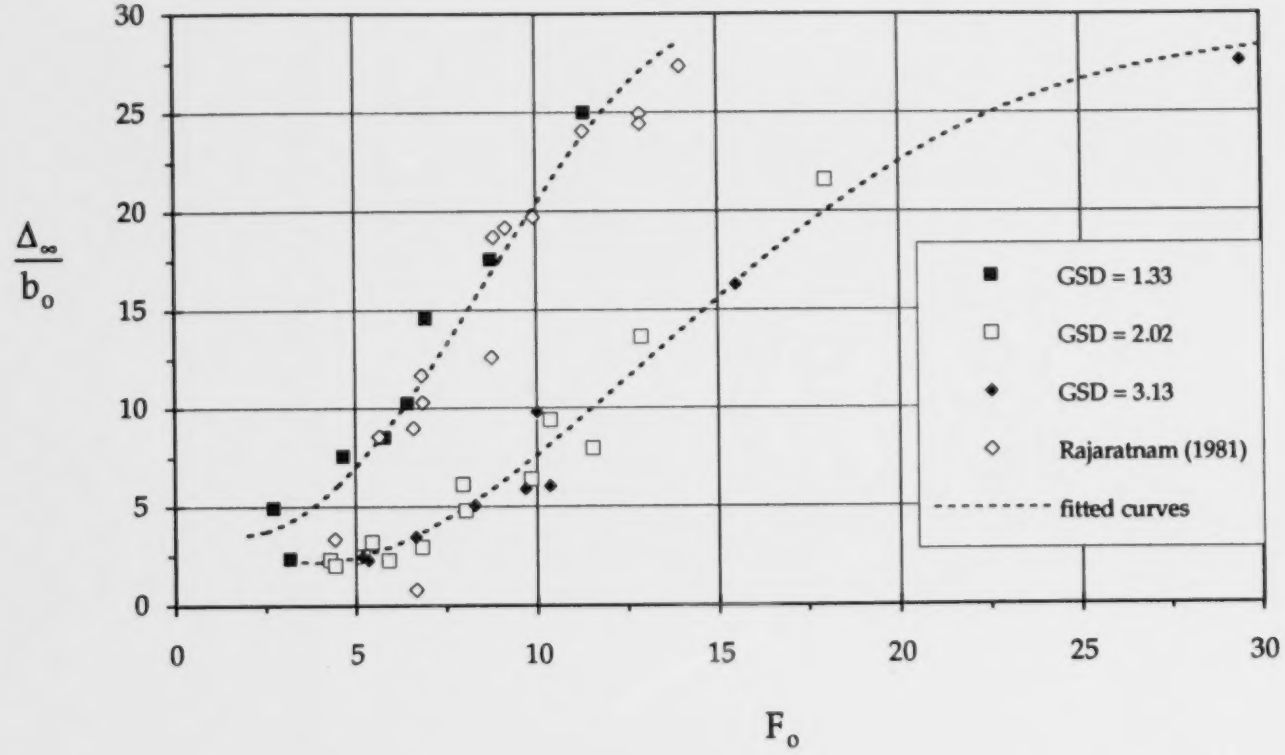

Figure 5–14: Variation of the dune height with F_o

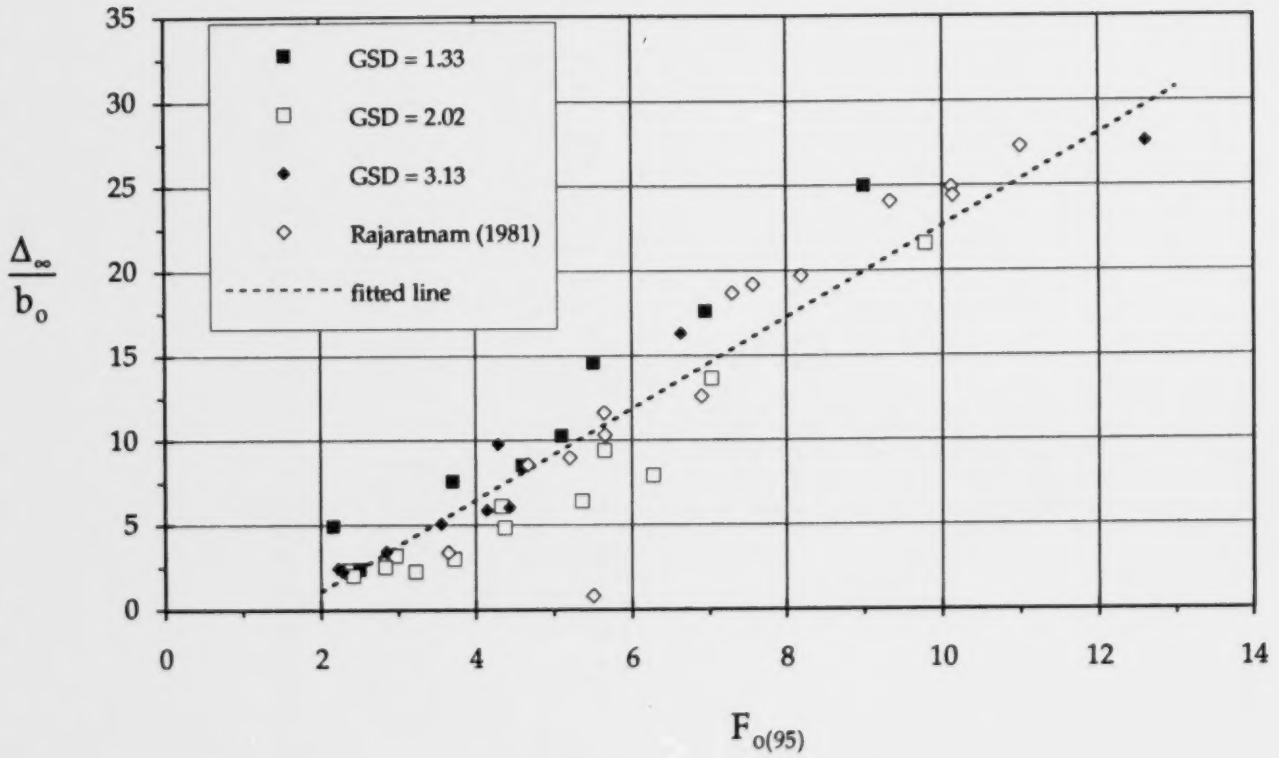

Figure 5–15: Variation of the dune height with $F_{o(95)}$

CHAPTER 6

Generalized Study of Erosion by Circular Horizontal Turbulent Jets †

6.1 Introduction

In the field of hydraulic engineering, erosion by circular wall jets is perhaps one the most common types of erosion by jets. It can be found at the outlets of circular culverts or storm drainage pipes which may be free or submerged depending on the tail water conditions. Upstream of the culvert or pipe, there is a backwater effect due to the constriction of the approach flow. As the flow enters the culvert, some of the potential energy is converted to kinetic energy. The nature of the flow in the culvert is influenced by its length, gradient, roughness and upstream and downstream water levels. At the outlet, if unprotected, the excess kinetic energy can cause a substantial scour resulting in channel instability and eventually the failure of the structure. This can be through localized erosion which encourages undermining of the culvert and/or instability of the embankment (gully scour) as reported by Stevens (1969), Bohan (1970) and Smith (1985), among others. Gully scour could be found where there is sufficient differential in elevation between the outlet and the section of stable channel downstream. The scour usually starts at a point where the channel is stable and progresses upstream and could completely undermine the outlet structure. To prevent this problem, the design usually entails building a riprapped (rock or blocks) culvert outlet stilling basin for low flows or an energy dissipator in the form of a rigid (i.e. concrete, steel) boundary basin for large flows.

There has been quite a number of investigations on this subject in the past few decades. Some of these are by Stevens (1969), Laushey et al. (1967), Rajaratnam and Berry (1977), Abt et al. (1984) and Lim (1995). In this chapter,

---

† Submitted to the Journal of Hydraulic Research, International Association of Hydraulic Research (IAHR).

the results of experimental studies on water jets on sand and gravel beds and air jets on a bed of canola seeds will be presented. An attempt will also be made to review and summarize the results from previous investigations. Over three hundred and fifty data sets on scour size have been compiled from many sources and the results of the re-analysis are presented in the sections below.

6.2 Literature Review

It appears that the first major published research studies on scour due to circular wall jets were the theses of Clarke (1961), Ofwona (1965), Opie (1967) and Stevens (1969). A good attention was given to it at the twelfth congress of the International Association for Hydraulic Research held at Colorado State University, Fort Collins, U.S.A. in 1967. At this congress, Seaburn and Laushey presented their research investigation into velocity of culvert jets for incipient motion and Laushey et al. presented results on magnitude and rate of erosion at culvert outlets. A few years later, reports on scour estimation and design of outlets were published by Bohan (1970) and Fletcher and Grace (1972 and 1974) at the United States Army Engineer Waterways Experiment Station in Vicksburg, Mississippi. Another important earlier study was by Simons and Stevens (1971). They presented a detailed analysis and control methods for scour control in rock basins. Since then, the literature on the subject has grown substantially and there has been improved knowledge on the analysis and control methods of scour downstream of circular wall jets. The following paragraphs present the rest of the review almost in chronological order and according to author or research institute.

Stevens (1969) performed an extensive laboratory work on culvert erosion using typical prototype values for the rock size, culvert diameter and flow discharges. Design curves for estimating the scour depth were given. A constant value for relative sediment size, d_e/d, which depends on the tail water depth h_d and the discharge Q, was suggested for the prevention of scour. The term d_e, which is the effective diameter, is the cube root of the average volume of the rock sizes and d is the diameter of the culvert. Simons and Stevens (1971) presented a detailed examination and analysis of scour in rock basins at pipe outlets based mainly on the experimental results of Stevens (1969).

Rajaratnam and Berry (1977) studied the erosion of loose beds of sand and polystyrene by jets of air and water. The characteristic lengths of the eroded bed in terms of the jet diameter d were found to be mainly functions of the densimetric particle Froude number, F_o. The erosion profiles were found to be similar both in the unsteady and asymptotic states. Rajaratnam and Diebel (1981) found that the relative tail water depth and relative width of the downstream channel do not affect the maximum depth of scour significantly whereas they reduce significantly the distance at which it occurs. In these studies, any characteristic length of scour during the erosion process was found to vary linearly with the logarithm of time up to some time after which the variation became non-linear and eventually reached an end state.

Abt et al. (1984) compiled data from many experiments performed at the Colorado State University Hydraulics Laboratory, Fort Collins and proposed equations for the dimensions of scour based on a non-dimensional discharge intensity Q_i, geometric standard deviation of bed material size σ_g and the ratio of median bed material size D to culvert diameter d. Q_i is defined as $Q/\sqrt{(gd^5)}$ where g is the acceleration due to gravity. Mendoza (1980), who also worked in the same laboratory, examined the headwall influence on scour. It was noticed that the headwall helps to prevent undermining of the culvert barrel and protect the embankment from excavating on both sides of the culvert outlet. Its effects on the scour hole dimensions were found to be insignificant. A foundation depth for the headwall equal to the maximum scour depth was recommended. Abt et al. (1985) examined the effect of culvert slope on scour and found that a sloped culvert can increase the characteristic lengths of scour from 10 to 40% over the characteristic lengths for a horizontal jet. Abt et al. (1987) investigated the influence of culvert shape on scour. The results showed that a significant influence exists. The experimental data from four different shapes were correlated to Q_i which was re-defined as $Q/\sqrt{(gR_h^5)}$ where R_h is the hydraulic radius of the culvert. These studies generally showed that the scour lengths increased as a power function of time before reaching an end state.

Lim and Chin (1992) investigated the effect of sediment non-uniformity on scour. For the non-uniform sediment, a shorter time was required for scour to reach equilibrium and also, the maximum scour depth was found to decrease

as the sediment gradation increased. Recently, Lim (1995) compiled a large database on maximum scour depth below unsubmerged full-flowing culvert outlets. The scour data were correlated with F_o and an equation for an enveloping curve was proposed. Scouring of non-cohesive beds by cantilevered circular horizontal jets of different drop heights has been investigated by Robinson (1971), Blaisdell and Anderson (1988a,b) and Doehring and Abt (1994), among others. These studies have proposed methods for predicting the anticipated scour hole size and may be used to design a stable pool energy dissipator.

6.3 Experiments and Compiled Data

Two different sets of experiments were performed. The first set was on water jets on sand and gravel beds and the second set was on air jets on a bed of canola seeds. The experimental set-ups are shown in Figure 6-1(a-b). The experiments were run until the asymptotic state was reached. The transient profiles of the eroded bed were measured in one of the experiments in the first set (Table 6-1(a)). The details of the asymptotic values of the characteristic lengths of the scoured bed for the two sets of experiments are given in Table 6-1(b). The definition sketch for the scour hole lengths is shown in Figure 6-2(a).

The first set consisted of twelve experiments which was performed in a tank, 3.53 m long, 1.09 m wide and 1.22 m deep. Three nozzles of diameters 5, 19 and 25.4 mm were used and were mounted on the side of the tank. The sand and gravel beds were 0.25 m deep and were supported by an elevated false bed of height of 0.31 m (see Figure 6-1(a)). The median size of the sand was 0.242 mm with a geometric standard deviation of 1.46 while the respective values for the gravel were 7.2 mm and 1.33. The jets were produced through the nozzles by pumping water from the far end corner of the tank in such a way as not to affect the flow around the scour hole. The velocity of the jet at the nozzle was measured using a Prandtl tube of external diameter of 3 mm. During the experiments, water was continuously supplied into the tank to account for losses and a constant tail water depth was ensured by having an over flow arrangement.

The air for the second set of experiments was supplied by the compressed air supply of the University (see Figure 6-1(b)). A 12.5 mm diameter nozzle was used for all the experiments. The velocity of the jet at the nozzle was measured by means of a pressure tap installed on the jet apparatus. A calibration had earlier been obtained between the pressure readings and the velocity measurements in the potential core of the jet using a 3 mm external diameter total head tube. The median size of the canola seeds was 1.47 mm with a geometric standard deviation of 1.12. The sediment size distribution curves are shown in Figure 6-3. The experiments were seven in number and were performed in a wooden container that has a length of 1.8m , a depth of 0.01m and a diverging width (in the downstream direction) varying from 0.3 to 1.18m.

Over three hundred and fifty sets of data have been compiled from thirteen sources including the present study. The database comprises of scour data on jets of water on gravel and sand beds and air jets on beds of sand, polystyrene and canola seeds. The ranges of the scour data are summarized in Table 6-2 and the experimental data from other investigations are given in Table 6-3 (a-l). It is interesting to note that in this database, D varies from 0.24 to 178 mm, d from 2.4 to 914 mm, jet submergences (equal to h_d/d) from -0.35 to large values, relative density difference, $\Delta\rho/\rho$, from 1.65 to 2189 and F_o from 0.65 to 99.6. $\Delta\rho$ is the difference between the mass densities of the bed material and the fluid and ρ is the mass density of the fluid. F_o is the densimetric particle Froude number which can be interpreted as a measure of the ratio of the tractive force of a wall jet on a grain to its resistive force. It is defined as $U_o/\sqrt{(gD\Delta\rho/\rho)}$, wherein, U_o is the jet velocity at the culvert outlet.

6.4 Scour hole Characteristics

6.4.1 Description of the Scour Process

A description of the scour process for experiment number 12 (see Tables 6-1(a-b)) will be given. The deeply submerged jet is 5 mm at the nozzle and has a velocity of 5.52 m/s. The bed is of sand with a median size of 0.242 mm and F_o is equal to 88.2. Immediately the jet was turned on, the sand particles close to the nozzle were blown out as big sediment clouds upwards and mainly downstream. The flow was very turbulent and the scouring at this

stage was very vigorous. Most of the eroded particles were transported as suspended load. This made observations quite difficult. The concentration of the suspended particles was seen to decrease in a vertical plane from the bed upwards. After a few seconds, a definite shape of the eroded bed could be seen and further erosion occurred mainly by the transport of the eroded material away as bed load. The sand particles were transported along the bed and at the crest of the ridge, the finer particles were propelled into suspension and settled some distance from the ridge whereas the coarser particles toppled over the crest of the ridge and rolled or slid down its downstream slope. After a few hours, the rate of erosion had decreased considerably. The bed load ceased to move continuously. It was noticed that the sand particles around the impingement area of the jet, which was mainly just downstream of x_O, periodically moved upwards and slid back. Some eventually made their way over the crest.

Migrating small dunes were formed on the upstream slope of the ridge a few hours later (see Figure 6-4(a)). They were usually 5 or 6 in number. They had an average height of about 4 to 6 mm and were spaced about 60 to 100 mm apart. They migrated very slowly up the slope and fall off at the crest of the ridge. A new dune was constantly being formed to maintain the total number as the furthermost dune was about to topple over the crest. The dunes remained noticeable throughout the rest of the test run. The periodic sliding of the sand particles around the impingement area still continued especially just downstream of the peaks of the small dunes. It was noticed that the bed armored a little. This was not unexpected because the particle size geometric standard deviation σ_g (equal to $\sqrt{(d_{84}/d_{16})}$) which is 1.46 is just outside the range ($\sigma_g < 1.35$) generally recommended for non-armoring sediment mixtures (Little and Mayer (1976) and Breusers and Raudkivi (1991)). Another interesting observation noticed at the latter stages of the run was at the downstream end of the scour hole. The movement of the particles occurred mainly in the form of a few scattered weak puffs which appeared to have been caused by turbulent bursts. These particles were entrained by the jet and transported to the impingement area where they took part in the periodic sliding and dune migration. Figure 6-4(b) shows the shape of the scour hole at the asymptotic state. These observations were similar to those made when the water jets eroded the gravel bed except for the periodic

sliding, migrating dunes and the scattered turbulent bursts. Figure 6-4(c) shows the scour hole area of the eroded gravel bed. It can be seen that the bed is segregated with the coarsest particles lying at the bottom of the hole.

The observations on the air jets on canola seeds were different. At the beginning of scour, the scour rate was high and the grains were blown and thrown upwards, settling at far distances away from the nozzle. A scour hole without a ridge was formed at this stage. After a few minutes, the scouring was less vigorous and a ridge was gradually being formed. There were now fewer grains being projected into the air and most of the grains in transportation were confined to a region within close proximity to the bed. It was noticed that the grains on the sides of the scour hole were sliding individually or in groups and were propelled by the jet at high velocities before or when they reached the bottom of the scour hole, along with those particles already moving with the jet. These grains formed the ridge which stretched from one side of the scour hole to the other. After a few hours the asymptotic state was reached and the number of grains being propelled out of the scour hole could be counted. Compared to the first set of experiments, the scour hole was found to have a small ridge and a very elongated shape. Figure 6-4(d) shows an eroded bed of canola seeds.

6.4.2 Evolution of Scour hole with Time

It has been observed by many researchers such as Laursen (1952), Stevens (1969) and Rajaratnam and Berry (1977) to mention a few, that scour grows continuously with time and eventually an equilibrium state (sometimes refereed to as the asymptotic state) is attained. Many equations have been proposed for the relationship between scour dimensions and time t. A semi-logarithmic form of equation was used by Rouse (1940), Laursen (1952) and Rajaratnam and Berry (1977). A power law form was used by Bohan (1970) and Shaihk (1980) and a hyperbolic form was proposed by Blaisdell and Anderson (1981) to predict the ultimate scour dimensions.

The growth of scour with time was studied in experiment number 12 of the first set of experiments. Figure 6-5 shows the evolution of the longitudinal profile of an eroded bed with time. It can be seen that an equilibrium state was not attained even after 186 hours. It is also interesting

to note that the difference between two consecutive profiles at any location x along the bed appears to increase with increasing distance from the nozzle. This suggests that the eroded bed profile attains an equilibrium state at earlier times for locations closer to the nozzle. This has been further substantiated in Figure 6-6, which shows the variation of rate of scour $\partial\varepsilon / \partial t$, with distance x. ε is the depth of scour below the original bed level. It can be seen that at any particular time, the rate of scour increases with increasing distance from the nozzle and at any particular distance, it decreases with increasing time. Figure 6-7 shows the growth of some of the characteristic lengths of the scour hole with time. It appears that the equations for these relationships could be expressed in the power form.

6.4.3 Geometric Similarity of Scour hole

The scour hole produced by a circular wall jet is somewhat elliptical in shape at any section taken parallel to the original bed level and the maximum depth is usually located just downstream of the mid point of the maximum scour hole length x_o, that is, approximately $0.57 \pm 0.28 x_o$, (95% confidence limit) based on all the compiled data. It has been observed by Laursen (1952), Rajaratnam and Berry (1977) among others, that the scour hole is similar both in the unsteady and end states. Figure 6-7 shows the variation of x_m/ε_m and x_o/ε_m with time. ε_m is the maximum scour depth and x_m is the distance from the outlet where ε_m occurs. It appears that these ratios could be assumed to be constant with time. Using all the compiled data (not just those at the asymptotic state), the ratios of the length scales of the scour hole have been plotted against F_o. Equation (6-1) expresses the relationship between these lengths, where $\bar{\beta}$ is the mean ratio and κ is its standard deviation. Table 6-4 shows the values for these coefficients, wherein, $\bar{b}_m$ is the maximum half-width of the scour hole and V_s is the volume of the scoured material.

$$\frac{l_c}{\varepsilon_m} = \bar{\beta} \pm \kappa \quad \text{or} \quad \frac{V_s}{\varepsilon_m^3} = \bar{\beta} \pm \kappa \qquad (6\text{-}1)$$

Equation (6-2), as plotted in Figure 6-8, shows that the ratio x_m/ε_m might be considered fairly constant if the data of Stevens (1969) are excluded. The same arguments could be made for the ratio x_o/ε_m which is given by

equation (6-3) and plotted in Figure 6-9. Scour holes from Stevens (1969) had big rocks and were quite shallow and this might have created a lot of errors in measuring the scour lengths. The ratios $\bar{b}_m/\varepsilon_m$ and V_s/ε_m^3 are expressed by equations (6-4) and (6-5) and plotted in Figures 6-10 and 6-11 respectively. The latter has a mean value of 16.77 and a large standard deviation of 20.96. The standard deviations for these mean ratios are relatively high and it is therefore advised that caution should be exercised when using them.

Table 6-4: Ratios of length scales

Ratios	$\bar{\beta}$	κ	Remarks	Figure no.	Equation no.
x_m/ε_m	4.36	3.08	without Stevens' data	6-8	(6-2)
x_o/ε_m	8.81	6.52	"	6-9	(6-3)
$\bar{b}_m/\varepsilon_m$	2.40	1.8	all data	6-10	(6-4)
V_s/ε_m^3	16.77	20.96	all data	6-11	(6-5)

The same arguments could be made for the ratio x_o/ε_m which is given by equation (6-3) and plotted in Figure 6-9. Scour holes from Stevens (1969) had big rocks and were quite shallow and this might have created a lot of errors in measuring the scour lengths. The ratios $\bar{b}_m/\varepsilon_m$ and V_s/ε_m^3 are expressed by equations (6-4) and (6-5) and plotted in Figures 6-10 and 6-11 respectively. The latter has a mean value of 16.77 and a large standard deviation of 20.96. The standard deviations for these mean ratios are relatively high and it is therefore advised that caution should be exercised when using these equations.

6.5 Dimensional Considerations

Dimensional arguments could be used to develop expressions for estimating the characteristic lengths of scour. This method does not produce a unique set of non-dimensional parameters for a fixed number of variables. One has to decide which of these parameters has a physical meaning pertaining to the problem. For circular wall jet erosion, it can be argued that at equilibrium, any characteristic length of the scoured bed $l_{c\infty}$, is a function of the following parameters.

$$l_{c\infty} = f_1\left(U_o, d, \rho, \mu, D, g, \Delta\rho, (\text{or } g\Delta\rho), \sigma_g, S_p, B, h_d\right) \qquad (6\text{-}6)$$

where S_p is the pipe slope and B is the downstream channel width.
Equation (6-6) is based on the assumptions that:
i) the bed is non-cohesive
ii) the invert of the pipe outlet is at the same as the bed level
iii) the slope of the bed is the same as the slope of the pipe
iv) the pipe is flowing full
v) there is no transitional bed between the pipe and the non-cohesive bed
vi) the turbulence in the flow is not directly accounted for

A review of the existing formulae shows that in most cases, any characteristic length of scour is usually expressed in terms of the pipe size and correlated mainly to a discharge intensity Q_i or the densimetric particle Froude number F_o as shown by equations (6-7) and (6-8) respectively.

$$\frac{l_{c\infty}}{d} = f_2\left(\frac{U_o}{\sqrt{gd}} \text{ or } Q_i = \frac{Q}{\sqrt{gd^5}}, R_e = \frac{\rho U_o d}{\mu}, \frac{D}{d}, \frac{\Delta\rho}{\rho}, \sigma_g, S_p, \frac{B}{d \text{ or } D}, s = \frac{h_d}{d}\right) \qquad (6\text{-}7)$$

$$\frac{l_{c\infty}}{d} = f_3\left(F_o = \frac{U_o}{\sqrt{g\frac{\Delta\rho}{\rho}D}}, R_e = \frac{\rho U_o d}{\mu}, \frac{D}{d}, \sigma_g, S_p, \frac{B}{d \text{ or } D}, s = \frac{h_d}{d}\right) \qquad (6\text{-}8)$$

Physically, Q_i is some form of Froude number that could be interpreted as a measure of the ratio of the kinetic energy to the potential energy of the flow whereas F_o, as defined earlier, can be interpreted as a measure of the ratio of the tractive force of a wall jet on a grain to its resistive force. The former has been used by Stevens (1969), Mendoza et al. (1983), Abt et al. (1985) and the latter by Rajaratnam and Diebel (1981) and Lim (1995). In this chapter, F_o will be used for correlation because of its physical meaning which incorporates both the flow and sediment properties. The use of Q_i for correlation applies only to a particular sediment size and could be modified for the use of a variety of sediment sizes by adding a non-dimensional sediment size D/d, as shown by Abt et al. (1984). For very turbulent flows,

the viscous effect is known to be negligible and the Reynolds number R_e can be removed from the analysis. The effects of other important non-dimensional parameters are discussed in later sections.

6.6 Characteristic Lengths of the Eroded Bed

6.6.1 Equilibrium Maximum Scour Depth

Some of the recently proposed equations for the equilibrium maximum scour depth downstream of circular wall jets are:

Rajaratnam and Diebel (1981)

$$\frac{\varepsilon_{m\infty}}{d} = 0.41F_o - 0.67 \tag{6-9}$$

Abt et al. (1984)

$$\frac{\varepsilon_{m\infty}}{d} = \frac{3.65}{\sigma_g^{0.4}}\left[\left(\frac{Q}{\sqrt{gd^5}}\right)\left(\frac{d_{50}}{d}\right)^{0.2}\right]^{0.57} \tag{6-10}$$

Breusers and Raudkivi (1991)

$$\frac{\varepsilon_{m\infty}}{d} = 0.65\left(\frac{U_o}{u_{*c}}\right)^{1/3} \quad \text{for} \quad 30 \le \frac{U_o}{u_{*c}} \le 500 \tag{6-11}$$

$$\left(\text{i.e. about } 6.36 \le F_o \le 106.1\right)$$

Lim (1995)

$$\frac{\varepsilon_{m\infty}}{d} = 0.45F_o \quad \text{for} \quad 1 \le F_o \le 10 \tag{6-12a}$$

$$\frac{\varepsilon_{m\infty}}{d} = 4.5 \quad \text{for } F_o \ge 10 \tag{6-12b}$$

Equation (6-9) is based on seventeen data sets in the F_O range of 3.1 to 18.3 and the relative submergence s in the range of 0.2 to 3.4. Equation (6-10) is based mainly on the data of Mendoza (1980), Shaihk (1980) and Kloberdanz

(1982). Their experiments were performed with unsubmerged jets eroding sand beds. Lim (1995) re-expressed equation (6-10) as equation (6-13). His analysis showed that the predictions of this equation on the effect of d_{50}/d on $\varepsilon_{m\infty}/d$ are contrary to the findings of Breusers and Raudkivi (1991) and poor predictions were obtained when the equation was applied to data having values of d_{50}/d outside the range the equation was developed for.

$$\frac{\varepsilon_{m\infty}}{d} = \frac{3.68}{\sigma_g^{0.4}} F_o^{0.57} \left(\frac{d_{50}}{d}\right)^{0.4} \qquad (6\text{-}13)$$

$$\frac{\varepsilon_{m\infty}}{d} = 1.1 F_o^{0.33} \qquad (6\text{-}14)$$

The poor prediction was attributed to the narrow range of d_{50}/d (0.02 to 0.03, if one data set is excluded). This appears to be true and might explain the reason why d_{50} has a positive exponent (the scour depth becomes proportional to $(d_{50})^{0.114}$). Lim (1995) re-expressed equation (6-11), which is Breusers and Raudkivi's (1991) equation as equation (6-14). The equation is based on the data of Bohan (1970) and Abt et al. (1984). Equation (6-12) was proposed by Lim (1995) and it is an envelop for the experimental data of his study, Opie (1967), Laushey et al. (1967), Bohan (1970), Rajaratnam and Diebel (1981) and Abt et al. (1995). Equation (6-12b) is based mainly on data points obtained from Bohan (1970) especially in the region of F_O greater than 20. Without these data, it will not be possible to develop this equation.

Bohan's (1970) data used for equation (6-12b) correspond to a test duration time of 5 hours and appear to be extrapolated data obtained from his scour length-time equations. This time does not correspond to the asymptotic (or equilibrium) state because Bohan (1970) reported that a limiting state was not reached in similar tests (F_O equal to 22.6 and 47.9) that were run for approximately 24 hours. Intuitively and based on the results of Rajaratnam and Berry (1977), the time it takes for the growth of scour to reach an asymptotic (or equilibrium) state should increase with F_O. Therefore, at very high values of F_O, it appears reasonable to at least expect that this time will be in terms of days, probably weeks and not a few hours. The results of experiment number 12 further confirm this. Bohan's (1970) data have been

further extrapolated to an arbitrary time of 72 hours to obtain better estimates of the asymptotic maximum scour depths and these will be treated as the asymptotic values in this study.

Figure 6-12 shows the plot of the asymptotic relative maximum scour depth against F_O using data from thirteen sources. The abscissa of this figure (and for some of the other figures) is in logarithm scale to prevent crowding of data points with low F_O values, which apply to most of the data. Some of the plotted data are from scour tests with the pipe/culvert flowing partially. In such cases, d has been re-defined as $\sqrt{(4A/\pi)}$, where A is the area of flow at the pipe outlet. In this figure, all the data appear to follow the same trend up to about F_O equal to 10 and beyond that, the data are split into two groups. The upper set of data belongs mainly to Clarke (1961) and have high values of s. An examination of his data shows that they are quite close to equilibrium data. Also in this group are three data points from the present study which are about 50% lower in value compared to Clarke's (1961) data. This might be attributed to armoring as a result of the value of σ_g, which is 1.46, compared to 1.13 and 1.15 for the sands used by Clarke (1961). The lower set of data belongs mainly to Bohan (1972) (corresponding to 72 hours) and have low values of s. It does appear that the effect of s on equilibrium maximum scour depth is not very pronounced until beyond F_O equal to 10. Equation (6-15) is proposed as a best fit equation for all the data before F_O equal to 10 and all the data beyond this point with s much greater than 1. These data, which will be referred henceforth to as 'Set 1', can be enveloped by a line expressed as equation (6-16). 'Set 2' refers to all the data beyond F_O equal to 10 with s less than 1.

$$\frac{\varepsilon_{m\infty}}{d} = 0.45\,F_o - 0.31 \qquad (6\text{-}15)$$

$$\frac{\varepsilon_{m\infty}}{d} = 0.5(F_o + 1) \qquad (6\text{-}16)$$

6.6.1.1 Effect of Jet Submergence

The effect of jet submergence s on the relative equilibrium maximum scour depth was found from Figure 6-12 to be very pronounced beyond F_O

equal to 10. For deep submergence, the scour depth was more and its difference from the corresponding scour depth for low submergence increased with increasing F_o. For low values of F_o, the data have been re-categorized according to the value of s as shown in Figure 6-13. For partial flow, s has been re-defined as h_d/d_b, where d_b is the depth of flow at pipe outlet. It appears that for F_o less than about 3, data in the range $0 < s \leq 0.5$ have slightly higher values of scour depth and the data in the range $s \geq 1$ have the least values. This trend is however, reversed at F_o greater than about 7.5.

Figure 6-14 shows the experimental results for unsubmerged flows ($s \leq 1$) only. Equation (6-17) is proposed as a set of equations, that envelopes almost all the data. They are modified forms of Lim's (1995) equations (equation (6-12)). The equations of Lim (1995) and Breusers and Raudkivi (1991) are also plotted on this figure for comparison. It can be seen that equation (6-12b) might not be quite reliable especially at very high F_o values. Data on equilibrium scour depth are needed in this range to obtain a more reliable equation.

$$\frac{\varepsilon_{m\infty}}{d} = 0.5F_o \qquad \text{for} \qquad 0.6 \leq F_o \leq 10 \qquad (6\text{-}17a)$$

$$\frac{\varepsilon_{m\infty}}{d} = 4.75 + 0.025F_o \qquad \text{for} \qquad 10 < F_o \leq 100 \qquad (6\text{-}17b)$$

6.6.1.2 Effect of Drop Height

The effect of drop height on scour by circular horizontal jets issuing from cantilevered outlets has been investigated by investigators such as Robinson (1969), Blaisdell and Anderson (1989) and Doehring and Abt (1994). Figure 6-2(b) shows a definition sketch for scour from cantilevered outlets. The data from these studies have been re-analyzed to conform with the present approach. F_o has been re-defined as F_d to reflect the height of the drop as given by equation (6-18). The difference in culvert (pipe) invert elevation and elevation of tail water level is refereed to as h_p. Also from these studies, the tail water depths were very shallow and a depth of 0.5d will be assumed in this analysis.

$$F_d = \sqrt{F_o^2 + \frac{2\left(h_p + 0.5d\right)}{D\Delta\rho/\rho}} \qquad (6\text{-}18)$$

$$\frac{\varepsilon_{m\infty}}{d} = 10.5\left\{1 - \exp\left[-0.35\left(F_d - 2\right)\right]\right\} - 0.5 \qquad (6\text{-}19)$$

Figure 6-15 shows the plot of the equation proposed by Blaisdell and Anderson (1989) (equation (6-19)) and the data of Robinson (1969), Smith and Johnson (1983) and Doehring and Abt (1994). The data of Rajaratnam (1981), which were obtained from circular impinging vertical jets with minimum tail water, are also plotted for comparison. In this case, the jet angle with the bed is at its maximum and greater than the jet angles used by the other investigators. Figure 6-15 shows some considerable scatter and this might be due to the difference in the experimental set-up and procedure. Blaisdell and Anderson's (1989) equation predicts very conservative values that envelope the rest of the data for F_d less than 14. It was developed using scour data from suspended-sediment-removed-tests and asymptotic data computed using an extrapolating method (Blaisdell et al. (1981)) on time-dependent scour depth data. The data of Robinson (1969) and Doehring and Abt (1994) appear to be static scour depths. Smith and Johnson (1983) obtained their data from scour holes at equilibrium with downstream dunes removed. Due to the degree of scatter in Figure 6-15, it appears reasonable to use the conservative equation proposed by Blaisdell and Anderson (1989) to estimate scour depths at overhanging pipe outlets.

6.6.2 Other Length Scales

The other length scales that will be discussed are the distance of the location of the maximum scour depth $x_{m\infty}$, the length of the scour hole $x_{o\infty}$, the maximum half-width of the scour hole $\bar{b}_{m\infty}$, the distance of the location of the dune $x_{c\infty}$, the height of the dune Δ_∞ and the cube root of the scoured material $V_s^{1/3}$.

Figure 6-16 shows the plot of $x_{m\infty}/d$ against F_o. A mean and an enveloping curve, given by equations (6-20) and (6-21) respectively, could be

used for Set 1 data. There were not enough Set 2 data in the literature to suggest a relationship.

$$\frac{x_{m\infty}}{d} = 1.69\,F_o - 0.65 \qquad (6\text{-}20)$$

$$\frac{x_{m\infty}}{d} = 1.8\,(F_o + 2) \qquad (6\text{-}21)$$

The relationship between the relative scour hole length $x_{o\infty}/d$ and F_o is shown in Figure 6-17. Following the previous approach, a mean and an enveloping curve have been proposed for Set 1 data. The equations for these curves are respectively equations (6-22) and (6-23). Equation (6-24) could be used as a predictor that envelops Set 2 data.

$$\frac{x_{o\infty}}{d} = 2.98\,F_o - 0.81 \qquad (6\text{-}22)$$

$$\frac{x_{o\infty}}{d} = 3.3\,(F_o + 2) \qquad (6\text{-}23)$$

$$\frac{x_{o\infty}}{d} = 68\log F_o - 41 \qquad (6\text{-}24)$$

The relation between the relative maximum half-width of the scour hole $\bar{b}_{m\infty}/d$ and F_o for Set 1 data is given by equation (6-25) and shown in Figure 6-18. Equations (6-26) and (6-27) have been proposed for the enveloping curves for Set 1 and Set 2 data respectively.

$$\frac{\bar{b}_{m\infty}}{d} = 0.86\,F_o - 0.17 \qquad (6\text{-}25)$$

$$\frac{\bar{b}_{m\infty}}{d} = 0.9(F_o + 2) \qquad (6\text{-}26)$$

$$\frac{\bar{b}_{m\infty}}{d} = 28\log F_o - 20.2 \qquad (6\text{-}27)$$

The relative distance of the location of maximum dune height $x_{c\infty}/d$ for Set 1 data can be related to F_o as given by equation (6-28) and shown in Figure 6-19. Set 2 data do not exist for this length scale. The plot of the relative dune height against F_o is shown in Figure 6-20. It has been categorized according to the value of s. There are not enough data to properly establish the effect of s on Δ_∞/d. It appears that between F_o equal to 8 and 20, Δ_∞/d has the highest value when s is greater than 4. The relationship between the relative scoured volume V_s/d^3 and F_o for F_o less than about 20 is given by equation (6-29) and shown in Figure 6-21.

$$\frac{x_{c\infty}}{d} = 3.72F_o + 5.89 \qquad (6\text{-}28)$$

$$\frac{V_{s\infty}}{d^3} = 0.3\,F_o^3 \qquad (6\text{-}29)$$

6.7 Effect of relative density difference $\Delta\rho/\rho$

It was observed as mentioned in the last paragraph of section 6.4.1, that the scour holes produced by the air jets had smaller ridges and more elongated shapes. The reason for this is believed to be the mode of transport which is governed by both F_o and the relative density difference $\Delta\rho/\rho$. The effects of the latter on the characteristic lengths of scour will be addressed in this section. These effects had been earlier examined by Rajaratnam (1977). The results indicate that the same relationship could be used to correlate $\varepsilon_{m\infty}$ with F_o for both the air and water jet experiments. This was also found to be true for the analysis of $x_{m\infty}$ and $\bar{b}_{m\infty}$, but not for Δ_∞.

Figure 6-22 shows that the relative maximum scour depth can be described by the same relationship for both the air and water jet experiments. The distance of its location $x_{m\infty}$ is however a bit further for the air jet experiments and this can be described by equation (6-30).

$$\frac{x_{m\infty}}{d} = -0.43 + 2.21F_o \qquad (6\text{-}30)$$

Figure 6-23 shows that the scour hole widths for the air jet experiments are slightly smaller and the scour hole lengths are approximately 88% longer at

F_o equal to 3 and this difference decreases to 34% at F_o equal to 100. These relationships could be described by equations (6-31) and (6-32) respectively.

$$\frac{\bar{b}_{m\infty}}{d} = -1.62 + 0.85F_o \qquad (6\text{-}31)$$

$$\frac{x_{o\infty}}{d} = 2.28 + 3.75F_o \qquad (6\text{-}32)$$

It appears that the distance of the ridge can be described by the same relationship for all the fluid-sediment systems as shown in Figure 6-24. This figure also shows that the ridge height for the water jet experiments ($s > 4$) have the higher values. It is higher by about at least 250 % at F_o equal to 10 and this difference decreases to about 25% at F_o equal to 50.

6.8 Effects of other non dimensional parameters

The effect of relative channel width B/d on maximum scour depth has been studied by Rajaratnam and Diebel (1981) and recently by Lim (1995). B/d had values of 1, 3, 3.5 and 86 in the former study and 5, 10 and 66.7 in the latter study. Their results both indicate that the effect is minimal. Abt et al. (1985) investigated the effect of slope on scour. Their results show, as earlier discussed in section 6.2; that there could be an increment of 10 to 40% in maximum scour dimensions over those for a horizontal culvert.

It is generally known that armoring of the bed by the larger bed particles occurs in very non-uniform beds resulting in smaller scour holes than in uniform beds. This is believed to occur when σ_g is greater than 1.3 according to Little and Mayer (1976). An examination of the compiled data shows that there are not enough data in this range to effectively quantify the effect of σ_g on scour depth. Abt et al. (1984) attempted to incorporate σ_g into a scour depth equation and obtained equation (6-10). It shows that the scour depth $\varepsilon_{m\infty}$ is proportional to $\sigma_g^{-0.4}$. Breusers and Raudkivi (1991) pointed out that three out of five sets of data used for the correlation were essentially uniform material and the effect of σ_g on scour depth may not be well defined by this equation. Lim and Chin (1992) also examined the effect of σ_g using three sand mixtures all having a median diameter of 1.65 and σ_g equal to 1.25, 1.78

and 2.5. Their results showed that under similar conditions, the scour depth is about half the value of that with uniform sediment.

6.9 Conclusions

An analysis of over three hundred and fifty sets of scour data at pipe outlets, obtained from thirteen sources including the present experimental study has been presented. The present experimental study comprised of air jets on canola seeds and water jets on sand and gravel beds. The whole database covers wide ranges of flow submergence, jet sizes and strengths, bed material size, relative channel width and relative density difference.

In one of the experiments, the study of scour growth at high densimetric particle Froude number F_O (F_O=88.2) revealed that it could take over a week for the asymptotic state to be reached. It was also noticed that the equilibrium state was being reached earlier at sections closer to the nozzle. Similarity of the scour hole was checked both in the unsteady and asymptotic states by determining the ratios between the characteristic lengths of the scour hole. It appears that these ratios could be considered fairly constant and ranges for these ratios have been suggested.

It was re-established that the characteristic lengths of scour are mainly functions of the densimetric particle Froude number F_O. Equations were proposed for the relationships between these lengths and F_O and were compared to some of the existing scour equations. The effect of the tail water depth in terms of jet size on the asymptotic characteristic lengths of the scour hole was found to be pronounced when F_O is greater than 10. In this range and for a given F_O, the maximum scour depth was found to be lager for deep submergence flow compared to low submergence. The difference between these depths appear to increase with increasing F_O. Similar results were obtained in the analysis of the other characteristic lengths. Compiled scour data at overhanging outlets showed considerable scatter and were enveloped by the equation of Blaisdell and Anderson (1989).

The effects of the relative density difference on the characteristic lengths of scour were determined. For a given F_O, the maximum scour depth and the distance of the location of the ridge were the same for all the fluid jet-

sediment systems. The distance of the location of maximum scour and the scour hole length had higher values for the air jet-sediment systems. The opposite was the case for the maximum width of the scour hole and the height of the ridge.

6.10 References

Abt, S. R., Donell, C. A., Ruff, J. F. and Doehring, F. K. (1985), Culvert Slope Effects on Outlet Scour, Journal of Hydraulic Engineering, Vol. 111, No. 10, pp. 1363 - 1367.

Abt, S. R., Kloberdanz, R. L. and Mendoza, C. (1984), Unified Culvert Scour Determination, Journal of Hydraulic Engineering, Vol. 110, No. 10, pp. 1475 - 1479.

Abt, S. R., Ruff, J. F., Doehring, F. K. and Donell, C. A. (1987), Influence of Culvert Shape on Outlet Scour, Journal of Hydraulic Engineering, Vol. 113, No. 3, pp. 393 - 400.

Blaisdell, F.W., Anderson, C.L. and Hebaus, G.G. (1981), Ultimate Dimensions of Local Scour, Journal of Hydraulics Division, ASCE, Vol. 107, No. HY3, pp. 327 - 337.

Bohan, J. P. (1970), Erosion and Rip rap Requirements at Culvert and Storm Drain Outlets, U.S. Army Engineer Waterways Experiment Station, Research Report H-70-2, Vicksburg, Mississippi. 50 pp.

Breusers, H.N.C. and Raudkivi, A.J. (1991), Scouring, International Association of Hydraulic Research - Hydraulic Structures Design Manual, A.A. Balkerma, Rotterdam, 143 pp.

Clarke, F.R.W. (1962), The Action of Submerged Jets on Movable Material, Thesis presented to the University of London for the Degree of Master of Science. 202 pp.

Ead, S.A. (1990), Effect of Supercritical Flow on Local Scour Downstream of Pipe Culverts,' M.S. thesis, Ain Shams University, Cairo, Egypt. 194 pp.

Fletcher, B.P. and Grace, J.L. Jr. (1972), Practical Guidance for Estimating and Controlling Erosion at Culvert Outlets, Report H-72-50, U.S. Army Waterways Experiment Station, Vicksburg, Mississippi. 39 pp.

Fletcher, B.P. and Grace, J.L. Jr. (1974), Practical Guidance for Design of lined Channel Expansions at Culvert Outlets, U.S. Army Engineer Waterways Experiment Station, Research Report H-74-9, Vicksburg, Mississippi. 91 pp.

Kloberdanz, R.L. (1982), Localized Culvert Scour in Non-cohesive Bed Material, M.S. thesis, Colorado State University, Fort Collins, Colorado. 98 pp.

Laursen, E.M. (1952), Observations on the Nature of Scour, Proceedings of Fifth Hydraulic Conference, Bulletin 34, University of Iowa, Iowa City, Iowa, pp. 179-197.

Laushey, L. M., Ulrich, K. and Ofwona, M. P. (1967), Magnitude and Rate of Erosion at Culvert Outlets, Proceedings, Twelfth Congress of the International Association for Hydraulic Research, Vol. 3, pp. 338 - 345.

Lim, S. Y. and Chin, C. O. (Wang S. S. (ed.)) (1992), Scour by Circular Wall jets with Non-uniform Sediments, Advances in Hydro-science and Engineering, Vol. 1, pp. 1989 - 1994.

Lim, S.Y. (1995), Scour below Unsubmerged Full-flowing Culvert Outlets, Proceedings of the Institution of Civil Engineers, Water, Maritime and Energy, Vol. 112, pp. 136 - 149.

Little, W.C. and Mayer, P.G. (1976), Stability of Channel Beds by Armoring, ASCE, Journal of Hydraulic Division, Vol. 102, No. HY11, Proc. Paper 12519, pp. 1647 - 1661.

Mendoza, C. (1980), Headwall Influence on Scour at Culvert Outlets, M.S. thesis, Colorado State University, Fort Collins, Colorado. 186 pp.

Mendoza, C., Abt, S. R. and Ruff, J. F. (1983), Headwall Influence on Scour at Culvert Outlets, Journal of Hydraulic Engineering, Vol. 109, No. 7, pp. 1056 - 1060.

Ofwona, M.P. (1965), Time Progression of Erosion at Culvert Outlets, M.S. thesis, University of Cincinnati, 88pp.

Opie, T. R. (1967), Scour at Culvert Outlets, M.S. thesis, Colorado State University, Fort Collins, Colorado. 82 pp.

Rajaratnam, N. and Berry, B. (1977), Erosion by Circular Turbulent Wall Jets, Journal of Hydraulic Research, Vol. 15, No. 3, pp. 277 - 289.

Rajaratnam, N. and Diebel, M. (1981), Erosion Below Culvert-like Structures, Sixth Canadian Hydrotechnical Conference, pp. 469 - 484.

Seaburn, G. E. and Laushey, L. M. (1967), Velocity of Culvert Jets for Incipient Erosion, Proceedings, Twelfth Congress of the International Association for Hydraulic Research, Vol. 3, pp. 1 - 8.

Shaihk, A. (1980), Scour in Gravel Culvert Outlets, M.S. thesis, Colorado State University, Fort Collins, Colorado. 105 pp.

Simons, D. B. and Stevens, M. A. (Shen, H.W. (ed.)) (1971), River Mechanics: Chapter 24, Scour Control in Rock Basins at Culvert Outlets, Published by Shen, H.W., P. O. Box 606, Fort Collins, Colorado, U. S. A., 80521.

Smith, C. D. (1985), Hydraulic Structures, University of Saskatchewan Printing Services, 364 pp.

Smith, C. D. and Johnson, S. R. (1983), Scour Control at Overhanging Pipe Outlets, Sixth Canadian Hydrotechnical Conference, pp. 581 - 597.

Stevens, M. A. (1969), Scour in Rip rap at Culvert Outlets, Ph.D. Dissertation, Colorado State University, Fort Collins, Colorado. 203 pp.

Table 6-1(a): Experimental Data for Evolution of Scour with Time

Test Run number	12		
Jet Velocity:	5.52 m/s	Sand Size:	0.242 mm
Jet Size:	5 mm	GSD:	1.46
Jet Submergence:	124	F_O:	88.2

t=2 mins		t=5 mins.		t=13 mins.		t=30 mins.		t=1 hr.		t=3 hr.		t=8 hr.		t=21 hr.		t=45 hr.		t=90 hr.		t= 186 hr.	
x (mm)	ε (mm)	x (mm)	ε (mm)	x (mm)	ε (mm)	x (mm)	ε (mm)	x (mm)	ε (mm)	x (mm)	ε (mm)	x (mm)	ε (mm)	x (mm)	ε (mm)	x (mm)	ε (mm)	x (mm)	ε (mm)	x (mm)	ε (mm)
10	14.2	20	14.8	20	17	20	14.8	20	15.5	20	15	20	14.5	20	14.2	20	14.2	20	17.3	80	26.40
20	14.8	60	18	70	20.5	70	20.5	70	21.5	70	21.5	70	21.5	70	21.8	70	23.5	70	24.3	120	34.37
40	14	100	26.5	120	33.5	120	34.7	120	35	120	35.8	120	36.5	120	36.5	120	36.7	120	36	220	63.36
70	19.2	140	36.7	170	44.7	170	45	170	46.5	170	49	170	51.5	170	50.5	170	51.8	170	51	270	74.21
100	24.5	180	42.5	220	52	220	54	220	55	220	60	220	61.5	220	62.8	220	63.8	220	63.8	320	84.00
130	33.8	220	48.5	270	54.7	270	59.7	270	62.5	270	66.7	270	69.2	270	72.5	270	74.3	270	75.1	370	91.20
160	38	260	51.8	300	58	300	61.5	300	64.5	320	73.2	320	76.5	320	80	320	82.5	320	83.8	420	96.77
190	42	290	52.5	330	57.3	330	61.8	330	66	350	75.8	360	80.5	370	85.8	370	88.8	370	91.1	470	99.46
220	46	320	54	360	57.5	360	62	360	66	380	77.3	400	81.5	400	90	400	91	420	95.2	520	99.46
250	48.5	350	53.5	390	54.7	390	60	390	66	410	77	440	83.7	430	89.9	430	92.2	450	96	570	97.92
280	50.5	380	50	440	46.5	420	57.8	420	64	440	76.3	480	81.5	460	89.9	460	93.2	480	96	620	92.93
310	50.5	420	44	480	39.7	450	53	470	57.7	470	75.5	520	77.5	490	88	490	93.7	510	96	670	84.58
340	49.5	460	41.5	520	31	480	49	520	47	520	67	560	73.5	520	87.5	520	93.7	540	96	720	75.65
370	49	500	28.5	570	14	520	41.8	570	31.5	570	61.5	600	65.8	570	81.8	550	89.8	570	93.8	770	60.77
400	44	540	15.5	610	2.5	550	30.5	620	8.2	620	37	640	48.5	620	70.5	580	86.5	620	86.8	820	41.28
440	39	580	9	650	-19	580	14	670	-12.5	640	35.5	680	32.5	670	56.7	620	78.5	670	75.3	870	14.88
480	31.7	620	-1	660	-16.5	610	11	720	-42	670	18.5	720	7.5	720	32.5	670	65.5	720	61.8	920	-12.00
540	10.5	650	-12	705	-25.5	660	-19.5	730	-43.5	720	-13.3	770	-14	770	7.5	720	48.5	770	43	970	-36.87
555	4.5	685	-13.5	720	-17	690	-26.2	735	-42	735	-23.5	820	-40.5	820	-15.8	770	28	820	19.8	1020	-61.63
590	5.5	700	-6.5	740	-6.5	720	-36.5	765	-47.5	745	-22.5	850	-61.5	870	-38.5	820	3.7	870	-13.5	1070	-68.36
615	1	720	-5.5	770	-4	730	-41	780	-38	770	-29.5	860	-57.5	920	-61.2	870	-29.5	920	-30.7	1120	-76.80
660	1.5	730	-4.5	820	-12	760	-23	810	-19.5	820	-56.3	910	-67.5	935	-69.3	920	-50.5	970	-62.4	1170	-85.64
720	0.5	750	-0.5	835	-3.5	780	-13.3	840	-16	830	-62.5	925	-70.3	945	-64	960	-66.2	1020	-66.2	1220	-65.00
820	-2	785	-8.5	880	-6	820	-12	870	-14.5	840	-58.5	940	-61	1000	-75.5	980	-60	1040	-61.2	1270	-34.56
		800	-2.5	890	-3	850	-14	890	-7	870	-60.5	970	-40.5	1030	-62.5	1020	-62.8	1110	-74.5	1320	-7.68
		840	-4	920	-3	865	-3	930	-13	900	-43.3	1005	-15	1060	-48.8	1050	-67.3	1140	-64.2	1370	-5.28
		920	-1	1020	-0.5	910	-10	940	-7	930	-21.5	1020	-14.2	1090	-27.5	1060	-61.2	1180	-57.2	1420	-3.36
		1070	0	1120	-0.5	920	-6	1020	-4.5	960	-15.5	1045	-8	1110	-12.2	1102	-62	1220	-35	1520	-3.36
						1020	-2.5	1120	-3	1015	-11.5	1070	-11	1170	-6.5	1120	-53.8	1255	-10.7		
						1120	-2	1220	-2	1020	-8	1120	-9	1270	-6.5	1150	-35.3	1320	-7.2		
						1220	-1	1320	-0.5	1070	-6.5	1220	-5	1370	-3	1181	-10	1420	-4.5		
										1120	-5.5	1320	-2.5	1520	-2.5	1220	-9	1520	-4.5		
										1220	-3.5					1320	-4.5				
										1320	-2					1420	-2.5				
																1520	-3				

Table 6-1(b): Experimental Results

#	Series	Time (hr.)	U_o (m/s)	d (mm)	D (mm)	σ_g	$\Delta\rho/\rho$	$\varepsilon_{m\infty}$ (mm)	$x_{m\infty}$ (mm)	$x_{o\infty}$ (mm)	$x_{c\infty}$ (mm)	Δ_∞ (mm)	$\bar{b}_{m\infty}$ (mm)	x_b (mm)	h_d/d	B/d	$\varepsilon_{m\infty}/d$	F_o
1	Water	94	5.43	25.40	7.2	1.33	1.65	130.5	588	1110	1381	174.5	323.5	780	24.4	43	5.14	15.91
2	jets on	34	2.73	25.40	7.2	1.33	1.65	79.0	407	735	949	118.5	175	540	24.4	43	3.11	8.00
3	Sand/	84	4.23	25.40	7.2	1.33	1.65	107.7	509	945	1213	153.0	235	640	24.4	43	4.24	12.39
4	Gravel	73	3.48	25.40	7.2	1.33	1.65	87.5	506	770	981	125.0	194.5	500	24.4	43	3.44	10.19
5		219	4.72	25.40	7.2	1.33	1.65	128.5	521	1050	1328	172.5	291.5	700	24.4	43	5.06	13.83
6		15	2.15	25.40	7.2	1.33	1.65	59.5	240	512	650	39.0	103.5	340	0.75	43	2.34	6.29
7		12	4.01	25.40	7.2	1.33	1.65	87.0	355	940	1240	76.5	243	685	0.75	43	3.43	11.73
8		18	5.39	25.40	7.2	1.33	1.65	99.0	370	1120	1590	109.0	358	880	0.75	43	3.90	15.79
9		20	5.06	19.00	7.2	1.33	1.65	64.4	550	940	1220	77.8	226.5	830	0.75	57.5	3.39	14.82
10		72	4.30	5.00	0.242	1.46	1.65	72.0	360	635	775	61.5	143	480	124	218.4	14.40	68.70
11		108	4.87	5.00	0.242	1.46	1.65	95.5	430	790	920	65.0	185.5	530	124	218.4	19.10	77.81
12		186	5.52	5.00	0.242	1.46	1.65	99.46	520	900	1170	85.63	-	-	124	218.4	19.89	88.20
1	Air	26	52.04	12.5	1.47	1.12	892.1	56.5	385	633	750	48.2	-	-	∞	47.6	4.52	14.51
2	jets on	24	20.33	12.5	1.47	1.12	892.1	21.8	145	280	325	5	34.13	200	∞	47.6	1.744	5.67
3	Canola	19	25.47	12.5	1.47	1.12	892.1	30.2	235	359	415	16.3	47.625	250	∞	47.6	2.416	7.10
4	seeds	18	37.34	12.5	1.47	1.12	892.1	38.8	275	499	585	23	70.645	320	∞	47.6	3.104	10.41
5		22	41.16	12.5	1.47	1.12	892.1	40	265	493	585	23.3	72.23	300	∞	47.6	3.2	11.48
6		17	32.84	12.5	1.47	1.12	892.1	26.5	195	395	450	10.2	46.83	250	∞	47.6	2.12	9.16
7		25	80.03	12.5	1.47	1.12	892.1	77	490	830	975	55.5	152.5	455	∞	47.6	6.16	22.31

Table 6-2: Summary of the Complied Data

#	1 Name	2 Table No.	3 Remarks	4 # of Data Sets	5 Scour time (hr.)	6 $d^{\dagger}$ (mm)	7 $D^{\dagger}$ (mm)	8 σ_g	9 $\Delta\rho/\rho$	10 $\varepsilon_{max}/d^{\ddagger}$	11 $d/D^{\S}$	12 $h_d/d^{\S}$	13 B/d	14 $Fo^{\ddagger}$
1	Clarke (1962)*	6 - 3(a)	water jet/sand	26	4 - 138.8	(3) 2.4 - 14.3	(2) 0.82 - 2.02	1.13 - 1.15	1.65	7.1 - 50	1.2 - 74.4	19.5 - 117.4	(3) 79 - 474	13.5 - 99.6
			air jet/sand	12	0.42 - 3	(2) 2.4 - 4.8	(3) 0.44 - 2.02	1.13 - 1.31	2189	8.7 - 32.6	1.2 - 5.4	-	(2) 558 - 2563	17.9 - 78.6
2	Ofwona (1965)*	6 - 3(b)		7	2 - 12	(2) 40.4 - 50.8	(4) 7.4 - 22.2	1 - 1.48	1.5 - 1.65	1.06 - 1.89	106 - 133.3	minimum	(2) 7.5 - 9.4	2.07 - 3.35
3	Opie (1967)*	6 - 3(c)	partial flow	7	>1	(3) 309 - 914	(5) 25.3 - 204.2	1 - 1.69	1.64 -1.72	0.48 - 1.4	3.3 - 21.3	0.34 - 0.6	(3) 6.7 - 13.8	1.72 - 4.88
			full flow	13	>1	(3) 309 - 914	(5) 25.3 - 204.2	1 - 1.18	1.64 - 1.72	0.34 - 1.21	2.2 - 12.2	0.37 - 1.1	(4) 3.9 - 13.8	1.69 - 3.44
4	Stevens (1969)	6 - 3(d)	partial flow	76	1 - 6	(4) 158 - 914	(10) 14 - 178	1.05 - 4.29	1.65 - 1.7	0.06 - 2.38	1.8 - 22.2	-0.35 - 3	(4) 2.6 - 13.5	0.68 - 4.97
			full flow	70	1 - 6	(4) 158 - 914	(10) 14 - 178	1.14 - 4.29	1.65 - 1.8	0.1 - 1.25	2.5 - 30	-0.11 - 1.53	(4) 2.6 - 13.5	1.23 - 6.06
5	Bohan (1972)*	6 - 3(e)	shorter duration	30	0.33 & 0.5	(3) 68 - 305	0.25	1.33	1.65	1.02 - 5.05	273 - 1219	0 & 1	(3) 16 - 71.4	13.62 - 98.72
			longer duration	3	21 - 24	101	0.25	1.33	1.65	2.69 - 3.5	406	0 & 1	48	22.55 - 47.86
6	Rajaratnam and Berry (1977)	6 - 3(f)	air jet/ polystyrene	14	nse††	(2) 6.4 - 23.5	1.4	uniform	859	0.29 - 4.61	4.5 - 16.8	-	(2) 45.4 - 168	2.93 - 13.31
			air jet/sand	12	nse	(2) 6.4 - 23.5	1.4	uniform	2189	0.43 - 3.6	4.5 - 16.8	-	(2) 45.4 - 16.8	2.72 - 10
			water jet/sand	4	nse	25.4	1.4	uniform	1.65	3.2 - 4.6	18.1	24	43	8.51 - 12.05
7	Mendoza (1980)*	6 - 3(g)	Headwall	7	16.67	101.6	1.85	1.33	1.65	1.52 - 2.77	54.6	0.4	11.8	3.19 - 18.31
			No - Headwall	7	16.67	101.6	1.85	1.33	1.65	1.49 - 2.70	54.6	0.4	11.8	3.19 - 18.31
8	Shaihk (1980)*	6 - 3(h)	uniform bed	4	5.27	260	7.62	1.32	1.65	1.35 - 2.52	34.1	0.45±0.05	23.4	4.76 - 11.62
			graded bed	4	5.27	260	7.34	4.78	1.65	1.07 - 2.19	35.4	0.45±0.05	23.4	4.85 - 11.84
9	Rajaratnam and Diebel (1981)	6 - 3(i)		17	< 64.6	(2) 12.7 - 25.4	1.05	uniform	1.65	0.66 - 6.5	12.1 - 24.2	0.2 - 3.39	(4) 1 - 86.6	3.13 - 17.93
10	Kloberdanz (1982)*	6 - 3(j)		6	5.27	101.6	2	4.38	1.65	0.45 - 2.45	50.8	0.45	11.8	2.14 - 14.17
11	Ead (1990)*	6 - 3(k)		18	< 3.33	(3) 25 - 100	0.707	2.275	1.65	1.37 - 3.22	35.9 - 141.4	< 2	(3) 4.5 - 18	10.95 - 20.84
12	Lim (1995)	6 - 3(l)		20	22 - 100	(2) 15 - 26	1.65	1.25	1.65	0.81 - 4.87	9.1 - 15.8	0.47	(3) 5 - 66.7	1.91 - 24.6
13	present study (1995)	6 - 2	water jet/gravel	12	12 - 219	(3) 5 - 25.4	(2) 0.24 - 7.2	1.33 - 1.46	1.65	2.34 - 19.44	2.64 - 20.66	0.75 - 124	43 - 218.4	6.3 - 88.2
			air jet/ canola seed	7	17 - 26	12.5	1.47	1.12	892	1.74 - 6.16	8.5	-	47.6	5.67 - 22.31
	Summary of all Data			376	0.33 - 219	2.4 - 914	0.24 - 178	1 - 4.38	1.5 - 2189	0.06 - 50	1.2 - 1219	-0.35 - -	1 - 2563	0.68 - 99.6

Note: All the pipes or jet outlets were full flowing, unless otherwise stated.

* The experimental data from this study could not be guaranteed to correspond to the asymptotic state
† The number in brackets represents the number of pipe sizes used
‡ For partial flow, d is defined as $\sqrt{(4A/\pi)}$
§ For partial flow, d is defined as d_h, the flow depth at pipe outlet
†† Scour time was not stated but asymptotic state was reached

Table 6 - 3(a): Clarke (1961)

	Seies	Expt. No.	D (mm)	d (mm)	U_o (m/s)	ε_m (mm)	x_m (mm)	x_o (mm)	$\bar{b}_m$ (mm)	x_c (mm)	x_e (mm)	Δ (mm)	h_d/d	ε_m/d	F_o
1	Water	34	0.82	4.78	6.25	116.8	442.0	774.7	217.2	998.2	-	-	58.5	24.4	54.3
2	jets on	42	0.82	4.78	4.10	79.8	315.0	561.3	157.5	718.8	858.5	91.4	58.5	16.7	35.6
3	sand	45	0.82	4.78	5.28	90.9	375.9	655.3	180.3	820.4	983.0	102.9	58.5	19.0	45.8
4		49	0.82	4.78	2.45	58.7	213.4	391.2	113.0	513.1	599.4	59.4	58.5	12.3	21.2
5		39	0.82	4.78	9.22	144.5	508.0	911.9	256.5	1155.7	1376.7	144.8	58.5	30.2	80.0
6		48	0.82	4.78	7.87	134.4	497.8	873.8	260.4	1122.7	1338.6	143.0	58.5	28.1	68.3
7		53	0.82	2.38	6.21	62.7	228.6	419.1	116.8	546.1	645.2	69.6	117.4	26.4	53.9
8		55	0.82	2.38	6.37	60.5	236.2	419.1	123.2	546.1	652.8	72.9	66.7	25.4	55.3
9		59	0.82	2.38	7.97	68.8	271.8	469.9	137.2	607.1	729.0	81.5	66.7	28.9	69.1
10		60	0.82	2.38	2.77	36.3	134.6	238.8	71.1	312.4	373.4	47.2	66.7	15.3	24.0
11		54	0.82	2.38	9.20	85.3	330.2	581.7	167.6	754.4	896.6	94.0	117.4	35.9	79.8
12		56	0.82	2.38	9.31	84.3	330.2	584.2	165.1	759.5	906.8	96.5	66.7	35.4	80.8
13		57	0.82	2.38	4.29	43.4	160.0	292.1	90.2	378.5	457.2	55.1	66.7	18.2	37.2
14		58	0.82	2.38	10.50	92.5	370.8	640.1	184.2	838.2	1000.8	105.2	66.7	38.8	91.1
15		61	0.82	2.38	4.05	46.7	149.9	289.6	87.6	368.3	442.0	49.3	117.4	19.6	35.2
16		62	0.82	2.38	2.40	36.3	106.7	213.4	67.3	276.9	332.7	40.9	117.4	15.3	20.9
17		63	0.82	2.38	7.84	78.2	284.5	500.4	148.6	640.1	772.2	86.4	117.4	32.9	68.0
18		64	0.82	2.38	11.48	105.4	388.6	675.6	193.0	866.1	1049.0	108.2	117.4	44.3	99.6
19		69	0.82	14.3	1.94	101.1	439.4	711.2	203.2	876.3	1041.4	101.3	19.5	7.1	16.8
20		70	0.82	14.3	2.84	114.3	497.8	784.9	226.1	972.8	1153.2	110.2	19.5	8.0	24.6
21		71	2.02	4.78	6.25	86.1	312.4	558.8	152.4	693.4	840.7	90.9	58.5	18.0	34.6
22		72	2.02	4.78	9.22	113.5	401.3	739.1	210.8	937.3	1127.8	122.7	58.5	23.8	51.0
23		73	2.02	4.78	4.10	63.8	228.6	411.5	116.8	525.8	629.9	74.2	58.5	13.3	22.7
24		74	2.02	4.78	2.45	43.7	137.2	264.2	81.3	342.9	411.5	51.3	58.5	9.1	13.5
25		75	2.02	4.78	7.87	98.0	348.0	647.7	189.2	891.5	977.9	111.5	58.5	20.5	43.5
26		76	2.02	2.38	11.48	64.5	241.3	449.6	120.7	569.0	683.3	78.7	117.4	27.1	63.5
1	Air	79	2.02	2.38	178.61	29.0	165.1	293.4	52.7	348.0	-	21.1	--	12.2	27.12
2	jets on	77	2.02	2.38	329.92	55.1	265.4	439.4	101.6	499.1	-	45.5	--	23.2	50.09
3	sand	78	2.02	2.38	264.37	38.6	215.9	383.5	73.0	447.0	-	30.5	--	16.2	40.14
4		82	2.02	4.78		65.3	304.8	519.4	107.3	584.2	-	47.0	--	13.7	-
5		89	0.82	2.38	178.61	-	-	440.7	-	-	-	-	--	-	42.56
6		87	0.82	2.38	178.61	45.0	251.5	454.7	85.1	-	-	-	--	18.9	42.56
7		88	0.82	2.38	329.92	-	-	660.4	-	-	-	-	--	-	78.62
8		86	0.82	2.38	329.92	77.5	389.9	692.2	153.7	760.7	-	32.3	--	32.6	78.62
9		81	2.02	4.78	117.82	41.4	224.8	384.8	74.9	442.0	-	32.8	--	8.7	17.89
10		80	2.02	4.78	161.06	58.9	269.2	483.9	99.1	544.8	-	42.7	--	12.3	24.45
11		91	0.44	2.38	329.92	-	-	928.4	-	-	-	-	--	-	107.33
12		90	0.44	2.38	178.61	-	-	580.4	-	-	-	-	--	-	58.11

Table 6-3(b): Ofwona (1965)

#	Time (hr.)	d (mm)	D (mm)	B (mm)	U_o (m/s)	ε_m (mm)	V_s (m^3*10^4)	B/d	ε_m/d	F_o
1	7.0	40.4	7.4	381	0.78	42.67	3.00	9.43	1.06	2.26
2	12.0	40.4	7.4	381	0.99	76.20	16.17	9.43	1.89	2.88
3	11.3	40.4	7.4	381	0.84	57.91	7.10	9.43	1.43	2.45
4	4.0	40.4	16.5	381	1.36	46.34	3.70	9.43	1.15	2.64
5	8.7	50.8	7.4	381	0.71	65.90	10.65	7.50	1.30	2.07
6	2.0	40.4	22.2	381	1.77	50.18	8.49	9.43	1.24	2.95
7	3.0	40.4	15.9	381	1.70	44.94	6.10	9.43	1.11	3.35

Table 6-3(c): Opie (1967)

#	Run #	D (mm)	σ_g	$\Delta\rho/\rho$	d (m)	d_b/d	Q (m^3/s)	A (m^2)	U_o (m/s)	ε_m (m)	x_o (m)	$\bar{b}_m$ (m)	x_m (m)	V_s (m^3)	h_d/d_b	$\varepsilon_{m=}/d$	F_o
1	B10	91.4	1.10	1.64	0.31	1	0.23	0.08	3.05	0.24	1.83	0.91	0.91	0.22	0.39	0.79	2.51
2	B12	91.4	1.10	1.64	0.31	1	0.19	0.08	2.56	0.22	1.37	0.91	0.76	0.15	0.39	0.71	2.10
3	B18	91.4	1.10	1.64	0.31	1	0.23	0.08	3.04	0.16	1.58	-	0.91	-	0.49	0.52	2.50
4	C22	99.1	1.03	1.72	0.31	1	0.21	0.08	2.79	0.12	1.22	0.82	0.91	0.03	0.46	0.37	2.20
5	D24	99.1	1.03	1.72	0.44	0.79	0.36	0.13	2.78	0.49	1.68	0.91	1.22	0.54	0.37	1.20	2.20
6	D25	99.1	1.03	1.72	0.44	0.74	0.27	0.12	2.17	0.18	1.52	0.61	0.91	0.09	0.34	0.46	1.72
7	D26	99.1	1.03	1.72	0.44	1	0.54	0.15	3.49	0.45	3.35	1.30	1.74	1.21	0.43	1.02	2.76
8	D27	99.1	1.03	1.72	0.44	1	0.40	0.15	2.64	0.37	2.13	0.91	1.34	0.53	0.37	0.83	2.08
9	E38	25.3	1.03	1.65	0.31	1	0.17	0.08	2.20	0.37	2.29	0.91	1.37	0.67	0.43	1.21	3.44
10	E39	25.3	1.03	1.65	0.31	0.72	0.11	0.06	1.84	0.26	2.13	0.76	0.91	0.25	0.60	0.95	2.88
11	F42	204.2	0.99	1.64	0.44	1	0.47	0.15	3.06	0.21	1.52	0.15	1.37	0.01	0.43	0.48	1.69
12	F43	204.2	0.99	1.64	0.44	1	0.63	0.15	4.08	0.34	2.93	0.99	2.13	0.43	0.50	0.76	2.24
13	F44	204.2	0.99	1.64	0.44	1	0.64	0.15	4.15	0.15	4.15	0.84	2.13	0.19	1.10	0.34	2.28
14	G54	204.2	0.99	1.64	0.91	0.77	1.83	0.54	3.40	0.34	3.66	1.37	1.22	1.12	0.57	0.40	1.87
15	G55	204.2	0.99	1.64	0.91	1	2.70	0.66	4.11	0.52	3.96	1.60	1.98	2.23	0.48	0.57	2.26
16	G58	204.2	0.99	1.64	0.91	0.87	2.28	0.60	3.77	0.52	3.66	1.68	2.29	2.15	0.44	0.59	2.08
17	G59	204.2	0.99	1.64	0.91	1	2.77	0.66	4.21	0.55	4.57	1.87	1.83	4.04	0.45	0.60	2.32
18	H62	31.7	1.69	1.72	0.91	0.74	1.82	0.52	3.49	0.79	5.33	2.21	2.13	6.09	0.50	0.97	4.88
19	K66	92.0	1.18	1.72	0.91	0.67	1.70	0.47	3.66	0.67	4.27	1.83	2.13	4.27	0.53	0.87	3.00
20	K67	92.0	1.18	1.72	0.91	1	2.71	0.66	4.13	0.79	5.49	2.44	4.88	19.81	0.38	0.87	3.38

Table 6-3(d): Stevens (1969) Full Flow

#	Series #	B (m)	d (m)	D (mm)	σ_g	S_p (%)	Q (m^3/s)	d_b (mm)	h_{du} (mm)	ε_m (mm)	x_m (mm)	x_o (mm)	$\bar{b}_m$ (mm)	x_b (mm)	x_e (mm)	h_d (mm)	$\varepsilon_{m\infty}/d$	F_o
1	BS 10	1.83	0.31	88.90	1.98	1	0.22937	309.4	121.9	228.6	1036.3	1828.8	883.9	1219.2	3657.6	-	0.74	2.54
2	BS 12	1.83	0.31	88.90	1.98	1	0.19227	309.4	121.9	219.5	762.0	1310.6	716.3	731.5	2712.7	-	0.71	2.13
3	BS 18	0.91	0.31	88.90	1.98	1	0.22880	309.4	152.4	161.5	914.4	1889.8	624.8	1127.8	-	-	0.52	2.54
4	BS 19	0.91	0.31	88.90	1.98	1	0.22597	309.4	167.6	161.5	914.4	1737.4	594.4	1097.3	-	-	0.52	2.51
5	CS 21	1.83	0.31	81.28	1.28	1	0.13592	309.4	112.2	61.0	396.2	487.7	106.7	396.2	-	-	0.20	1.58
6	CS 22	1.83	0.31	81.28	1.28	1	0.20954	309.4	143.3	121.9	883.9	1402.1	426.7	853.4	2834.6	-	0.39	2.43
7	D 26	3.35	0.44	81.28	1.28	0	0.53519	442.0	189.0	451.1	1737.4	3413.8	1158.2	2225.0	6096.0	128.0	1.02	3.04
8	D 27	3.35	0.44	81.28	1.28	0	0.40493	442.0	164.6	365.8	1341.1	2133.6	914.4	1219.2	4358.6	109.7	0.83	2.30
9	ES 38	1.83	0.31	24.89	1.29	1	0.16565	309.4	134.1	374.9	1463.0	2286.0	914.4	1219.2	-	-	1.21	3.47
10	F 42	1.98	0.44	177.80	1.25	0	0.47006	442.0	192.0	213.4	1371.6	1767.8	320.0	1066.8	1767.8	182.9	0.48	1.81
11	F 43	1.98	0.44	177.80	1.25	0	0.62580	442.0	222.5	335.3	2133.6	2987.0	853.4	2225.0	5730.2	176.8	0.76	2.40
12	F 44	1.98	0.44	177.80	1.25	0	0.63713	442.0	487.7	152.4	2133.6	4206.2	838.2	1219.2	-	487.7	0.34	2.45
13	G 55	2.44	0.91	177.80	1.25	0	2.69860	914.4	442.0	518.2	1981.2	3962.4	1600.2	2133.6	8839.2	426.7	0.57	2.42
14	G 59	6.10	0.91	177.80	1.25	0	2.76656	914.4	411.5	579.1	1828.8	4572.0	1874.5	2438.4	-	381.0	0.63	2.48
15	H 63	6.10	0.91	30.48	4.29	0	2.79487	914.4	304.8	1066.8	1828.8	8138.2	-	-	-	396.2	1.17	6.06
16	K 67	6.10	0.91	76.20	2.66	0	2.70992	914.4	350.5	853.4	4876.8	5577.8	2438.4	3352.8	-	335.3	0.93	3.72
17	L 79	2.13	0.16	13.72	1.26	0	0.02209	157.9	83.8	152.4	457.2	853.4	312.4	457.2	1524.0	79.2	0.97	2.39
18	L 80	2.13	0.16	13.72	1.26	0	0.02209	157.9	103.6	70.1	457.2	990.6	205.7	457.2	1706.9	99.1	0.44	2.39
19	L 83	2.13	0.16	13.72	1.26	0	0.02203	157.9	83.8	140.2	609.6	914.4	289.6	304.8	1676.4	82.3	0.89	2.39
20	L 84	2.13	0.16	13.72	1.26	0	0.02203	157.9	103.6	27.4	304.8	457.2	144.8	137.2	-	97.5	0.17	2.39
21	L 85	2.13	0.16	13.72	1.26	0	0.02226	157.9	91.4	79.2	670.6	1127.8	228.6	228.6	-	85.3	0.50	2.41
22	L 94	2.13	0.16	13.72	1.26	0	0.02744	157.9	50.3	155.4	381.0	609.6	335.3	304.8	1066.8	35.1	0.98	2.97
23	L 95	2.13	0.16	13.72	1.26	0	0.02733	157.9	68.6	167.6	457.2	792.5	373.4	457.2	1432.6	61.0	1.06	2.96
24	L 96	2.13	0.16	13.72	1.26	0	0.02733	157.9	85.3	143.3	762.0	1097.3	327.7	609.6	1981.2	83.8	0.91	2.96
25	L 97	2.13	0.16	13.72	1.26	0	0.02744	157.9	105.2	57.9	457.2	1188.7	152.4	457.2	1828.8	100.6	0.37	2.97
26	L 98	2.13	0.16	13.72	1.26	0	0.02744	157.9	134.1	42.7	609.6	-	121.9	914.4	-	128.0	0.27	2.97
27	L 99	2.13	0.16	13.72	1.26	0	0.02744	157.9	185.9	33.5	762.0	1524.0	91.4	762.0	-	179.8	0.21	2.97
28	L 100	2.13	0.16	13.72	1.26	0	0.02750	157.9	89.9	97.5	685.8	1463.0	266.7	457.2	-	86.9	0.62	2.98
29	L 101	2.13	0.16	13.72	1.26	0	0.03426	157.9	33.5	155.4	304.8	609.6	312.4	304.8	1097.3	12.2	0.98	3.71
30	L 102	2.13	0.16	13.72	1.26	0	0.03440	157.9	41.1	170.7	396.2	670.6	335.3	365.8	1127.8	9.1	1.08	3.73
31	L 103	2.13	0.16	13.72	1.26	0	0.03455	157.9	54.9	182.9	457.2	883.9	419.1	457.2	1432.6	35.1	1.16	3.74
32	L 104	2.13	0.16	13.72	1.26	0	0.03440	157.9	68.6	198.1	609.6	1143.0	487.7	762.0	-	61.0	1.25	3.73
33	L 105	2.13	0.16	13.72	1.26	0	0.03440	157.9	79.2	182.9	609.6	1280.2	411.5	838.2	-	76.2	1.16	3.73
34	L 106	2.13	0.16	13.72	1.26	0	0.03455	157.9	91.4	121.9	792.5	1981.2	274.3	762.0	-	85.3	0.77	3.74
35	L 107	2.13	0.16	13.72	1.26	0	0.03426	157.9	155.4	100.6	1371.6	-	228.6	1676.4	-	147.8	0.64	3.71

Table 6-3(d): Stevens (1969) Full Flow (Continued)

#	Series #	B (m)	d (m)	D (mm)	σ_g	S_p (%)	Q (m^3/s)	d_b (mm)	h_{du} (mm)	ε_m (mm)	x_m (mm)	x_o (mm)	$\bar{b}_m$ (mm)	x_b (mm)	x_e (mm)	h_d (mm)	$\varepsilon_{m\infty}/d$	F_o
36	L 108	2.13	0.16	13.72	1.26	0	0.03455	157.9	123.4	94.5	1371.6	-	205.7	1524.0	-	120.4	0.60	3.74
37	L 109	2.13	0.16	13.72	1.26	0	0.02735	157.9	25.9	137.2	182.9	518.2	289.6	243.8	883.9	-18.3	0.87	2.96
38	LS 150	2.13	0.16	13.72	1.26	3.75	0.01133	157.9	164.6	24.4	76.2	548.6	91.4	228.6	1005.8	231.6	0.15	1.23
39	LS 157	2.13	0.16	13.72	1.26	3.75	0.02209	157.9	176.8	30.5	152.4	487.7	121.9	152.4	1127.8	240.8	0.19	2.39
40	MS 197	2.13	0.16	29.46	1.37	3.75	0.03540	157.9	24.4	182.9	396.2	716.3	312.4	457.2	1447.8	85.3	1.16	2.62
41	MS 198	2.13	0.16	29.46	1.37	3.75	0.03540	157.9	39.6	195.1	548.6	792.5	327.7	457.2	1767.8	109.7	1.24	2.62
42	MS 199	2.13	0.16	29.46	1.37	3.75	0.03540	157.9	61.0	137.2	685.8	1005.8	289.6	533.4	1935.5	129.5	0.87	2.62
43	MS 200	2.13	0.16	29.46	1.37	3.75	0.03540	157.9	77.7	85.3	609.6	1021.1	182.9	457.2	1950.7	143.3	0.54	2.62
44	MS 201	2.13	0.16	29.46	1.37	3.75	0.03540	157.9	102.1	42.7	609.6	853.4	83.8	381.0	-	169.2	0.27	2.62
45	MS 202	2.13	0.16	29.46	1.37	3.75	0.03540	157.9	158.5	18.3	304.8	396.2	22.9	304.8	-	225.6	0.12	2.62
46	M 203	0.91	0.16	29.46	1.37	0	0.03095	157.9	54.9	125.0	533.4	792.5	281.9	457.2	1524.0	61.0	0.79	2.29
47	M 208	0.91	0.16	29.46	1.37	0	0.03525	157.9	38.1	173.7	579.1	792.5	304.8	487.7	1524.0	36.6	1.10	2.61
48	M 212	0.91	0.16	29.46	1.37	0	0.02735	157.9	33.5	82.3	365.8	487.7	167.6	304.8	1219.2	29.0	0.52	2.02
49	M 213	0.91	0.16	29.46	1.37	0	0.02735	157.9	48.8	64.0	335.3	487.7	152.4	304.8	-	48.8	0.41	2.02
50	M 214	0.91	0.16	29.46	1.37	0	0.03540	157.9	57.9	143.3	609.6	853.4	221.0	533.4	1493.5	56.4	0.91	2.62
51	M 215	0.91	0.16	29.46	1.37	0	0.03525	157.9	73.2	94.5	609.6	883.9	221.0	457.2	1554.5	73.2	0.60	2.61
52	M 216	0.91	0.16	29.46	1.37	0	0.03525	157.9	91.4	42.7	457.2	609.6	137.2	457.2	-	91.4	0.27	2.61
53	M 217	0.91	0.16	29.46	1.37	0	0.03525	157.9	114.3	15.2	243.8	259.1	38.1	121.9	-	115.8	0.10	2.61
54	M 218	0.91	0.16	29.46	1.37	0	0.02735	157.9	50.3	73.2	304.8	609.6	205.7	304.8	1158.2	50.3	0.46	2.02
55	M 219	0.91	0.16	29.46	1.37	0	0.02735	157.9	70.1	42.7	304.8	426.7	83.8	304.8	914.4	70.1	0.27	2.02
56	M 220	0.91	0.16	29.46	1.37	0	0.03143	157.9	36.6	152.4	457.2	640.1	289.6	426.7	1325.9	35.1	0.97	2.32
57	M 221	0.91	0.16	29.46	1.37	0	0.02735	157.9	47.2	57.9	335.3	533.4	182.9	304.8	-	47.2	0.37	2.02
58	M 222	0.91	0.16	29.46	1.37	0	0.03157	157.9	56.4	121.9	548.6	838.2	228.6	381.0	1493.5	56.4	0.77	2.33
59	M 224	0.91	0.16	29.46	1.37	0	0.03143	157.9	70.1	61.0	304.8	746.8	205.7	335.3	-	71.6	0.39	2.32
60	M 225	0.91	0.16	29.46	1.37	0	0.03143	157.9	91.4	36.6	182.9	457.2	152.4	304.8	-	93.0	0.23	2.32
61	M 226	0.91	0.16	29.46	1.37	0	0.04106	157.9	64.0	146.3	762.0	1082.0	350.5	762.0	1889.8	64.0	0.93	3.04
62	M 241	0.91	0.16	29.46	1.37	0	0.02735	157.9	29.0	61.0	243.8	502.9	198.1	548.6	670.6	12.2	0.39	2.02
63	M 242	0.91	0.16	29.46	1.37	0	0.02747	157.9	25.9	82.3	304.8	457.2	213.4	304.8	670.6	0.0	0.52	2.03
64	M 243	0.91	0.16	29.46	1.37	0	0.03157	157.9	36.6	131.1	381.0	533.4	243.8	304.8	1036.3	6.1	0.83	2.33
65	M 262	2.13	0.16	29.46	1.37	0	0.02733	157.9	13.7	88.4	274.3	426.7	160.0	304.8	975.4	6.1	0.56	2.02
66	M 263	2.13	0.16	29.46	1.37	0	0.03143	157.9	22.9	164.6	457.2	609.6	228.6	457.2	1036.3	9.1	1.04	2.32
67	M 264	2.13	0.16	29.46	1.37	0	0.03596	157.9	30.5	185.9	457.2	685.8	259.1	502.9	1219.2	15.2	1.18	2.66
68	M 265	2.13	0.16	29.46	1.37	0	0.04120	157.9	61.0	158.5	762.0	1188.7	312.4	457.2	1981.2	61.0	1.00	3.05
69	P 277	2.13	0.16	62.23	1.14	0	0.03398	157.9	45.7	30.5	152.4	-	-	-	-	45.7	0.19	1.73
70	P 278	2.13	0.16	62.23	1.14	0	0.04361	157.9	51.8	30.5	152.4	-	-	-	-	51.8	0.19	2.22

Table 6-3(d): Stevens (1969) Partial Flow

#	Series #	B (m)	d (m)	D (mm)	σ_g	S_p (%)	Q (m^3/s)	d_b (mm)	h_{du} (mm)	ε_m (mm)	x_m (mm)	x_o (mm)	$\bar{b}_m$ (mm)	x_b (mm)	x_e (mm)	h_d (mm)	d_b/d	A (m^2)	$\varepsilon_{m\infty}/d$	F_o
1	LS 139	2.13	0.16	13.72	1.26	3.75	0.00736	38.7	-30.5	88.4	152.4	304.8	144.8	152.4	609.6	31.7	0.25	0.00372	1.28	4.20
2	LS 140	2.13	0.16	13.72	1.26	3.75	0.00745	39.6	-6.1	88.4	228.6	304.8	175.3	213.4	640.1	56.4	0.25	0.00385	1.26	4.11
3	LS 141	2.13	0.16	13.72	1.26	3.75	0.00742	39.6	18.3	106.7	304.8	640.1	221.0	396.2	1066.8	83.8	0.25	0.00385	1.52	4.09
4	LS 142	2.13	0.16	13.72	1.26	3.75	0.00736	40.5	36.6	70.1	762.0	1143.0	137.2	762.0	1950.7	102.1	0.26	0.00397	0.99	3.93
5	N 266	2.13	0.50	41.76	1.05	0	0.02209	128.0	30.5	42.7	228.6	365.8	121.9	304.8	-	30.5	0.26	0.03955	0.19	0.68
6	N 268	2.13	0.50	41.76	1.05	0	0.02209	128.0	50.3	48.8	228.6	365.8	121.9	228.6	-	50.3	0.26	0.03955	0.22	0.68
7	N 269	2.13	0.50	41.76	1.05	0	0.02209	128.0	15.2	48.8	228.6	335.3	83.8	228.6	-	6.1	0.26	0.03955	0.22	0.68
8	LS 143	2.13	0.16	13.72	1.26	3.75	0.00745	42.7	64.0	30.5	304.8	762.0	91.4	304.8	1371.6	128.0	0.27	0.00427	0.41	3.70
9	N 270	2.13	0.50	41.76	1.05	0	0.03143	157.9	24.4	48.8	228.6	457.2	106.7	304.8	-	15.2	0.32	0.05297	0.19	0.72
10	N 271	2.13	0.50	41.76	1.05	0	0.03525	157.9	18.3	82.3	304.8	563.9	167.6	213.4	823.0	6.1	0.32	0.05297	0.32	0.81
11	N 272	2.13	0.50	41.76	1.05	0	0.03525	157.9	39.6	79.2	487.7	609.6	144.8	457.2	1036.3	39.6	0.32	0.05297	0.31	0.81
12	N 273	2.13	0.50	41.76	1.05	0	0.03525	157.9	76.2	51.8	335.3	579.1	-	-	-	76.2	0.32	0.05297	0.20	0.81
13	N 275	2.13	0.50	41.76	1.05	0	0.04361	157.9	56.4	100.6	548.6	838.2	205.7	609.6	1737.4	56.4	0.32	0.05297	0.39	1.00
14	MS 194	2.13	0.16	29.46	1.37	3.75	0.01121	52.4	0.0	36.6	335.3	426.7	76.2	365.8	-	61.0	0.33	0.00568	0.43	2.86
15	MS 195	2.13	0.16	29.46	1.37	3.75	0.01119	52.7	18.3	18.3	106.7	121.9	38.1	91.4	-	82.3	0.33	0.00573	0.21	2.83
16	LS 145	2.13	0.16	13.72	1.26	3.75	0.01119	53.0	0.0	106.7	304.8	548.6	213.4	304.8	853.4	62.5	0.34	0.00577	1.24	4.11
17	LS 146	2.13	0.16	13.72	1.26	3.75	0.01124	53.6	21.3	158.5	533.4	883.9	266.7	609.6	1493.5	85.3	0.34	0.00586	1.83	4.07
18	LS 147	2.13	0.16	13.72	1.26	3.75	0.01104	53.9	36.6	109.7	609.6	1219.2	198.1	685.8	2072.6	105.2	0.34	0.00591	1.27	3.97
19	LS 151	2.13	0.16	13.72	1.26	3.75	0.01124	54.3	36.6	109.7	609.6	1188.7	167.6	609.6	2087.9	102.1	0.34	0.00596	1.26	4.01
20	LS 148	2.13	0.16	13.72	1.26	3.75	0.01124	54.6	61.0	79.2	1066.8	1402.1	167.6	990.6	2255.5	125.0	0.35	0.00600	0.91	3.98
21	L 114	2.13	0.16	13.72	1.26	0	0.00750	59.1	13.7	79.2	182.9	274.3	152.4	152.4	670.6	4.6	0.37	0.00669	0.86	2.38
22	L 117	2.13	0.16	13.72	1.26	0	0.00742	61.6	22.9	61.0	182.9	365.8	137.2	152.4	914.4	15.2	0.39	0.00707	0.64	2.23
23	L 115	2.13	0.16	13.72	1.26	0	0.00742	63.4	36.6	33.5	152.4	335.3	121.9	152.4	-	32.0	0.40	0.00735	0.35	2.14
24	LS 161	2.13	0.16	13.72	1.26	3.75	0.01657	67.1	24.4	198.1	609.6	1112.5	365.8	685.8	1889.8	91.4	0.42	0.00792	1.97	4.44
25	LS 162	2.13	0.16	13.72	1.26	3.75	0.01657	67.1	39.6	170.7	701.0	1341.1	274.3	914.4	2194.6	112.8	0.42	0.00792	1.70	4.44
26	MS 190	2.13	0.16	29.46	1.37	3.75	0.01671	67.1	3.0	91.4	381.0	670.6	137.2	304.8	1219.2	67.1	0.42	0.00792	0.91	3.05
27	LS 163	2.13	0.16	13.72	1.26	3.75	0.01657	67.7	61.0	118.9	1005.8	1676.4	221.0	1066.8	-	125.0	0.43	0.00801	1.18	4.39
28	MS 191	2.13	0.16	29.46	1.37	3.75	0.01651	67.7	21.3	109.7	548.6	944.9	160.0	533.4	1463.0	89.9	0.43	0.00801	1.09	2.98
29	MS 192	2.13	0.16	29.46	1.37	3.75	0.01659	68.3	42.7	67.1	457.2	792.5	121.9	457.2	533.4	108.2	0.43	0.00811	0.66	2.96
30	LS 160	2.13	0.16	13.72	1.26	3.75	0.01657	68.6	6.1	149.4	381.0	701.0	312.4	381.0	1143.0	67.1	0.43	0.00816	1.47	4.31
31	L 116	2.13	0.16	13.72	1.26	0	0.00742	68.9	59.4	6.1	-	0.0	0.0	-	-	53.3	0.44	0.00821	0.06	1.92
32	L 113	2.13	0.16	13.72	1.26	0	0.01121	76.2	4.6	91.4	152.4	304.8	182.9	152.4	685.8	-13.7	0.48	0.00936	0.84	2.54
33	L 86	2.13	0.16	13.72	1.26	0	0.01124	76.5	30.5	109.7	243.8	396.2	221.0	213.4	914.4	18.3	0.48	0.00940	1.00	2.54
34	LS 159	2.13	0.16	13.72	1.26	3.75	0.01657	77.1	12.2	240.8	609.6	1249.7	502.9	762.0	2164.1	74.7	0.49	0.00950	2.19	3.70
35	MS 176	2.13	0.16	29.46	1.37	3.75	0.02209	77.7	12.2	167.6	533.4	685.8	205.7	457.2	1402.1	74.7	0.49	0.00960	1.52	3.33
36	LS 152	2.13	0.16	13.72	1.26	3.75	0.02209	78.0	12.2	253.0	609.6	1249.7	518.2	838.2	2194.6	73.2	0.49	0.00964	2.28	4.86
37	LS 153	2.13	0.16	13.72	1.26	3.75	0.02209	78.3	33.5	225.6	762.0	1417.3	442.0	990.6	2316.5	99.1	0.50	0.00969	2.03	4.84
38	MS 177	2.13	0.16	29.46	1.37	3.75	0.02209	78.6	24.4	152.4	579.1	944.9	205.7	533.4	1524.0	97.5	0.50	0.00974	1.37	3.28
39	LS 154	2.13	0.16	13.72	1.26	3.75	0.02209	78.9	45.7	201.2	914.4	1554.5	342.9	1066.8	2438.4	115.8	0.50	0.00980	1.80	4.78

Table 6-3(d): Stevens (1969) Partial Flow (Continued)

#	Series #	B (m)	d (m)	D (mm)	σ_g	S_p (%)	Q (m^3/s)	d_b (mm)	h_{du} (mm)	ε_m (mm)	x_m (mm)	x_o (mm)	$\bar{b}_m$ (mm)	x_b (mm)	x_e (mm)	h_d (mm)	d_b/d	A (m^2)	$\varepsilon_{m\infty}/d$	F_o
40	L 87	2.13	0.16	13.72	1.26	0	0.01119	79.2	48.8	67.1	335.3	609.6	167.6	182.9	1127.8	45.7	0.50	0.00985	0.60	2.41
41	MS 178	2.13	0.16	29.46	1.37	3.75	0.02209	79.2	45.7	118.9	685.8	1066.8	205.7	533.4	1950.7	112.8	0.50	0.00985	1.06	3.25
42	LS 155	2.13	0.16	13.72	1.26	3.75	0.02209	79.9	64.0	189.0	1219.2	1859.3	320.0	1219.2	-	131.1	0.51	0.00994	1.68	4.72
43	MS 179	2.13	0.16	29.46	1.37	3.75	0.02209	81.7	70.1	61.0	609.6	1188.7	99.1	304.8	-	140.2	0.52	0.01023	0.53	3.13
44	LS 158	2.13	0.16	13.72	1.26	3.75	0.02209	82.3	85.3	146.3	1066.8	1905.0	266.7	1295.4	-	149.4	0.52	0.01033	1.28	4.54
45	MS 180	2.13	0.16	29.46	1.37	3.75	0.02209	83.8	97.5	30.5	228.6	-	-	-	-	161.5	0.53	0.01057	0.26	3.03
46	L 88	2.13	0.16	13.72	1.26	0	0.01110	84.4	73.2	15.2	243.8	335.3	53.3	228.6	-	67.1	0.53	0.01066	0.13	2.21
47	L 111	2.13	0.16	13.72	1.26	0	0.01654	90.8	-3.0	100.6	152.4	365.8	198.1	152.4	640.1	-32.0	0.58	0.01167	0.83	3.01
48	M 239	0.91	0.16	29.46	1.37	0	0.01657	91.4	9.1	24.4	152.4	228.6	91.4	121.9	-	-3.0	0.58	0.01176	0.20	2.04
49	L 90	2.13	0.16	13.72	1.26	0	0.01657	92.7	36.6	121.9	304.8	457.2	236.2	243.8	914.4	24.4	0.59	0.01195	0.99	2.94
50	M 209	0.91	0.16	29.46	1.37	0	0.01642	92.7	21.3	45.7	304.8	457.2	114.3	304.8	457.2	19.8	0.59	0.01195	0.37	1.99
51	L 91	2.13	0.16	13.72	1.26	0	0.01648	94.8	57.9	134.1	457.2	701.0	243.8	243.8	1371.6	51.8	0.60	0.01228	1.07	2.85
52	M 210	0.91	0.16	29.46	1.37	0	0.01679	95.7	41.1	34.1	182.9	304.8	76.2	243.8	304.8	41.1	0.61	0.01242	0.27	1.96
53	L 92	2.13	0.16	13.72	1.26	0	0.01657	99.1	76.2	54.9	609.6	944.9	175.3	167.6	1554.5	71.6	0.63	0.01294	0.43	2.72
54	K 66	6.10	0.91	76.20	2.66	0	1.70184	609.6	320.0	670.6	2438.4	4267.2	1828.8	1828.8	7772.4	304.8	0.67	0.46534	0.87	3.29
55	L 93	2.13	0.16	13.72	1.26	0	0.01657	111.3	103.6	9.1	152.4	0.0	0.0	0.0	0.0	99.1	0.70	0.01475	0.07	2.38
56	LS 144	2.13	0.16	13.72	1.26	3.75	0.00745	112.8	112.8	33.5	76.2	198.1	99.1	91.4	685.8	178.3	0.71	0.01497	0.24	1.06
57	LS 149	2.13	0.16	13.72	1.26	3.75	0.01113	112.8	112.8	45.7	243.8	487.7	114.3	304.8	1127.8	178.3	0.71	0.01497	0.33	1.58
58	ES 39	1.83	0.31	24.89	1.29	1	0.10647	222.5	134.1	259.1	914.4	2072.6	655.3	823.0	-	-	0.72	0.05790	0.95	2.90
59	LS 164	2.13	0.16	13.72	1.26	3.75	0.01657	114.3	114.3	61.0	457.2	1066.8	137.2	304.8	1676.4	179.8	0.72	0.01519	0.44	2.31
60	H 62	6.10	0.91	30.48	4.29	0	1.82077	676.7	335.3	792.5	2133.6	5334.0	2209.8	2316.5	-	350.5	0.74	0.52128	0.97	4.97
61	LS 156	2.13	0.16	13.72	1.26	3.75	0.02209	117.3	118.9	91.4	914.4	1493.5	182.9	914.4	-	184.4	0.74	0.01561	0.65	3.00
62	D 25	3.35	0.44	81.28	1.28	0	0.26618	329.2	112.8	134.1	914.4	1585.0	609.6	762.0	3200.4	121.9	0.74	0.12260	0.34	1.89
63	G 54	2.44	0.91	177.80	1.25	0	1.83493	701.0	396.2	335.3	1219.2	3657.6	1371.6	1767.8	7315.2	457.2	0.77	0.54050	0.40	2.00
64	M 261	2.13	0.16	29.46	1.37	0	0.02209	125.0	9.1	67.1	304.8	396.2	144.8	228.6	-	-3.0	0.79	0.01663	0.46	1.92
65	L 81	2.13	0.16	13.72	1.26	0	0.02203	128.0	42.7	131.1	304.8	518.2	289.6	304.8	914.4	30.5	0.81	0.01701	0.89	2.75
66	L 110	2.13	0.16	13.72	1.26	0	0.02203	128.0	13.7	118.9	152.4	426.7	236.2	182.9	716.3	-24.4	0.81	0.01701	0.81	2.75
67	M 204	0.91	0.16	29.46	1.37	0	0.02195	128.0	27.4	61.0	304.8	487.7	106.7	228.6	-	24.4	0.81	0.01701	0.41	1.87
68	M 240	0.91	0.16	29.46	1.37	0	0.02203	128.0	22.9	42.7	182.9	259.1	99.1	152.4	-	4.6	0.81	0.01701	0.29	1.88
69	M 223	0.91	0.16	29.46	1.37	0	0.02172	131.1	45.7	48.8	533.4	365.8	137.2	228.6	-	45.7	0.83	0.01738	0.33	1.81
70	M 205	0.91	0.16	29.46	1.37	0	0.02206	134.1	47.2	76.2	304.8	609.6	152.4	304.8	1097.3	47.2	0.85	0.01773	0.51	1.80
71	G 58	6.10	0.91	177.80	1.25	0	2.28234	792.5	350.5	506.0	2286.0	3657.6	1737.4	2133.6	7620.0	344.4	0.87	0.60491	0.58	2.22
72	L 77	2.13	0.16	13.72	1.26	0	0.02203	137.2	42.7	140.2	304.8	487.7	281.9	152.4	975.4	30.5	0.87	0.01807	0.92	2.59
73	L 78	2.13	0.16	13.72	1.26	0	0.02209	137.2	64.0	161.5	381.0	670.6	342.9	304.8	1371.6	57.9	0.87	0.01807	1.07	2.59
74	L 82	2.13	0.16	13.72	1.26	0	0.02203	137.2	64.0	155.4	457.2	731.5	335.3	335.3	1493.5	57.9	0.87	0.01807	1.02	2.59
75	L 112	2.13	0.16	13.72	1.26	0	0.02260	137.2	77.7	152.4	533.4	838.2	304.8	457.2	1554.5	73.2	0.87	0.01807	1.00	2.65
76	M 206	0.91	0.16	29.46	1.37	0	0.02220	137.2	67.1	45.7	274.3	365.8	76.2	304.8	-	67.1	0.87	0.01807	0.30	1.78

Table 6 - 3(e): Bohan (1972)

#	Series	Time (hr.)	D (mm)	d (mm)	h_d (mm)	Q (m^3/s)	U_o (m/s)	x_o (mm)	$\bar{b}_m$ (mm)	ε_m (mm)	V_s (m^3)	ε_m/d	F_o
1	Shorter	0.33	250	304.8	0	0.13337	1.83	3960	780	720	2.61	2.36	28.73
2	duration	0.33	250	304.8	0	0.15574	2.13	4270	1220	770	3.34	2.53	33.55
3		0.33	250	304.8	0	0.17783	2.44	4880	-	810	4.36	2.67	38.31
4		0.33	250	304.8	0	0.20020	2.74	5180	-	850	6.17	2.8	43.13
5		0.33	250	304.8	0	0.22229	3.05	5180	-	890	7.36	2.91	47.88
6		0.33	250	304.8	0	0.26674	3.66	6100	-	950	10.65	3.1	57.46
7		0.33	250	304.8	0	0.33414	4.58	-	-	1020	13.17	3.35	71.98
8		0.33	250	101.5	0	0.00994	1.23	1220	500	260	0.07	2.52	19.31
9		0.33	250	101.5	0	0.01138	1.41	1070	430	270	0.08	2.67	22.11
10		0.33	250	101.5	0	0.01280	1.58	1220	380	280	0.09	2.79	24.86
11		0.33	250	101.5	0	0.01424	1.76	1520	530	300	0.14	2.91	27.67
12		0.33	250	101.5	0	0.02464	3.04	2290	840	360	0.35	3.5	47.86
13		0.33	250	101.5	0	0.03695	4.57	3050	1220	400	0.97	3.94	71.79
14		0.33	250	101.5	0	0.04927	6.09	3660	1220	430	1.43	4.24	95.72
15		0.33	250	68.3	0	0.00317	0.87	670	170	160	0.02	2.36	13.62
16		0.33	250	68.3	0	0.00371	1.01	760	190	170	0.03	2.53	15.93
17		0.33	250	68.3	0	0.00425	1.16	820	170	180	0.03	2.67	18.24
18		0.33	250	68.3	0	0.00476	1.3	850	180	190	0.03	2.8	20.42
19		0.33	250	68.3	0	0.00530	1.45	1010	210	200	0.05	2.91	22.73
20		0.33	250	68.3	0	0.00634	1.73	1220	290	210	0.07	3.11	27.23
21		0.33	250	68.3	0	0.00793	2.17	1370	330	230	0.09	3.35	34.04
22		0.5	250	101.5	101.5	0.01161	1980	460	170	0.15	1.72	22.55	
23		0.5	250	101.5	101.5	0.01274	1.57	2130	380	200	0.15	1.94	24.75
24		0.5	250	101.5	101.5	0.02464	3.04	3960	530	350	0.41	3.45	47.86
25		0.5	250	101.5	101.5	0.03681	4.55	4720	530	440	0.63	4.38	71.51
26		0.5	250	101.5	101.5	0.04927	6.09	4630	1220	510	1.58	5.05	95.72
27		0.5	250	68.3	68.3	0.00317	0.87	1010	90	70	0.01	1.01	13.62
28		0.5	250	68.3	68.3	0.00371	1.01	1130	120	90	0.02	1.38	15.93
29		0.5	250	68.3	68.3	0.00425	1.16	1310	140	120	0.03	1.69	18.24
30		0.5	250	68.3	68.3	0.00926	2.53	2130	240	240	0.12	3.48	39.75
31	Longer	21	250	101.5	0	0.01161	1.43	3050	840	270	0.41	2.69	22.55
32	duration	23.75	250	101.5	0	0.02464	3.04	5490	-	360	2.32	3.5	47.86
33		24	250	101.5	101.5	0.02464	3.04	5030	610	350	1.06	3.45	47.86

Table 6 - 3(f): Rajaratnam and Berry (1977)

	Series	Expt. No.	U_o (m/s)	d (mm)	S_s	D (mm)	ρ kg/m^3	$\varepsilon_{m\infty}$ (mm)	$x_{m\infty}$ (mm)	$\bar{b}_{m\infty}$ (mm)	$x_{o\infty}$ (mm)	$x_{c\infty}$ (mm)	Δ_{∞} (mm)	$\varepsilon_{m\infty}/d$	$x_{m\infty}/d$	F_o
1	Air jet on	111	10.06	23.50	1.041	1.4	1.21	7	131	20	262	274	1	0.29	5.58	2.93
2	Polystyrene	112	14.33	23.50	1.041	1.4	1.21	18	213	50	369	427	8	0.78	9.08	4.17
3	beds	113	19.20	23.50	1.041	1.4	1.21	29	244	77	439	549	11	1.23	10.38	5.59
4		114	22.25	23.50	1.041	1.4	1.21	37	259	91	509	579	13	1.56	11.03	6.48
5		115	27.13	23.50	1.041	1.4	1.21	48	335	118	616	701	15	2.05	14.27	7.90
6		116	30.78	23.50	1.041	1.4	1.21	52	381	138	695	808	17	2.23	16.22	8.96
7		117	34.44	23.50	1.041	1.4	1.21	61	411	160	750	817	18	2.59	17.51	10.03
8		118	41.45	23.50	1.041	1.4	1.21	78	488	192	890	1006	21	3.31	20.76	12.07
9		119	45.72	23.50	1.041	1.4	1.21	88	518	215	997	1122	21	3.74	22.05	13.31
10		121	24.08	6.35	1.041	1.4	1.21	13	116	29	204	232	2	2.02	18.24	7.01
11		122	29.57	6.35	1.041	1.4	1.21	16	122	36	219	250	7	2.50	19.20	8.61
12		123	34.75	6.35	1.041	1.4	1.21	19	152	46	250	305	9	2.98	24.00	10.11
13		124	41.15	6.35	1.041	1.4	1.21	25	158	59	293	335	11	3.98	24.96	11.98
14		125	45.72	6.35	1.041	1.4	1.21	29	183	68	323	366	14	4.61	28.80	13.31
15	Air jet on	211	14.94	23.50	2.65	1.4	1.21	12	122	28	280	335	5	0.49	5.19	2.72
16	Sand beds	212	20.42	23.50	2.65	1.4	1.21	21	183	46	378	427	8	0.88	7.78	3.72
17		213	26.82	23.50	2.65	1.4	1.21	32	244	71	472	549	12	1.36	10.38	4.89
18		214	31.09	23.50	2.65	1.4	1.21	38	274	84	533	610	14	1.62	11.68	5.67
19		215	35.05	23.50	2.65	1.4	1.21	47	335	94	600	701	16	1.98	14.27	6.39
20		216	40.54	23.50	2.65	1.4	1.21	55	381	121	683	792	18	2.32	16.22	7.39
21		217	46.33	23.50	2.65	1.4	1.21	65	427	137	762	853	18	2.78	18.16	8.45
22		218	52.73	23.50	2.65	1.4	1.21	76	457	163	856	975	21	3.24	19.46	9.62
23		221	20.42	6.35	2.65	1.4	1.21	3	61		137			0.43	9.60	3.72
24		222	32.61	6.35	2.65	1.4	1.21	12	91	26	177	213	5	1.82	14.40	5.95
25		223	47.55	6.35	2.65	1.4	1.21	19	152	42	247	290	10	2.93	24.00	8.67
26		224	54.86	6.35	2.65	1.4	1.21	23	152	50	287	335	11	3.60	24.00	10.01
27	Water jet on	331	1.28	25.40	2.65	1.4	1000	81	366	-	-	808	94	3.20	14.40	8.50
28	Sand beds	332	1.57	25.40	2.65	1.4	1000	94	457	-	-	957	122	3.68	18.00	10.43
29		333	1.68	25.40	2.65	1.4	1000	98	457	-	-	957	116	3.84	18.00	11.14
30		334	1.81	25.40	2.65	1.4	1000	117	512	-	-	1137	134	4.60	20.16	12.05

Table 6 - 3(g): Mendoza (1980)

Run #	Condition	d (mm)	Q (m^3/s)	U_o (m/s)	D (mm)	ε_m (mm)	x_o (mm)	V_s (m^3)	ε_m/d	x_o/d	V_s/d^3	F_o
1	Headwall	101.6	0.0045	0.55	1.86	155	1534	0.067	1.52	15.10	63.56	3.19
2	Headwall	101.6	0.0067	0.83	1.86	185	1662	0.092	1.82	16.36	87.52	4.79
3	Headwall	101.6	0.009	1.11	1.86	206	1796	0.132	2.03	17.68	125.43	6.39
4	Headwall	101.6	0.0112	1.38	1.86	218	1862	0.151	2.15	18.33	143.85	7.98
5	Headwall	101.6	0.015	1.85	1.86	243	2117	0.24	2.39	20.84	228.51	10.65
6	Headwall	101.6	0.0206	2.54	1.86	281	2571	0.469	2.77	25.31	447.2	14.65
7	Headwall	101.6	0.0258	3.18	1.86	281	3098	0.608	2.77	30.49	579.7	18.31
8	No - headwall	101.6	0.0045	0.55	1.86	151	1490	0.069	1.49	14.67	66.24	3.19
9	No - headwall	101.6	0.0067	0.83	1.86	175	1732	0.091	1.73	17.05	86.88	4.79
10	No - headwall	101.6	0.009	1.11	1.86	221	1703	0.13	2.17	16.76	124.37	6.39
11	No - headwall	101.6	0.0112	1.38	1.86	241	1969	0.21	2.38	19.38	200	7.98
12	No - headwall	101.6	0.015	1.85	1.86	284	2299	0.507	2.79	22.63	483.28	10.65
13	No - headwall	101.6	0.0206	2.54	1.86	263	2634	0.495	2.59	25.92	471.74	14.65
14	No - headwall	101.6	0.0258	3.18	1.86	274	3189	0.629	2.70	31.39	600	18.31

Table 6 - 3(h) Shaihk (1980)

Run #	d (mm)	D (mm)	σ_g	d_b (mm)	d_b/d	Area (m^2)	Q (m^3/s)	U_o (m/s)	ε_m (mm)	$\bar{b}_m$ (mm)	x_o (mm)	V_s (m^3)	ε_m/d	$\bar{b}_m/d$	x_o/d	V_s/d^3	F_o
1	260	7.62	1.32	150	0.59	0.0323	0.054	1.67	351	767	2033	0.345	1.35	2.95	7.82	19.65	4.76
2	260	7.62	1.32	260	1.00	0.0531	0.108	2.04	452.4	1209	3151	1.027	1.74	4.65	12.12	58.43	5.82
3	260	7.62	1.32	260	1.00	0.0531	0.163	3.06	559	1489.8	5959	2.429	2.15	5.73	22.92	138.20	8.72
4	260	7.62	1.32	260	1.00	0.0531	0.217	4.08	655.2	1843.4	7210	4.633	2.52	7.09	27.73	263.60	11.62
5	260	7.34	4.78	150	0.59	0.0323	0.054	1.67	278.2	581.1	2460	0.165	1.07	2.24	9.46	9.37	4.85
6	260	7.34	4.78	260	1.00	0.0531	0.108	2.04	377	1158.3	2530	0.623	1.45	4.455	9.73	35.47	5.93
7	260	7.34	4.78	260	1.00	0.0531	0.163	3.06	465.4	1857.7	4534	1.834	1.79	7.145	17.44	104.33	8.88
8	260	7.34	4.78	260	1.00	0.0531	0.217	4.08	569.4	1857.7	5652	3.942	2.19	7.145	21.74	224.3	11.84

Table 6 - 3(i): Rajaratnam and Diebel (1981)

	Expt. #	d (mm)	D (mm)	U_o (m/s)	h_d (mm)	B (mm)	$\varepsilon_{m\infty}$ (mm)	$x_{m\infty}$ (mm)	$x_{c\infty}$ (mm)	Δ_∞ (mm)	h_d/d	B/d	$\varepsilon_{m\infty}/d$	$x_{m\infty}/d$	F_o
1	A11	12.7	1.05	1.25	22.6	1092	36.5	176.8	420.6	18.3	1.78	85.98	2.87	13.92	9.59
2	A12	12.7	1.05	1.63	24.1	1092	61.6	210.3	573	17.1	1.90	85.98	4.85	16.56	12.50
3	A13	12.7	1.05	1.8	43	1092	60.1	268.2	640	30.5	3.39	85.98	4.73	21.12	13.81
4	A14	12.7	1.05	2.32	42.7	1092	82.6	313.9	825	32.3	3.36	85.98	6.50	24.72	17.80
5	A15	12.7	1.05	0.58	25.6	1092	12.5	85.3	200	16.2	2.02	85.98	0.98	6.72	4.45
6	A16	12.7	1.05	1.79	10.2	1092	65.4	240.8	688.8	22.3	0.80	85.98	5.15	18.96	13.73
7	A17	12.7	1.05	1.48	10.2	1092	54.3	201.2	597.4	15.2	0.80	85.98	4.28	15.84	11.35
8	A18	12.7	1.05	1.08	2.5	1092	34.1	85.3	-	19.1	0.20	85.98	2.69	6.72	8.28
9	A19	12.7	1.05	1.29	2.5	1092	38.4	140.2	402.3	10.6	0.20	85.98	3.02	11.04	9.90
10	B11	12.7	1.05	2.13	32	38.1	76.2	192	-	11.3	2.52	3.00	6.00	15.12	16.34
11	B12	12.7	1.05	1.53	31.7	38.1	43.6	161.5	-	14.7	2.50	3.00	3.43	12.72	11.74
12	B21	25.4	1.05	0.45	22.3	88.9	25.3	85.3	359.7	14	0.88	3.50	1.00	189.56	3.45
13	B22	25.4	1.05	0.53	23.5	88.9	25.6	146.3	365.8	15.2	0.93	3.50	1.01	276.04	4.07
14	B23	25.4	1.05	0.71	29.3	88.9	32	222.5	512.1	13.1	1.15	3.50	1.26	313.38	5.45
15	B24	25.4	1.05	0.41	22.2	88.9	16.8	54.9	259.1	14	0.87	3.50	0.66	133.90	3.14
16	B25	25.4	1.05	1.41	16.5	25.4	79.3	298.7	-		0.65	1.00	3.12	211.84	10.82
17	B26	25.4	1.05	0.9	6.7	88.9	51.2	100.6	-	14.9	0.26	3.50	2.02	111.78	6.90

Table 6 - 3(j) Kloberdanz (1982)

Run #	d (mm)	Q (m^3/s)	U_o (m/s)	D (mm)	ε_m (mm)	$\bar{b}_m$ (mm)	x_o (mm)	V_s (m^3)	ε_m/d	$\bar{b}_m/d$	x_o/d	V_s/d^3	F_o
1	101.6	0.0031	0.38	2	46	148	813	0.0029	0.45	1.46	8.00	2.75	2.14
2	101.6	0.0042	0.52	2	57	351	1149	0.0072	0.56	3.45	11.31	6.85	2.91
3	101.6	0.0051	0.63	2	69	220	1059	0.0085	0.68	2.17	10.42	8.09	3.49
4	101.6	0.0102	1.26	2	115	459	1094	0.0260	1.13	4.52	10.77	24.82	6.99
5	101.6	0.0156	1.92	2	174	690	1619	0.0981	1.71	6.79	15.94	93.58	10.68
6	101.6	0.0207	2.55	2	249	1011	1956	0.1848	2.45	9.95	19.25	176.24	14.17

Table: 6 - 3(k): Ead (1990)

Run #	d (mm)	Q (m^3/s)	U_o (m/s)	D (mm)	h_d/d	ε_m (mm)	x_m (mm)	x_o (mm)	ε_m/d	F_o
1	25	0.00065	1.32	0.707	free*	64	300	730	2.54	12.38
2	25	0.0008	1.63	0.707	free	65	400	940	2.60	15.24
3	25	0.0010	2.04	0.707	free	81	450	960	3.22	19.04
4	50	0.0023	1.17	0.707	free	111	300	620	2.22	10.95
5	50	0.0030	1.53	0.707	free	134	490	1170	2.67	14.28
6	50	0.0040	2.04	0.707	free	156	600	1190	3.11	19.04
7	75	0.00633	1.43	0.707	free	152	700	1850	2.03	13.39
8	75	0.00825	1.87	0.707	free	167	750	1920	2.23	17.46
9	75	0.00985	2.23	0.707	free	185.5	1050	1720	2.47	20.84
10	100	0.00935	1.19	0.707	free	156.5	450	1480	1.57	11.13
11	100	0.01299	1.65	0.707	free	146	600	1630	1.46	15.46
12	100	0.01696	2.16	0.707	free	195.5	1250	1800	1.96	20.19
13	75	0.00633	1.43	0.707	1.27	105	500	1120	1.40	13.39
14	75	0.00633	1.43	0.707	1.5	102.5	600	1120	1.37	13.39
15	75	0.00633	1.43	0.707	2	111	630	1160	1.48	13.39
16	100	0.01299	1.65	0.707	1.2	143	650	1280	1.43	15.46
17	100	0.01299	1.65	0.707	1.5	149	650	1280	1.49	15.46
18	100	0.01299	1.65	0.707	2	147.5	700	1280	1.48	15.46

* Free means that the jet is unsubmerged and h_d/d was not measured.

Table: 6 - 3(l): Lim (1995)

	Run #	Time (hr.)	U_o (m/s)	d (mm)	$\varepsilon_{m\infty}$ (mm)	$\bar{b}_{m\infty}$ (mm)	$x_{o\infty}$ (mm)	$V_{s\infty}$ (mm^3)	$\varepsilon_{m\infty}/d$	$\bar{b}_{m\infty}/d$	$x_{o\infty}/d$	$V_{s\infty}/d^3$	B/d	F_o
1	H6	78	2.826	15	73	230	877	9000	4.87	15.33	58.47	2666.67	66.67	17.29
2	H9	46	4.02	15	65	285	1156	12500	4.33	19.00	77.07	3703.70	66.67	24.60
3	H10	65	1.464	15	48	130	400	1500	3.20	8.67	26.67	444.44	66.67	8.96
4	H11	24	0.72	15	21	50	100	65	1.40	3.33	6.67	19.26	66.67	4.41
5	H12	22	1.012	15	30	80	215	375	2.00	5.33	14.33	111.11	66.67	6.19
6	H13	47	2.065	15	61	140	500	2510	4.07	9.33	33.33	743.70	66.67	12.64
7	H14	24	0.45	15	13	-	-	-	0.87	-	-	-	66.67	2.75
8	H15	46	2.41	15	64	257.5	620	3900	4.27	17.17	41.33	1155.56	66.67	14.75
9	H16	25	1.8	15	51	160	430	1500	3.40	10.67	28.67	444.44	66.67	11.01
10	J1	97	0.521	26	37	85	412	700	1.42	3.27	15.85	39.83	10	3.19
11	J2	68	0.68	26	29	72.5	330	550	1.12	2.79	12.69	31.29	10	4.16
12	J3	70	0.312	26	30	62.5	170	300	1.15	2.40	6.54	17.07	10	1.91
13	J4	72	0.425	26	30	55	376	350	1.15	2.12	14.46	19.91	10	2.60
14	J5	94	1.053	26	57	85	480	4500	2.19	3.27	18.46	256.03	10	6.44
15	J6	69	1.25	26	65	95	560	3980	2.50	3.65	21.54	226.45	10	7.65
16	K1	55	1.25	26	56	-	660	2500	2.15	-	25.38	142.24	5	7.65
17	K2	66	1.003	26	46	-	537	1750	1.77	-	20.65	99.57	5	6.14
18	K3	99	0.747	26	28	-	410	860	1.08	-	15.77	48.93	5	4.57
19	K4	71	0.531	26	26	-	365	750	1.00	-	14.04	42.67	5	3.25
20	K5	95	0.421	26	21	-	180	340	0.81	-	6.92	19.34	5	2.58

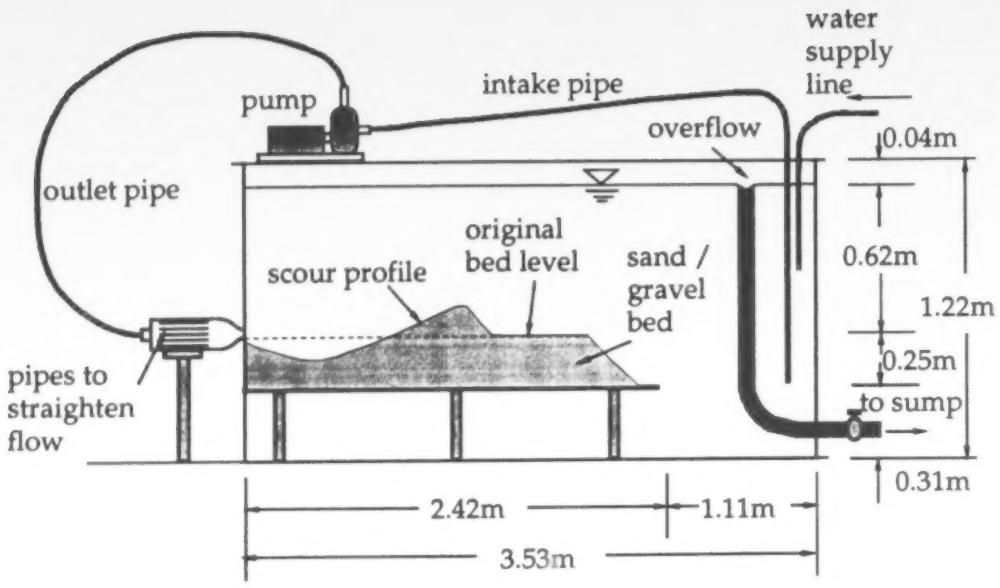

(a) Set-up for the water jet experiments

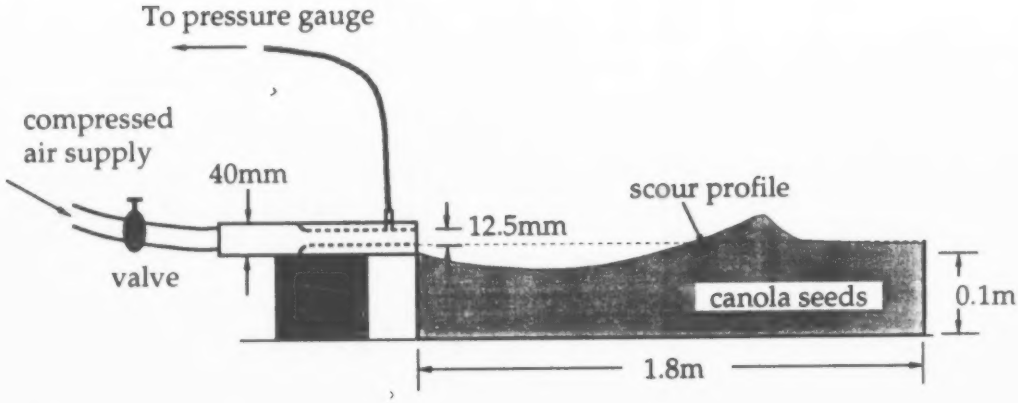

(b) Set-up for the air jet experiments

Figure 6 - 1(a - b): Set-up for the experiments

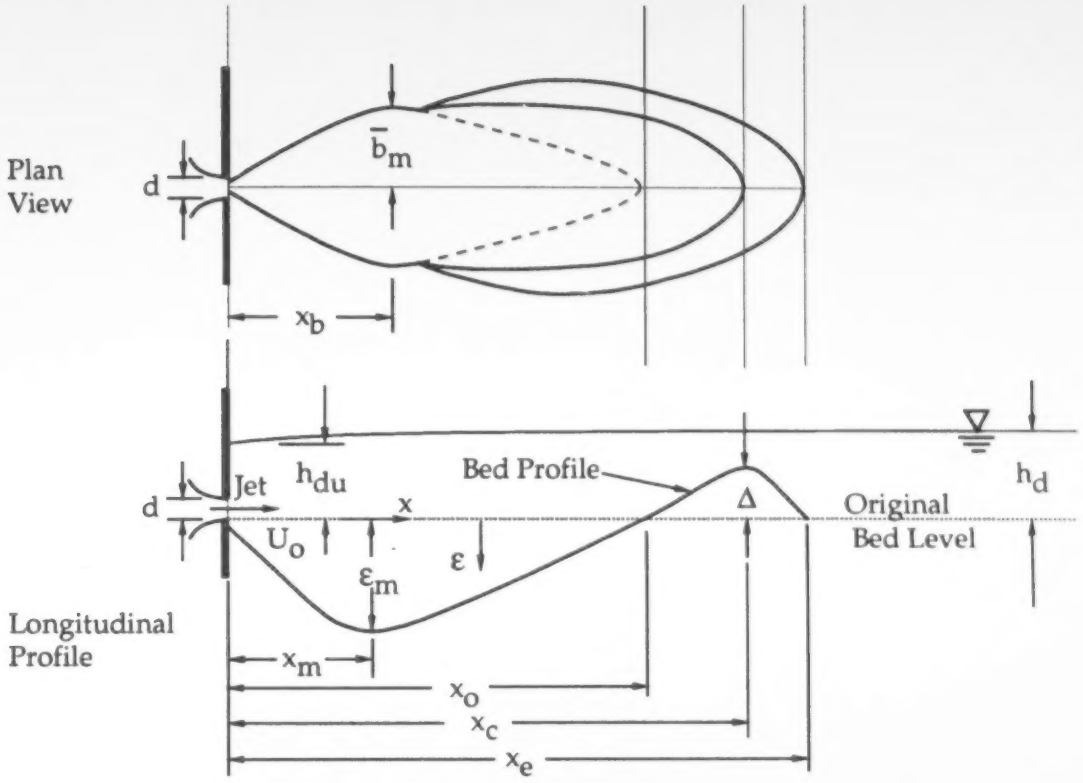

Figure 6 - 2(a) Definition Sketch for Wall Jet Erosion

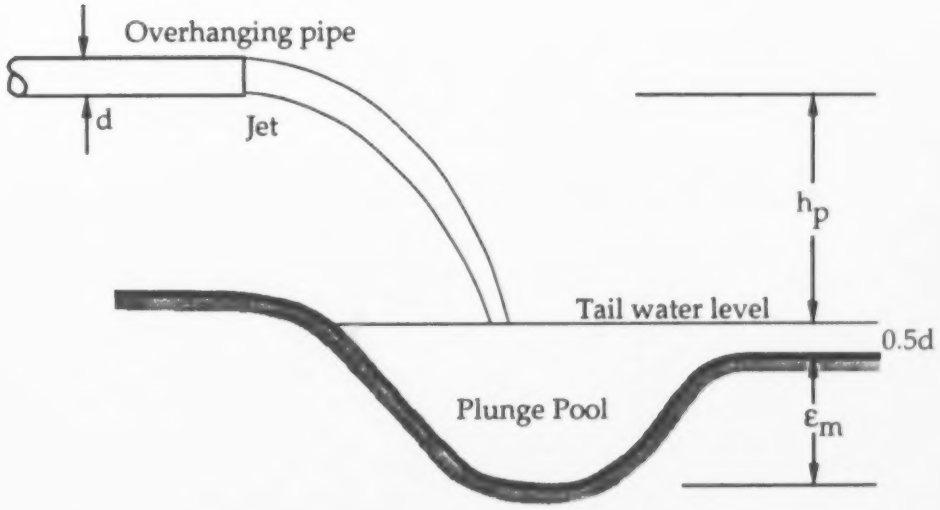

Figure 6 - 2(b): Definition Sketch for
Overhanging Pipe Outlet Erosion

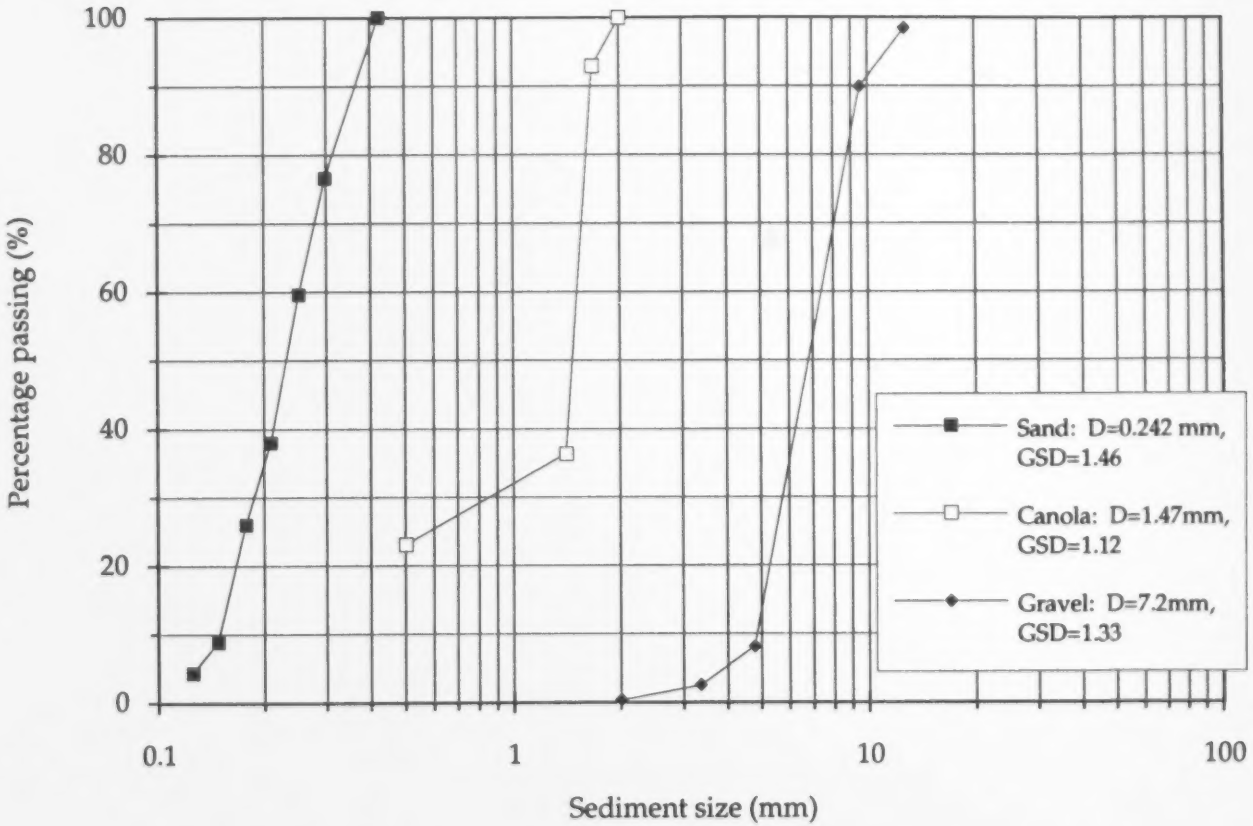

Figure 6-3: Sediment size distribution curves

Figure 6-4(a): Migrating Dunes

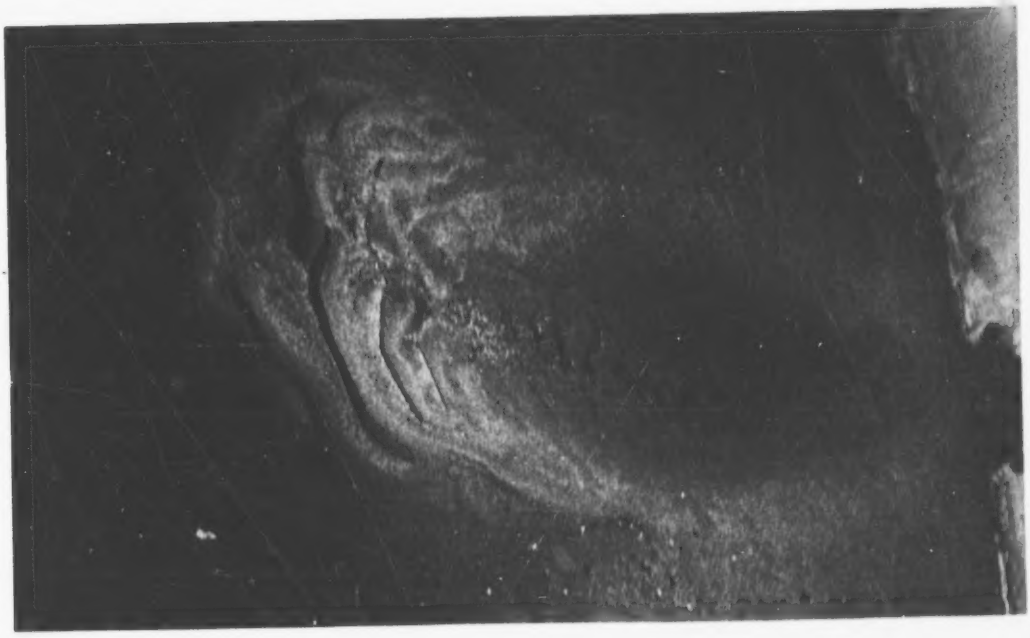

Figure 6-4(b): Eroded Sand Bed

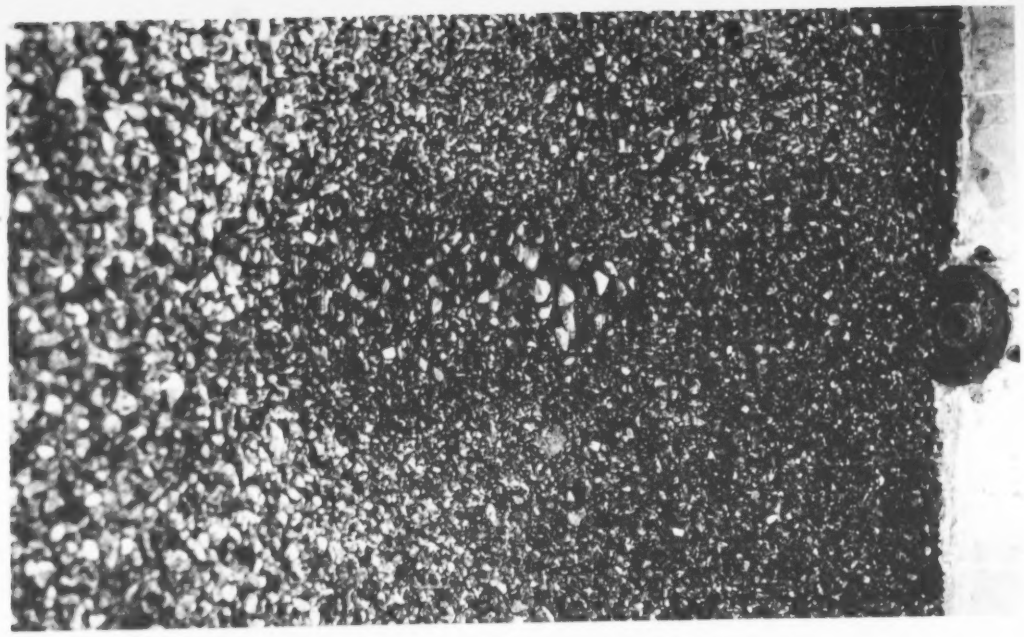

Figure 6-4(c): Eroded Gravel Bed

Figure 6-4(d): Eroded Bed of Canola Seeds

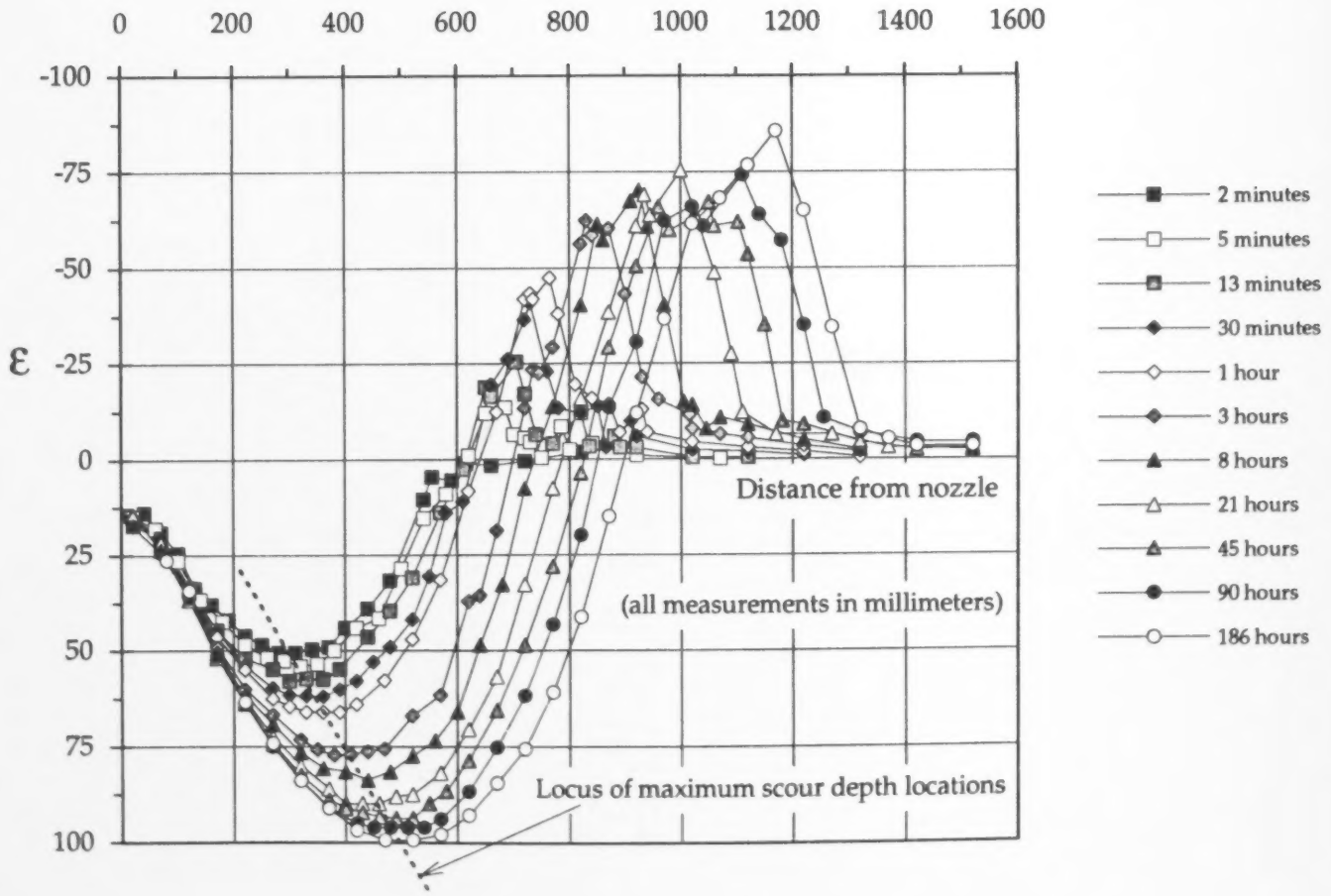

Figure 6 – 5: Variation of longitudinal profile of the eroded bed with time

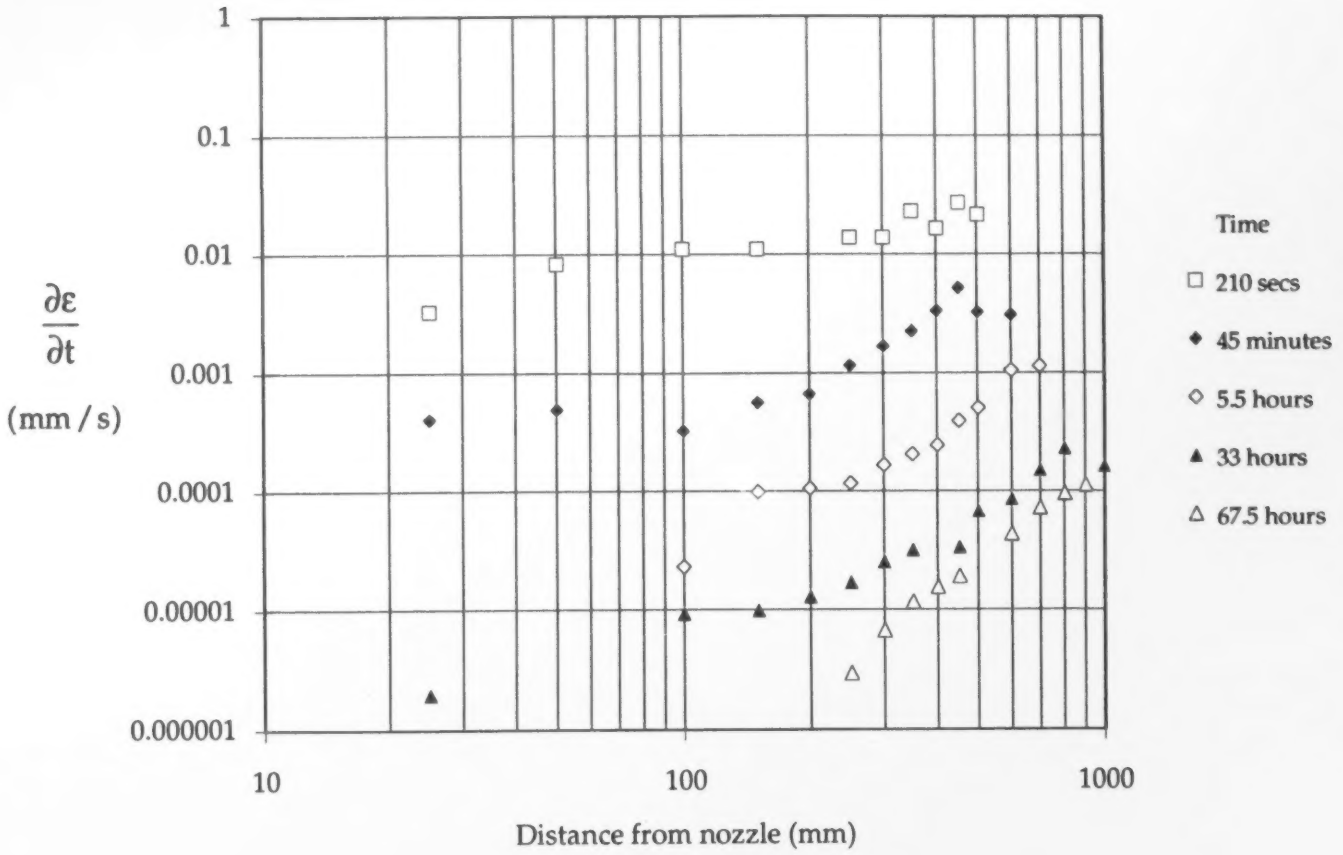

Figure 6–6: Variation of the rate of erosion with distance

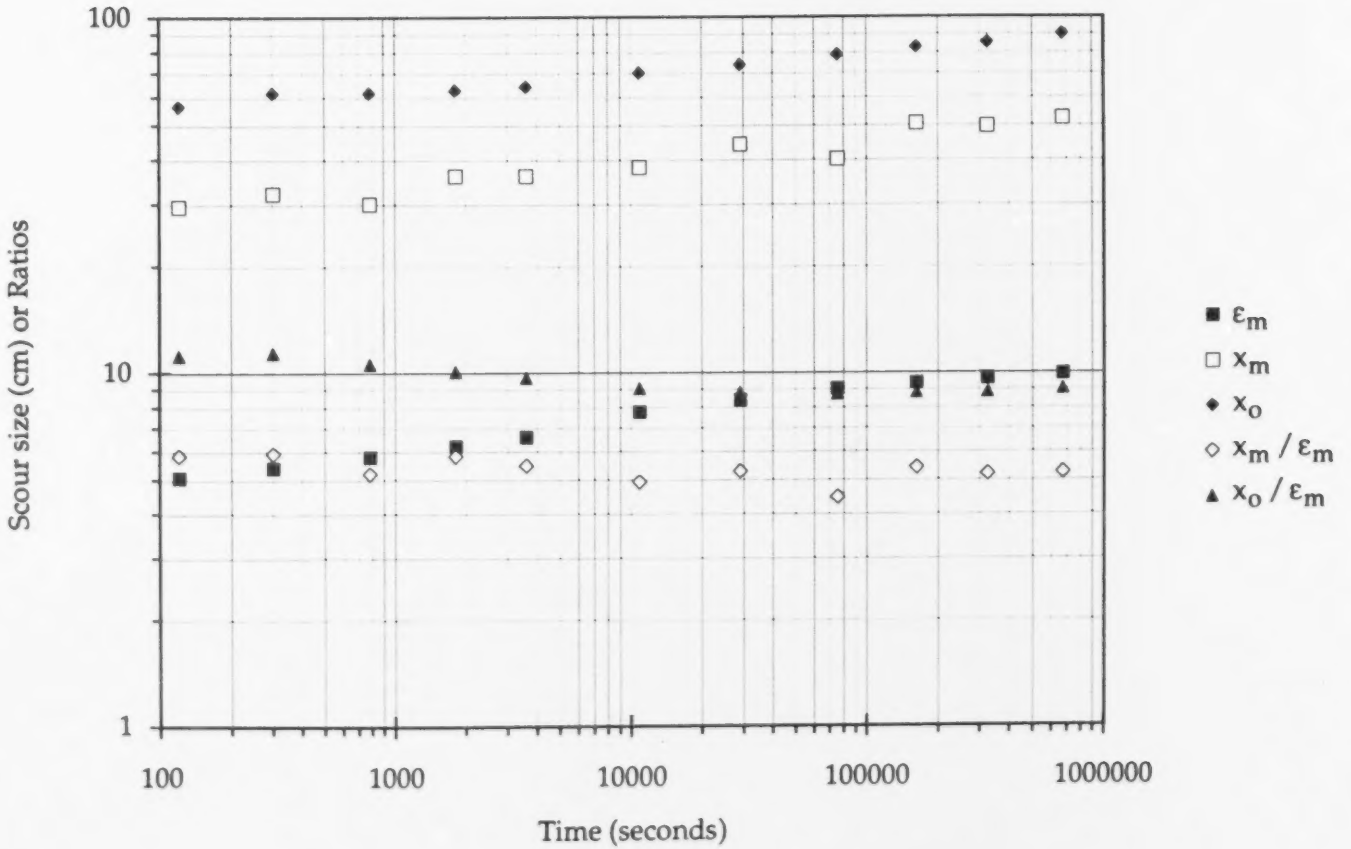

Figure 6–7: Variation of the characteristic lengths of the scour hole of the eroded bed with time

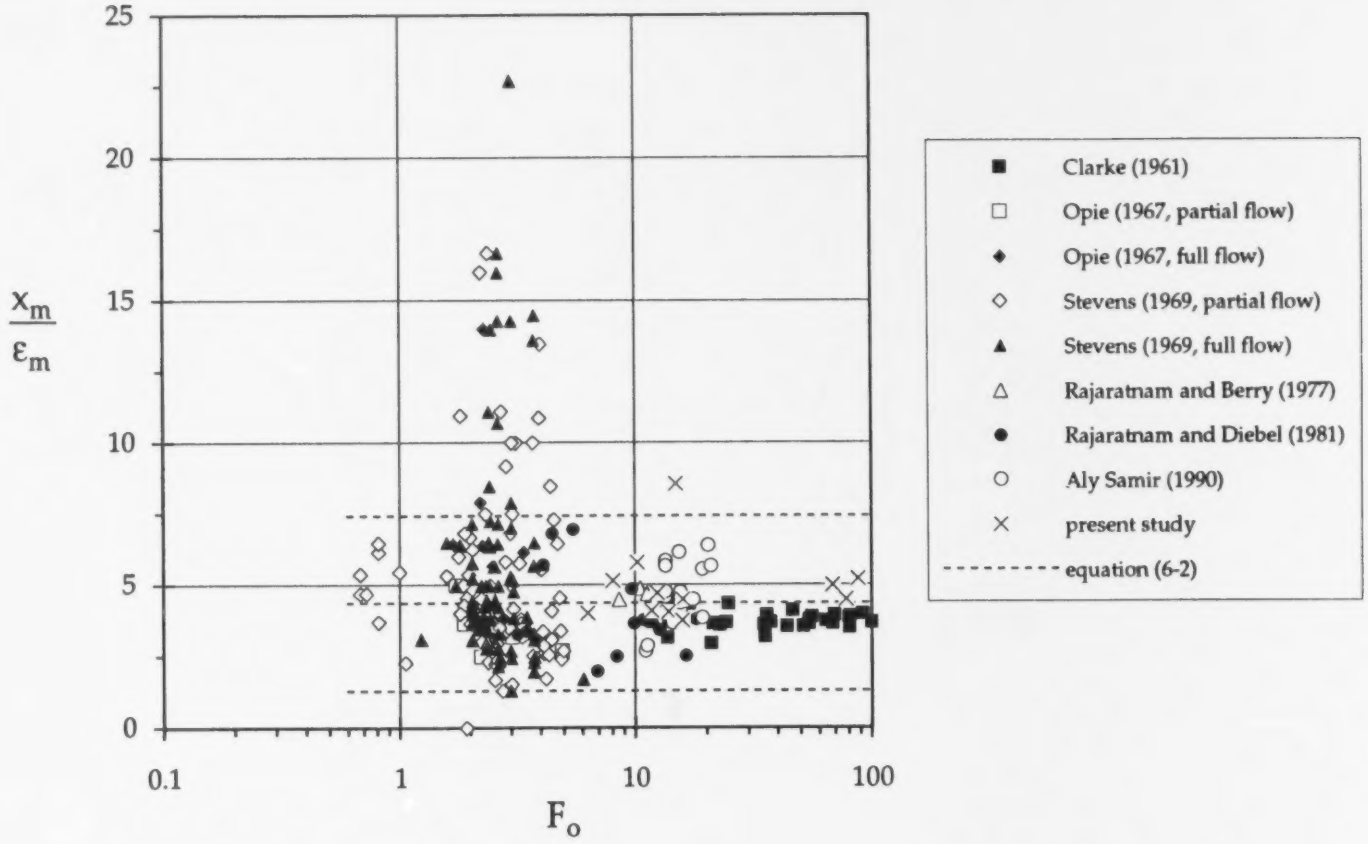

Figure 6–8: Variation of x_m / ε_m with F_o

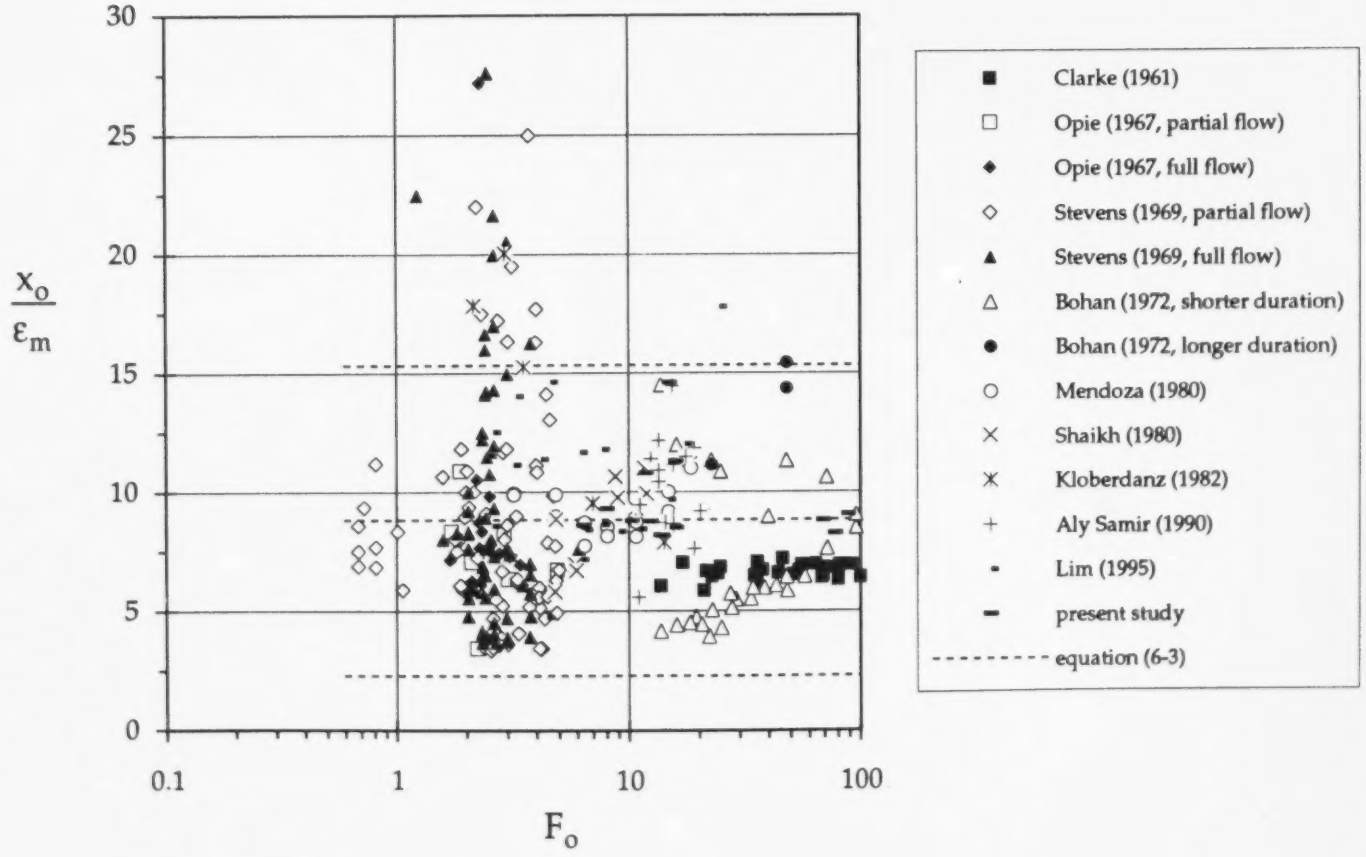

Figure 6 – 9: Variation of x_o / ε_m with F_o

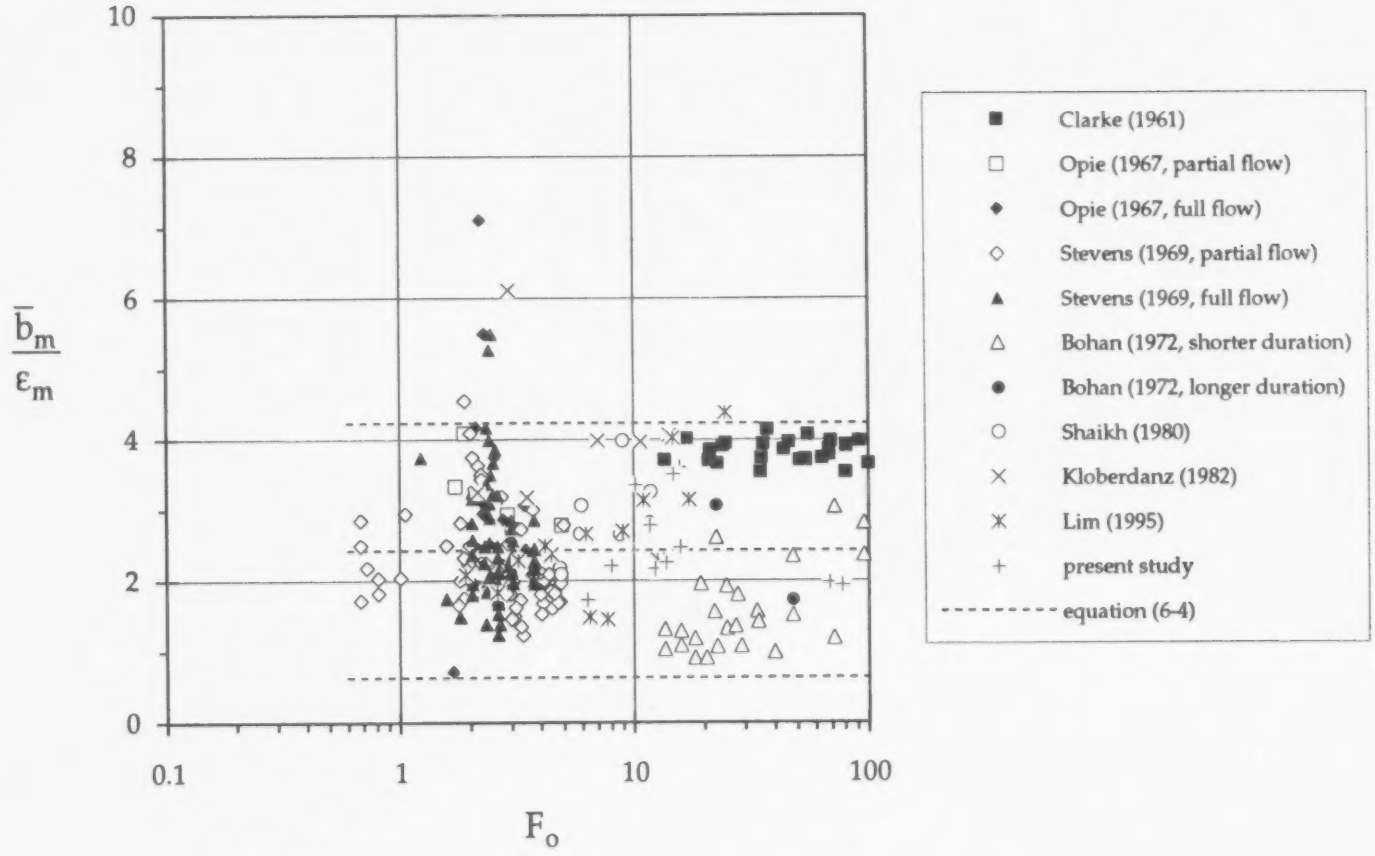

Figure 6 – 10: Variation of $\bar{b}_m / \varepsilon_m$ with F_o

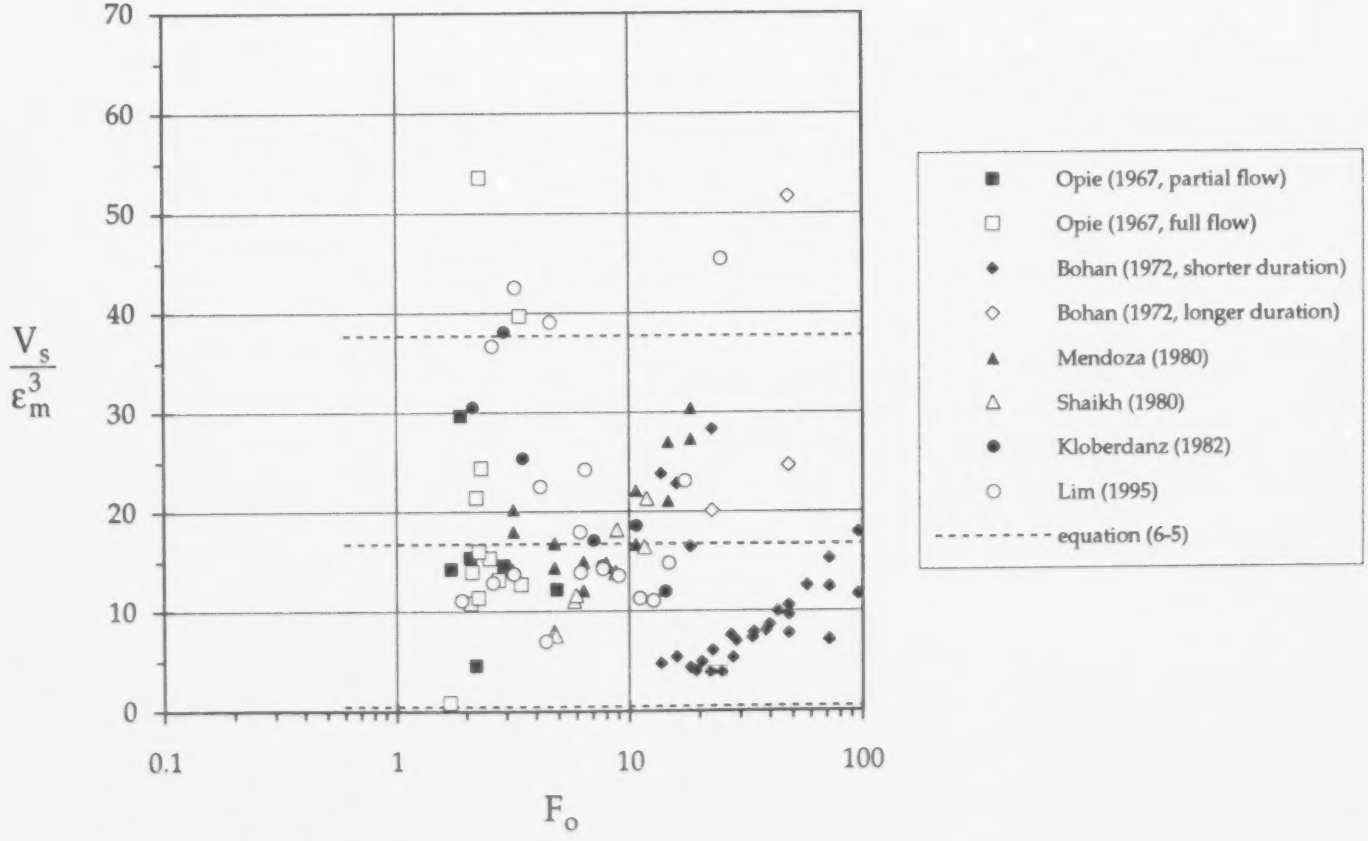

Figure 6 – 11: Variation of V_s / ε_m^3 with F_o

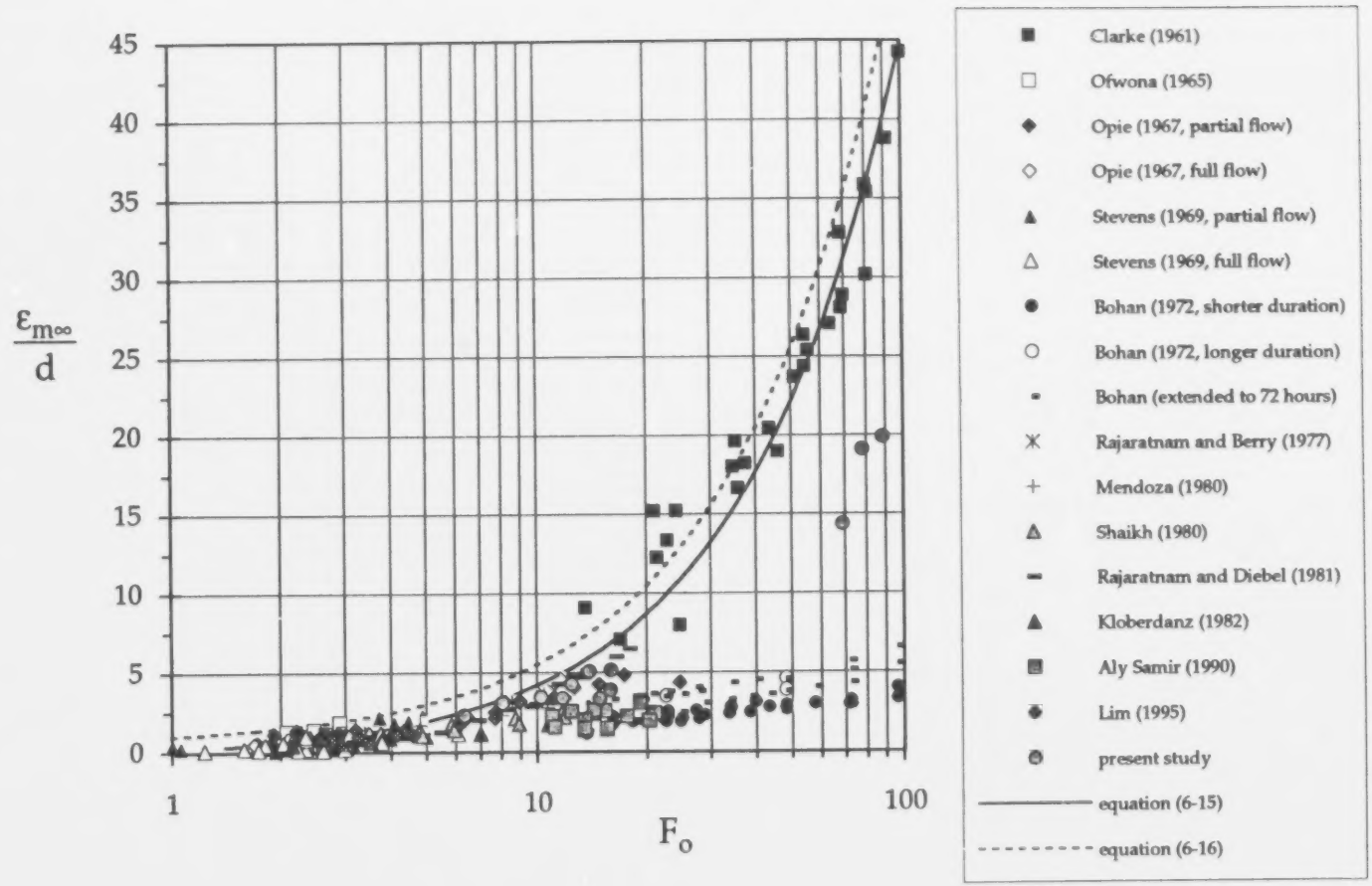

Figure 6–12: Variation of relative maximum scour depth with F_o

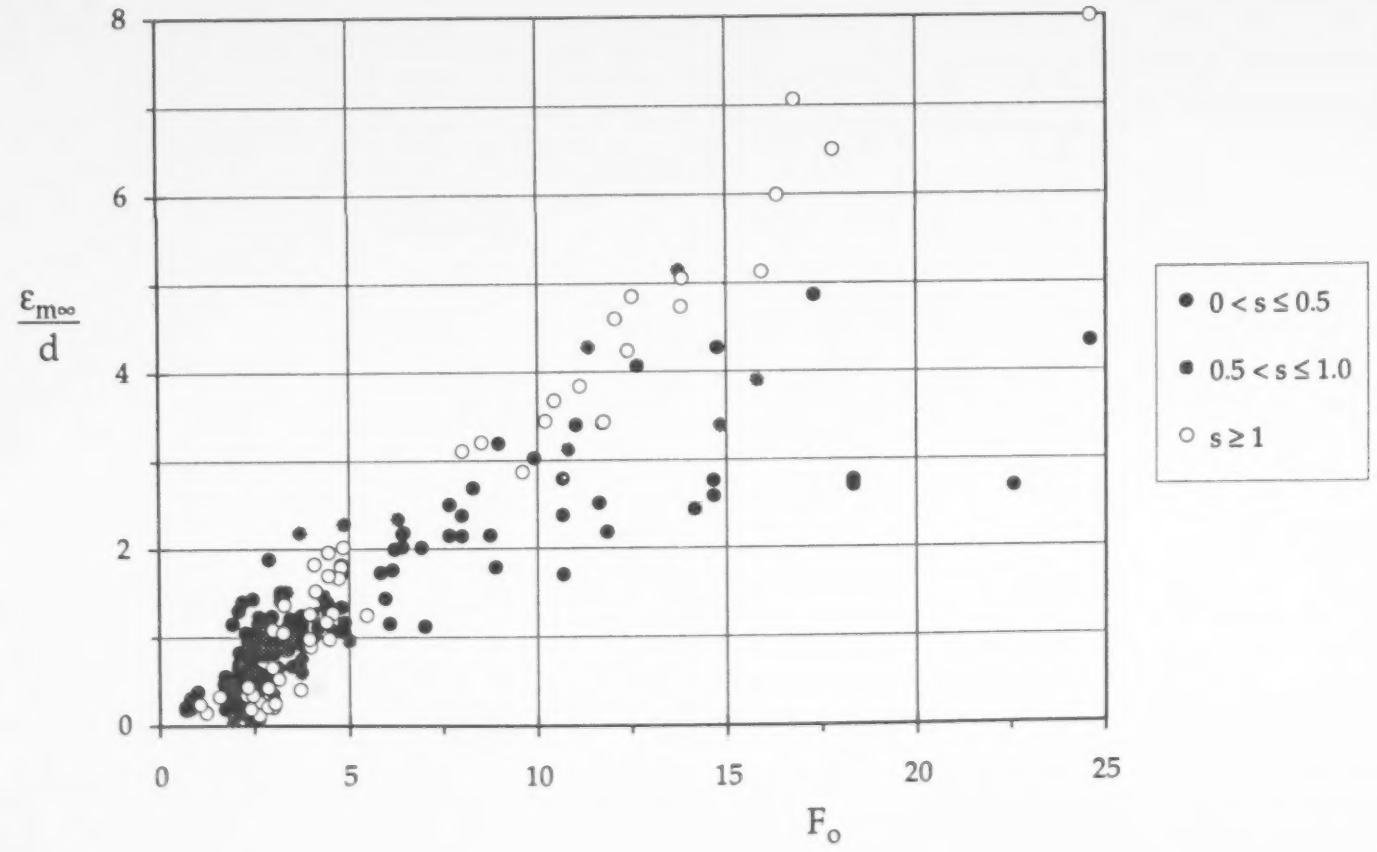

Figure 6 – 13: Effect of submergence on relative maximum scour depth

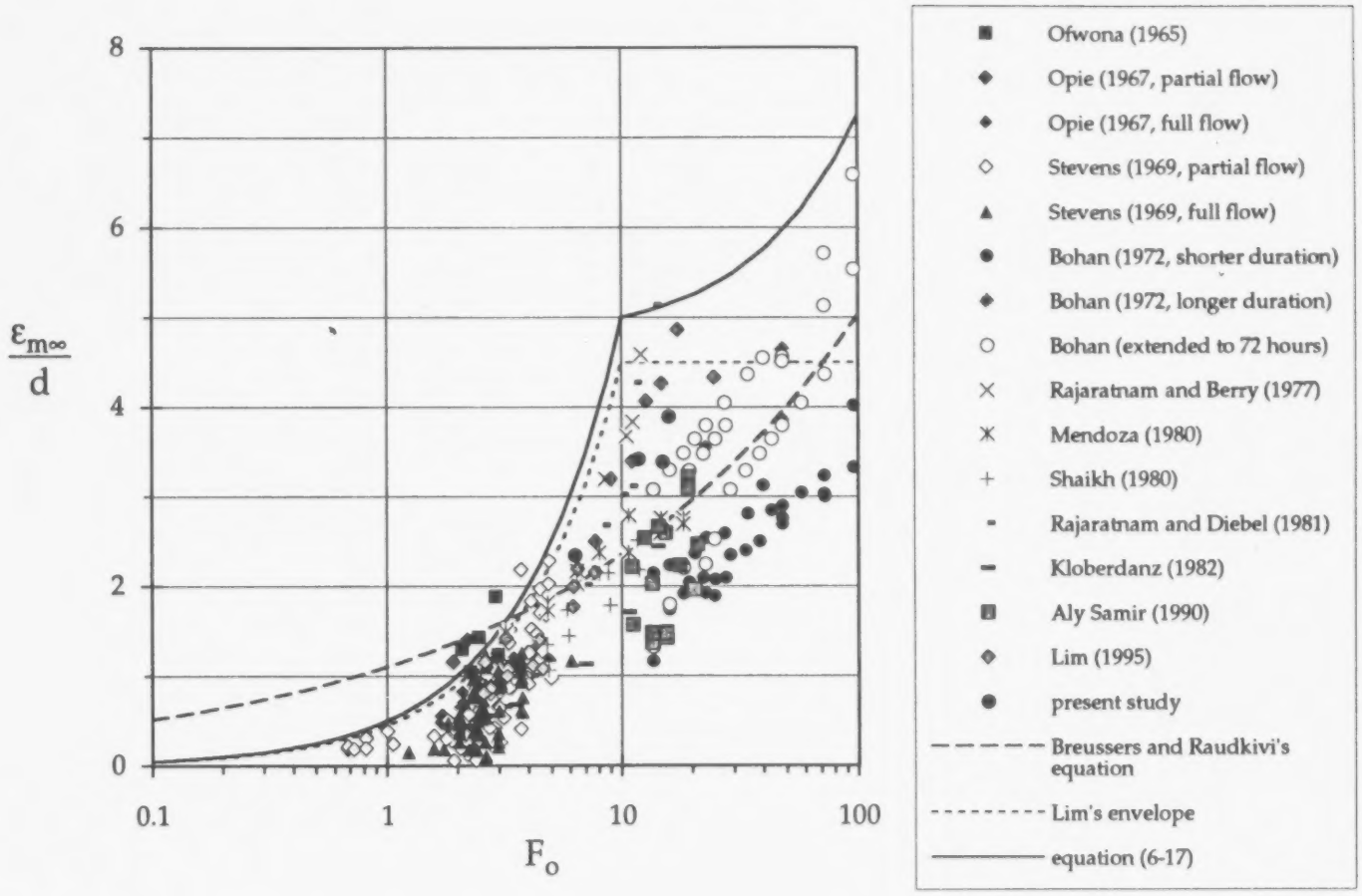

Figure 6 – 14: Variation of relative maximum scour depth with F_o for unsubmerged flows

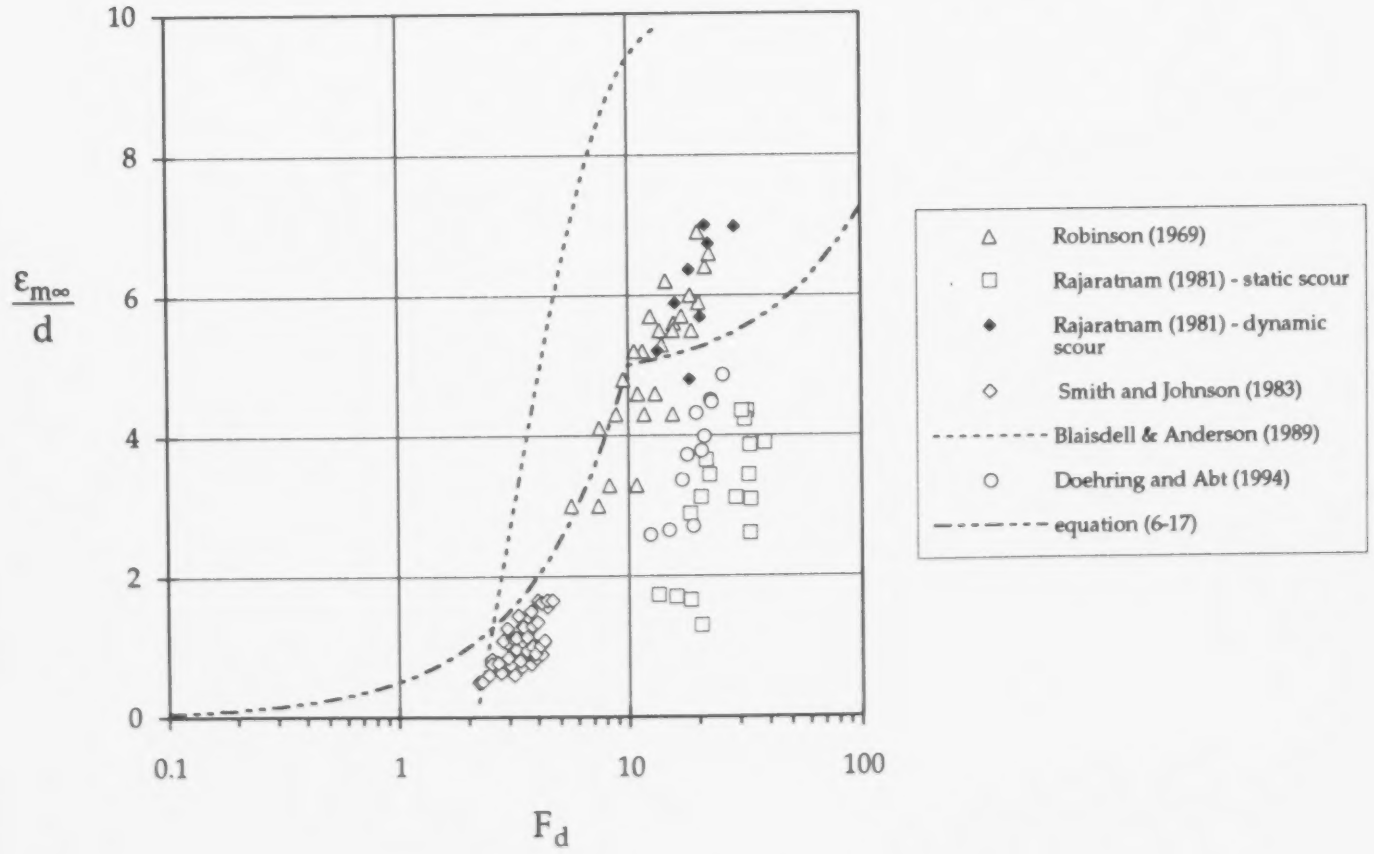

Figure 6-15: Variation of relative maximum scour depth with F_d for overhanging pipes

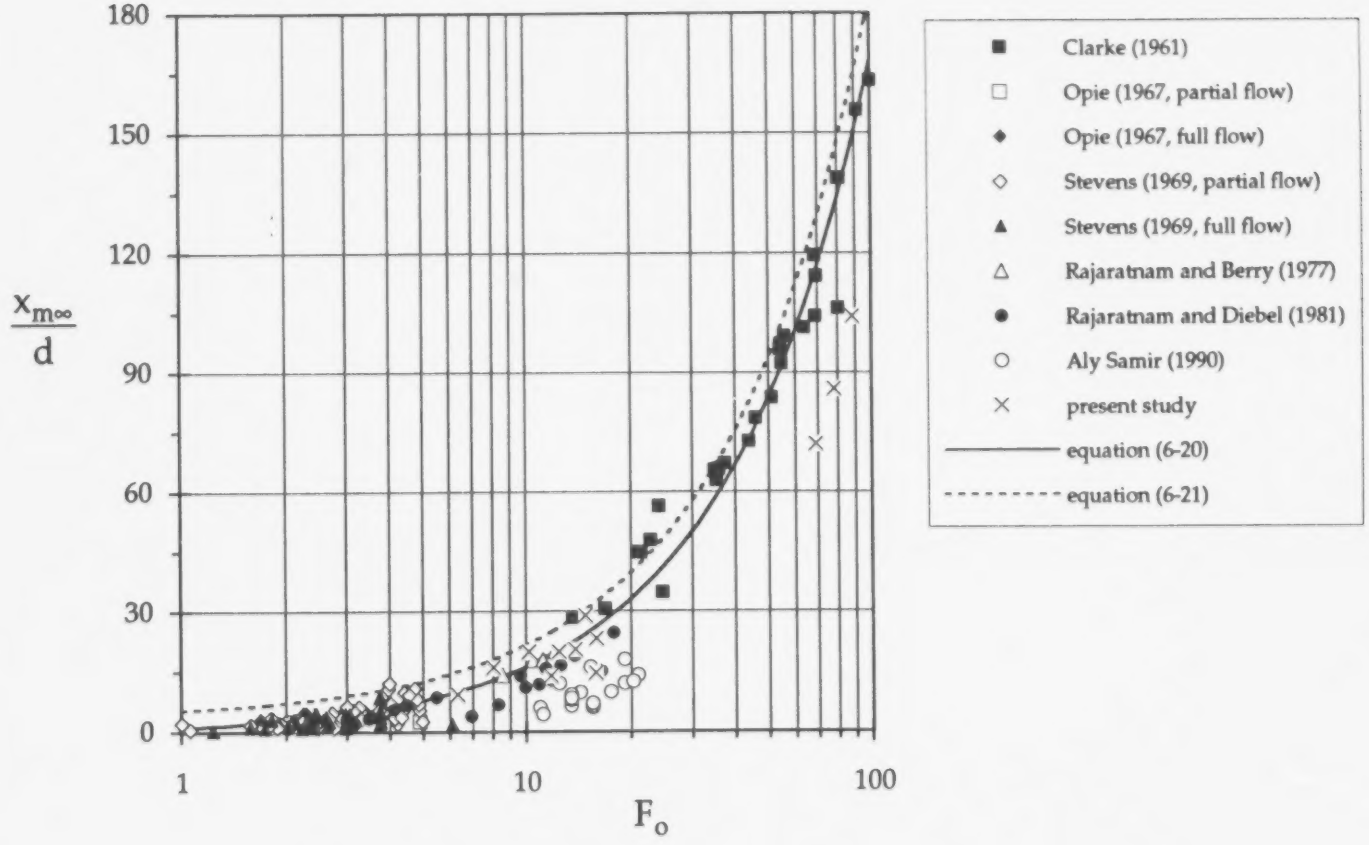

Figure 6 – 16: Variation of relative distance of the maximum scour depth with F_o

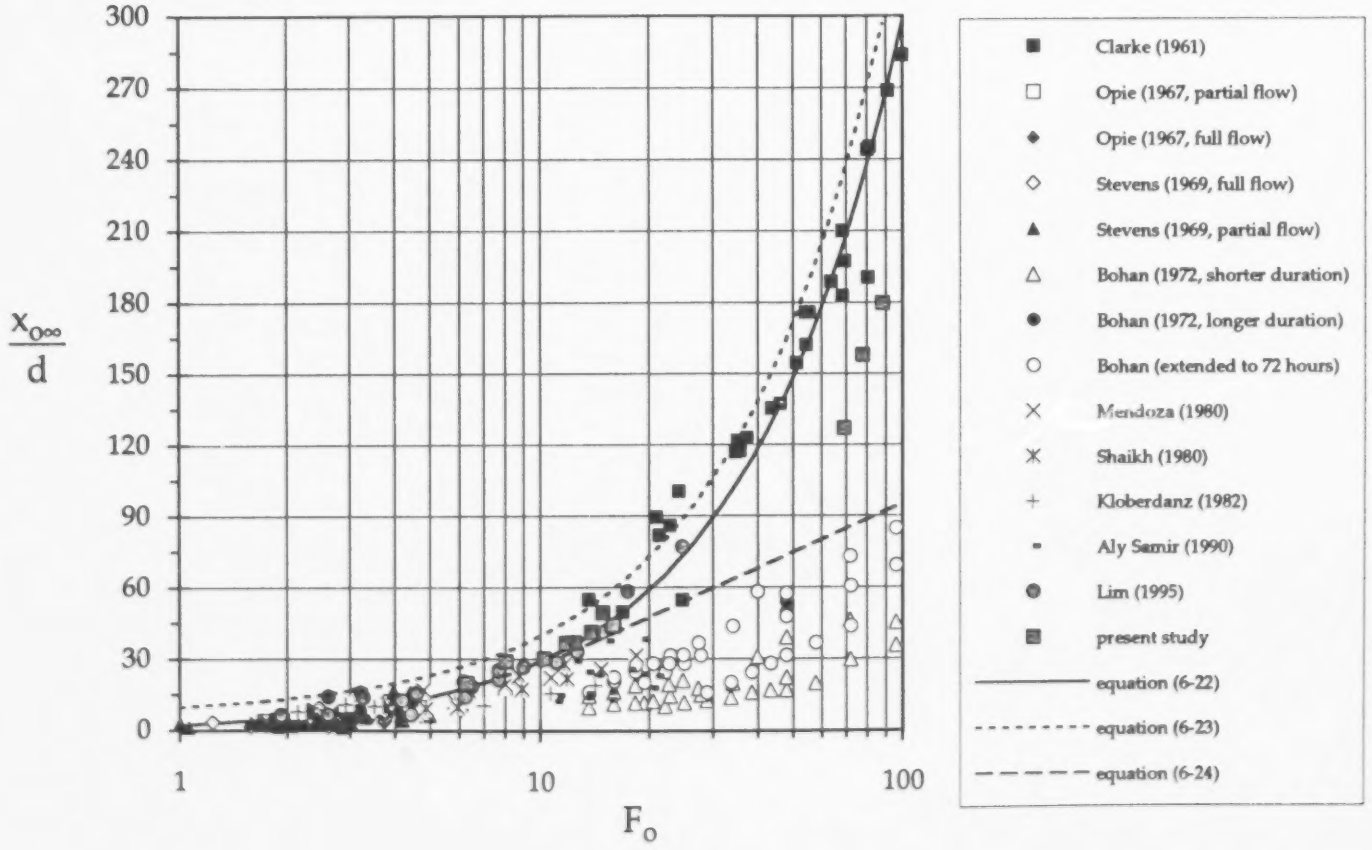

Figure 6 – 17: Variation of relative scour hole length with F_o

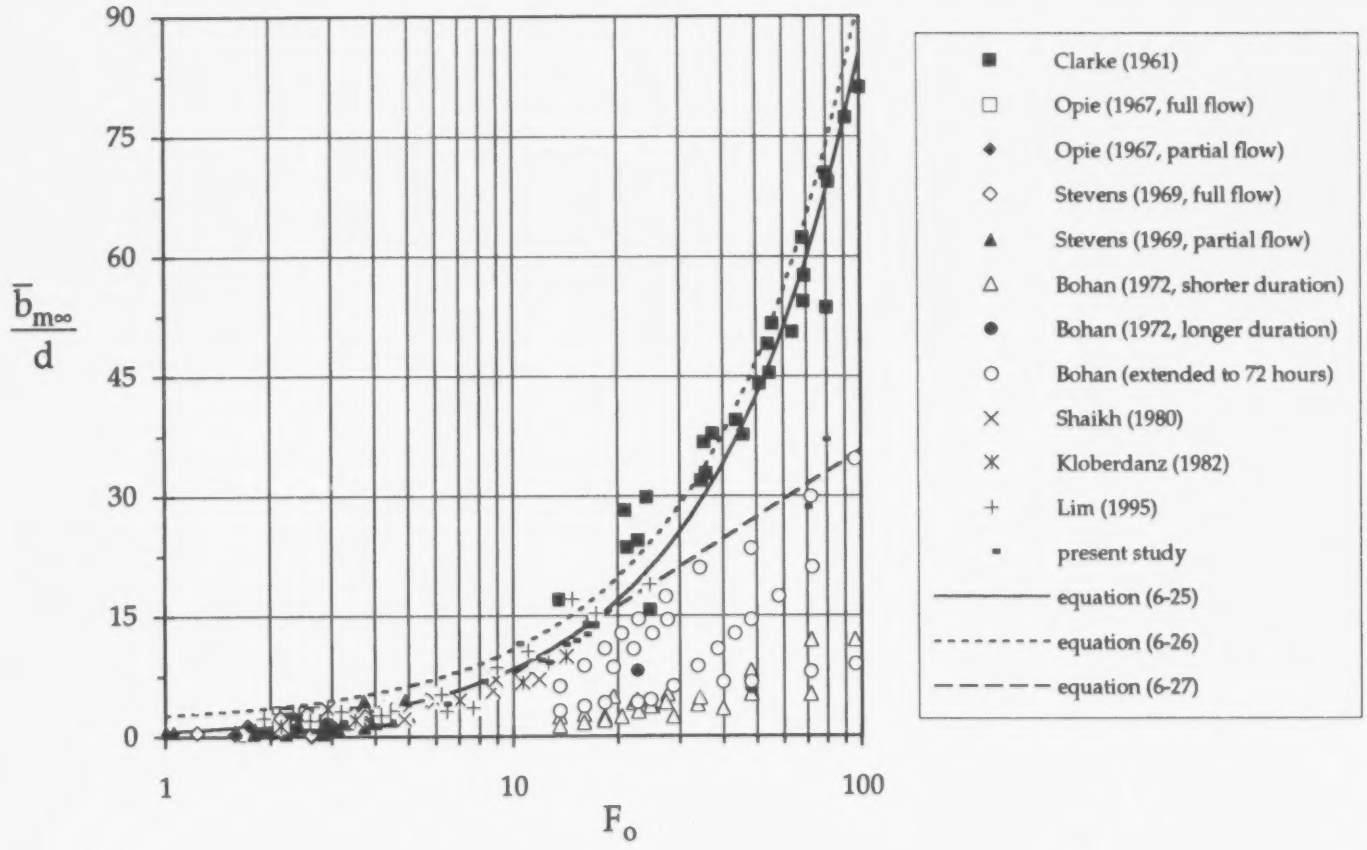

Figure 6 – 18: Variation of relative maximum scour hole half width with F_o

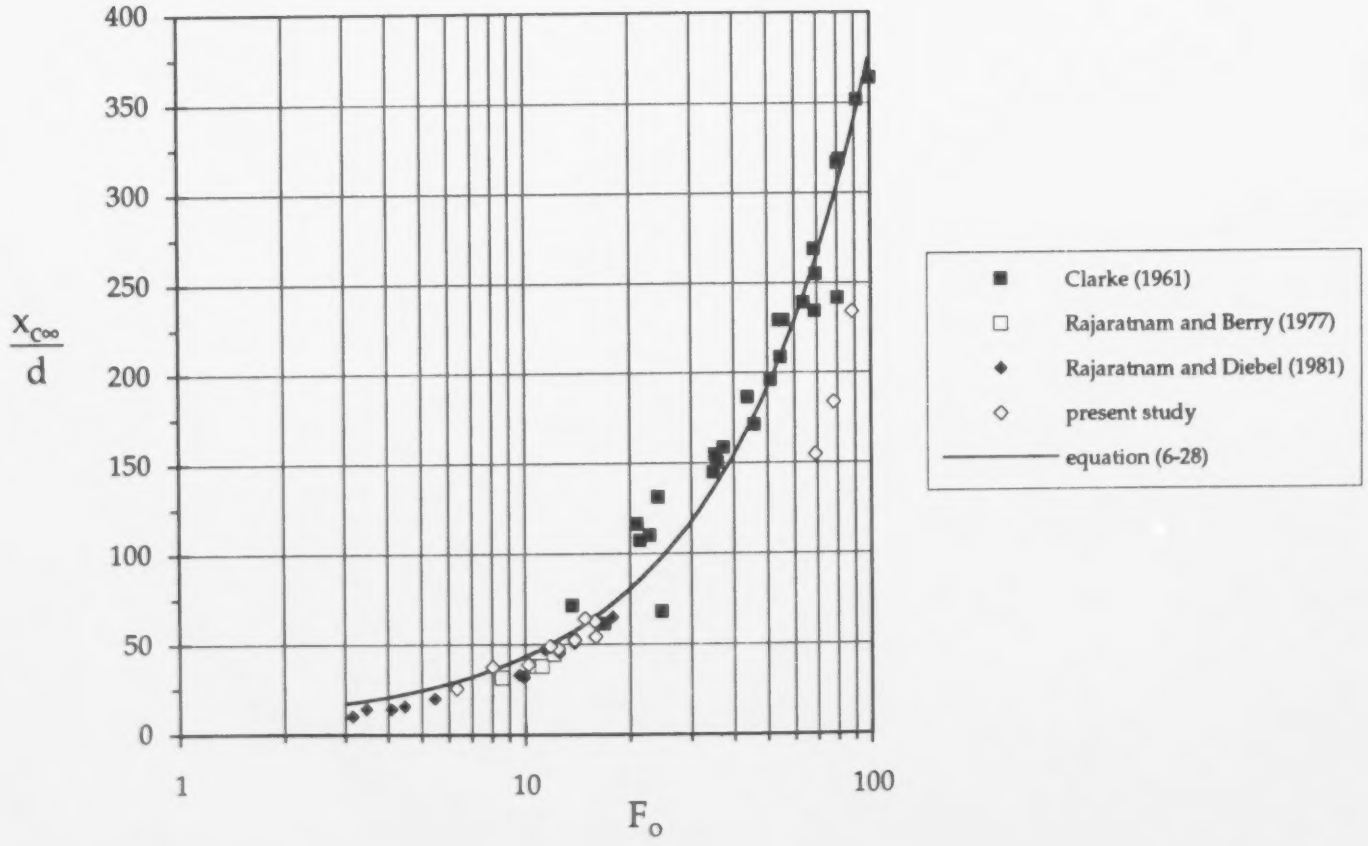

Figure 6 – 19: Variation of relative distance of dune with F_o

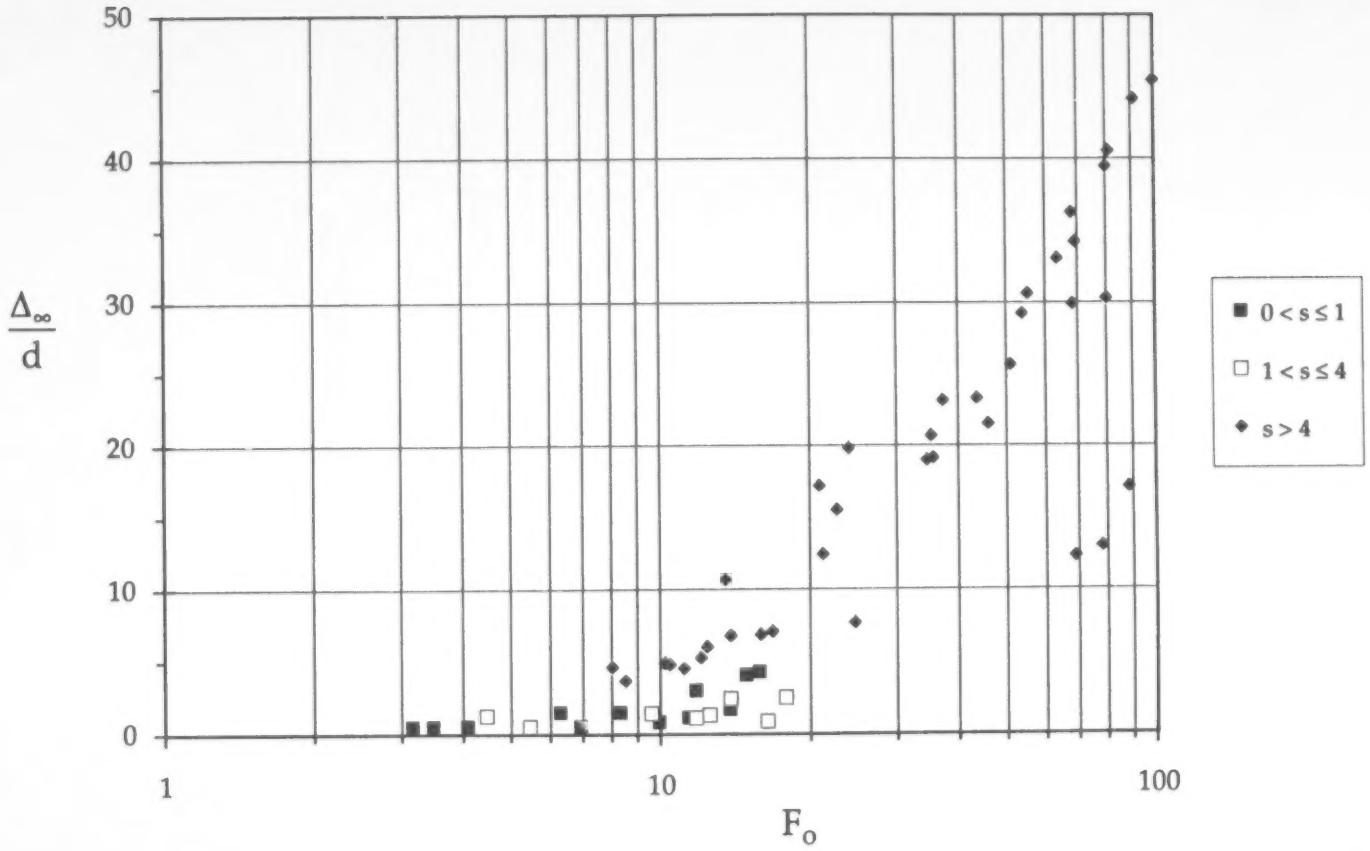

Figure 6 – 20: Variation of relative dune height with F_o

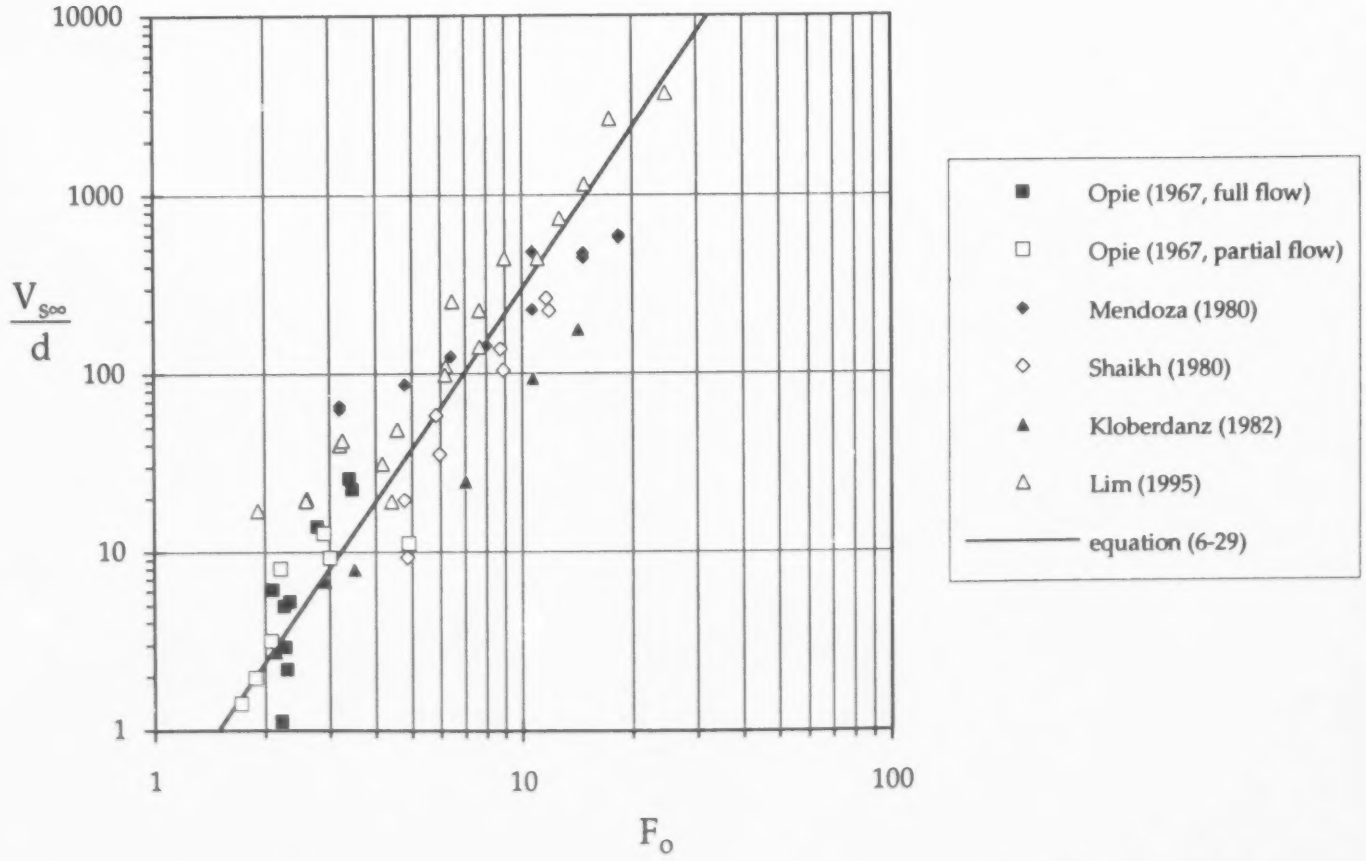

Figure 6 – 21: Variation of relative volume of scour with F_o

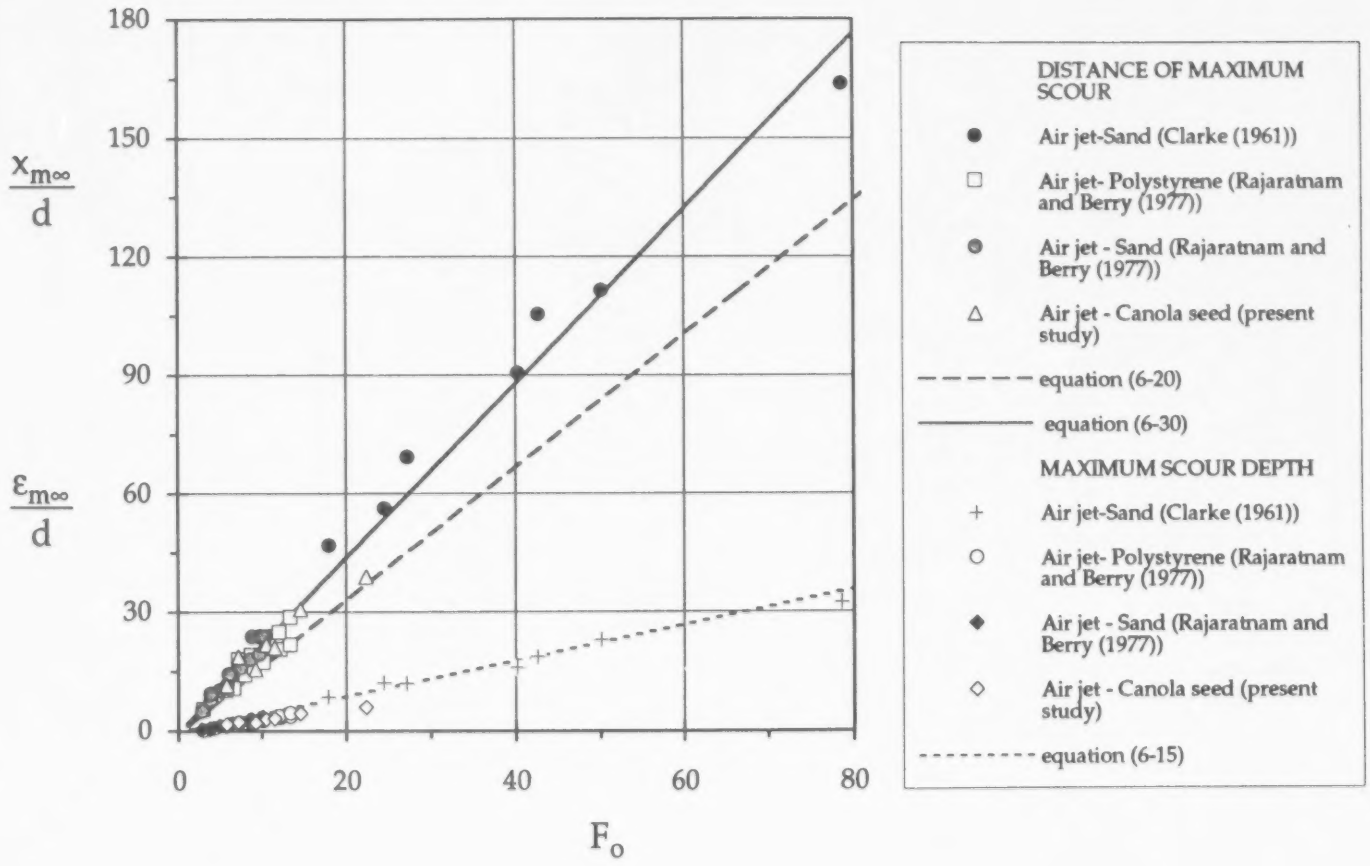

Figure 6 – 22: Variation of $(\varepsilon_{m\infty} / d)$ and $(x_{m\infty} / d)$ with F_o for other fluid – sediment systems

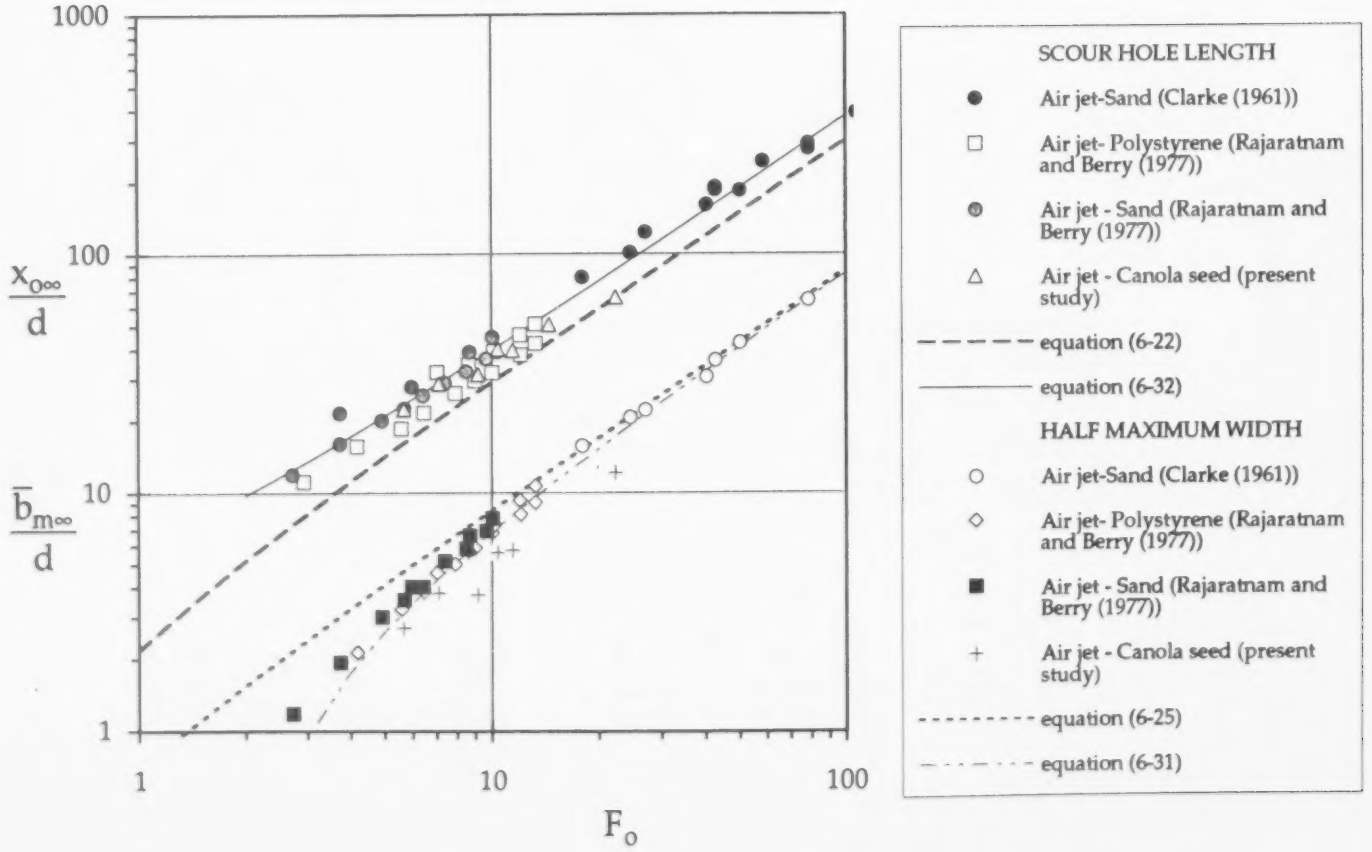

Figure 6 – 23: Variation of $\left(\bar{b}_{m\infty} / d\right)$ and $\left(x_{o\infty} / d\right)$ with F_o for other fluid – sediment systems

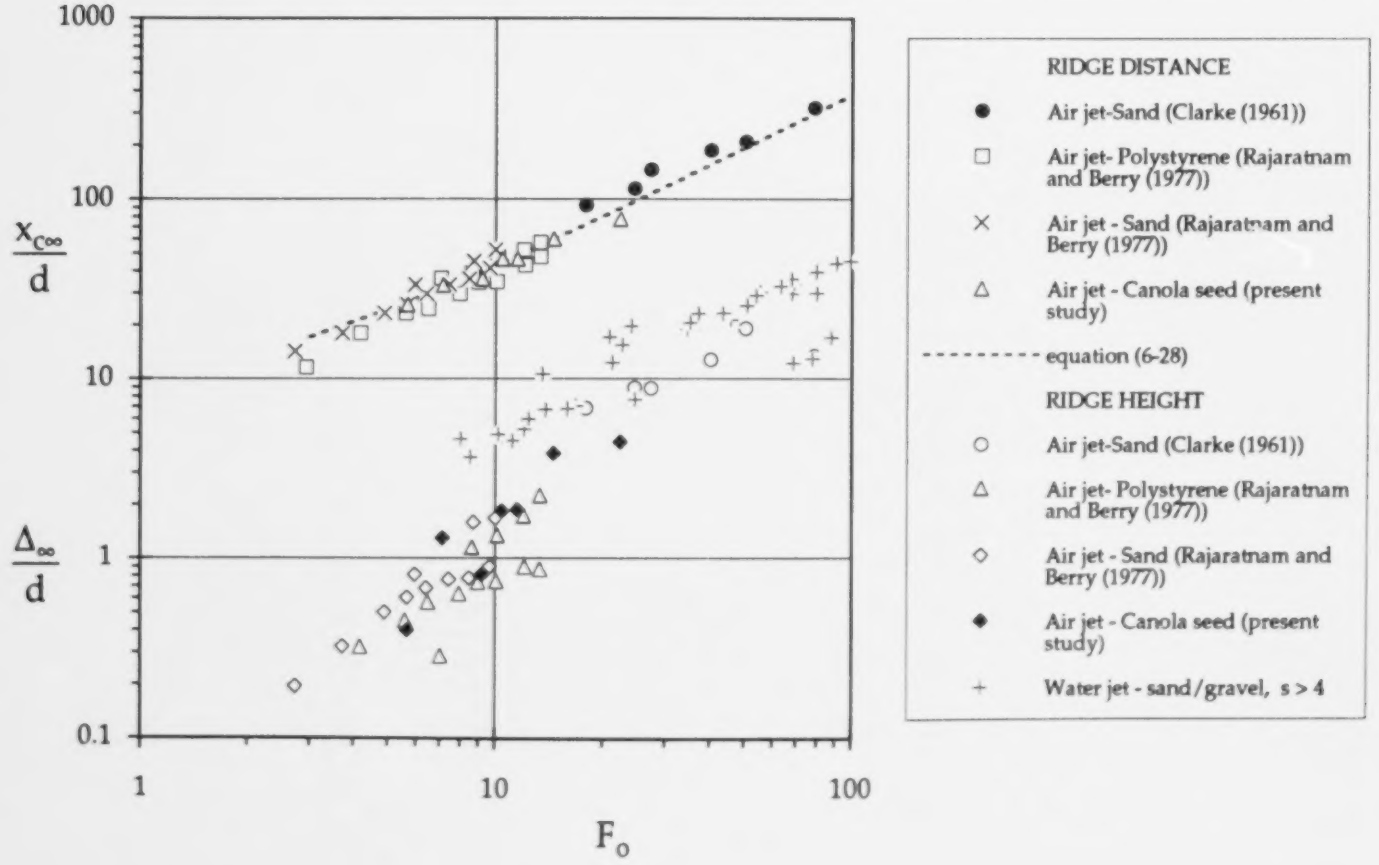

Figure 6 – 24: Variation of (Δ_∞ / d) and $(x_{c\infty} / d)$ with F_o for other fluid – sediment systems

CHAPTER 7

General Discussion

7.1 General Discussion

In the preceding five chapters, five problems on erosion by jets were studied. In this last chapter, a brief general discussion on each of these contributions is presented.

The first contribution, is the development of empirical equations for the characteristic lengths of scour below obliquely impinging submerged turbulent water jets for angles of impingement equal to 10, 30, 45 and 60 degrees. The scour lengths were found to be mainly functions of the erosion parameter E_p. The derived equations could be used to estimate the size of plunge pool scour below free trajectory jets issuing from flip bucket spillways or outlets of arch dams. The proposed scour depth equation was tested on two prototype cases and the results were found to be encouraging.

This study has been quite simplified by neglecting some factors such as the outlet conditions, the dispersion of the jet in air before entering into the plunge pool and the complex nature of the prototype bed material. These factors could substantially affect the scour size. Locher and Hsu (1984) and Mason and Arumugan (1985) addressed some of these issues and most of them are still unresolved. Further research is therefore needed in these areas to enable the development of better equations.

The study in Chapter 3 is an extension of an earlier study by Rajaratnam and Aderibigbe (1993). The success in this study, which involved using screens to reduce scour caused by deeply submerged plane wall jets, prompted the idea to investigate such effects in the case of impinging jets. The major advantage the screen has over a solid apron is that it can not be damaged by uplift pressures. The screen also helps in the dissipation of some

of the energy from the jet by the interaction of the smaller jets issuing from the screen openings in the eroded space below the screen.

In the impinging circular jet experiments, which were more extensive, the dynamic scour depth reduction ranged from 47 to 84% and the reduction or increment in scour hole radius ranged from a reduction of 16% to an increment of 75%. One of the interesting results was the development of simple approximate equations which are independent of flow and sediment properties that could be used to quantify the reductions or increments in the scour lengths. It will be interesting if this method is taken a step further by putting this idea into practice at least for some small to medium scale hydraulic structures.

As a third contribution, Chapter 4 examined the erosion of non-cohesive beds by circular impinging vertical turbulent jets for erosion parameter E_c less than 5. This study can be regarded as a simplified study of erosion below jets issuing from cantilevered circular pipe outlets and square gates of dams. This study also gives an appreciation of erosion by impinging plane jets. It was interesting to discover two distinct flow regimes as a result of the interaction of the jet with the bed and classify them according to E_c. The Strongly Deflected Flow Regime (SDJR) was well formed at E_c much greater than 0.35 and the Weakly Deflected Flow Regime (WDJR) at E_c much less than 0.35. The complied sets of scour data were obtained from five sources and it was pleasing to obtain good correlations from them. As mentioned earlier, further research will the needed in the areas of jet dispersion in air, effects of outlet conditions and non-uniformity and cohesiveness of bed material to enable the development of better equations.

The fourth contribution, which is Chapter 5, examined the effects of sediment gradation on erosion by deeply submerged plane turbulent wall jets. In most of the past studies, nearly uniform sand or gravel was used to model the prototype sediment bed which is generally non-uniform (σ_g > 1.35). These produced conservative estimates of the scour hole size because the armoring process was not simulated. In this study, three sand mixtures having median sizes and particle size geometric standard deviations σ_g of 7.2 mm and 1.33, 1.15 mm and 2.09 and 1.62 mm and 3.13 respectively were used.

One of the interesting observations was the interaction of the unstable jet with the bed. The jet continuously moved between a position along the bed to a horizontal direction and produced a deeper and shallower maximum scour depth respectively. This eventually resulted in an unstable armor layer. The shallower maximum scour depth was on the average less than the deeper maximum scour depth by about 30%, which is fairly substantial. The eroded bed was quite segregated with the coarsest section lying approximately between 0.37 and 0.75 of the scour hole length. It was not very surprising to discover that the median size of the particles in this section was approximately equal to the d_{95} of the original sand mixture. This size proved to be the effective size of the sediment mixture for obtaining a good correlation for the depth of scour rather than d_{50} for defining the densimetric particle Froude number F_O. The average reduction due to armoring in the maximum scour depth and dune height was found to be about 60% and 50% for the scour hole length and the distance of the dune. The major practical value of this study is showing that the characteristic lengths of the scoured bed can be reduced by at least 50% if the particle size geometric standard deviation is greater than 2. Further research is recommended to determine if these reductions are same for sediment mixtures with σ_g greater than 3.5.

Chapter 6 presents the fifth contribution. In this chapter, the analysis of over three hundred and fifty sets of scour data at pipe outlets, obtained from thirteen sources including the present experimental study was presented. The present experimental study comprised of air jets on canola seeds and water jets on sand and gravel beds. The whole database covers wide ranges of flow submergence, jet sizes and strengths, bed material size, relative channel width and relative density difference. For this reason, the results from this study could be viewed with much reliability.

One of the interesting results was the study of scour growth at a high densimetric particle Froude number F_O (F_O=88.2) which revealed that the scoured bed was still growing after a week. The equilibrium state was found to be gradually reached earlier at sections closer to the nozzle. The measurement of scour rates at different locations along the bed confirmed this. This clarifies the notion, as some might believe, that the entire scoured

bed profile reaches an equilibrium state at the same time. It was re-established that the characteristic lengths of scour are mainly functions of F_O. The analysis further showed that the effect of jet submergence (h_d/d) on the asymptotic characteristic lengths of the scour hole is only very pronounced when F_O is greater than 10. Beyond this, it appears that the scour size for the deep submergence case is bigger and the difference seems to increase with increasing F_O. The effects of the relative density difference on the characteristic lengths of scour were studied and interesting results were obtained. For a given F_O, the maximum scour depth and the distance of the location of the ridge were the same for all the fluid jet-sediment systems. The distance of the location of maximum scour and the scour hole length had higher values for the air jet-sediment systems and the opposite was the case for the maximum width of the scour hole and the height of the ridge. This study can be further extended to examine the effects of the difference in the elevation between the bed and the jet, the cohesiveness of the bed and the turbulence and fluctuations in the flow.

7.2 Application of Results to Prototype Cases

In the previous chapters, scour by different types of jets were examined and equations for the characteristic lengths of scour were proposed. These equations essentially show that any characteristic relative length of scour is mainly a function of the erosion parameter as given by equation (7-1). One important question that needs to be answered is the applicability of these proposed equations to prototype cases.

$$\frac{l_{c\infty}}{d \text{ or } b_o} = f_{1 \text{ or } 2}\left(F_o = \frac{U_o}{\sqrt{g\frac{\Delta\rho}{\rho}D}}\right) \qquad \text{(for wall jet erosion)} \qquad (7\text{-}1a)$$

$$\frac{l_{c\infty}}{d} = f_3\left(E_c = \frac{U_o}{\sqrt{g\frac{\Delta\rho}{\rho}D}}\frac{d}{h_t}\right) \qquad \text{(for circular impinging jet erosion)} \qquad (7\text{-}1b)$$

$$\frac{l_{c\infty}}{h_t} = f_4\left(E_p = \frac{U_o}{\sqrt{g\frac{\Delta\rho}{\rho}D}}\sqrt{\frac{2b_o}{h_t}}\right) \quad \text{(for plane impinging jet erosion)} \quad (7\text{-}1c)$$

It was earlier shown that the scour equations developed are independent of the scale of the model experiment. The scour data used covered wide ranges of the bed material size, the impinging distance and the jet size and velocity. In some cases (Opie (1967) and Stevens (1969)), the flow and the scour data could be deemed to be close to field data. Therefore, it appears that these equations could be used at a much larger scale, that is, at the prototype scale, provided the same conditions prevail. Unfortunately, the conditions are not the same. In the laboratory setting, it is quite difficult to model some factors in the prototype setting that could substantially affect the scour hole size. Some of these factors are the outlet conditions, aeration, the wind effect, the irregularities of the spilled discharge and the non-uniformity and cohesiveness of the bed material. These factors also vary from site to site. This suggests that for a particular type of jet erosion, no single expression can be assumed applicable to all cases. However, it appears that the functional relationship as given by equation (7-1) is still valid. The coefficients and the exponents in the final form of equation (7-1) should therefore reflect the prevalent conditions at each site. For small scale structures, it is not usually economically justifiable to perform model studies, therefore, some of the proposed scour equations could be used to obtain reasonable estimates of the scour size. For large scale structures, model studies have to be done. The results can then be used to determine the final form of equation (7-1).

Another important feature of equation (7-1) is that it satisfies the relevant criteria for similarity between model and prototype. This implies that based on equation (7-1a), equation (7-2) must be satisfied for the same F_o in the model and the prototype. The general criteria for scour modeling are geometrical similarity, Froude number similarity and similarity of sediment transport. The expressions for these criteria are given by equations (7-3) to (7-5) respectively for circular wall jet erosion.

$$\left(\frac{l_{c\infty}/d}{F_o}\right)_{model} = \left(\frac{l_{c\infty}/d}{F_o}\right)_{prototype} \qquad (7\text{-}2)$$

$$\frac{l_{c\infty\,(model)}}{l_{c\infty\,(prototype)}} = \frac{d_{(model)}}{d_{(prototype)}} = \frac{Length_{\,(model)}}{Length_{\,(prototype)}} \qquad (7\text{-}3)$$

$$\frac{U_{\,(model)}}{U_{\,(prototype)}} = \sqrt{\frac{d_{(model)}}{d_{(prototype)}}} = \sqrt{\frac{Length_{\,(model)}}{Length_{\,(prototype)}}} \qquad (7\text{-}4)$$

$$\frac{U_{o\,(model)}}{U_{o\,(prototype)}} = \frac{U_{c\,(model)}}{U_{c\,(prototype)}} = \sqrt{\frac{(gD\Delta\rho/\rho)_{(model)}}{(gD\Delta\rho/\rho)_{\,(prototype)}}} \qquad (7\text{-}5)$$

It can be seen that by combining equations (7-3) and (7-5), equation (7-2) can be obtained. Equations (7-3) and (7-4) will be applicable for scaling velocity of flow.

7.3 References

Breusers, H.N.C. and Raudkivi, A.J. (1991), Scouring, International Association of Hydraulic Research - Hydraulic Structures Design Manual, A.A. Balkerma, Rotterdam, pp. 143.

Locher, F.A. and Hsu, T.S. (1984), Energy Dissipation at High Dams, Chapter 5 - Developments in Hydraulic Engineering - 2 (Editor: P. Novak), Elsevier Applied Science Publishers Ltd., pp. 183 - 238.

Mason, P.J. and Arumugam, K. (1985), Free Jet Scour Below Dams and Flip Buckets, Journal of Hydraulic Engineering, Vol. 111, No. 2, pp. 220 - 235.

Rajaratnam, N. and Aderibigbe, O. (1993), A method for Reducing Scour below Vertical Gates, Proc. Inst. of Civil Engineers, Water, Maritime and Energy, Vol. 101, pp. 73 - 83.